# ALTERATION AND INFILTRATION: DOCUMENTING CONTROLS ON SKARN FORMATION AT MINERAL HILL, SECHELT, SOUTHWESTERN BRITISH COLUMBIA

by

**KATHARINE R. MCCONAGHY**

B.A. Western State College of Colorado, 1998

A THESIS SUBMITTED IN PARTIAL FULFILLMENT OF THE REQUIREMENTS FOR

THE DEGREE OF MASTER OF SCIENCE

in

THE FACULTY OF GRADUATE STUDIES

(Department of Earth and Ocean Sciences)

We accept this thesis as conforming to the required standard

THE UNIVERSITY OF BRITISH COLUMBIA

July, 2001

Department of Earth and Ocean Sciences

The University of British Columbia
Vancouver, Canada

Date 7/26/01

# ABSTRACT

The Mineral Hill wollastonite deposit is hosted by a north-west trending calcareous roof pendant enclosed within Late Jurassic plutons of the southwestern Coast Plutonic Complex. The study area consists of calcite marble, other meta-sediments and skarn in contact with a dioritic component of the Crowston Lake Pluton. The area is cross-cut by two Cretaceous-aged dike generations (D2 and D3).

Detailed mapping, petrography, petrology and O and C stable isotope analyses has led to the interpretation of a complex infiltration history of the study area. High temperature mineral production (i.e. wollastonite), skarn $^{18}O/^{16}O$ ratios, and extensive $SiO_2$ metasomatism indicate magmatic volatiles infiltrated and exchanged with the roof pendant during Late Jurassic pluton emplacement creating spatially extensive wollastonite and garnet skarn. Homogeneously depleted marble $^{18}O$ values near the wollastonite skarn boundary require interaction with a low $\delta^{18}O$ fluid (meteoric) at high temperatures. Because very low $\delta^{18}O$ values (< 5 permil) for marble are spatially associated with the pluton, and because both D2 and D3 dikes preserve textures that indicate a cold crust at the time of emplacement, a high temperature meteroic fluid must have infiltrated pre- to syn- skarn formation during the Late Jurassic. Finally, low $\delta^{18}O$ values preserved in D2 and D3, require at least one low $\delta^{18}O$ fluid interaction event either during Cretaceous syn-dike emplacement (D2 and D3, or D3) as a response to thermal activity or during a post-Cretaceous high temperature event.

This study also documents the nature and evolution of permeability at the wollastonite skarn/marble boundary within a 450 m by 150-200 m map area. Because syn-metamorphic permeability is destroyed by compaction, I used reaction transport theory to deduce paleo-fluid flow geometry. The distribution of multiple tracers (i.e. $SiO_2$, degraphitization, and $^{18}O/^{16}O$) are used in order to distinguish between infiltration sides in which flow is parallel to the alteration

boundary and infiltration fronts in which flow is perpendicular to interface geometry. At Mineral Hill, a dominance of infiltration sides and field observations support an irregular and interfingering contact between wollastonite skarn and marble. This geometry may be controlled by reaction infiltration instabilities (RII) at the reaction front which are derived from positive feedback coupling between infiltration and reaction [*Ortoleva et al.*, 1987]. RII requires dissolution at the reaction front which allows fluid to focus into areas of high permeability.

# TABLE OF CONTENTS

# LIST OF TABLES

# LIST OF FIGURES

# LIST OF PLATES

# ACKNOWLEDGMENTS

Foremost, I would like to thank my supervisor Greg Dipple for remaining enthusiastic about this project. His candid personality made him a joy to work with and I thank him for his great perspective and patience. He is not only a great advisor, but a brilliant and encouraging teacher for whom I hold in the highest regards. I would also like to thank Mati Raudsepp and Steve Rowins for being on my committee.

Thanks to Rudy Riepe and his family for not only allowing me to study skarn on their property, but for also sharing their home. I thank Rudy Riepe for always being energetic, generous and sharing his vast knowledge of geology, Greg Riepe for being an excellent and hard-working field assistant, and Connie Riepe for opening her heart to a stranger in a way that should truly be commended.

I am grateful to the office and technical staff in the Department of Earth and Ocean Sciences. Beyond doubt, they are the most important and helpful people in the building. Without them, I would have run circles around myself and what took three years to complete would have taken five.

Finally, I'd like to give a shout out to all my homies in the house: yo homies! In particular, I'd like to thank my boyz Slinky K and Brudda Is for starting it all off and keeping me sane (by comparison). I have never met such polar opposites who kept me so enthralled by their mere presence. I owe much more to these two than I can express.

I leave with this thought: as sculptor Henry Moore once declared to poet Donald Hall, "The secret to life is to have a task, something you devote your entire life to, something you bring everything to, every minute of the day for your whole life. And the most important thing is-- *it must be something you cannot possibly do*."

# CHAPTER 1: OVERVIEW

## 1.1 Introduction

The Mineral Hill property is located approximately 60 kilometers due west-north-west of Vancouver and 5.5 kilometers north of Sechelt on the Sechelt Peninsula of British Columbia. The Sechelt Peninsula is located at the south-western end of the Coast Plutonic Complex (CPC), a north-west-trending concentration of Late Jurassic to Tertiary plutonic rocks, and is comprised of elongated and deformed calcareous roof pendants. The majority of these roof pendants are tentatively correlated to carbonates of the Upper Triassic Quatsino Formation [*Ditson*, 1987; *Ray and Kilby*, 1996]. At Mineral Hill, a north-west-trending pendant is completely enclosed by the Late Jurassic Crowston Lake and Snake Bay Plutons. These intrusions vary in composition from gabbro to quartz-diorite and quartz-diorite to granodiorite, respectively, and are likely responsible for altering the host sediments to calcite and dolomite marbles and calcic exoskarn (i.e. sedimentary protolith).

The study area at Mineral Hill is located in a 450 meter by ~200 meter south-eastern portion of the pendant (see Fig. 1.1). The study area consists of calcite marble, other meta-sediments and skarn in contact with a dioritic component of the Crowston Lake Pluton. Late dike phases (D2 and D3) crosscut marble and skarn units. Chapter Two of this thesis documents the rock units sampled within the study area at Mineral Hill in terms of field, textural and petrographic descriptions. Intact samples (I) were taken directly from outcrop as well as fall rock (FR) collected from loose material usually located below outcrops of similar lithology. Petrographic descriptions of units are provided in terms of mineral assemblages (prograde and retrograde), peak-metamorphic equilibrium phases, and macro- and micro textures observed in the field and using optical and scanning electron microscopy (SEM) (Notation defined in Table 1.1). Chapter Three describes rock units in terms of their whole-rock geochemistry, interprets

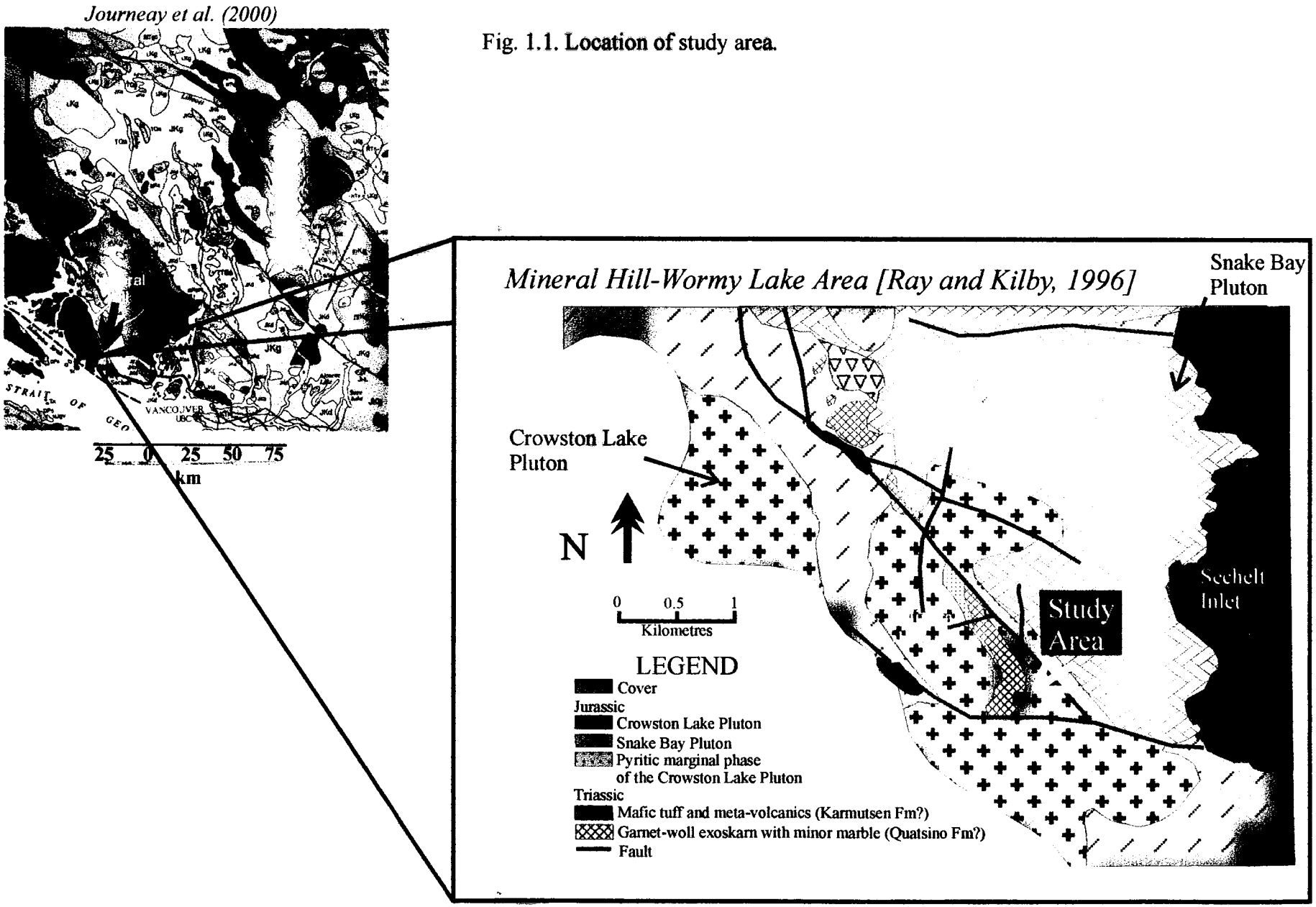


Fig. 1.1. **Location of study area.**

Table 1.1. Notation for minerals and rocks

**Minerals**

| | | | |
|---|---|---|---|
| apa | apatite | ank | ankerite |
| chl | chlorite | alb | albite |
| bt | biotite | qtz | quartz |
| zeo | zeolite | rut | rutile |
| ttn | titanite | par | paragonite |
| pyr | pyrite | ilm | ilmenite |
| ser | sericite | olig | oligoclase |
| apo | apophyllite | amph | amphibole |
| gr | grossular | st | staurolite |
| gnt | garnet | ky | kyanite |
| pl | plagioclase feldspar | an | anorthite |
| ksp | potassium feldspar | pyr | pyrope |
| gph | graphite | spe | spessartine |
| phl | phlogopite | andr | andradite |
| musc | muscovite | hed | hedenbergite |
| ent | enstatite | di | diopside |
| clz | clinozoisite | | |
| woll | wollastonite | | |
| cc | calcite | | |
| opq | opaques | | |

**Rocks**

| | |
|---|---|
| g-w skarn | garnet-wollastonite skarn |
| woll skarn | wollastonite skarn |
| gnt skarn | garnet skarn |
| gr marble | green marble |
| cpx skarn | clinopyroxene skarn |
| qtz vein | quartz vein |
| bk marble | black marble |
| g-b marble | grey and bleached marble |

geochemical controls of skarn zonation, estimates volume change caused by reaction of marble to form wollastonite skarn, fluid-rock ratios and time-integrated fluid fluxes over the duration of skarn formation. Whole-rock compositions of all meta-sedimentary and skarn units within the study area are plotted in A-S-C-F ternary space and graphically compared to seven meta-sedimentary units documented in the literature, twelve common sedimentary rocks, and end-member chemical compositions of eleven minerals. Igneous whole-rock chemistry from this study were augmented with data from *Ray and Kilby* [1996] and classified using five NEWPET plots. Petrographic and petrologic data and observations are used to estimate volume changes caused by reaction from marble to wollastonite skarn, through graphical passive enrichment of immobile elements (element ratios) and calculations using *Grant's* [1986] mass balance approaches. Moreover, reaction transport theory is used to interpret geochemical controls (infiltration vs. protolith) on zonation of skarn in the study area. Chapter Four describes the stable isotope geochemistry of all units in respect to common oxygen and carbon reservoirs. The nature and evolution of permeability during skarn formation is delineated by the spatial extent of multiple reactions (alteration fronts): $SiO_2$, degraphitization, and $^{18}O/^{16}O$. The distinction between infiltration sides and infiltration fronts due to the distribution of multiple tracers allows us to image the flow geometry at the wollastonite skarn/marble interface. Finally, the complex fluid history in the field area recorded by oxygen isotope alteration in skarn, marble and igneous units is interpreted.

## 1.2 Regional Geology

The Coast Plutonic Complex (CPC), a northwest trending belt approximately 1700 km long and 50-175 km wide, is the largest single concentration of plutonic rock on the western North American margin [*Friedman et al.*, 1995]. It is composed of Jurassic- to Tertiary-aged plutonic rocks which represent a suite of subduction-related magmatic intrusions which conceal

the contact between the morphogeological Insular and Intermontane belts of the Canadian Cordillera [*Friedman et al.*, 1995; *Cui and Russell*, 1995]. The CPC makes up a substantial part of the Coast Belt which *Journey and Freidman* [1993] subdivided into eastern, central, and western structural and lithological domains. Moreover, the CPC has been subdivided into northern and southern isotopic domains. Nd and Sr isotopic data for plutonic rocks from the northern CPC show dominantly Late Cretaceous-Tertiary intrusions to have been contaminated by juvenile material and "old, recycled crustal material" [*Samson et.al.*, 1991]. On the basis of Nd, Sr, and Pb radiogenic isotope characteristics, *Cui and Russell* [1995] concluded that Late Jurassic to Late Cretaceous intrusions in the southern CPC are juvenile in origin and resulted from partial melting of mantle-derived materials with little to no interaction with old continental crust. However, these intrusions may have had chemical interaction with older, isotopically primitive terranes (e.g. Wrangellia).

*Friedman et al.* [1995] concluded that the Coast Plutonic Complex in the southwestern portion of the southern Coast Belt was generated in an isotopically juvenile magmatic arc. Here, the CPC intrudes the Wrangellian terrane, currently preserved primarily as deformed roof pendants [*Friedman et al.*, 1995]. The Wrangellia terrane is primarily comprised of rocks of oceanic and volcanic arc affinity, which are dominated by juvenile isotopic values.

The Mineral Hill property lies in the Caron Mountain Range, specifically within the Crowston Lake and Snake Bay Plutons of the southern CPC, southwestern British Columbia. The plutons at Mineral Hill were mapped as an early Coast Plutonic suite of granitic rock. Earlier authors associate pluton emplacement in the Late Jurassic inferred through correlation with similar intrusive bodies that have been dated by isotopic methods [*Ray and Kilby,* 1996]. They intrude amphibolites, marble and meta-volcanics correlated with Wrangellian strata [*Roddick and Woodsworth*, 1979; *Friedman and Armstrong*, 1995]. The meta-sediments studied at Mineral Hill are part of a roof pendant preserved within the Crowston Lake Pluton, which ranges in

composition from gabbro to quartz diorite [*Ray and Kilby*, 1996]. The roof pendant at Mineral Hill is a discontinuous, elongate, northwestwardly trending belt. Various stages of intense deformation are observed within the pendant including isoclinal folding of metasediments and skarn and boudinaged early and late igneous sill phases (D1 and D2). Although the pendant has not been dated, it is believed to be comprised of Upper Triassic Vancouver Island Group sediments. Units of layered to massive, fine to medium grained mafic metatuffs and metabasalts located in the northern portion of the roof pendant at Mineral Hill may be members of the Triassic Karmutsen Formation or the Jurassic Bowen Island Group metavolcanic sequence [*Ray and Kilby*, 1996]. The calcic to dolomitic meta-sediments are tentatively correlated with the Triassic Quatsino Formation [*Goldsmith and Kallock*, 1988; *Ray and Kilby*, 1996]. The unaltered Quatsino Formation of Vancouver Island is generally comprised of a gradational sequence between lower and upper limestone members. The lower member is a massive to poorly bedded, pure to cherty limestone. The cherty inclusions are dark-grey to brown-grey and occur at many levels within the member [*Eastwood*, 1968; *Muller et al.*, 1974; *Jeletzky*, 1976]. The upper member is predominantly medium to thinly well-bedded argillaceous limestones, which commonly contain nodules and laminations of brown-grey, dark-grey and black chert [*Eastwood*, 1968; *Muller, et al.*, 1974; *Jeletzky*, 1976]. In the study area, the roof pendant is comprised of similar calcic sediments. No pre-Jurassic volcanic rocks are observed.

## 1.3 Local Geology

### 1.3.1 Introduction

The study area at Mineral Hill is located in a 450 meter by ~200 meter southeastern area of the northwest-trending pendant (see Fig. 1.1). The study area consists of calcite marble, other meta-sediments and skarn in contact with a dioritic component of the Late Jurassic Crowston Lake Pluton (Fig. 1.2). The intrusion is likely responsible for thermal and metasomatic alteration

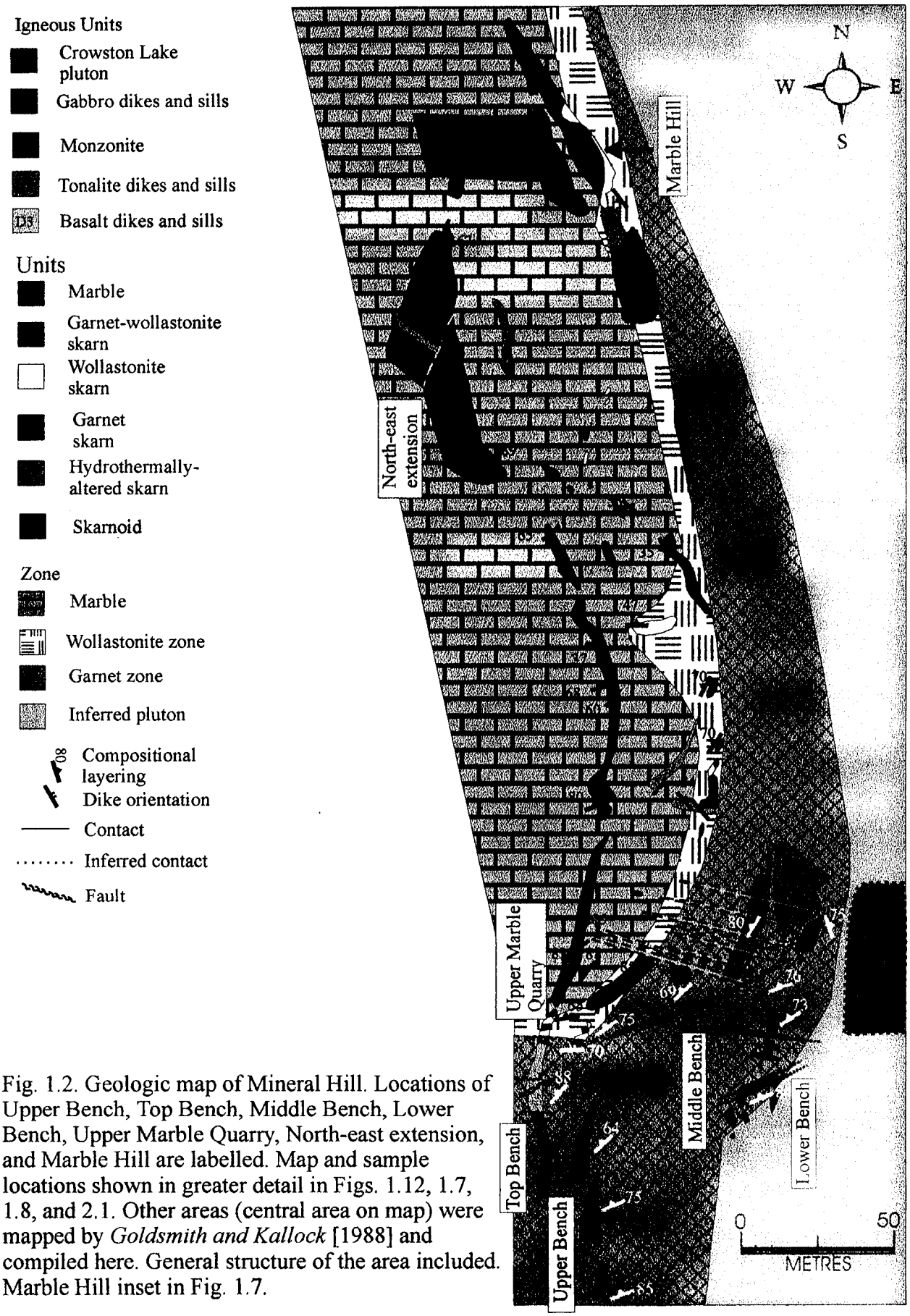


Fig. 1.2. Geologic map of Mineral Hill. Locations of Upper Bench, Top Bench, Middle Bench, Lower Bench, Upper Marble Quarry, North-east extension, and Marble Hill are labelled. Map and sample locations shown in greater detail in Figs. 1.12, 1.7, 1.8, and 2.1. Other areas (central area on map) were mapped by *Goldsmith and Kallock* [1988] and compiled here. General structure of the area included. Marble Hill inset in Fig. 1.7.

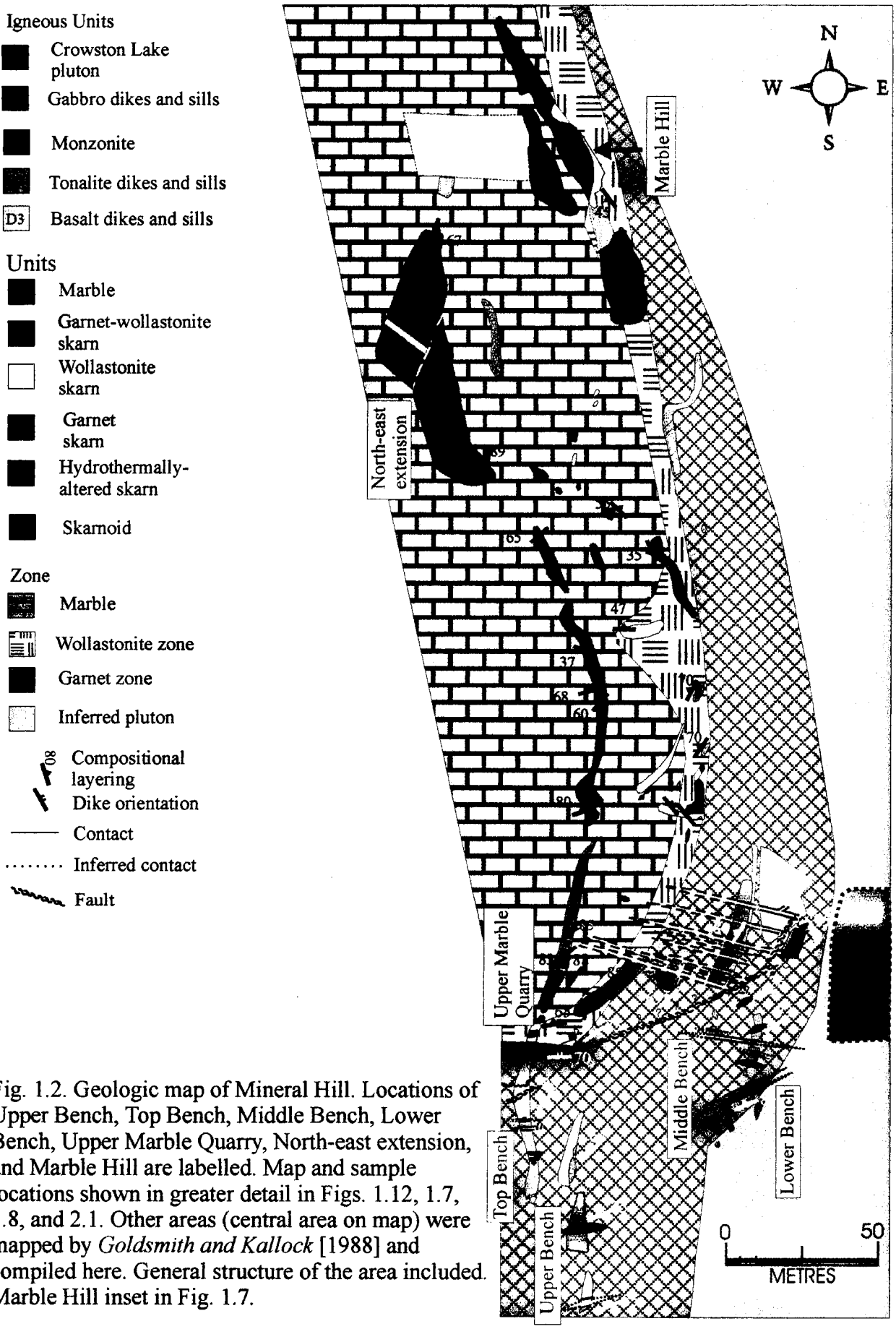


Fig. 1.2. Geologic map of Mineral Hill. Locations of Upper Bench, Top Bench, Middle Bench, Lower Bench, Upper Marble Quarry, North-east extension, and Marble Hill are labelled. Map and sample locations shown in greater detail in Figs. 1.12, 1.7, 1.8, and 2.1. Other areas (central area on map) were mapped by *Goldsmith and Kallock* [1988] and compiled here. General structure of the area included. Marble Hill inset in Fig. 1.7.

of host sediments to calcite marble and calcic exoskarn. Tonalitic and basaltic dike phases, D2 and D3, respectively, crosscut marble and skarn units, whereas gabbroic and tonalitic sill phases, D1 and D2, conform with compositional layering defined by meta-sedimentary and skarn units.

### 1.3.2 Structure

Skarn and meta-sediment units within the field area are intensely deformed. *Goldsmith and Kallock* [1988] mapped and diamond-drilled within the study area. They noted that primary bedding/compositional layering was accentuated by banded skarn assemblages (i.e. garnet skarn) and that the original limestone bedding had been transposed during plastic deformation. They also defined the structure of the area which was confirmed by structural measurements taken during detailed quarry mapping in this study (App. 1). The structure defined by compositional layering suggests a regional fold in the central portion of the map area (Fig. 1.2). Structure measurements taken during field mapping (this study) reveal compositional layering in the Top Bench, Upper Bench and Upper Marble Quarry generally trends north-east/south-west and dips near vertical to the northwest (Figs. 1.3b and 1.4). Although, there is a greater degree of variation in compositional layering possibly due to a fault and/or proximity to the Crowston Lake Pluton, structure in the middle bench is similar (Figs. 1.3a and 1.5). Compositional layering at Marble Hill, north of the aforementioned map areas, generally trends north-west/ south-east, and dips near vertical, confirming a change in strike direction and suggest the existence of a regional fold (Figs. 1.6 and 1.7). Dikes D2 and D3 are localized in the fold axis. These dikes strike predominantly to the east and dip near vertical (Figs. 1.6b and 1.5). D2 sills within the axis have ductile boudinage structures. Some D1 dikes have the same trend, however, three D1 structures strike north-west/south-east and have a shallower dip (Fig. 1.6b). Compositional layering of marble and skarn units proximal to the Crowston Lake Pluton generally strike parallel-to-subparallel to the contact (Figs. 1.8 and 1.7).

A)

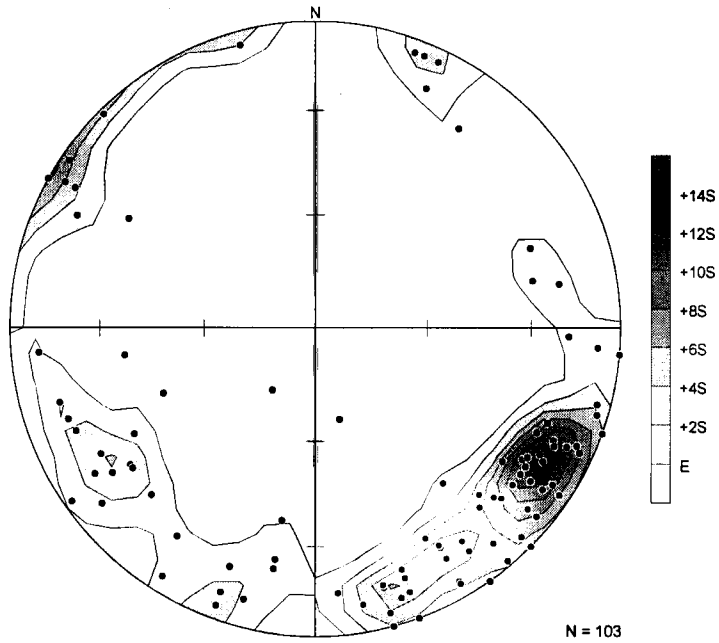


B)

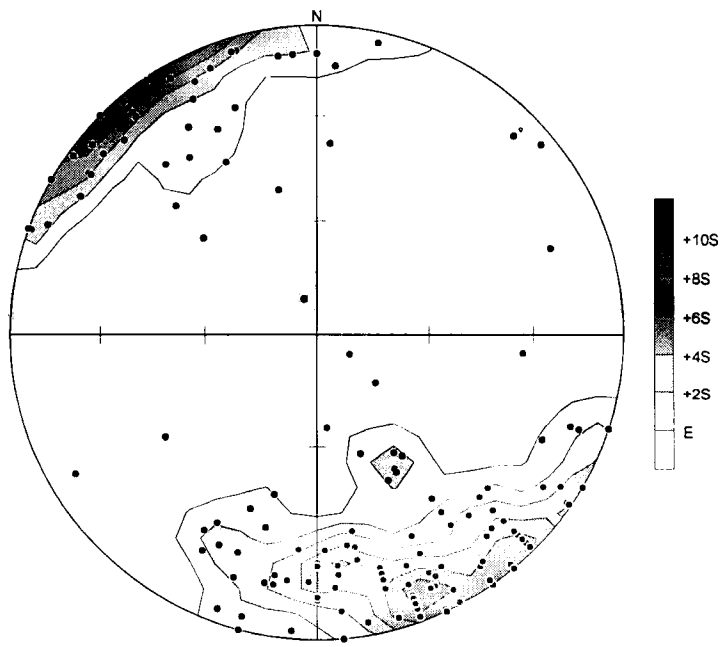


Fig.1.3. A) Contoured stereonet of compositional layering measurements from Middle Bench suggest NE-SW strike direction and near vertical dip direction although variation exists (see Fig. 1.6). B) Contoured stereonet of compositional layering measurements from Upper Bench, Top Bench, and Upper Marble Quarry suggest NE-SW strike direction and near vertical dip direction (see Fig. 1.4).

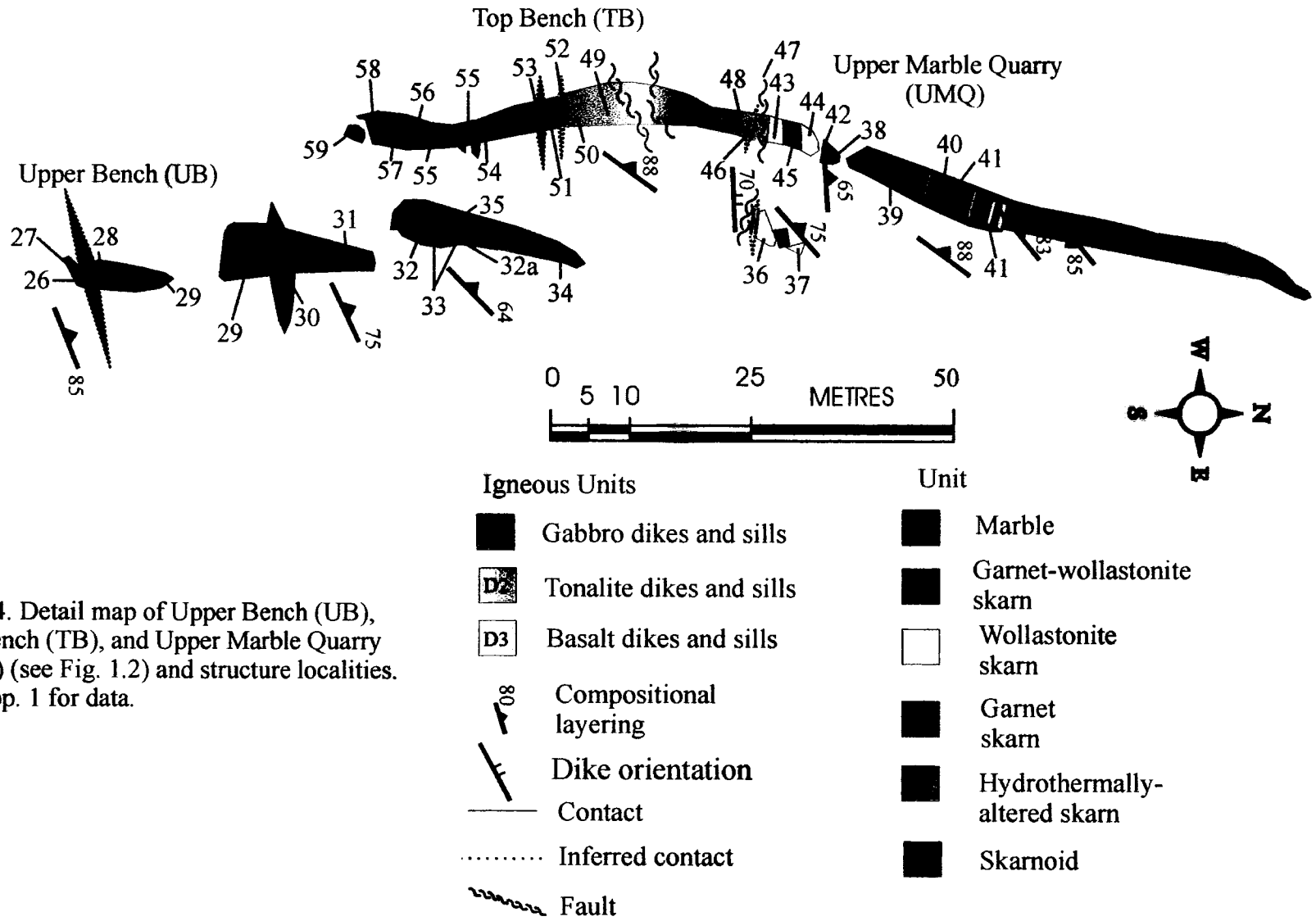


Fig. 1.4. Detail map of Upper Bench (UB), Top Bench (TB), and Upper Marble Quarry (UMQ) (see Fig. 1.2) and structure localities. See App. 1 for data.

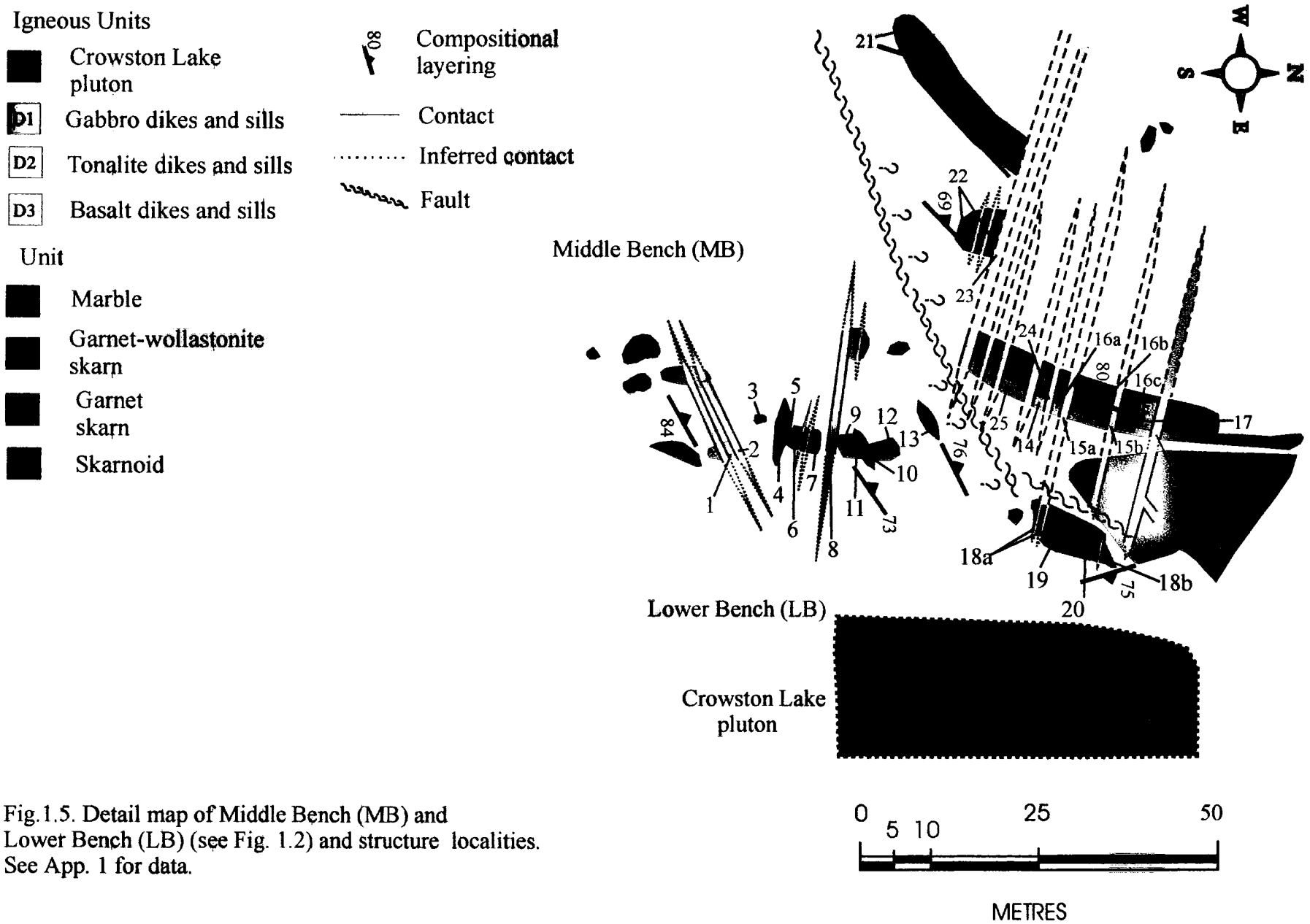


Fig.1.5. Detail map of Middle Bench (MB) and Lower Bench (LB) (see Fig. 1.2) and structure localities. See App. 1 for data.

A)

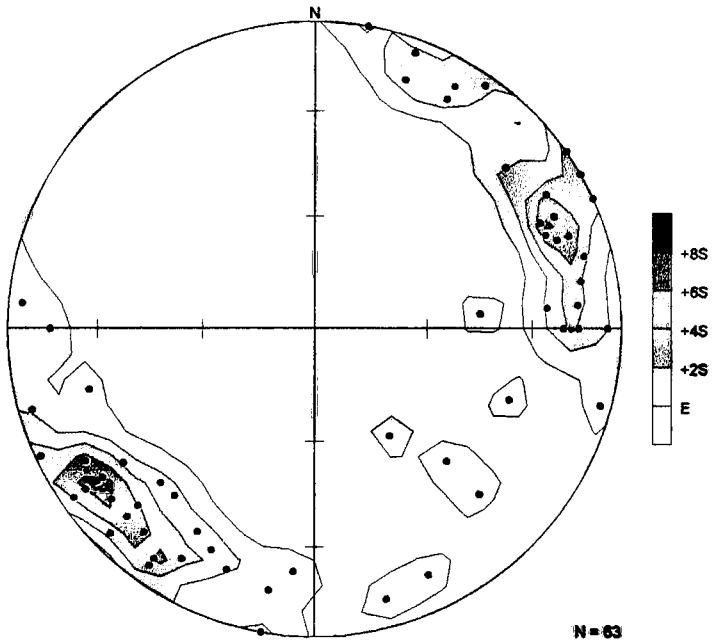


B)

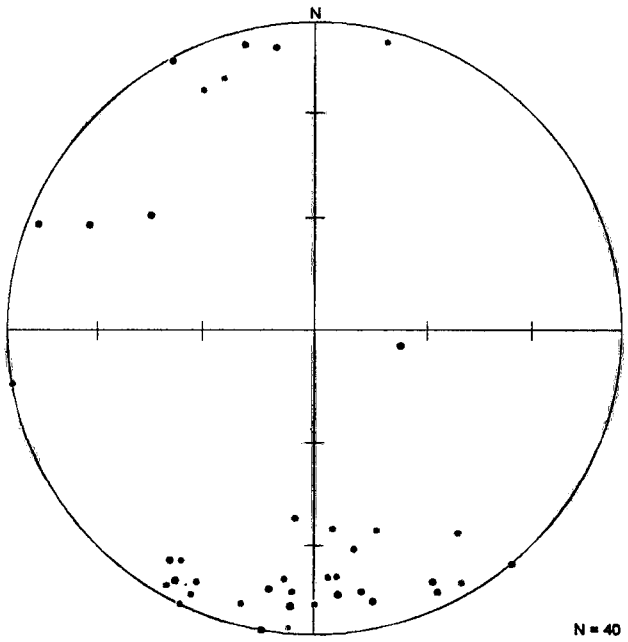


Fig. 1.6. A) Contoured stereonet of compositional layering measurements from Marble Hill suggest NW-SE strike direction and near vertical dip direction (see Fig. 1.8). B) Stereonet of structural measurements of igneous dikes and sills. Red= D1, orange= D2, green= D3. Generally all dike generations strike east with a near vertical dip. Three D1 strike to the NW with an average dip of ~60 degrees (see Fig. 1.2).

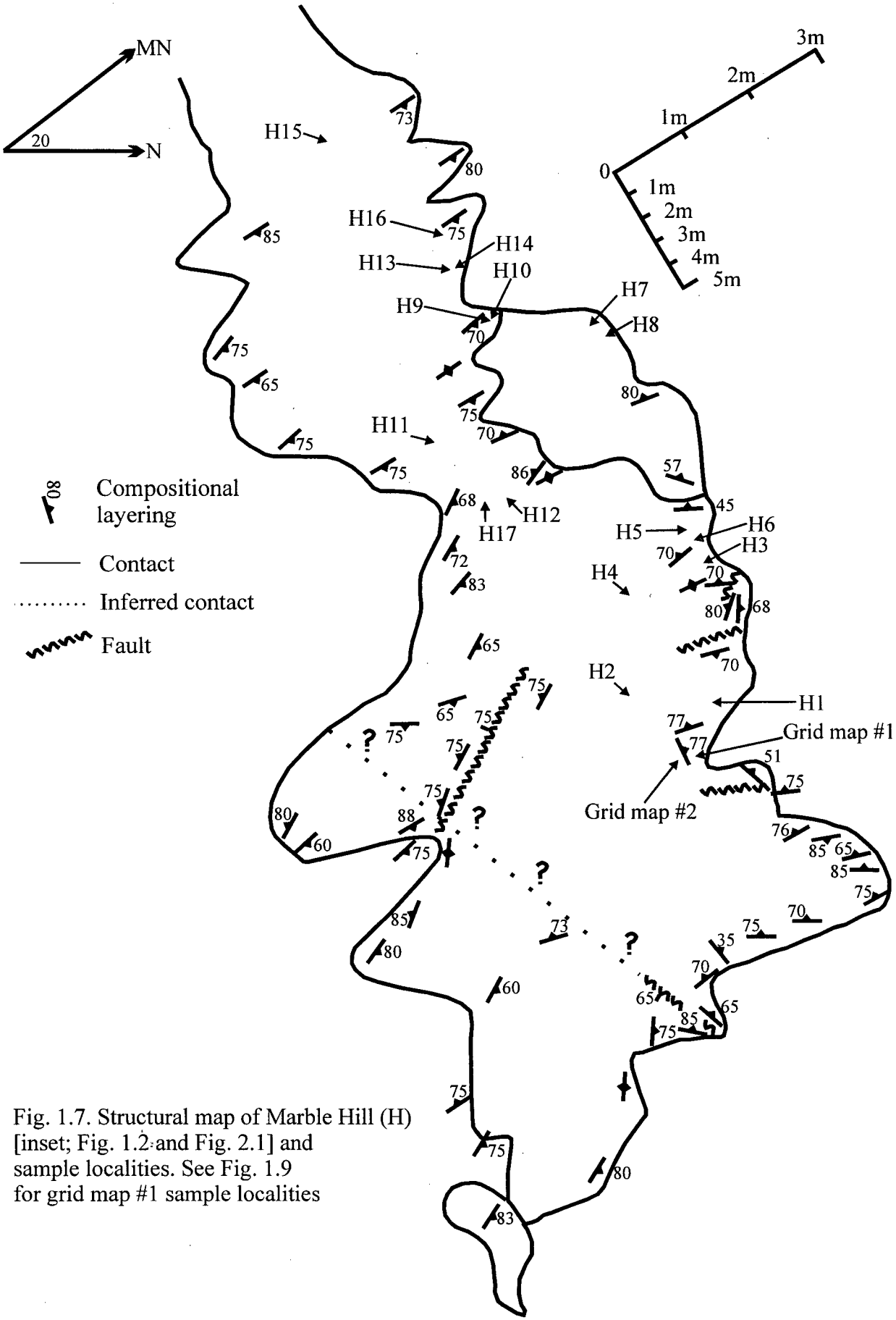


Fig. 1.7. Structural map of Marble Hill (H) [inset; Fig. 1.2 and Fig. 2.1] and sample localities. See Fig. 1.9 for grid map #1 sample localities

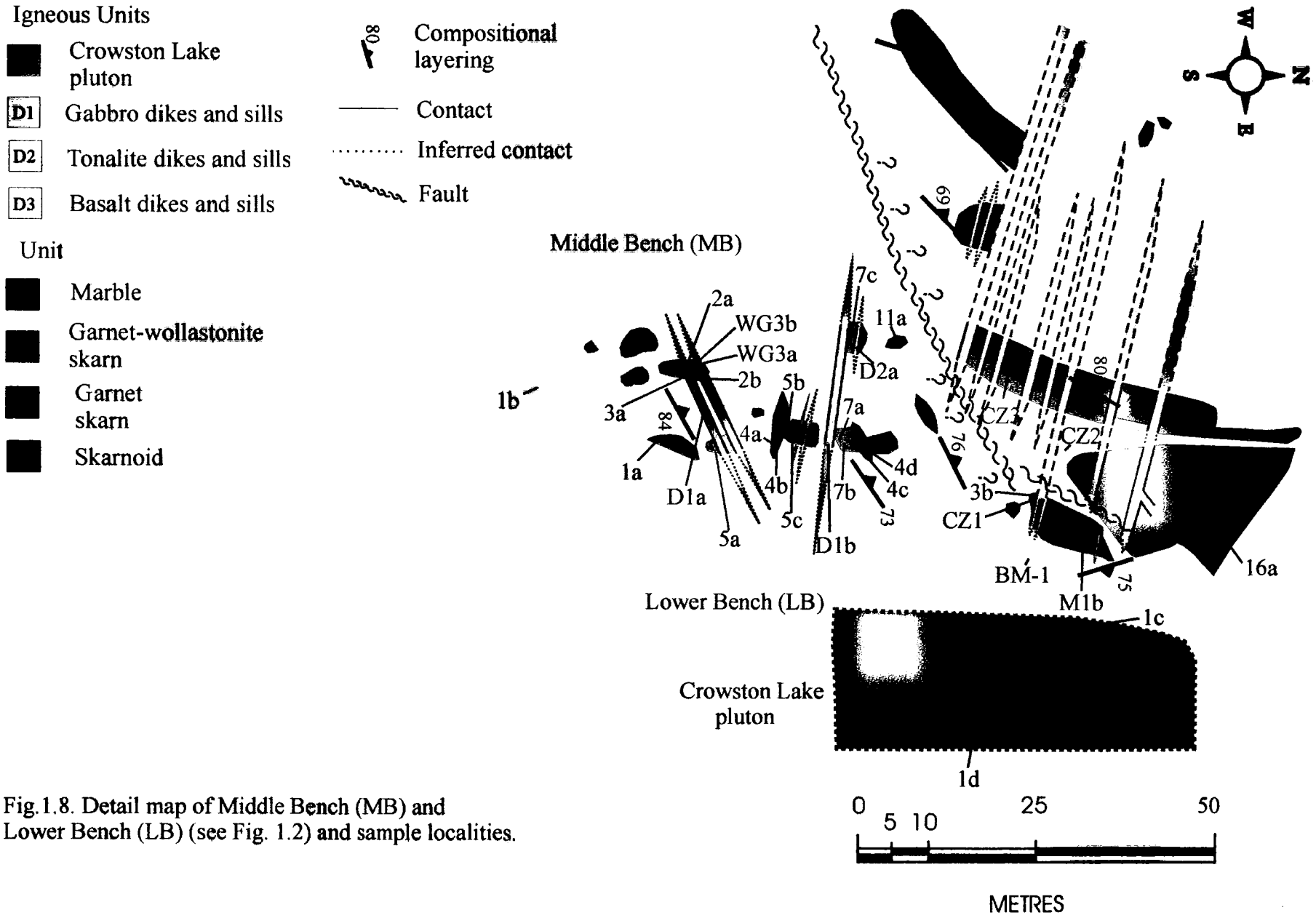


Fig.1.8. Detail map of Middle Bench (MB) and Lower Bench (LB) (see Fig. 1.2) and sample localities.

Brittle deformation is observed as faults within meta-sediments, skarn, and all igneous units (including D3) (Figs. 1.4, 1.5 and 1.7). Retrograde skarn assemblages are observed primarily in the proximity of brittle faults and pluton contacts. Two main faults have been mapped on the Mineral Hill property by previous workers outside of the study area: the north-northwesterly trending and near vertical (80-90 degree) Wormy Lake Fault (WLF) and the more east-west trending steeply dipping Snake Creek Fault (SCF) [*Ray and Kilby*, 1996; *Murphy*, 1999] (Fig. 1.1). The WLF is parallel to the regional northwest trend and has approximately 800 meters of sinistral movement. The SCF cross cuts and displaces the WLF approximately 2 kilometers to the west by dextral movement. *Murphy* [1999] contends that dextral movement cut off, ductily deformed and drag folded skarn. Extension on the eastern side of the roof pendant resulted in brittle tension fractures (intruded by later dike phases). On the western boundary, shortening is observed by compressional crenulation folds. Moreover, dextral displacement along the SCF shifted a large portion of the Crowston Lake Pluton to the west [*Murphy*, 1999].

### 1.3.3 Prograde Skarn Episodes

*Ray and Kilby* [1996] identified three prograde skarn episodes associated with igneous activity at Mineral Hill. The first skarn episode is the most spatially extensive and accompanied the intrusion of the Late Jurassic Crowston Lake Pluton and associated gabbroic dikes and sills (D1). Skarn is characterized by garnet-wollastonite-pyroxene mineral assemblages. Ductile deformation includes intense flow folding (isoclinal) as well as boudinaged D1 sills. The first skarn episode is the main focus of this study and was mapped within a 450m by ~200m area. The interface of the skarn front and marble pendant was mapped within 2m by 2m map areas (Fig 1.9, 1.10, and 1.11) in order to document the skarn geometry and alteration outboard the skarn front. The interface occurs as wollastonite skarn in contact with proximal bleached marble to distal grey marble (see Fig. 1.11). Bleached marble rarely extends more than a few centimeters

## Grid Map 1 (GM1)

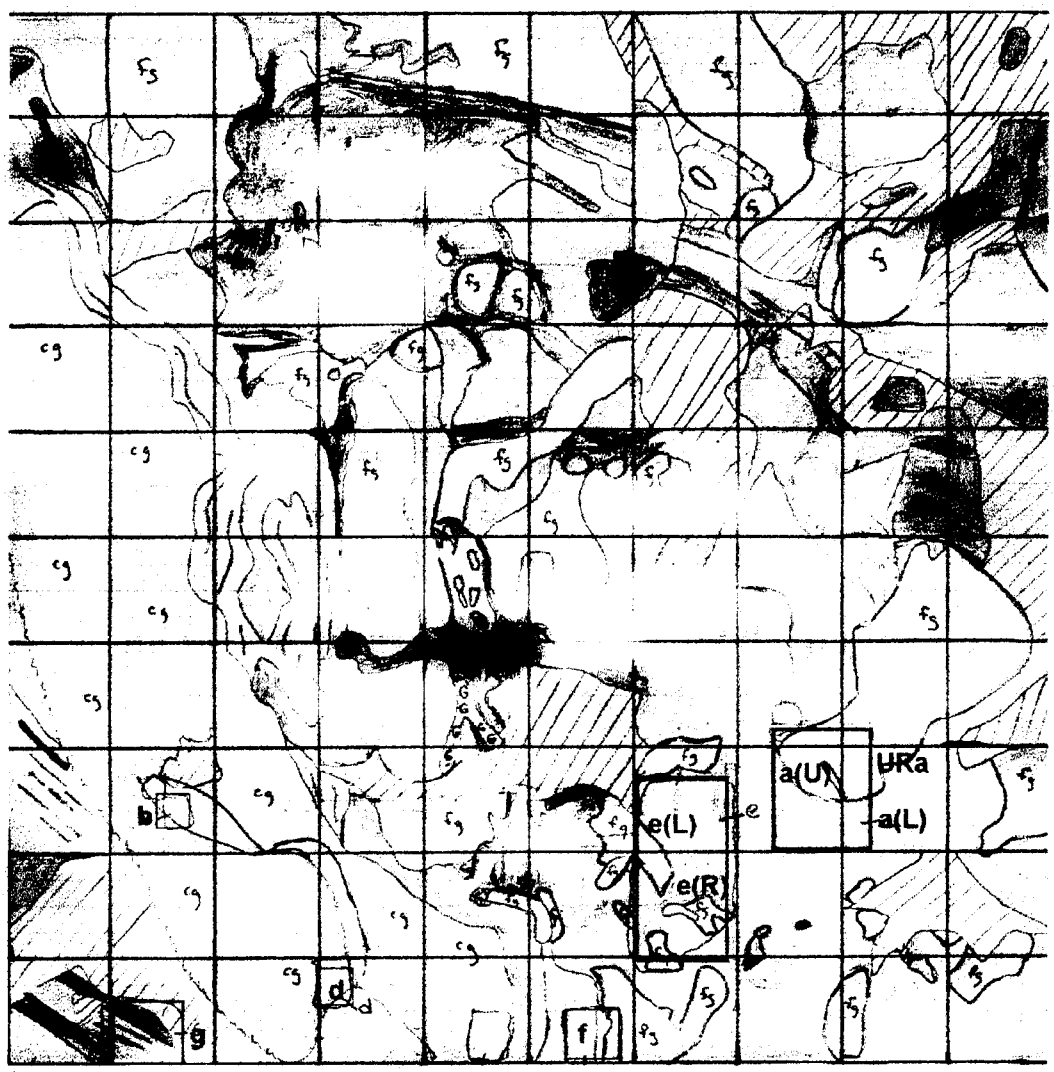


fg fine-grained wollastonite skarn

cg coarse-grained wollastonite skarn

garnet-bearing wollastonite skarn

bleached marble

grey marble

quartz vein

outcrop covered

calcite vein

**grid orientation 032/66NE**

Fig. 1.9. Grid Map 1. Scale is 2 meters by 2 meters. Sample localities in black boxes and labeled according to sample designation (i.e. sample GM1a(U), came from locality a(U)). Stable isotope values for each area presented in Table 4.1. Petrography presented in Table 2.2. Geochemistry presented in Table 3.2.

## Grid Map 2 (GM2)

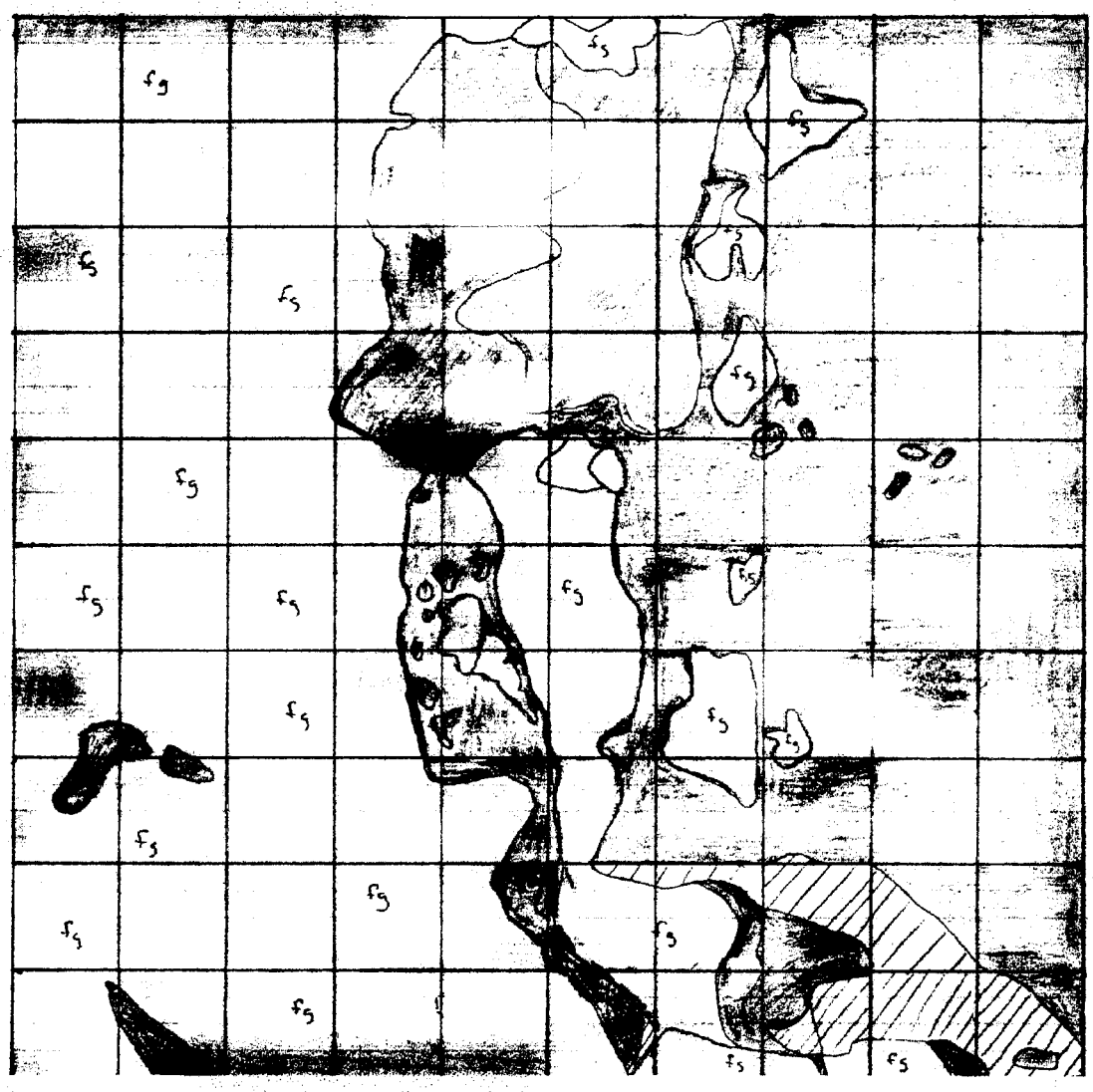

fg fine-grained wollastonite skarn

bleached marble

grey marble

outcrop covered

**grid orientation 290/55NE**

Fig. 1.10. Grid Map 2 is located directly above (in outcrop) GM1 (see Fig. 1.9) at Marble Hill. Scale is 2 meters by 2 meters. No samples were collected from GM2.

## Grid Map 3 (GM3)

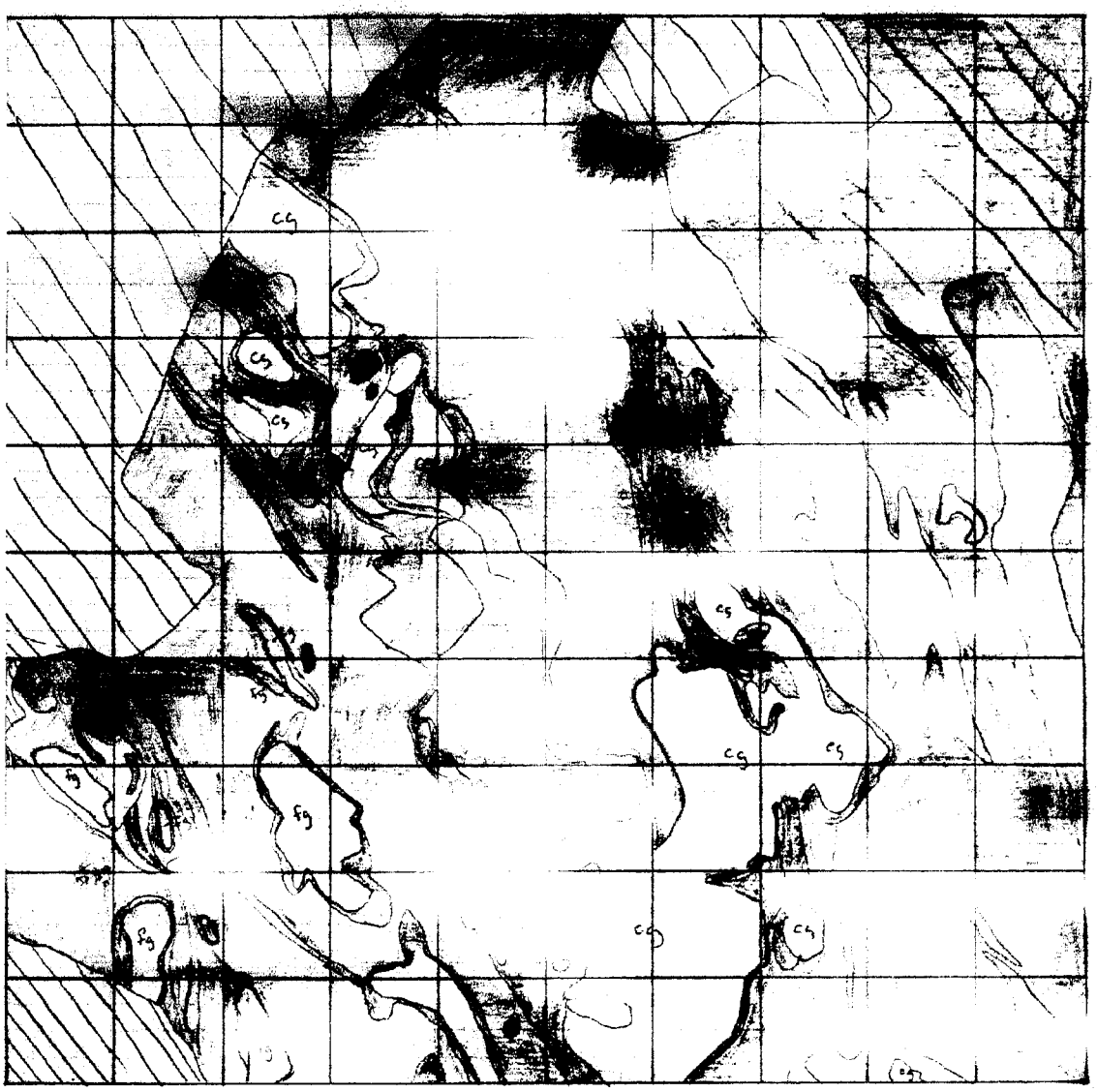

fg fine-grained wollastonite skarn

cg coarse-grained wollastonite skarn

bleached marble

grey marble

unidentified black material (augens)

outcrop covered

**grid orientation 340/60E**

Fig. 1.11. Grid Map 3 is located in the Upper Marble Quarry. Scale is 2 meters by 2 meters. No samples collected from GM3.

outboard of wollastonite skarn. Moreover, the interface does not represent a planar boundary, but occurs as fingering lobes of wollastonite skarn extending irregularly into marble (see Figs. 1.9 and 1.10). This geometry suggests fluid infiltration into pervious rocks, where fluid is not restricted to structural conduits. Mechanisms allowing fluid infiltration into rocks undergoing metamorphism in which permeability is essentially destroyed by compaction is described later in this thesis.

Porphyritic tonalitic dikes and sills (D2), the second pulse of igneous activity, intrude skarn and marble. *Ray and Kilby* [1996] observed D2 crosscutting the Crowston Lake Pluton. Garnet-epidote reaction skarn is observed along the margins of D2 but is not observed to exceed two centimeters in width. Reaction skarn differs from the first skarn-forming event since the introduction of exotic components outside the sedimentary section is not required even though metasomatic zoning is displayed. Reaction skarn often forms due to the local exchange of fluid (bimetasomatism) by diffusive mass transfer in which fluid travels no more than a few centimeters [*Einaudi and Burt*, 1982]. Boudinaged D2 sills are fractured parallel to stretching. These fractures are infilled with epidote. D2 are altered proximal to the fractures, observed as color change from dark to light green in hand sample and greater plagioclase abundance in thin section.

Emplacement of basaltic dikes (D3) cross-cutting boudinaged D2 sills represent the final pulse of igneous activity in the field area. These dikes predominantly strike east and in places show brittle deformation features (e.g. Upper Marble Quarry; see Fig. 1.12). Reaction skarn occurs along the margins of D3, but is not observed to exceed four centimeters in width. Reaction skarn occurs as proximal garnet and distal wollastonite were D3 intrudes bleached and grey marble [*Ray and Kilby*, 1996].

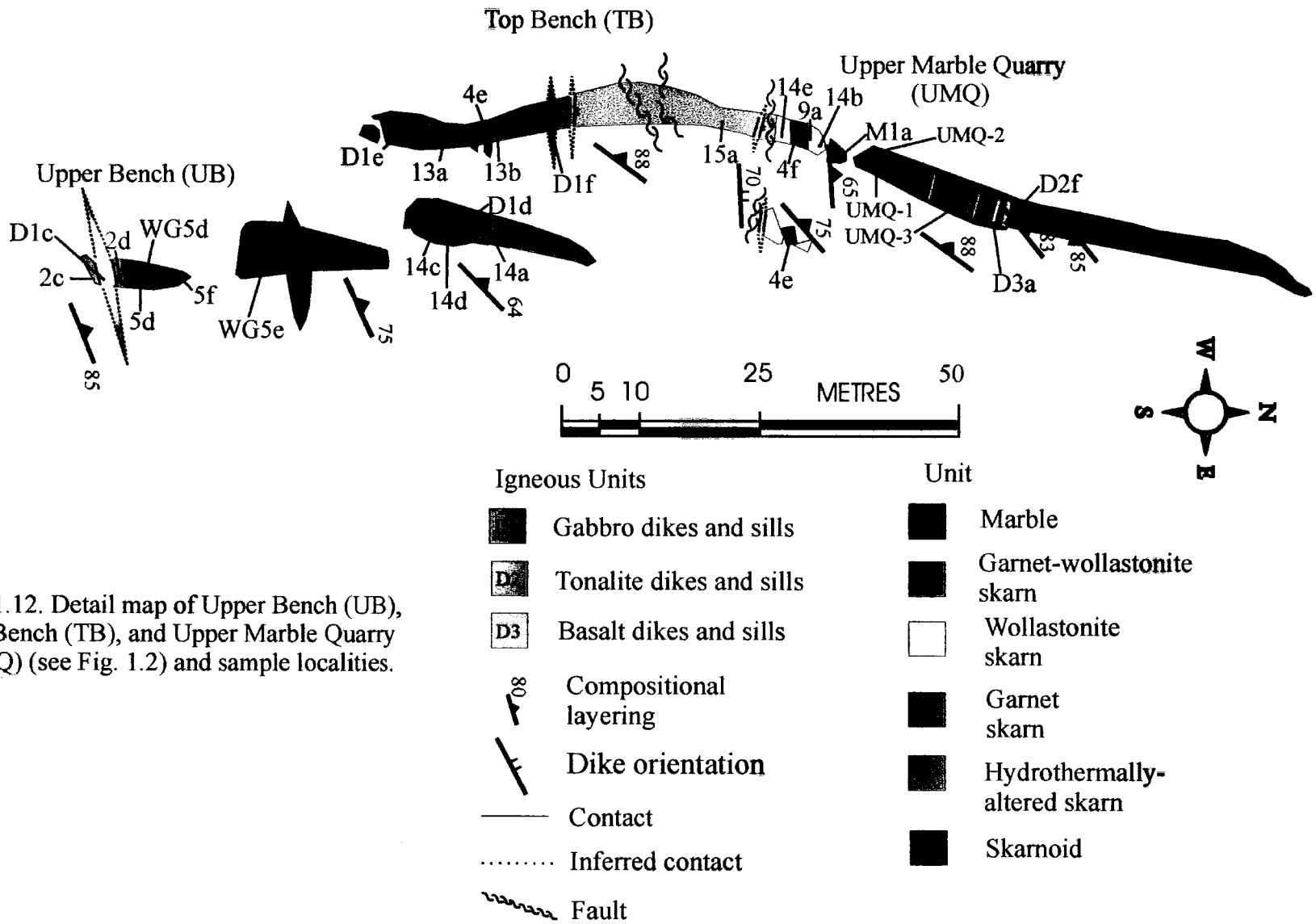


Fig. 1.12. Detail map of Upper Bench (UB), Top Bench (TB), and Upper Marble Quarry (UMQ) (see Fig. 1.2) and sample localities.

### 1.3.4 Summary of results: overview

The following section gives an overview of the main conclusions of this thesis within the context of an overall geologic history of skarn formation at Mineral Hill.

A calcareous roof pendant tentatively correlated with the Quatsino Formation of the Vancouver Island Group was enclosed within the Late Jurassic Crowston Lake Pluton, which was probably emplaced near surface and comprises a juvenile portion of the southern CPC. Meteoric fluid infiltrated and isotopically (oxygen) altered marble near pluton and to a lesser extent distal marble (relative to pluton contact). Magmatic volatiles exsolved off of the pluton pervasively altering the roof pendant creating calcic exoskarn. Spatial extent of wollastonite skarn represents the spatial extent of the geochemical $SiO_2$ front. Large scale zonation patterns within skarn are partially controlled by infiltration of magmatic fluid and protolith composition. Positive feedback coupling between infiltration and reaction may have resulted in heterogeneous permeability within marble and focused flow into areas of high permeability producing a skarn/marble boundary that is highly irregular and fingered. Laminated and nodule-rich marble interleaved with pure marble gave rise to two geochemically different wollastonite skarns: A and B. The former is generally higher in concentrations of immobile elements (i.e. Al, Ti, Zr, V, Yb, Y and HREEs). Rare earth element patterns suggest mobility of LREEs. Passive enrichment of immobiles support a calculation of ~ 20% volume loss associated with the formation of wollastonite skarn B from average pure marble samples from the field area. This may have created transient syn-metamorphic porosity at the reaction front.

Intrusion of D2 and D3 events, correlated to Early Cretaceous extension, cross cut skarn and marble units. Reaction skarn occurs along the margins of both dike phases, as garnet-epidote and garnet-wollastonite, respectively. This indicates preservation of high temperature alteration although porphyritic and aphanitic textures within D2 and D3 reflect a cold crust at the time of emplacement. Low $\delta^{18}O$ alteration preserved in D2 and D3 suggest high temperature meteoric

fluid infiltration either syn-Cretaceous as a response to thermal perturbations or a post-D3 low $^{18}O$ fluid event.

# CHAPTER 2: ROCK UNIT DESCRIPTIONS

## 2.1 Intrusive rocks

Intrusive igneous rocks identified within the map area at Mineral Hill include the Crowston Lake Pluton and associated gabbroic dikes and sills, monzonite, tonalitic dikes and sills , and basaltic dikes. They were classified by mineral content and rock texture. Mineral assemblages were identified in polished thin section using a petrographic microscope and, in some samples where petrographic examination was difficult, scanning electron microscope (SEM). Mineral assemblages for intrusive rocks are presented in Table 2.1.

### 2.1.1 Crowston Lake Pluton

The mafic Crowston Lake Pluton outcrops along the eastern portion of the map area (Fig. 1.8). It is typically dioritic-to-gabbroic in composition and locally pegmatitic. The pluton is a black and white spotted, fine-to-medium grained (0.5-2 millimeters) and equigranular. Pegmatitic phases are coarser-grained (> 1 millimeter), often more felsic, and contain biotite. Near the contact with meta-sedimentary wall rocks, the pluton is foliated and contains late-stage quartz veins parallel to foliation.

The dominant mineralogy is plagioclase, orthopyroxene, and hornblende. Isolated cores of clinopyroxene within hornblende are observed in sample LB1c. Apatite is present as an accessory mineral. Rims of orthopyroxene and hornblende are altered to hornblende and chlorite, respectively, indicating at least two pulses of retrograde alteration. Subsolidus hornblende growth is evident in foliated samples as randomly oriented hornblende grains overgrowing pre-existing hornblende with a preferred orientation. Sample MB1a was collected near the pluton-wall rock contact and displays a weak alignment of plagioclase in thin section. Samples MB1b and LB1d were collected further from the pluton-wall rock contact; neither displays a grain-shape preferred orientation although deformation microstructures (e.g. deformation twins in

Table 2.1. Mineral assemblages of intrusive rocks at Mine

| | | Samples from Mineral Hill, Sechelt, British Columbia | | | | | | | | | | | | | | Analytical methods | | |
|---|---|---|---|---|---|---|---|---|---|---|---|---|---|---|---|---|---|---|
| | | Mineralogy | | | | | | | | | | | | | | | | |
| Sample | Description | Hand Specimen | Thin Section | Alteration | Clinopyroxene | Orthopyroxene | Garnet | Plag/K-spar | Quartz | Wollastonite | Calcite | Hornblende | Epidote | Opaques | Other phases | Majors | Traces (Cr2O3, Sc, V, Zn) | Stable Isotopes | SEM |
| **LB1c** | foliated diorite sample close to wall rocks | I[1] | pts[3] | | cores | cores | | X[4] | | | | X-R[5] | | R | apa,chl(R) | | | | |
| **LB1d** | foliated diorite farther from wall rocks | I | pts | X | | X | | X | | | | X-R | | R | chl(R) | [8]+ | + | + | |
| **MB1a** | diorite near contact | I | pts | X | | X | | X | | | | X-R | V | R | chl(R,V) | + | + | + | |
| **MB1b** | diorite farther from contact | I | pts | X | | X | | Ca-X | | | | X-R | | Fe, Ti, Al , Cr, Mn | chl(R),bt | + | + | + | + |
| **MBd1a** | equigranular gabbro with qtz/plag veins | I | pts | X | ? | X? | | X | V[6] | | | X-R | V | R | chl(R) | + | + | + | |
| **MBd1b** | porphrytic gabbro | I | pts | X | | X | | X | | | | X | R | R | zeo, chl(R) | + | + | + | |
| **UBd1c** | foliated equigranular (0.5-1mm) gabbro | I | pts | | X | | | XX | | | | | | R | | | | | |
| **UBd1d** | vfg, black,foliated equigranular diorite | I | pts | | | | | X | | | | X | | R | chl | | | | |
| **TBd1e** | equigranular (2-3mm) gabbro | I | pts | | X | | | XX | | | | | R | R | chl | | | | |
| **TBd1f** | porphrytic diorite-gabbro | I | pts | X | X | | | X | | | | X | | pyr(R) | zeo(V) | + | + | + | + |
| **MBFRd2** | altered porphrytic tonalite | I | pts | X | | | | Ca-XX | X | | | X-R | V | Fe,Ti | chl(R, V), apa, ttn | + | + | + | + |
| **MBd2b** | altered porphrytic tonalite | I | | | | | | | | | | | | | | | | | |
| **UBd2c** | altered porphrytic tonalite | I | pts | | X | X | | X | | | | X | | R | chl,veins | | | | |
| **UBFRd2** | altered porphrytic tonalite with epidote veins | FR[2] | pts | X | | | | X | V | | | X | V | R | chl(V) | + | + | + | |
| **MBd2a** | porphyrtic tonalite (unaltered) | FR | pts | X | | | | XX | | | | X | | R | chl(R) | + | + | + | |
| **UBd3a** | basalt dike | I | pts | X | X | | | Ca-XX | | | | R | R | Pb, Zn, Fe | zeo(R)?, chl(R), ttn | + | + | + | + |
| **UBFRd3a** | basalt dike with light green alteration rims | FR | pts | X | X | | VUG[7] | X | | skarn | | X-R? | | | zeo(VUG), chl(R) | + | + | + | |
| **UBFRd3b** | basalt dike with light green alteration rims | FR | | | | | | | | | | | | | | | | | |
| **UBFRd3c** | basalt dike with light green alteration rims | FR | | | | | | | | | | | | | | | | | |
| **Monz-1** | non-foliated monzonite | I | pts | | | | | X | X | | | | ? | R | bt, chl | | | | |
| **Monz-2** | non-foliated monzonite | I | pts | | | | | X | X | | | X | ? | R | bt | | | | |

[1] I-intact sample
[2] FR-fall rock sample
[3] pts-polished thin section
[4] X-mineral present
[5] R-replacement
[6] V-mineral in vein
[7] VUG-mineral in vug
[8] +-analysis done

plagioclase) were observed for all samples. Late mineralization includes Fe, Ti, Al, Cr, and Mn-bearing opaques (identified by SEM) and epidote veins.

### 2.1.2 Monzonite

Black and white spotted, medium-grained (1-2 millimeters) equigranular monzonite outcrops west of Marble Hill (Fig. 2.1). The dominant mineralogy is plagioclase/ K-feldspar, quartz, hornblende, and biotite. Retrograde minerals include biotite and chlorite, replacing hornblende and biotite, respectively. Late mineralization includes epidote and opaques. No foliation or alignment of minerals is evident macro- or microscopically. However, in thin section, plagioclase displays deformation twins and plagioclase and quartz display undulose extinction. Monzonite is interpreted as a pegmatitic phase of the Crowston Lake Pluton, since it is more felsic and contains a hydrous phase. The outcrop has been oxidized to a rusty color.

### 2.1.3 D1: Gabbroic dikes and sills- first generation

The oldest dikes and sills (D1) in the map area are generally gabbroic in composition. They were interpreted by *Ray and Kilby* [1996] as spatially and temporally related to the Crowston Lake Pluton. There are two phases of the first dike generation distinguished primarily by texture, but related geochemically and mineralogically.

The first phase is black and white, fine-to-medium (0.5-3 millimeters) equigranular, and is clearly foliated with proximity to the wall rocks. Sills of this phase are boudinaged (Plate 2.1). Mineralogy includes pyroxenes (possibly one phase; pigeonite), plagioclase, and +/- hornblende and K-feldspar. Plagioclase and K-feldspar show undulose extinction and plagioclase shows deformation twinning. Replacement reactions include chlorite replacing pyroxene, and hornblende overgrowing pre-existing hornblende. Late mineralization includes epidote, pyrite, and other opaques. Sample MBd1a has quartz and epidote veins.

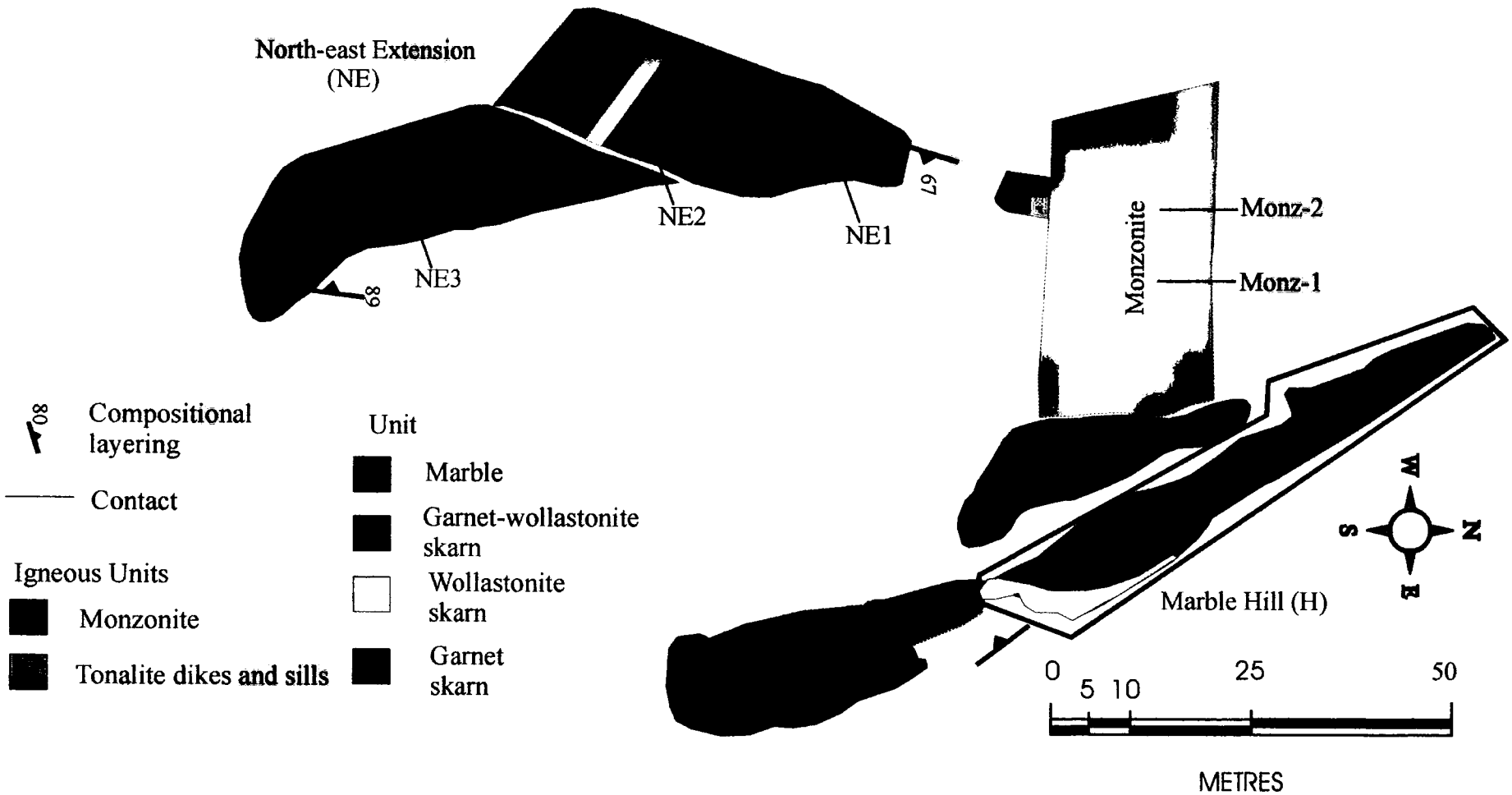


Fig. 2.1. Detail map of North-east Extension (NE) and Marble Hill (H) (see Fig. 1.2) and sample localities for NE. See Fig. 1.7 and Fig. 1.9 for sample localities at H (inset).Structure compiled from *Goldsmith and Kallock* [1988].

Plate 2.1. Rigidly boudinaged gabbroic sill within compositionally layered garnet skarn.

Plate 2.2. D2 tonalitic sill fractures infilled with epidote. Dike and sills are altered to a pale green color resulting from the increase in plagioclase content adjacent to epidote veins.

The second phase (samples MBd1b and TBd1f) is porphyritic with a blue-green fine-grained matrix. The phenocrysts in this phase is coarse-grained euhedral hornblende and pyroxene (2-10 millimeters), and fine-to-medium grained plagioclase (0.5-2 millimeters ). The groundmass consists of very-fine grained (< 1 millimeter) randomly oriented plagioclase. Retrograde alteration minerals include chlorite, zeolite, epidote and pyrite. Zeolite occurs in vein in sample TBd1f. This second phase appears to be an intermediate between first phase gabbroic/dioritic dikes and sills and tonalitic dikes and sills on the basis of geochemistry (see *Whole-rock chemistry*), grain size and, on the basis of texture, cooling history.

### 2.1.4 D2: Tonalitic dikes and sills- second generation

The second generation dikes and sills are tonalitic in composition and contain white feldspar phenocrysts set in an aphanitic groundmass. The groundmass is typically altered and green in handle sample but rarely is unaltered and black. D2 dikes and sills are located primarily in the center of the map area (Fig. 1.2 and 1.8). Altered and unaltered dikes were sampled.

Sample MBFRd2 is black and porphyritic with 1millimeter plagioclase and >1centimeter hornblende phenocrysts in an aphanitic plagioclase and hornblende matrix. Accessory minerals include apatite and titanite. Late mineralization includes Fe and Ti-bearing opaques, epidote veins and K-feldspar veins.

Altered second generation dikes and sills (Samples MBd2a, MBd2b, Ubd2c, and UBFRd2) are porphyritic with plagioclase, and +/- hornblende and pyroxene phenocrysts in an green aphanitic plagioclase, hornblende, and +/- K-feldspar matrix which has been altered to randomly oriented chlorite. Phenocrysts range from 0.5-2 millimeters with the exception of sample UBFRd2 which has 5-8 millimeter hornblende phenocrysts. Plagioclase phenocrysts in these samples typically show deformation twins. Sills are boudinaged and are fractured perpendicular to stretching infilled with epidote. Adjacent to epidote veins, the sills have been

altered to a pale green color resulting from the increase in plagioclase content in the matrix material (Plate 2.2). Quartz and chlorite veins also occur. Late mineralization includes opaques and epidote. Garnet-epidote reaction skarn occurs along the margins of these tonalitic dikes and sills where in contact with marble. Reaction skarn has not been observed to exceed two centimeters in width.

### 2.1.5 D3: Basaltic dikes-third generation

The final generation of dikes does not display ductile deformation textures or structures although, in places, brittle deformation is observed. Moreover, no sills are observed for this intrusive generation. It appears clear that the third generation dikes are not chemically, temporally, or genetically related to the two earlier dike episodes. These dikes intruded after the tonalitic dikes and sills indicated from cross-cutting relationships (Plate 2.3).

The third generation dikes are dark green and very fine-grained (< 1 millimeter) to aphanitic with light green alteration rims. Mineralogy includes primarily plagioclase (>80 percent), clinopyroxene, and +/- hornblende and K-feldspar. Titanite occurs as an accessory mineral. Retrograde chlorite, hornblende, and zeolite is present. Late Pb, Zn, and Fe-bearing opaque minerals are observed (SEM) in sample UBd3a. There is no grain shape preferred orientation within the matrix.

Compositionally and texturally these dikes are basaltic and are not related to the first or second dike generation [*Ray and Kilby*, 1996; *Chapter 3*, this study].

Reaction skarn occurs along the margins of D3 basalt dikes as proximal garnet and distal wollastonite, where adjacent to marble (Plate 2.4). Reaction skarn has not been observed to exceed four centimeters in width.

Plate 2.3. Ductile boudinaged tonalitic sill (light green with yellow rims) cross cut by later basaltic dike (dark green) in grey and bleached marble of upper marble quarry.


Plate 2.4. Reaction skarn on the margin of a D3 basaltic dike occurs as proximal garnet (brown) and distal wollastonite (white) where adjacent to marble (grey).

## 2.2 Meta-sedimentary and Skarn Units

Nine meta-sedimentary and/or skarn units were distinguished in the map area. Meta-sedimentary and skarn units at Mineral Hill were subdivided based on their appearance in the field (e.g. color and texture) and peak mineral assemblage (i.e. equilibrium phases). Peak mineral assemblages were identified in polished thin section using a petrographic microscope and, in some samples where petrographic examination was difficult, scanning electron microscope (SEM). Mineral assemblages are presented in Table 2.2. Peak mineral assemblages are presented in Table 2.3. Some thin sections were cut across skarn boundaries, and therefore represent more than one rock unit as determined by changes in peak mineral assemblages or changes in dominant mineral.

### 2.2.1 Marble

Two marble units were identified at Mineral Hill: green marble, and grey and bleached marble. There are no significant geochemical differences between the marbles. Mineralogically, marbles are similar however, grey marble contains graphite.

#### *Green Marble*

On outcrop scale, green marble is bluish-green, medium-to-coarse grained (1-6 millimeters), and often massive. Green marble is distinguished by green color and limited occurrence within the map area. In places, green marble occurs as lenses within garnet zone skarn units. In these cases, it is unclear if green marble is derived from vein or marble that has been boudinaged and pinched-out during transposed bedding (Plate 2.5). Peak mineralogy is

Table 2.2. Mineral assemblages of meta-sedimentary and skarn samples from Mineral Hill

| | | | | | Samples from Mineral Hill, Sechelt, British Columbia Mineralogy | | | | | | | | | | | | Analytical methods | | | |
|---|---|---|---|---|---|---|---|---|---|---|---|---|---|---|---|---|---|---|---|---|
| Sample | Description | Hand Specimen | Thin Section | Alteration | Clinopyroxene | Orthopyroxene | Garnet | Plag/K-spar | Quartz | Wollastonite | Calcite | Hornblende | Epidote | Rhodonite | Opaques | Other phases | Majors | Traces | Stable Isotopes | SEM |
| MB2a | garnet-wollastonite skarn | I[1] | pts[3] | | | | | | | | | | | | R | | | | | |
| MB2b | garnet-wollastonite skarn | I | pts | | | | X[4] | ? | | X | | | | tr[9] -R[5] | R | ser-R | | | | |
| UB2c | garnet-wollastonite skarn | I | pts | X-mn[8] | | | X | ? | ? | X | | | R | | R | | [7]+ | + | + | |
| UB2d | garnet-wollastonite skarn | I | pts | | | | X | | | X | | | R | | R | | | | | |
| MB3a | garnet-wollastonite skarn | I | pts | | | | X | ? | | X | | | R | | | | | | | |
| MB5a | garnet-wollastonite skarn (> 3mm) | I | | | | | | | | | | | | | | | | | | |
| MB5b | garnet-wollastonite skarn (1-2mm) | I | pts | X-no | | | X | | | X | X | | | | | | + | + | + | |
| MB5c | garnet-wollastonite skarn | I | pts | | | | X | ? | | X | X | | | | R | | | | | |
| UB5d | garnet- wollastonite skarn | I | pts | | | | X | | | X | | | | | R | | | | | |
| UB5f | interlayered with f-g mafic intrusive garnet-wollastonite skarn? | I | pts | | X | | | | | X | | | | | R | | | | | |
| TB9a | garnet-wollastonite skarn | I | pts | | X | | X | | X | X | | | | | mn | | + | + | + | |
| MB9b | garnet-wollastonite skarn | FR[2] | pts | | X | | X | | ? | X | V[6] | | | | R | | | | | |
| WG3a | garnet wollastonite skarn | I | pts | X-mn | | | X | | | X | X , V | | | | | apo | + | + | + | |
| WG3b | garnet wollastonite skarn | I | pts | X-mn | | | X | | | X | | | | | R | | + | + | + | |
| WG5b-1 | garnet wollastonite skarn | I | pts | X-no | mn | | X | | | X | X | | | | | | + | + | + | |
| WG5b-2 | garnet wollastonite skarn | I | pts | X-no | | | X | | | X | X | | | | | | + | + | + | |
| WG5d | garnet wollastonite skarn | I | pts | X-no | | | X | | | X | mn (V) | | | | | | + | + | + | |
| MB4b | garnet-wollastonite skarn | I | pts | | tr | | Ti-gr | ? | | X | 3 | | | | R | apa | + | + | + | + |
| UB5e | garnet skarn & clinopyroxene skarn | I | pts | X-mn | X | | X | X | X | X | V | | | | R | | | | | |
| WG5e | garnet skarn | I | pts | | X | | gr | | | X | V | | | | R | apo(V) | + | + | + | + |
| TB13a | brown massive garnetite with woll & qtz veins | I | pts | X-no | X | | X-80 | | V | X | V | | | | | | + | + | + | |
| TB13b | brown massive garnetite with woll stringers | I | pts | | X | | X-80 | | ? | X, V | V | | | | | | | | | |
| MB3b | clinopyroxene skarn | I | pts | X-mn | X | | X | | X | X | X | | R | | R | | + | + | + | |
| FRW1a | wollastonite skarn | FR | pts | X-mn | X | | | X | | X | X | | | | R | | + | + | + | |
| FRW1b | wollastonite skarn | FR | pts | X-mn | X | | X | | X | X | X | | | | R | | + | + | + | |
| FRW1c | wollastonite skarn | FR | pts | X-mn | X | | ? | X | | X | X | | | | R | | + | + | + | |
| FRW1d(w) | wollastonite skarn | FR | pts | X-no | | | | X | | X | V | | | | tr(R) | | + | + | + | |
| TB14e | wollastonite skarn | I | pts | | X | | | | | X | | | | | | | | | | |
| 00H4 | wollastonite skarn | I | pts | X-no | | | | | | X | V | | | | R | | + | + | + | |
| 00H4b | wollastonite skarn | I | pts | X-no | | | | | | X | X | | | | R | | + | + | + | |
| 00H10 | wollastonite skarn | I | pts | X-mn | | | X | | | X | X(V) | | | | R | | + | + | + | |
| 00H1 | wollastonite skarn | I | pts | X-mn | | | | | | X | V | | | | R | apo(V) | + | + | + | |
| 00H2 | wollastonite skarn | I | pts | X-mn | X-mn | | X | | | X | V | | | | R | apo(V) | + | + | + | |
| 00H5 | wollastonite skarn | I | pts | X-mn | | | X-mn | | | X | | | | | R | | + | + | + | |
| 00H7 | wollastonite skarn | I | pts | X-mn | | | X | | | X | V | | R | | | apo(V) | + | + | + | |
| 00H8 | wollastonite skarn | I | pts | X-no | | | X | | | X | V | | | | | apo(V) | + | + | + | |
| 00H11 | wollastonite skarn | I | pts | X-no | X | | | | | X | | | | | | | + | + | + | |
| 00H3 | wollastonite skarn | I | pts | X-no | | | X-mn | | | X | V | | | | | | + | + | + | |
| 00H6 | wollastonite skarn | I | pts | X-mn | | | | | | X | | | | | R | | + | + | + | |
| 00H13 | wollastonite skarn | I | pts | X-no | | | | | | X | | | | | | | + | + | + | |

Samples from Mineral Hill, Sechelt, British Columbia

| | | | | | Mineralogy | | | | | | | | | | | | Analytical methods | | | |
|---|---|---|---|---|---|---|---|---|---|---|---|---|---|---|---|---|---|---|---|---|
| Sample | Description | Hand Specimen | Thin Section | Alteration | Clinopyroxene | Orthopyroxene | Garnet | Plag/K-spar | Quartz | Wollastonite | Calcite | Hornblende | Epidote | Rhodonite | Opaques | Other phases | Majors | Traces | Stable Isotopes | SEM |
| a1(L) | wollastonite skarn | I | pts | X-no | | | | | | X | V | | | | | | + | + | + | |
| a3(L) | wollastonite skarn | I | pts | X-no | | | | | | X | X | | | | | | + | + | + | |
| a4(U) | wollastonite skarn | I | pts | X-no | X | | X-mn | | | X | V | | | | | | + | + | + | |
| a5(U) | wollastonite skarn | I | pts | X-mn | X | | X | | | X | V | | | | R | | + | + | + | |
| URa2 | wollastonite skarn | I | pts | X-no | | | | | | X | V | | | | | | + | + | + | |
| e(L)-1 | wollastonite skarn | I | pts | X-mn | | | | | | X | V | | | | R | | + | + | + | |
| e(R)-1 | wollastonite skarn | I | pts | X-no | mn | | X | | | X | V | | | | | | + | + | + | |
| e(R)-3 | wollastonite skarn | I | pts | X-no | | | | | | X | V | | | | | | + | + | + | |
| f1 | wollastonite skarn | I | pts | X-no | | | | | | X | V | | | | | | + | + | + | |
| g1 | wollastonite skarn | I | pts | X-mod[10] | X | | X | | | X | V | | | | | | + | + | + | |
| g2 | wollastonite skarn | I | pts | X-mod | mn | | | | | X | V | | | | | | + | + | + | |
| GM1h | wollastonite skarn | I | pts | X-no | | | | | | X | V | | | | | | + | + | + | |
| UB4e(w) | wollastonite skarn | I | pts | X-no | | | | | X | X | X | | | | | | + | + | + | |
| TB15a | "grunge rock" | I | pts | | X | | X | | | X | | | R | | R | | | | | |
| | adjacent to brittle fault | | | | | | | | | | | | | | | | | | | |
| MB16a | grunge rock' | I | pts | | | | | | | | | | | | | | | | | |
| UB14a | calc-silicate skarnoid | I | pts | | X | | | X | | | | | R | | R | | | | | |
| TB14b | calc-silicate skarnoid | I | pts | | X | | X | | X | X | | | | | R | | | | | |
| UB14c | calc-silicate skarnoid | I | pts | X | X | | | X | | | | | R | | R | chl-mn(R) | + | + | + | |
| UB14d | calc-silicate skarnoid | I | pts | | | | | X | | | | X | | | R | | | | | |
| MB8a | gt, cpx floating | I | | | | | | | | | | | | | | | | | | |
| | in crs.qtz (breccia?) | | | | | | | | | | | | | | | | | | | |
| CZ-1 | calc-silicate skarnoid | I | pts | | | | X | X | X | X | | | R | | R | bt | + | + | | |
| CZ-2 | calc-silicate skarnoid | I | pts | | | | X | X | X | X | | | | | | | + | + | | |
| CZ-3 | calc-silicate skarnoid | I | pts | X | | | | X | | | | X | R | | R | chl(R) | + | + | | |
| MB7a | massive quartz (1-2mm) | I | pts | X | | | | | X | | | | X, R | | R | | + | + | + | |
| | and epidote unit | | | | | | | | | | | | | | | | | | | |
| MB7b | qtz(?) and epidote (1-2mm) | I | | | | | | | | | | | | | | | | | | |
| MB7c | quartz and epidote unit | I | pts | | | | | | X | | | | X | | R | | | | | |
| MB11a | quarzite(vein?) | I | pts | | X | | Ti-grt? | XX | X | | | | ? | | R | | | | | |
| MB11b | plag, qtz, & epidote | I | | | | | | | | | | | | | | | | | | |
| | (1-2mm) unit | | | | | | | | | | | | | | | | | | | |
| 00H7 | quartz vein | I | pts | X-no | | | | | X | | V | | | | | | + | + | + | |
| FRW1d(m) | bleached marble | FR | pts | | X | | | X | | X | X | | | | | | + | + | + | |
| UBM1a | grey and bleached marble | I | pts | | X | | ?2 | | X | X | X | | | | R | | + | + | + | |
| MBM1b | grey and bleached marble | I | pts | | | | X | | | X | X | | | | R | | | | | |
| UBFRM2a | grey and bleached marble | FR | pts | | X | | | Ca-pl | ? | ? | X | | | | R | apa | | | | + |
| UBFRM2b | grey and bleached marble | FR | pts | | X | | gr | | X | X | X | | | | R | ttn | | | | + |
| UBFRM2c | grey and bleached marble | FR | pts | | ? | | X | | V | V | X | | | | R | | + | + | + | |
| UBFRM2d | grey and bleached marble | FR | pts | | | | X | | X | X | X | | | | R | | | | | |
| UBFRM2e | grey and bleached marble | FR | pts | | X | | X | X | | X | X | | | | R | | | | | |
| UBFRM2f | grey and bleached marble | FR | pts | | X | | | | | X | X | | | | R | | | | | |
| UBFRM2g | grey and bleached marble | FR | pts | | X | | | | X | X | X | | | | R | | | | | + |
| UBFRM2h | grey and bleached marble | FR | pts | | X | | X | X | | X | X | | | | | | | | | |
| 00UMQ-1 | grey and bleached marble | I | pts | | X | | mn | | | X | X | | | | | | + | + | + | |

Samples from Mineral Hill, Sechelt, British Columbia

| | | | | | Mineralogy | | | | | | | | | | | | Analytical methods | | | |
|---|---|---|---|---|---|---|---|---|---|---|---|---|---|---|---|---|---|---|---|---|
| Sample | Description | Hand Specimen | Thin Section | Alteration | Clinopyroxene | Orthopyroxene | Garnet | Plag/K-spar | Quartz | Wollastonite | Calcite | Hornblende | Epidote | Rhodonite | Opaques | Other phases | Majors | Traces | Stable Isotopes | SEM |
| 00UMQ-2 | grey and bleached marble | I | pts | | X | | X | X | | X | X | | | | | | + | + | + | |
| 00UMQ-3 | grey and bleached marble | I | pts | | X | | X | | | X | X | | | | | | + | + | + | |
| 00NE-1 | grey and bleached marble | I | pts | | | | X | | | X | X | | | | | | + | + | + | |
| 00NE-2a | grey and bleached marble | I | pts | | | | | | | X | X | | | | | | + | + | + | |
| 00NE-2b | grey and bleached marble | I | pts | | X | | | | X | X | X | | | | | | + | + | + | + |
| 00NE-3a | grey and bleached marble | I | pts | | X | | | | | X | X | | | | | | + | + | + | |
| 00NE-3b2 | grey and bleached marble | I | pts | | X | | Ti-gnt | | | X | X | | | | | | + | + | + | + |
| 00H3 | grey and bleached marble | I | pts | | X | | X | | | X | X | | | | | | + | + | + | |
| 00H4 | grey and bleached marble | I | pts | | X | | | | | X | X | | | | | gph | + | + | + | |
| 00H4b | grey and bleached marble | I | pts | | X | | X | | | X | X | | | | | gph | + | + | + | |
| 00H6 | grey and bleached marble | I | pts | | X | | | | | X | X | | | | | | + | + | + | |
| 00H9 | grey and bleached marble | I | pts | | | | | | | X | X | | | | | | + | + | + | |
| 00H10 | grey and bleached marble | I | pts | | X | | X | | | X | X | | | | | gph | + | + | + | |
| 00H12 | grey and bleached marble | I | pts | | | | | | | | X | | | | | | + | + | + | |
| 00H13 | grey and bleached marble | I | pts | | | | | | | X | X | | | | | | + | + | + | |
| 00H14 | grey and bleached marble | I | pts | | X | | | | | X | X | | | | | | + | + | + | |
| 00H15 | grey and bleached marble | I | pts | | X | | | | | X | X | | | | | | + | + | + | |
| 00H16 | grey and bleached marble | I | pts | | X | | | | | X | X | | | | | | + | + | + | |
| a1(L) | grey and bleached marble | I | pts | | | | | | | X | X | | | | | | + | + | + | |
| a2(L) | grey and bleached marble | I | pts | | | | X | | | X(pods[11]) | X | | | | | | + | + | + | |
| a3(L) | grey and bleached marble | I | pts | | | | X | | | X | X | | | | | | + | + | + | |
| a4(U) | grey and bleached marble | I | pts | | | | X | | | X(pods) | X | | | | | | + | + | + | |
| URa1 | grey and bleached marble | I | pts | | | | X | | | X | X | | | | | | + | + | + | |
| URa2 | grey and bleached marble | I | pts | | | | | | | X | X | | | | | | + | + | + | |
| e(L)-1 | grey and bleached marble | I | pts | | | | | | | X | X | | | | | | + | + | + | |
| e(R)-2 | grey and bleached marble | I | pts | | X | | X | | | X | X | | | | | | + | + | + | |
| e(R)-3 | grey and bleached marble | I | pts | | | | X | | | X(pods) | X | | | | | | + | + | + | |
| e(R)-4 | grey and bleached marble | I | pts | | | | X | | | X | X | | | | | | + | + | + | |
| f1 | grey and bleached marble | I | pts | | | | X | | | X | X | | | | | | + | + | + | |
| g2 | grey and bleached marble | I | pts | | X | | X | | | X | X | | | | | | + | + | + | |
| GM1h | grey and bleached marble | I | pts | | X | | mn | | | X | X | | | | | | + | + | + | |
| BM-1 | black marble | I | pts | | ent? | | X | | | X | X | | | | R | apa, phl | + | + | + | + |
| MB4a | green marble | I | pts | | X | | X | X | | X | X | | | | R | | | | | |
| MB4c | green marble | I | pts | | X | | Ti-Mg-Fe gr | ksp | | X | X | | R | | pyr | apa, musc | + | + | + | + |
| MB4d | no description | I | | | | | | | | | | | | | | | | | | |
| UB4e(m) | green marble | I | pts | | X | | X | X | | X | X | | | | | | + | + | + | |
| TB4e | garnet skarn and green marble | I | pts | | X | | X | | | | X | | | | R | | + | + | + | |
| TB4f | garnet skarn and green marble | I | pts | X-no | X | | X | | | X | X | | | | | apo(V) | + | + | + | |
| 00UMQ-2 | augen | I | pts | | X | | Ti & gr | XX | X | X | X | | | | pyr | apa | + | + | + | + |
| 00NE-2b | augen | I | pts | | X | | | Ca-ksp | X | X | X | | | | Al, Mn (R) | | + | + | + | + |
| 00NE-3b2 | augen | I | pts | | X | | | Ca-pl | X | X | X | | | | | | + | + | + | + |
| BM-1 | augen | I | pts | | | | Mg,Fe, Ti-gr | | | ? | X | | clz | | R | Ca-Ti | + | + | + | + |

[1] I-intact sample

[2] FR-fall rock sample

[3] pts-polished thin section

[4] X-mineral present

[5] R-replacement

[6] V-mineral in vein

[7] +-analysis done

[8] mn-present in minor amounts

[9] tr-present in trace amounts

[10] mod-present in moderate amounts

[11] pods-mineral present in pods

Table 2.3. Peak mineral assemblage for meta-sedimentary and skarn samples from Mineral Hill

| | | | | | Peak Assemblage Mineralogy | | | | | | | | | | |
|---|---|---|---|---|---|---|---|---|---|---|---|---|---|---|---|
| Sample | Map Location | Hand Specimen | Clinopyroxene | Orthopyroxene | Garnet | Plag/K-spar | Quartz | Wollastonite | Calcite | Hornblende | Epidote | Other phases | lithology | texture | boundary type |
| **1)** | | | | | | | | | | | | | | | |
| **MB2b** | MB [10] | I [7] | | | X | | | X | | | | | g-w skarn | c.l [1] | |
| **UB2c** | UB [11] | I | | | X | | | X | | | | | g-w skarn | | |
| **UB2d** | UB | I | | | X | | | X | | | | | g-w skarn | c.l | |
| **MB3a** | MB | I | | | X | | | X | | | | | g-w skarn | c.l | |
| **UB5d** | UB | I | | | X | | | X | | | | | g-w skarn | c.l | |
| **WG3b** | MB | I | | | X | | | X | | | | | g-w skarn | | |
| **00H5** | H [14] | I | | | X | | | X | | | | | woll skarn | s.f [5] | |
| **00H7** | H | I | | | X | | | X | V | | | | woll skarn | w.f [3] | |
| **00H8** | H | I | | | X | | | X | V | | | | woll skarn | m.f. [4] | |
| **00H3** | H | I | | | X | | | X | V | | | | woll skarn | m-s.f. | **1,3** |
| **2)** | | | | | | | | | | | | | | | |
| **WG5b-2** | UB | I | | | X | | | X | X | | | | g-w skarn | | |
| **MB4b** | MB | I | | | Ti-gr | | | X | 3 | | | apa? | g-w skarn | c.l | |
| **MB5b** | MB | I | | | X | | | X | X | | | | g-w skarn | c.l | |
| **00H10** | H | I | | | X | | | X | X(V) | | | | woll skarn | w-m.f. | **1,2,3** |
| **WG3a** | MB | I | | | X | | | X | X (V) | | | | g-w skarn | c.l. | |
| **WG5d** | UB | I | | | X | | | X | mn [6] (V) | | | | g-w skarn | | |
| **a2(L)** | GM [13] | I | | | X | | | X(pods) | X | | | | marble | s.f. | **1** |
| **UBFRM2d** | UMQ [16] | FR [8] | | | X | | ? [9] | X | X | | | | marble | | |
| **00NE-1** | NE [15] | I | | | X | | | X | X | | | | marble | s.f. | |
| **a3(L)** | GM | I | | | X | | | X | X | | | | marble | s.f. | **1,2** |
| **a4(U)** | GM | I | | | X | | | X(pods) | X | | | | marble | s.f. | **1,2?,3** |
| **URa1** | GM | I | | | X | | | X | X | | | | marble | w-m.f. | **1** |
| **e(R)-3** | GM | I | | | X | | | X(pods) | X | | | | marble | s.f. | **1,3** |
| **e(R)-4** | GM | I | | | X | | | X | X | | | | marble | s.f. | **1** |
| **f1** | GM | I | | | X | | | X | X | | | | marble | s.f. | **1,3** |
| **MBM1b** | MB | I | | | X | | | X | X | | | | marble | | |
| **3)** | | | | | | | | | | | | | | | |
| **TB4f** | TB [12] | I | X | | X | | | X | | | | | gnt skarn | | |
| **MB9b** | MB | FR | X | | X | | | X | | | | | g-w skarn | c.l | |
| **WG5e** | UB | I | X | | gr | | | X | V | | | | gnt skarn | c.l. | |
| **TB13a** | TB | I | X | | X-80 | | | X | | | | | garnetite | | |
| **TB13b** | TB | I | X | | X-80 | | | X | | | | | garnetite | | |
| **00H2** | H | I | X-mn | | X | | | X | V | | | | woll skarn | m-s.f. | |
| **a4(U)** | GM | I | X | | X | | | X | V | | | | woll skarn | n.f. [2] | **1,2?,3** |
| **e(R)-1** | GM | I | mn | | X | | | X | V | | | | woll skarn | n.f. | |
| **a5(U)** | GM | I | X | | X | | | X | V | | | | woll skarn | n.f. | |
| **g1** | GM | I | X | | X | | | X | V | | | | woll skarn | m-s.f. | |
| **4)** | | | | | | | | | | | | | | | |
| **WG5b-1** | UB | I | mn | | X | | | X | X | | | | g-w skarn | | |
| **MB5c** | MB | I | X | | X | | | X | X | | | | g-w skarn | c.l | |
| **UBFRM2c** | UB | FR | X | | X | | | X | X | | | | marble | | |
| **00NE-3b2** | NE | I | X | | X | | | X | X | | | | marble | m.f. | |
| **00H3** | H | I | X | | X | | | X | X | | | | marble | m.f. | **1,3** |
| **00H4b** | H | I | X | | X | | | X | X | | | | marble | s.f | **1,3** |
| **00H10** | H | I | X | | X | | | X | X | | | | marble | s.f. | **1,2,3** |
| **e(R)-2** | GM | I | X | | X | | | X | X | | | | marble | s.f. | **1** |
| **g2** | GM | I | X | | X | | | X | X | | | | marble | m.f. | **1,3** |
| **GM1h** | GM | I | X | | mn | | | X | X | | | | marble | s.f. | **1,3** |
| **00UMQ-1** | UMQ | I | X | | mn | | | X | X | | | | marble | | |
| **00UMQ-3** | UMQ | I | X | | X | | | X | X | | | | marble | | |
| **TB4f** | TB | I | X | | X | | | X | X | | | | gr marble | | |
| **00UMQ-2** | UMQ | I | X | | Ti & gr | | ?(apa) | X | X | | | | augen | | |
| **5)** | | | | | | | | | | | | | | | |
| **FRW1a** | UMQ | FR | X | | | | | X | | | | | woll skarn | n.f | |
| **TB14e** | TB | I | X | | | | | X | | | | | woll skarn | c.l. | **3** |
| **00H11** | H | I | X | | | | | X | | | | | woll skarn | | |
| **g2** | GM | I | mn | | | | | X | V | | | | woll skarn | n.f. | **1,3** |
| **6)** | | | | | | | | | | | | | | | |
| **UBFRM2f** | UMQ | FR | X | | | | | X | X | | | | marble | | |
| **00H14** | H | I | X | | | | | X | X | | | | marble | s.f. | |
| **00H15** | H | I | X | | | | | X | X | | | | marble | s.f. | |
| **00H16** | H | I | X | | | | | X | X | | | | marble | s.f. | |
| **00NE-3a** | NE | I | X | | | | | X | X | | | | marble | m.f. | |
| **FRW1d(m)** | UMQ | FR | X | | | ? | | X | X | | | | marble | | |
| **00H4** | H | I | X | | | | | X | X | | | | marble | m.f. | **1,3** |
| **00H6** | H | I | X | | | | | X | X | | | | marble | m-s.f. | |
| **7)** | | | | | | | | | | | | | | | |
| **00H4** | H | I | | | | | | X | V | | | | woll skarn | m.f. | **1,3** |

**Peak Assemblage Mineralogy**

| Sample | Map Location | Hand Specimen | Clinopyroxene | Orthopyroxene | Garnet | Plag/K-spar | Quartz | Wollastonite | Calcite | Hornblende | Epidote | Other phases | lithology | texture | boundary type |
|---|---|---|---|---|---|---|---|---|---|---|---|---|---|---|---|
| **00H1** | H | I | | | | | | X | V | | | | woll skarn | m-s.f. | |
| **a1(L)** | GM | I | | | | | | X | V | | | | woll skarn | n.f. | **1,3** |
| **URa2** | GM | I | | | | | | X | V | | | | woll skarn | m.f. | **1,3** |
| **e(L)-1** | GM | I | | | | | | X | V | | | | woll skarn | n.f. | **1,2,3** |
| **e(R)-3** | GM | I | | | | | | X | V | | | | woll skarn | n.f. | **1,3** |
| **f1** | GM | I | | | | | | X | V | | | | woll skarn | n.f. | **1,3** |
| **GM1h** | GM | I | | | | | | X | V | | | | woll skarn | m.f. | **1,3** |
| **FRW1d(w)** | UMQ | FR | | | | | | X | V | | | | woll skarn | w.f | |
| **00H6** | H | I | | | | | | X | | | | | woll skarn | w.f. | |
| **00H13** | H | I | | | | | | X | | | | | woll skarn | m.f. | **1,3** |
| **8)** | | | | | | | | | | | | | | | |
| **FRW1b** | UMQ | FR | | | | | | X | X | | | | woll skarn | n.f | **2** |
| **FRW1c** | UMQ | FR | ? | | | | | X | X | | | | woll skarn | m.f | |
| **00H4b** | H | I | | | | | | X | X | | | | woll skarn | w.f | **1,3** |
| **a3(L)** | GM | I | | | | | | X | X | | | | woll skarn | n.f. | **1,2** |
| **00NE-2a** | NE | I | | | | | | X | X | | | | marble | s.f. | |
| **00H9** | H | I | | | | | | X | X | | | | marble | s.f. | |
| **00H13** | H | I | | | | | | X | X | | | | marble | s.f. | **1,3** |
| **a1(L)** | GM | I | | | | | | X | X | | | | marble | s.f. | **1,3** |
| **URa2** | GM | I | | | | | | X | X | | | | marble | s.f. | **1,3** |
| **e(L)-1** | GM | I | | | | | | X | X | | | | marble | s.f. | **1,2,3** |
| **9)** | | | | | | | | | | | | | | | |
| **CZ-1** | MB | I | | | X | X | X | X | | | | | skarnoid | | |
| **CZ-2** | MB | I | | | X | X | X | X | | | | | skarnoid | | |
| **10)** | | | | | | | | | | | | | | | |
| **TB9a** | TB | I | X | | X | | X | X | | | | | g-w skarn | c.l | |
| **UB5e** | UB | I | X | | X | | X | X | | | | | gnt skarn | | |
| **TB14b** | TB | I | X | | X | | X | X | | | | | skarnoid | | |
| **11)** | | | | | | | | | | | | | | | |
| **UBM1a** | UMQ | I | X | | X | | X | X | X | | | | marble | | |
| **UBFRM2b** | UMQ | FR | X | | gr | | X | X | X | | | | marble | | **1,2,3** |
| **MB3b** | MB | I | X | | X | | X | X | X | | | | cpx skarn | | |
| **12)** | | | | | | | | | | | | | | | |
| **MB7a** | MB | I | | | | | X | | | | X | | quartzite | V? | |
| **MB7c** | MB | I | | | | | X | | | | X | | quartzite | V? | |
| **13)** | | | | | | | | | | | | | | | |
| **UBFRM2g** | UMQ | FR | X | | | | X | X | X | | | | marble | | |
| **00NE-2b** | NE | I | X | | | | X | X | X | | | | marble | | |
| **00NE-3b2** | NE | I | X | | | | X | X | X | | | | augen | | |
| **14)** | | | | | | | | | | | | | | | |
| **UB4e(w)** | UB | I | | | | | X | X | | | | | woll skarn | n.f | |
| **00NE-2b** | NE | I | | | | | X | X | | | | opq | augen | | |
| **15)** | | | | | | | | | | | | | | | |
| **MB11a** | MB | I | | | | ? | X | | | | ? | | quartzite | V? | |
| **16)** | | | | | | | | | | | | | | | |
| **00H7** | H | I | | | | | X | | V | | | | qtz vein | | |
| **17)** | | | | | | | | | | | | | | | |
| **UB5e** | UB | I | X | | | X | X | X | | | | | cpx skarn | | |
| **18)** | | | | | | | | | | | | | | | |
| **MB4a** | MB | I | X | | X | X | | X | X | | | | gr marble | | |
| **MB4c** | MB | I | X | | Ti-Mg-Fe gr | ksp | | X | X | | | apa? | gr marble | | |
| **UB4e(m)** | UB | I | X | | X | X | | X | X | | | | gr marble | | |
| **00UMQ-2** | UMQ | I | X | | X | X | | X | X | | | | marble | | |
| **UBFRM2e** | UMQ | FR | X | | X | X | | X | X | | | | marble | | |
| **UBFRM2h** | UMQ | FR | X | | X | X | | X | X | | | | marble | | |
| **19)** | | | | | | | | | | | | | | | |
| **UB14a** | UB | I | X | | | X | | | | | | | skarnoid | | |
| **UB14c** | UB | I | X | | | X | | | | | | | skarnoid | | |
| **20)** | | | | | | | | | | | | | | | |
| **CZ-3** | MB | I | | | | X | | | | X | | | skarnoid | alignment | |
| **UB14d** | UB | I | | | | X | | | | X | | | skarnoid | | |
| **21)** | | | | | | | | | | | | | | | |
| **TB4e** | TB | I | X | | X | | | | X | | | | gnt skarn | | |
| **UBFRM2a** | UMQ | FR | X | | X | | | | X | | | apa | marble | | |
| **22)** | | | | | | | | | | | | | | | |
| **00H12** | H | I | | | | | | | X | | | | marble | | |
| **TB4e** | TB | I | | | | | | | X | | | | gr marble | | |
| **23)** | | | | | | | | | | | | | | | |
| **BM-1** | MB | I | ent? | | X | | | X | X | | apa | phl | bk. marble | | |
| **24)** | | | | | | | | | | | | | | | |
| **BM-1** | MB | I | | | Mg,Fe, Ti-gr | | | X | X | | clz | | augen | | |

[1] c.l.-compositionally layered
[2] n.f.-non-foliated
[3] w.f.-weakly-foliated
[4] m.f.-moderately foliated
[5] s.f.-strongly foliated
[6] mn-minor amounts
[7] I-intact sample
[8] FR-fall rock sample
[9] ?-unsure identification
[10] MB-middle bench
[11] UB-upper bench
[12] TB-top bench
[13] GM-grid map 1 sample
[14] H-Marble Hill
[15] NE-northeast extension
[16] UMQ-upper marble quarry

**boundary type:**

**1** samples with wollastonite grains in marble far from boundary / cc + qtz = woll + $CO_2$

**2** samples with area near boundary containing cc and woll indicating presence of reactants and products resulting from the reaction cc + $SiO_2$(aq) = woll +$CO_2$

**3** samples with sharp boundary between marble and wollastonite skarn

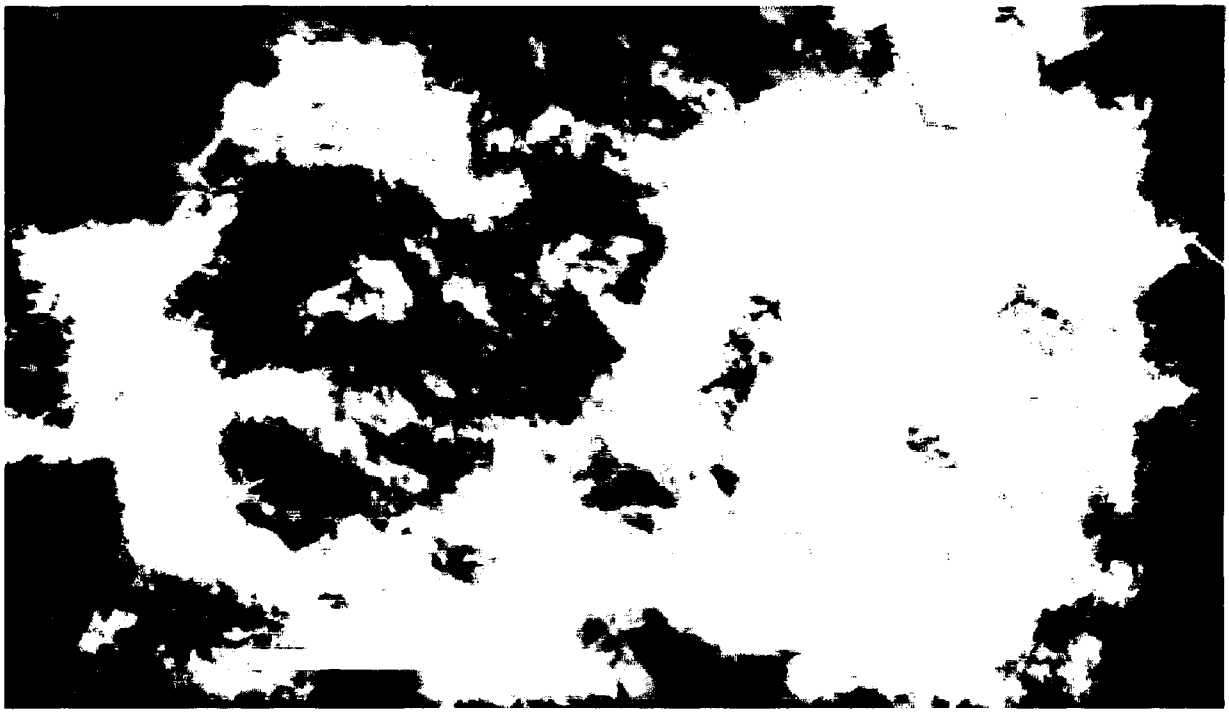

Plate 2.5. Green marble within garnetite. Scale bar = 4.5 cm.

Plate 2.6. Skarnoid cliff exposure

calcite and +/- wollastonite, garnet, calcic-clinopyroxene and plagioclase/K-feldspar with or without trace amounts of apatite. Late opaque minerals are observed.

***Grey and Bleached Marble***

Grey and bleached marble is located in the Upper Marble Quarry (Fig. 1.12) and extends north-eastward to Marble Hill (Figs. 2.1 and 1.7). On outcrop scale, grey and bleached marble is grey and white, medium-to-coarse grained (1-10 millimeters), and thinly-to-medium layered (1-15 centimeters). Layering is defined by compositional differences between grey and bleached marble (i.e. disappearance of graphite in bleached marble). This layering may represent transposed bedding. A magnesium-rich (black) marble outcrops in the east central portion (Fig. 1.8; sample BM-1) of the map area, adjacent to a fault and the pluton-wall-rock contact.

Peak mineralogy is calcite and +/- wollastonite, and calcic-clinopyroxene with or without minor-to-trace amounts of garnet, quartz, plagioclase/K-feldspar, apatite, titanite and graphite. Black marble (BM-1) contains phlogopite in addition. In places the marble unit contains black augens composed of one or more of calcic-clinopyroxene, garnet, K-feldspar, apatite, calcite, quartz and wollastonite, however no augen contains the entire assemblage. Minerals in augen vary in abundance. Augen in black marble (BM-1) contains garnet, calcite, and clinozoisite. Late opaque and epidote mineralization are observed in marble and augen.

All marbles analyzed from Marble Hill and the northern extension of Mineral Hill are moderately-to-strongly foliated. The foliation is defined by grain-shape preferred orientation of calcite. In the Marble Hill samples (H), the foliation appears parallel-to-subparallel to the pluton contact. This observation is consistent with the pendant/pluton contact in the entire study area (see Fig. 1.8). This foliation may have resulted from contact metamorphism associated with pluton emplacement, or movement along Wormy-Lake fault. Generally, marbles in the Upper Marble Quarry of Mineral Hill are not foliated.

All marble samples examined contain wollastonite well away (> 2.5 mm) from the wollastonite-marble boundary in equilibrium with calcite (Table 2.3, (1)). The presence of wollastonite within marble is attributed to the presence of quartz within protolith limestone, formed by the reaction, calcite + $SiO_2$ (qtz) = wollastonite + $CO_2$ (see Fig. 2.2).

Wollastonite skarn commonly contains calcite, however the boundary between marble and wollastonite skarn is marked by a large increase in wollastonite abundance (in skarn). Two boundary types are observed in thin sections that display the wollastonite-marble contact (Fig. 2.3): Samples with a sharp boundary (<0.5 mm) between marble and wollastonite skarn (3) and samples in which calcite and wollastonite coexist over a scale > 0.5 mm (2). This latter occurrence indicates the presence of reactants and products from the reaction, calcite + $SiO_2$ (aq) = wollastonite + $CO_2$. Boundary types are tabulated as (3) and (2), respectively, in Table 2.3. Most samples show a sharp boundary between marble and wollastonite skarn. However, samples FRW1b, H10, a3(L), a4(U)?, e(L)-1, and UBFRM2b, contain areas of reactant and product phases.

### 2.2.2 Quartzite

Epidote-bearing quartzite was identified in the middle bench of the map area interspersed with garnet skarn. In outcrop, quartzite is white and green, fine-to-medium grained (1-2 millimeters) and massive. It is brecciated and intruded by small (< 6 inches wide), irregular, discontinuous, mafic dikes (Fig. 2.4). This unit may represent, highly silicified alterations of dike or skarn material, vein material or silica infiltration into brecciated garnet skarn. Peak mineralogy is quartz and epidote. Retrograde alteration is not observed. Late disseminated mineralization includes opaques.

Metasomatic vs. Thermal production
of Wollastonite

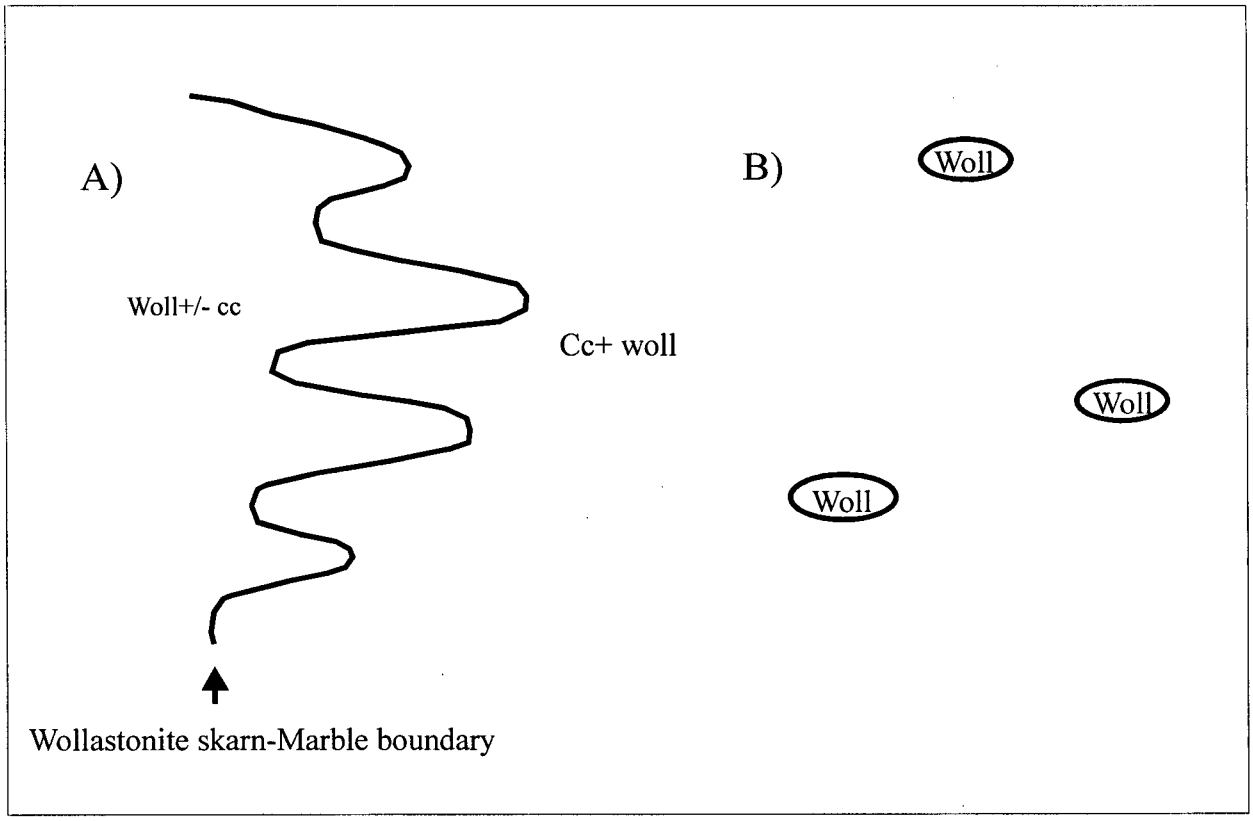


Two reactions:
A) $CaCO_3 + SiO_2$ (aq) = $CaSiO_3 + CO_2$

B) $CaCO_3 + SiO_2$ (qtz) = $CaSiO_3 + CO_2$

Fig. 2.2. Schematic of metasomatic vs. thermal production of wollastonite

Wollastonite Skarn-Marble Boundary

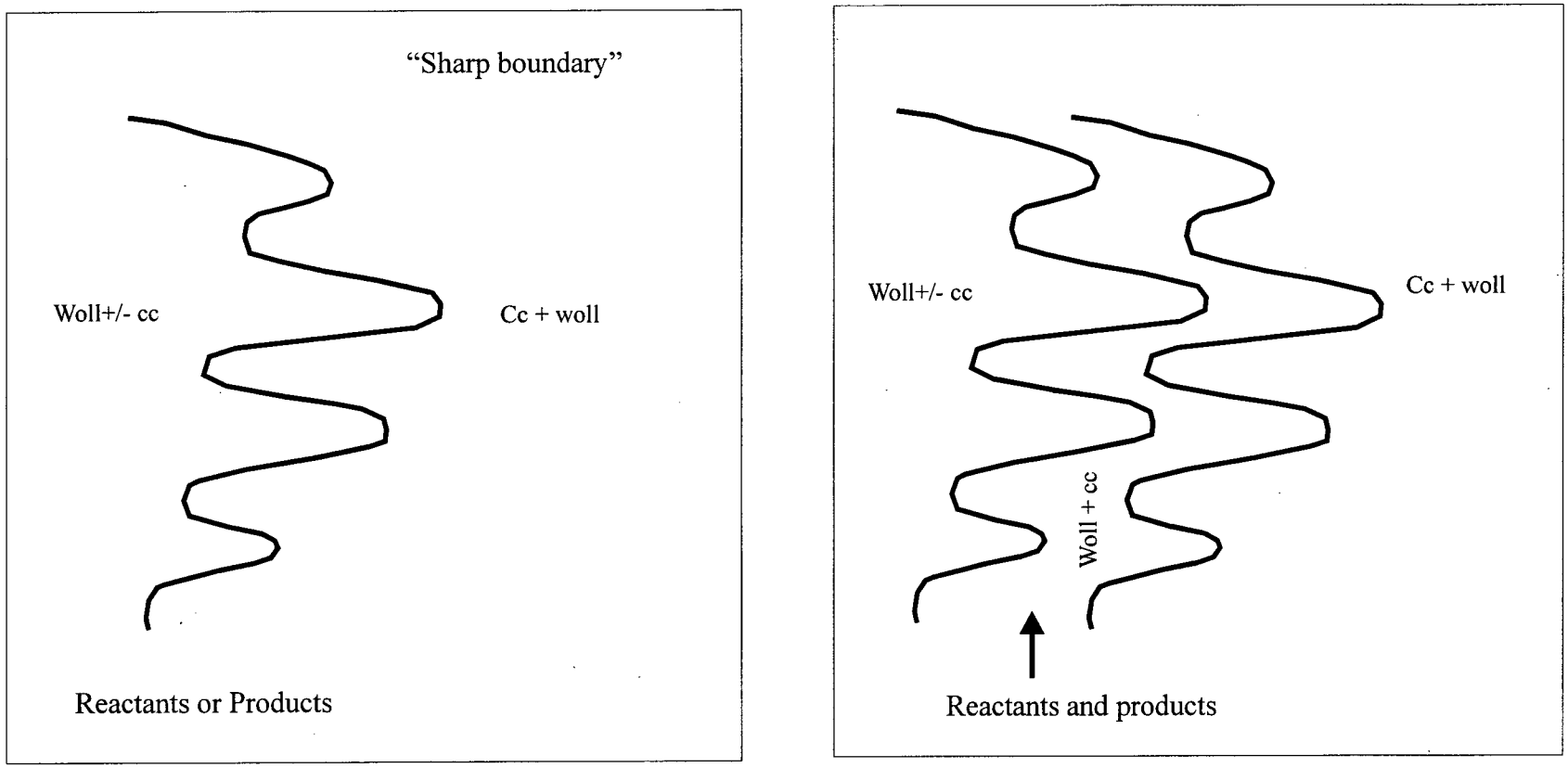


$$CaCO_3 + SiO_2\ (aq) = CaSiO_3 + CO_2$$

Fig. 2.3. Schematic of wollastonite skarn and marble boundary types seen in Mineral Hill samples

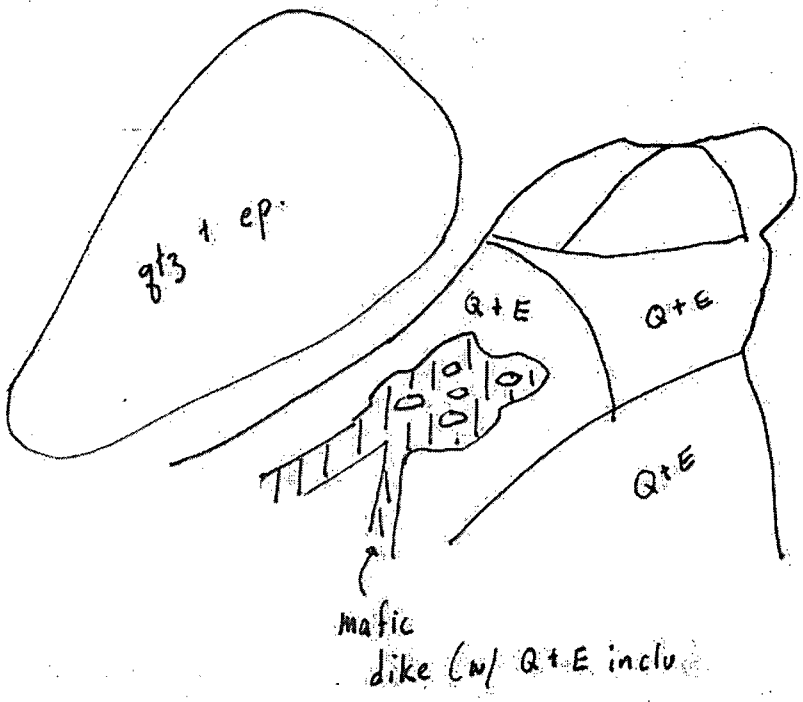


Fig 2.4. Sketch from field notebook of quartzite outcrop, cut by irregular mafic dike with inclusions of quartzite. Q= quartz, E=epidote, hash lines= mafic dike.

### 2.2.3 Skarnoid

Skarnoid is located within and interbedded with the main skarn body at Mineral Hill, and is best developed where extensively intruded by D2 and D3 (Fig. 1.8). On outcrop scale, skarnoid is a white-to-greenish, highly silicified, fine-to-medium grained unit (1-2 millimeters) and is resistant to weathering (often exposed as cliffs) (Plate 2.6). Skarnoid is located within the garnet zone due to field observations of garnet within this unit, and is interpreted to have had a silty-argillitic protolith on the basis of the abundance of feldspar in the peak mineral assemblage.

Skarnoid typically contains clinopyroxene, feldspar (plagioclase and/or alkali-feldspar), quartz, wollastonite, garnet and minor biotite, however no sample contains all of these minerals. Moreover, mineral abundance is highly variable. Retrograde chlorite is observed in some samples with late opaque and epidote mineralization. Altered skarnoid, especially in proximity to dikes, contains hornblende. Skarnoid is distinguished mostly on the basis of high plagioclase content in equilibrium with other calc-silicates (i.e. wollastonite, calcic-clinopyroxene, garnet). Alignment of acicular minerals is observed.

### 2.2.4 Skarn

Five skarn units were identified at Mineral Hill: wollastonite skarn, clinopyroxene skarn, garnet-wollastonite skarn, garnet skarn, and garnetite. Skarn units were subdivided based on mineral content and color. Some skarn units may derive from alteration of other pre-existing skarn assemblages or meta-sedimentary units. Garnet skarn is located proximal to the pluton-skarn contact. Garnet skarn is interlayered with garnetite, garnet-wollastonite skarn, and green marble. Both garnet and garnet-wollastonite skarn are compositionally layered, however only garnet skarn, especially in places where garnet exceeds 80 percent (garnetite), is texturally massive. Wollastonite skarn is distal to the pluton. It is the interface of wollastonite skarn and marble that denotes the periphery of the skarn body. This marble-wollastonite contact is sharp

within the quarry, however in other localities (Marble Hill; see Fig. 1.9) wollastonite skarn clearly interfingers with grey and bleached marble (indicating replacement of calcite by an infiltrating $SiO_2$ front) (Plate 2.7).

***Wollastonite skarn***

Wollastonite skarn appears along the periphery of the skarn body adjacent to marble (Fig. 1.2). Wollastonite skarn is a white, fine-to-coarse grained (0.5-10 millimeters) unit. In places, it appears to be compositionally layered (1-15 centimeters) with calcite and/or quartz, however the calcite and quartz may reflect transposed calcite and quartz veins. Both of these vein types are observed cross-cutting wollastonite skarn. Wollastonite skarn is distinguished from all units by white color due to dominant wollastonite content.

Peak mineralogy is wollastonite, +/- calcite, calcic-clinopyroxene and garnet. Sample UB4e(w) contains quartz . Generally, no retrograde alteration of peak minerals is observed, however there is late opaque minerals and apophyllite veins. Some samples have optically-unidentifiable fine-grained alteration alteration along cleavage planes (e.g. sample GM1g-W) Sample 00H7 contains late epidote mineralization.

Wollastonite skarn ranges from non-foliated to strongly- foliated, due to the mineral alignment of wollastonite, in the samples examined petrographically. However, wollastonite alignment is not always in the same direction as the marble foliation. Marble is often seen wrapping around wollastonite pods (few cm to ten's of cm) or augens (Plate 2.8). Both wollastonite skarn and wollastonite pods contain calcite veins. See *Grey and bleached marble* section (above) and Table 2.3 for boundary description.

Plate 2.7. Grid map locality (Marble Hill) showing interfingering relationship of wollastonite skarn and marble boundary.

Plate 2.8. Classic 'augen' within banded grey and bleached marble.

*Clinopyroxene skarn*

One sample, MB3b, was identified as clinopyroxene skarn on an outcrop scale. It appears as a green and white, medium-grained (~2 millimeters), compositionally layered unit. It is distinguished from other skarn units by minor garnet and green coloration. MB3b differs from calc-silicate skarnoid by greater clinopyroxene and quartz content and less plagioclase. However, they are very similar in grain size and location within the map area. Sample UB5e reveals clinopyroxene skarn assemblages within compositional layering. The clinopyroxene in sample UB5e is coarser-grained than in sample MB3b and skarnoid samples.

Peak mineralogy for clinopyroxene skarn is calcic-clinopyroxene, quartz, plagioclase/K-feldspar, and wollastonite with or without garnet. Late mineralization includes opaques. A microphotograph of sample UB5e shows garnet infilling late-porosity around clinopyroxene grains (Plate 2.9). This suggests the possible existence of a magnesium front producing clinopyroxene prior to the iron front that produced garnet.

*Garnet-wollastonite skarn*

Garnet-wollastonite skarn is white and greenish-brown and medium-to-coarse grained (1-3 millimeters), except sample UB2d which contains coarse-grained (up to 20 millimeters) wollastonite. It is typically compositionally layered on a scale of 1-5 centimeters (Plate 2.10). Compositional layering is defined by garnet dominant and wollastonite dominant alternating layers. Garnet-wollastonite skarn outcrops primarily within the garnet zone of the map area.

Peak mineralogy is wollastonite, garnet, and -/+ calcic-clinopyroxene and calcite. It is distinguished from garnet skarn on the basis of having wollastonite content greater than garnet (Plate 2.11). Calcite occurs as part of the peak assemblage and in veins (e.g. WG3a and WG5d). In some samples (e.g. MB2b, UB2d, MB3a, and MB5b), wollastonite content is less than 50 percent due to the presence of other minerals. In other cases, wollastonite content can reach up to

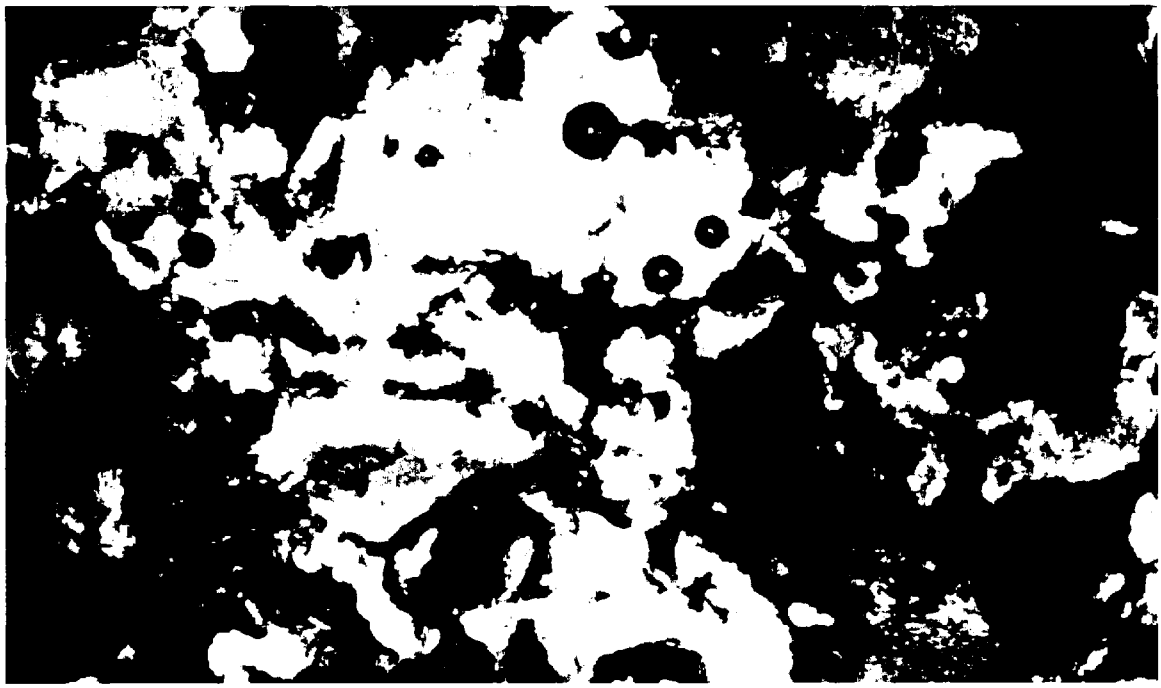

Plate 2.9. Microphotograph of garnet (isotropic) infilling late-porosity around clinopyroxene grains (cross-polarized light). L.d. is 1.25 mm (10x).

Plate 2.10. Compositionally-layered garnet-wollastonite skarn.

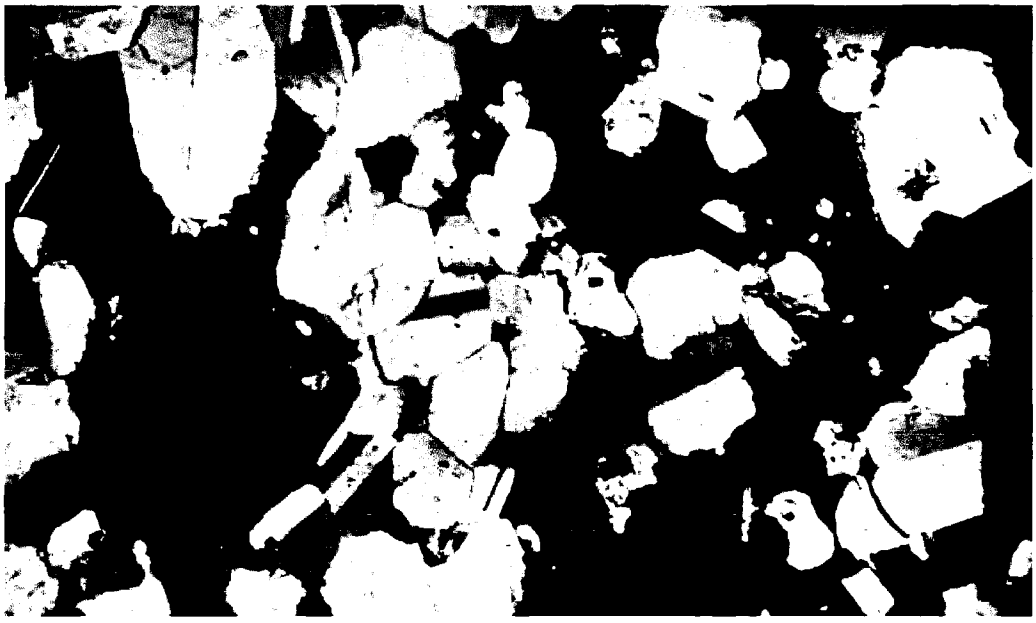

Plate 2.11. Microphotograph of garnet-wollastonite skarn. Garnet is isotopic and wollastonite has first-order birefringence in cross-polarized light. L.d. is 1.25mm (10x).

80 percent by volume (e.g. UB2c, MB5c, and MB4b). Apatite is present as an accessory mineral in MB4b. Some samples within this unit display clear and distinct compositional layering (e.g. UB2d, MB3a, and MB5b), while in others, compositional layering is not so clear on a macro-scale, but observed petrographically (e.g. MB5c, MB2b, UB5d, MB4b, MB9b, and TB9a). UB2c is the only sample of garnet-wollastonite skarn that does not display compositional layering in hand sample nor petrographically. In most garnet-wollastonite skarn samples, retrograde alteration is not observed, although sericite and rhodonite are identified in trace amounts in sample MB2b. Late mineralization in some samples includes pyrite, other opaques, epidote, and apophyllite (i.e. WG3a).

***Garnet skarn***

Garnet skarn is dark red-brown and green in outcrop, medium grained (1-3 millimeters) and often displays brown, green, and grey compositional layering on a 2-10 centimeter scale (Plate 2.12). Garnet skarn is rarely massive and in places is brecciated by coarse crystalline quartz veins. Garnet skarn is exclusively located within the garnet zone of the map area. Garnet skarn is distinguished from garnet-wollastonite skarn on the basis on having a garnet content greater than wollastonite and the presence of calcic-clinopyroxene.

Peak mineralogy is garnet, wollastonite, calcic-clinopyroxene, -/+ quartz (UB5e), and +/- calcite (TB4e). Calcite occurs as vein material in sample WG5e. TB4e was the only sample in which no wollastonite was identified. In some cases where garnet content reaches 75 percent, wollastonite does not exceed 10 percent volumetrically. Garnet skarn is especially evident on outcrop scale by the striking brown hue to the rock. Compositional layering of garnet, wollastonite, and calcic-clinopyroxene is common in this unit (e.g. UB5e, MB9b, and TB4f) and may be controlled in part by protolith composition. Retrograde alteration is not observed in garnet skarn, however late opaque mineralization and apophyllite veins are present.

Plate 2.12. Compositionally-layered garnet skarn.

***Garnetite***

Garnetite is a massive brown unit with wollastonite and quartz veinlets or stringers (Plates 2.13 and 2.14). Lenses of green marble are seen within this unit and may be (i) veins of calcite or (ii) representative protolith for garnetite (Plate 2.5). The latter interpretation implies that garnetite was formed by metasomatic alteration of marble. Garnetite occurs within the garnet zone of the map area and is only observed adjacent to garnet skarn (e.g. samples 13a and 13b; see Fig. 1.12).

Peak mineralogy is garnet, calcic-clinopyroxene, and wollastonite. Garnetite is distinguished from garnet skarn on the basis of garnet content exceeding 80 percent, although calcic-clinopyroxene and wollastonite are seen in equilibrium with garnet petrographically. No late or alteration minerals are observed in garnetite.

Plate 2.13. Ductile deformation of wollastonite veins within garnetite.

Plate 2.14. Brittle deformation of wollastonite veins within garnetite.

BLANK PAGE

# CHAPTER 3: WHOLE- ROCK CHEMISTRY- INFILTRATION AND PROTOLITH CONTROLS ON SKARN ZONATION

## 3.1 Introduction

Whole-rock geochemistry of representative samples of all units sampled at Mineral Hill, coupled with petrographical analyses, allows further and more accurate identification of igneous, meta-sedimentary and skarn rocks. By projecting geochemistry in SACF ternary space (defined in section 3.2) and comparing samples from Mineral Hill with meta-sedimentary rocks from *Ferry* [1988, 1989, and 1994] that formed at or near to isochemical condition and with chemical compositions of common sedimentary rocks compiled by *Brownlow* [1996], we can deduce either a protolith or a metasomatic origin for the units.

Furthermore, based on the distribution of minerals in skarn at Mineral Hill, the aforementioned geochemical observations, and basic principles of one-dimensional reaction-transport theory, we interpret controls on skarn zonation as either being primarily controlled by protolith composition or infiltration and interaction with external material (e.g. magmatic volatiles).

Because interaction with fluid affects the hydrodynamics of the system, we would expect to see a volume change at the reaction front (i.e. marble-wollastonite skarn boundary). Petrographic and petrologic data and observations are used to estimate volume changes caused by reaction at this interface, through graphical trends of immobile elements (element ratios) and calculations using *Grant's* [1986] mass balance approaches.

## 3.2 Method of Investigation

Samples collected at Mineral Hill were cut into ~8-10 $cm^3$ rock slabs with a water saw from the freshest part of each sample. Slabs were cleaned in an ultrasound bath of deionized distilled water and initially crushed to a size fraction less than 1.6 cm (pebble size) with a steel-

faced mechanical jaw crusher. Crushed samples were further ground to a powder in a tungsten carbide ring-mill. Powders were mixed and quartered in order to ensure sample homogeneity. A few grid map (GM) samples were too large to be cut with the water saw without destroying the integrity of the sample for detailed isotopic study described later in this thesis. These samples were initially cut with an oil saw, trimmed down to ~6 $cm^3$ slabs with a water saw, submersed in a Neutrad ultrasound bath, followed by an ultrasound bath in deionized water, ground, re-submersed in an ultrasound bath of deionized water, and crushed and powdered as described above.

Chemical analysis of thirty-one samples for ten major elements plus four trace elements, $Cr_2O_3$, Sc, V, and Zn, by X-ray fluorescence (XRF) were done by Geochemical Laboratories at McGill University. Reported data is presented in Table 3.1. Chemical analysis of forty-two samples for eleven major elements by XRF plus thirty-six trace elements by inductively coupled plasma mass spectrometry (ICP-MS) were done by ALS Chemex in North Vancouver, British Columbia. Reported data is presented in Table 3.2.

Eleven igneous rocks were analyzed including gabbro (N=6), tonalite (N=3), and basalt (N=2). Oxide and element abundances were converted to molar quantities, normalized to 100 percent, and plotted using NEWPET graphical software. All $Fe_2O_3$ was recalculated to FeO for igneous samples to circumvent the effects of 'variable oxidation'. This underestimates the degree of oxidation and favors calculation of amphibole, pyroxene and biotite. These analyses were plotted with and compared to correlating data from *Ray and Kilby* [1996]. Partial data from *Ray and Kilby* [1996] is presented in Table 3.3.

Sixty-two meta-sedimentary and skarn samples were analyzed including marble (N=29), wollastonite skarn (N=22), garnet-wollastonite skarn (N=3), clinopyroxene skarn (N=1), garnetite (N=1), garnet skarn (N=2), calc-silicate skarnoid (N=3), and quartzite (N=1). Oxide and element abundances were converted to molar quantities. The oxides analyzed are $SiO_2$, $TiO_2$,

Table 3.1. Whole-rock chemical analyses from Mineral Hill (McGill University). Major element oxides reported in grams; trace elements in ppm.

| | Sample | d1a | d1b | d1f | d2a | BFRd | UBFRd | FRd3a | UBd3a | LB1d | MB1a | MB1b | UB2c | MB4b | MB5b | TB13a | MB3b | UB14c | TB9a |
|---|---|---|---|---|---|---|---|---|---|---|---|---|---|---|---|---|---|---|---|
| | lithology | gabbro | gabbro | gabbro | tonalite | tonalite | tonalite | basalt | basalt | gabbro | gabbro | gabbro | gt-w skarn[1] | gt-w skarn | gt-w skarn | garnetite | cpx skarn[2] | skarnoid | woll skarn[3] |
| $SiO_2$ | % XRF | 51 | 56.26 | 54.54 | 62.21 | 65.79 | 64.56 | 49.56 | 51.83 | 51.1 | 50.49 | 45.56 | 43.2 | 38.88 | 41.26 | 35 | 71.55 | 55.13 | 55.86 |
| $TiO_2$ | % XRF | 0.928 | 0.624 | 0.631 | 0.366 | 0.259 | 0.255 | 0.669 | 0.626 | 0.911 | 0.879 | 0.36 | 0.614 | 1.088 | 0.481 | 0.39 | 0.235 | 0.653 | 0.173 |
| $Al_2O_3$ | % XRF | 18.81 | 18.25 | 17.6 | 17.84 | 17.8 | 17.9 | 19.28 | 18.96 | 20.06 | 18.84 | 21.37 | 15.39 | 12.37 | 4.06 | 7.91 | 7.15 | 19.91 | 2.18 |
| $Fe_2O_3$ | % XRF | 8.73 | 6.93 | 6.85 | 4.95 | 3.48 | 3.15 | 7.09 | 7.4 | 8.69 | 8.67 | 9.34 | 5.17 | 4.51 | 3.45 | 15.97 | 2.73 | 2.86 | 1.13 |
| MnO | % XRF | 0.142 | 0.124 | 0.13 | 0.083 | 0.097 | 0.104 | 0.131 | 0.138 | 0.135 | 0.133 | 0.142 | 0.131 | 0.108 | 0.136 | 0.918 | 0.169 | 0.109 | 0.146 |
| MgO | % XRF | 5.96 | 3.74 | 3.64 | 1.69 | 1.12 | 1.08 | 6.4 | 5.97 | 5.17 | 5.68 | 8.94 | 3.94 | 1.19 | 0.7 | 0.79 | 1.99 | 2.66 | 0.32 |
| CaO | % XRF | 8.71 | 5.5 | 9.08 | 4.12 | 4.49 | 4.97 | 11.03 | 8.31 | 9.29 | 10.07 | 10.66 | 28.09 | 38.82 | 44.52 | 35.31 | 14.73 | 10.56 | 37.5 |
| $Na_2O$ | % XRF | 3.47 | 4.53 | 3.92 | 4.55 | 5.55 | 4.89 | 3.02 | 3.57 | 3.9 | 3.15 | 2.14 | 0.15 | 0.06 | < d/l | 0.09 | 0.24 | 4.12 | 0.21 |
| $K_2O$ | % XRF | 1.19 | 2.1 | 1.32 | 3.63 | 1.12 | 1.8 | 0.76 | 1.19 | 0.26 | 1.24 | 0.17 | 0.09 | 0.03 | < d/l | 0.03 | 0.06 | 2.39 | 0.28 |
| $P_2O_5$ | % XRF | 0.258 | 0.253 | 0.239 | 0.255 | 0.23 | 0.234 | 0.195 | 0.196 | 0.221 | 0.434 | 0.05 | 0.728 | 0.921 | 2.959 | 3.332 | 0.459 | 0.415 | 1.532 |
| $Cr_2O_3$ | ppm | 158 | 44 | 44 | < d/l | < d/l | 19 | 214 | 178 | 87 | 141 | 360 | 70 | 207 | 253 | 81 | 140 | < d/l | 168 |
| Sc | ppm | 31 | 22 | 23 | < d/l | 14 | < d/l | 22 | 28 | 24 | 22 | 20 | 40 | 31 | 12 | 23 | 19 | < d/l | 11 |
| V | ppm | 199 | 123 | 129 | 44 | 19 | 25 | 145 | 155 | 199 | 240 | 86 | 240 | 165 | 200 | 146 | 105 | 91 | 273 |
| Zn | ppm | 74 | 62 | 50 | 67 | 42 | 46 | 94 | 61 | 67 | 50 | 75 | 372 | 181 | 100 | 66 | 137 | 46 | 140 |
| LOI | % | 1.39 | 2.29 | 2.29 | 0.75 | 0.43 | 0.93 | 2.04 | 2.09 | 1.06 | 1.22 | 1.58 | 2.47 | 2.09 | 2.42 | 0.41 | 0.84 | 1 | 0.69 |
| Total | % | 100.63 | 100.63 | 100.26 | 100.46 | 100.37 | 99.88 | 100.2 | 100.3 | 100.83 | 100.85 | 100.37 | 100.05 | 100.13 | 100.02 | 100.18 | 100.19 | 99.82 | 100.08 |

Table 3.1 (cont).

| | Sample | W1a | W1b | W1c | W1d(w) | UB4e(w) | MB4c | UB4e(mb) | TB4e | TB4f | UBM1a | FRM2c | W1d(mb) | MB7a | |
|---|---|---|---|---|---|---|---|---|---|---|---|---|---|---|---|
| | lithology | woll skarn | woll skarn | woll skarn | woll skarn | woll skarn | gr marble[4] | gr marble | gr marble | gr marble | g-b marble[5] | g-b marble | b marble[6] | quartzite (vein?) | |
| | | | | | | | | | | | | | | | Detection Limits(ppm |
| $SiO_2$ | % XRF | 50.59 | 51.71 | 51.51 | 48.75 | 50.15 | 10.31 | 11.4 | 0.19 | 9.89 | 1.62 | 7.27 | 9.98 | 70.23 | 60 |
| $TiO_2$ | % XRF | 0.048 | 0.029 | 0.034 | 0.077 | 0.114 | 0.587 | 0.031 | 0.005 | 0.026 | 0.043 | 0.349 | 0.016 | 0.431 | 35 |
| $Al_2O_3$ | % XRF | 1.05 | 0.4 | 0.37 | 1.11 | 1.13 | 3.34 | 0.34 | 0.05 | 0.25 | 0.45 | 2.57 | 0.27 | 12.44 | 120 |
| $Fe_2O_3$ | % XRF | 0.74 | 1.57 | 0.33 | 1.12 | 1.06 | 2.12 | 0.36 | 0.03 | 0.55 | 0.41 | 3.88 | 0.35 | 0.36 | 30 |
| MnO | % XRF | 0.133 | 0.215 | 0.223 | 0.147 | 0.12 | 0.032 | 0.047 | 0.058 | 0.056 | 0.048 | 0.082 | 0.042 | 0.02 | 30 |
| MgO | % XRF | 0.52 | 4.54 | 1.04 | 0.58 | 0.5 | 0.62 | 0.41 | 0.07 | 0.94 | 0.42 | 0.79 | 0.36 | 0.06 | 95 |
| CaO | % XRF | 46 | 37.91 | 46.04 | 46.26 | 46.16 | 49.15 | 52.86 | 55.47 | 52.37 | 54.2 | 48.16 | 52.69 | 14.01 | 15 |
| $Na_2O$ | % XRF | 0.03 | < d/l | < d/l | 0.03 | < d/l | 0.07 | 0.04 | 0.07 | 0.02 | 0.02 | 0.17 | < d/l | < d/l | 75 |
| $K_2O$ | % XRF | 0.02 | < d/l | 0.19 | < d/l | < d/l | 0.14 | 0.01 | < d/l | < d/l | 0.01 | 0.07 | < d/l | 0.05 | 25 |
| $P_2O_5$ | % XRF | 0.212 | 0.024 | 0.265 | 0.136 | 0.245 | 0.337 | 0.078 | 0.019 | 0.092 | 0.096 | 0.823 | 0.018 | 0.019 | 35 |
| $Cr_2O_3$ | ppm | 54 | 145 | 16 | 75 | 127 | 59 | 17 | < d/l | 22 | 16 | 119 | 15 | 15 | 15 |
| Sc | ppm | < d/l | < d/l | < d/l | 19 | 18 | 14 | 15 | 11 | 16 | < d/l | 12 | < d/l | < d/l | 10 |
| V | ppm | 70 | 86 | 53 | 117 | 498 | 74 | 30 | < d/l | 26 | 43 | 177 | 46 | 59 | 10 |
| Zn | ppm | 30 | 131 | 29 | 101 | 152 | 7 | 87 | 9 | 74 | < d/l | 23 | 25 | 7 | 2 |
| LOI | % | 0.65 | 3.71 | 0.14 | 1.89 | 0.36 | 33.66 | 34.31 | 44.06 | 35.98 | 42.84 | 36.16 | 36.38 | 2.43 | 100 |
| Total | % | 100.01 | 100.14 | 100.1 | 100.13 | 99.89 | 100.38 | 99.9 | 100.02 | 100.19 | 100.16 | 100.36 | 100.1 | 100.03 | |

[1] gt-w =garnet-wollastonite skarn
[2] cpx =clinopyroxene skarn
[3] woll =wollastonite skarn
[4] gr =green marble
[5] g-b =grey and bleached marble
[6] b =bleached marble

Note: The results are expressed as weight percent, the trace elements (BaO to Zn) as ppm (ug/g).
Total iron present has been recalculated as Fe2O3. In cases where most of the iron was originally in the ferrous state (usually the case with unaltered rocks) a higher total is the result.
Analyses done on fused beads prepared from ignited samples.
Detection limits are based on three times the background sigma values.
"int" indicates that there is interference from unusually high quantities of other trace elements.

Table 3.2. Whole-rock chemical analyses from Mineral Hill (ALS Chemex). Major element oxides reported in grams; trace elements reported in ppm.

| | Sample lithology | W1d (mb) marble | UBM1a marble | 00H3-M marble | 00NE-3a-M marble | 0-NE-2-M marble | 00UMQ-2-M marble | 00UMQ-1-M marble | 00H4-M marble | 00H10-M marble | 00H6-M marble | 00NE-1-M marble | GM1h-M marble | 00UMQ-3-M marble | 00H15-M marble | 00NE-3b-M marble | 00H12-M marble | 00H9-M marble | 00H13-M marble |
|---|---|---|---|---|---|---|---|---|---|---|---|---|---|---|---|---|---|---|---|
| Ba | ppm | 8 | 7 | 12 | 17 | 13 | 21 | 42.5 | 259 | 10 | 8.5 | 24 | 13 | 11 | 12.5 | 19 | 11.5 | 10 | 15 |
| Ce | ppm | 4 | 4 | 7 | 3 | 2 | 4 | 7 | 2.5 | 3 | 4.5 | 3 | 4.5 | 4.5 | 3 | 2.5 | 4.5 | 4.5 | 4 |
| Cs | ppm | <0.1 | <0.1 | <0.1 | 0.1 | <0.1 | <0.1 | <0.1 | <0.1 | <0.1 | <0.1 | <0.1 | <0.1 | 0.1 | <0.1 | <0.1 | <0.1 | <0.1 | <0.1 |
| Co | ppm | 9 | 7 | 3 | 2 | 3 | 3 | 2 | 3 | 3 | 3 | 2 | 3 | 4 | 3 | 3 | 4 | 3 | 2 |
| Cu | ppm | 10 | 10 | 10 | 5 | 5 | 10 | 5 | 5 | 10 | 5 | 5 | 20 | 10 | 5 | <5 | 25 | 15 | <5 |
| Dy | ppm | 0.5 | 0.4 | 0.4 | 0.2 | 0.3 | 0.3 | 0.3 | 0.2 | 0.4 | 0.2 | <0.1 | 0.4 | 0.7 | 0.3 | 0.2 | 0.4 | 0.3 | 0.4 |
| Er | ppm | 0.4 | 0.3 | 0.5 | 0.2 | 0.2 | 0.2 | 0.3 | 0.1 | 0.4 | 0.3 | 0.1 | 0.3 | 0.5 | 0.3 | 0.3 | 0.3 | 0.4 | 0.3 |
| Eu | ppm | 0.1 | 0.1 | 0.1 | <0.1 | <0.1 | 0.1 | 0.1 | 0.1 | 0.1 | 0.1 | <0.1 | 0.1 | 0.2 | 0.1 | 0.1 | 0.1 | 0.1 | 0.1 |
| Gd | ppm | 0.6 | 0.5 | 0.6 | 0.3 | 0.4 | 0.4 | 0.5 | 0.5 | 0.6 | 0.4 | 0.2 | 0.5 | 0.9 | 0.5 | 0.4 | 0.5 | 0.7 | 0.6 |
| Ga | ppm | <1 | <1 | <1 | <1 | <1 | <1 | <1 | <1 | <1 | <1 | <1 | <1 | <1 | <1 | <1 | <1 | <1 | <1 |
| Hf | ppm | <1 | <1 | <1 | <1 | <1 | <1 | <1 | <1 | <1 | <1 | <1 | <1 | <1 | <1 | <1 | <1 | <1 | <1 |
| Ho | ppm | 0.1 | 0.1 | 0.1 | <0.1 | <0.1 | <0.1 | 0.1 | <0.1 | 0.1 | <0.1 | <0.1 | 0.1 | 0.1 | 0.1 | <0.1 | <0.1 | 0.1 | 0.1 |
| La | ppm | 5 | 4 | 9 | 3.5 | 2.5 | 4 | 7 | 3.5 | 3.5 | 5 | 2 | 3.5 | 4.5 | 3 | 2.5 | 2.5 | 3.5 | 3 |
| Pb | ppm | <5 | <5 | 5 | <5 | 5 | <5 | <5 | 5 | <5 | <5 | <5 | <5 | <5 | <5 | <5 | <5 | <5 | <5 |
| Lu | ppm | <0.1 | <0.1 | <0.1 | <0.1 | <0.1 | <0.1 | <0.1 | <0.1 | <0.1 | <0.1 | <0.1 | <0.1 | <0.1 | <0.1 | <0.1 | <0.1 | <0.1 | <0.1 |
| Nd | ppm | 4 | 2.5 | 4 | 1.5 | 1.5 | 2.5 | 3 | 2 | 3 | 2.5 | 1.5 | 2.5 | 4 | 2 | 1.5 | 2 | 3 | 2 |
| Ni | ppm | <5 | <5 | <5 | <5 | <5 | <5 | <5 | <5 | <5 | <5 | <5 | 25 | 5 | <5 | <5 | 15 | <5 | <5 |
| Nb | ppm | <1 | <1 | <1 | <1 | <1 | <1 | <1 | <1 | <1 | <1 | <1 | <1 | 1 | <1 | <1 | <1 | <1 | <1 |
| Pr | ppm | 1.2 | 0.7 | 1.1 | 0.5 | 0.4 | 0.6 | 0.8 | 0.5 | 0.6 | 0.7 | 0.4 | 0.6 | 0.9 | 0.5 | 0.4 | 0.5 | 0.6 | 0.5 |
| Rb | ppm | 0.2 | 3 | 1.2 | 3 | 1.8 | 1 | 3.4 | 0.6 | 0.2 | <0.2 | 2.6 | <0.2 | 0.6 | 0.4 | 0.8 | 1.4 | 1 | 0.6 |
| Sm | ppm | 0.5 | 0.5 | 0.6 | 0.3 | 0.3 | 0.3 | 0.4 | 0.3 | 0.6 | 0.4 | 0.2 | 0.4 | 0.7 | 0.3 | 0.3 | 0.4 | 0.5 | 0.4 |
| Ag | ppm | <1 | <1 | <1 | <1 | <1 | <1 | <1 | <1 | <1 | <1 | <1 | <1 | <1 | <1 | 25 | <1 | <1 | <1 |
| Sr | ppm | 790 | 340 | 696 | 240 | 302 | 361 | 369 | 356 | 402 | 544 | 531 | 454 | 316 | 357 | 253 | 369 | 457 | 416 |
| Ta | ppm | <0.5 | <0.5 | <0.5 | <0.5 | <0.5 | <0.5 | <0.5 | <0.5 | <0.5 | <0.5 | <0.5 | <0.5 | <0.5 | <0.5 | <0.5 | <0.5 | <0.5 | <0.5 |
| Tb | ppm | <0.1 | <0.1 | <0.1 | <0.1 | <0.1 | <0.1 | <0.1 | <0.1 | <0.1 | <0.1 | <0.1 | <0.1 | 0.1 | <0.1 | <0.1 | <0.1 | <0.1 | <0.1 |
| Tl | ppm | <0.5 | <0.5 | <0.5 | <0.5 | <0.5 | <0.5 | <0.5 | <0.5 | <0.5 | <0.5 | <0.5 | <0.5 | <0.5 | <0.5 | <0.5 | <0.5 | <0.5 | <0.5 |
| Th | ppm | <1 | <1 | <1 | <1 | <1 | <1 | <1 | <1 | <1 | <1 | <1 | <1 | <1 | <1 | <1 | <1 | <1 | <1 |
| Tm | ppm | <0.1 | <0.1 | <0.1 | <0.1 | <0.1 | <0.1 | <0.1 | <0.1 | <0.1 | <0.1 | <0.1 | <0.1 | <0.1 | <0.1 | <0.1 | <0.1 | <0.1 | <0.1 |
| Sn | ppm | <1 | <1 | <1 | <1 | <1 | <1 | <1 | <1 | <1 | <1 | <1 | <1 | <1 | <1 | <1 | <1 | <1 | <1 |
| W | ppm | 25 | 14 | 14 | 10 | 9 | 5 | 7 | 12 | 16 | 14 | 8 | 9 | 18 | 13 | 8 | 16 | 9 | 8 |
| U | ppm | 1 | 4 | 3.5 | 3 | 3 | 5 | 3 | 3 | 2.5 | 2 | 2 | 2 | 5 | 2 | 2 | 3 | 2 | 3 |
| V | ppm | 55 | 55 | 60 | 55 | 55 | 70 | 60 | 50 | 70 | 45 | 40 | 145 | 80 | 90 | 60 | 45 | 75 | 50 |
| Yb | ppm | 0.3 | 0.3 | 0.3 | 0.1 | 0.2 | 0.2 | 0.3 | 0.1 | 0.3 | 0.1 | <0.1 | 0.3 | 0.4 | 0.3 | 0.2 | 0.4 | 0.4 | 0.2 |
| Y | ppm | 6.5 | 4.5 | 6 | 3.5 | 4 | 4 | 4.5 | 3.5 | 5.5 | 4 | 2 | 5.5 | 8.5 | 4.5 | 3.5 | 4.5 | 6.5 | 5 |
| Zn | ppm | 25 | 5 | 125 | 105 | 25 | 5 | <5 | 15 | 125 | 35 | 5 | 25 | 20 | 25 | 35 | 10 | 285 | 25 |
| Zr | ppm | 8.5 | 9 | 3 | 3 | <0.5 | 3 | 7 | <0.5 | 4 | <0.5 | <0.5 | 3.5 | 6 | 1.5 | <0.5 | 3 | 0.5 | <0.5 |
| $Al_2O_3$ | % XRF | 0.39 | 0.49 | 0.25 | 0.27 | 0.29 | 0.42 | 0.28 | 0.24 | 0.32 | 0.21 | 0.29 | 0.32 | 0.6 | 0.35 | 0.34 | 0.72 | 0.39 | 0.29 |
| CaO | % XRF | 53.68 | 54.95 | 54.68 | 55.08 | 54.72 | 55.22 | 55.16 | 54.91 | 53.79 | 55.59 | 54.49 | 53.92 | 52.45 | 52.68 | 54.85 | 53.11 | 53.6 | 54.25 |
| $Cr_2O_3$ | % XRF | <0.01 | <0.01 | <0.01 | <0.01 | <0.01 | <0.01 | <0.01 | <0.01 | <0.01 | <0.01 | <0.01 | <0.01 | <0.01 | <0.01 | <0.01 | <0.01 | <0.01 | <0.01 |
| $Fe_2O_3$ | % XRF | 0.27 | 0.27 | 0.05 | 0.1 | 0.09 | 1.18 | 0.31 | 0.03 | 0.23 | 0.01 | 0.01 | 0.19 | 1.18 | 0.09 | 0.1 | 0.21 | 0.22 | 0.09 |
| $K_2O$ | % XRF | 0.03 | 0.03 | 0.03 | 0.04 | 0.03 | 0.03 | 0.03 | 0.03 | 0.02 | 0.01 | 0.09 | 0.02 | 0.03 | 0.03 | 0.05 | 0.07 | 0.05 | 0.05 |
| MgO | % XRF | 0.25 | 0.27 | 0.16 | 0.23 | 0.22 | 0.31 | 0.28 | 0.21 | 0.32 | 0.17 | 0.23 | 0.36 | 2.93 | 1.46 | 0.24 | 0.46 | 0.28 | 0.18 |
| MnO | % XRF | 0.03 | 0.03 | 0.01 | 0.01 | 0.01 | 0.06 | 0.05 | 0.01 | 0.03 | 0.01 | 0.01 | 0.03 | 0.06 | 0.06 | 0.01 | 0.04 | 0.02 | 0.03 |
| $Na_2O$ | % XRF | <0.01 | <0.01 | <0.01 | <0.01 | <0.01 | <0.01 | <0.01 | <0.01 | <0.01 | <0.01 | <0.01 | <0.01 | <0.01 | <0.01 | <0.01 | <0.01 | <0.01 | <0.01 |
| $P_2O_5$ | % XRF | 0.01 | 0.09 | 0.13 | 0.05 | 0.06 | 0.07 | 0.03 | 0.07 | 0.08 | 0.07 | 0.04 | 0.06 | 0.09 | 0.07 | 0.03 | 0.07 | 0.08 | 0.11 |
| $SiO_2$ | % XRF | 9.86 | 1.65 | 3.45 | 0.89 | 0.89 | 1.61 | 1.19 | 1.04 | 4.91 | 1.92 | 2.89 | 7.37 | 1.51 | 5.47 | 1.54 | 4.29 | 4.3 | 5.55 |
| $TiO_2$ | % XRF | 0.01 | 0.03 | <0.01 | <0.01 | <0.01 | 0.03 | <0.01 | <0.01 | 0.01 | <0.01 | <0.01 | <0.01 | 0.03 | 0.01 | 0.02 | 0.03 | 0.01 | 0.01 |
| LOI | % | 34.71 | 41.41 | 40.41 | 42.54 | 42.83 | 40.11 | 41.99 | 42.72 | 39.56 | 41.21 | 41.08 | 36.99 | 40.22 | 39.05 | 42.17 | 40.28 | 40.27 | 38.78 |
| TOTAL | % | 99.24 | 99.22 | 99.17 | 99.21 | 99.14 | 99.04 | 99.32 | 99.26 | 99.27 | 99.2 | 99.13 | 99.26 | 99.1 | 99.27 | 99.35 | 99.28 | 99.22 | 99.34 |

Table 3.2.

| | Sample | BM-1-M | 00H14-M | GM1e (R)-G | GM1a (L)-G | W1d (w) | W1a | UB4e | W1b | W1c | 00H10-W | GM1h-W | 00H13-W | 00-H8-W | 00-H11-W | 00H1-W | 00H7-W | 00H4-W | 00H3-W |
|---|---|---|---|---|---|---|---|---|---|---|---|---|---|---|---|---|---|---|---|
| | lithology | marble | marble | marble | marble | woll skarn | woll skarn | woll skarn | woll skarn | woll skarn | woll skarn | woll skarn | woll skarn | woll skarn | woll skarn | woll skarn | woll skarn | woll skarn | woll skarn |
| Ba | ppm | 88.5 | 14.5 | 14.5 | 10 | 6.5 | 6 | 16.5 | 2.5 | 201 | 4 | 4.5 | 23 | 16.5 | 4.5 | 12.5 | 9.5 | 20.5 | 5 |
| Ce | ppm | 10.5 | 4.5 | 6 | 5.5 | 4.5 | 5 | 8 | 2 | 5 | 2 | 2 | 2 | 8 | 2.5 | 21.5 | 5 | 1.5 | 2 |
| Cs | ppm | 1.1 | <0.1 | <0.1 | <0.1 | <0.1 | <0.1 | <0.1 | <0.1 | <0.1 | <0.1 | <0.1 | <0.1 | <0.1 | <0.1 | <0.1 | <0.1 | <0.1 | <0.1 |
| Co | ppm | 10 | 4 | 3 | 3 | 8 | 9 | 17 | 12 | 6 | 13 | 13 | 4 | 10 | 3 | 14 | 6 | 4 | 5 |
| Cu | ppm | 5 | 5 | 15 | <5 | 30 | 15 | 5 | 5 | 5 | 5 | 5 | 5 | <5 | 5 | 5 | 10 | 5 | 5 |
| Dy | ppm | 1.2 | 0.3 | 0.4 | 0.6 | 1 | 0.4 | 1.5 | 0.5 | 0.8 | 0.8 | 0.5 | 0.7 | 1.7 | 0.8 | 0.8 | 0.7 | 0.6 | 0.5 |
| Er | ppm | 0.7 | 0.3 | 0.4 | 0.5 | 0.8 | 0.4 | 1 | 0.4 | 0.7 | 0.7 | 0.5 | 0.5 | 1.3 | 0.7 | 0.5 | 0.5 | 0.5 | 0.5 |
| Eu | ppm | 0.4 | 0.1 | 0.2 | 0.1 | 0.2 | 0.1 | 0.3 | 0.1 | 0.1 | 0.1 | 0.1 | 0.1 | 0.4 | 0.2 | 0.2 | 0.1 | <0.1 | 0.1 |
| Gd | ppm | 1.4 | 0.4 | 0.8 | 0.8 | 0.9 | 0.7 | 1.8 | 0.5 | 0.9 | 0.7 | 0.7 | 0.9 | 1.8 | 0.7 | 0.9 | 0.8 | 0.6 | 0.7 |
| Ga | ppm | 3 | <1 | <1 | 2 | 2 | 1 | 3 | 1 | 1 | 1 | 1 | 1 | 1 | 2 | 1 | <1 | <1 | <1 |
| Hf | ppm | <1 | <1 | <1 | <1 | <1 | <1 | <1 | <1 | <1 | <1 | <1 | <1 | <1 | 1 | <1 | <1 | <1 | <1 |
| Ho | ppm | 0.2 | 0.1 | 0.1 | 0.1 | 0.2 | 0.1 | 0.3 | 0.1 | 0.2 | 0.2 | 0.1 | 0.1 | 0.4 | 0.1 | 0.1 | 0.1 | 0.1 | 0.1 |
| La | ppm | 5 | 2.5 | 5 | 5 | 4.5 | 5.5 | 8.5 | 2 | 5 | 2.5 | 2.5 | 2.5 | 9.5 | 2.5 | 22 | 5 | 2 | 2.5 |
| Pb | ppm | <5 | <5 | <5 | <5 | <5 | <5 | <5 | 10 | <5 | <5 | <5 | 5 | 5 | 5 | <5 | <5 | <5 | <5 |
| Lu | ppm | 0.1 | <0.1 | <0.1 | <0.1 | 0.1 | <0.1 | 0.1 | <0.1 | <0.1 | <0.1 | <0.1 | <0.1 | 0.2 | <0.1 | <0.1 | <0.1 | <0.1 | <0.1 |
| Nd | ppm | 6 | 2 | 3.5 | 3.5 | 3.5 | 4 | 8 | 1.5 | 4 | 2.5 | 2 | 2.5 | 7.5 | 2.5 | 6.5 | 5 | 2 | 2 |
| Ni | ppm | 15 | <5 | 20 | 30 | 10 | <5 | 50 | <5 | <5 | 5 | 25 | 5 | 25 | <5 | <5 | <5 | <5 | 15 |
| Nb | ppm | 3 | <1 | <1 | <1 | 1 | <1 | 4 | <1 | <1 | <1 | <1 | <1 | 1 | 1 | 1 | <1 | <1 | <1 |
| Pr | ppm | 1.3 | 0.5 | 0.9 | 0.8 | 1 | 1 | 1.8 | 0.4 | 0.9 | 0.6 | 0.5 | 0.5 | 1.8 | 0.6 | 2 | 1.1 | 0.4 | 0.5 |
| Rb | ppm | 10.8 | <0.2 | <0.2 | <0.2 | 0.2 | 1.2 | 2.2 | 0.6 | 6.2 | 0.8 | 0.4 | 0.8 | 1.2 | 1 | 1.4 | 1.6 | 0.2 | 0.6 |
| Sm | ppm | 1.2 | 0.4 | 0.6 | 0.7 | 0.7 | 0.7 | 1.5 | 0.4 | 0.6 | 0.5 | 0.5 | 0.5 | 1.3 | 0.6 | 0.9 | 1 | 0.4 | 0.4 |
| Ag | ppm | <1 | <1 | <1 | <1 | <1 | <1 | 2 | <1 | <1 | 11 | <1 | <1 | <1 | <1 | <1 | <1 | <1 | 4 |
| Sr | ppm | 264 | 348 | 474 | 446 | 69.1 | 55.1 | 102.5 | 94.5 | 33 | 55.4 | 92.2 | 68.5 | 99.4 | 44.4 | 104 | 207 | 479 | 228 |
| Ta | ppm | <0.5 | <0.5 | <0.5 | <0.5 | <0.5 | <0.5 | <0.5 | <0.5 | <0.5 | <0.5 | <0.5 | <0.5 | <0.5 | <0.5 | 0.5 | 0.5 | <0.5 | <0.5 |
| Tb | ppm | 0.2 | <0.1 | <0.1 | 0.1 | 0.1 | <0.1 | 0.2 | <0.1 | 0.1 | 0.1 | 0.1 | 0.1 | 0.3 | 0.1 | 0.1 | 0.1 | <0.1 | 0.1 |
| Tl | ppm | <0.5 | <0.5 | <0.5 | <0.5 | <0.5 | <0.5 | <0.5 | <0.5 | <0.5 | <0.5 | <0.5 | <0.5 | <0.5 | <0.5 | <0.5 | <0.5 | <0.5 | <0.5 |
| Th | ppm | <1 | <1 | <1 | <1 | <1 | <1 | <1 | <1 | <1 | <1 | <1 | <1 | <1 | 1 | <1 | <1 | <1 | <1 |
| Tm | ppm | 0.1 | <0.1 | <0.1 | <0.1 | 0.1 | <0.1 | 0.1 | <0.1 | <0.1 | 0.1 | <0.1 | <0.1 | 0.1 | <0.1 | <0.1 | <0.1 | <0.1 | <0.1 |
| Sn | ppm | <1 | <1 | <1 | <1 | <1 | <1 | <1 | <1 | <1 | 1 | <1 | <1 | <1 | <1 | <1 | <1 | <1 | <1 |
| W | ppm | 13 | 16 | 9 | 9 | 21 | 41 | 70 | 69 | 29 | 53 | 135 | 40 | 66 | 35 | 75 | 56 | 37 | 57 |
| U | ppm | 14.5 | 1.5 | 3.5 | 4 | 6.5 | 7 | 16 | 1.5 | 12.5 | 10.5 | 5 | 4.5 | 6.5 | 25.5 | 5 | 1.5 | 4 | 1.5 |
| V | ppm | 60 | 40 | 115 | 240 | 150 | 90 | 650 | 115 | 70 | 85 | 205 | 160 | 150 | 45 | 75 | 80 | 25 | 60 |
| Yb | ppm | 0.6 | 0.1 | 0.3 | 0.3 | 0.8 | 0.4 | 1.1 | 0.3 | 0.5 | 0.5 | 0.4 | 0.4 | 1.2 | 0.5 | 0.3 | 0.5 | 0.3 | 0.4 |
| Y | ppm | 9.5 | 4.5 | 5 | 7 | 11.5 | 6 | 14.5 | 6 | 9.5 | 10.5 | 7 | 8.5 | 19 | 9.5 | 7.5 | 7.5 | 7 | 8 |
| Zn | ppm | 10 | 10 | 80 | 35 | 95 | 35 | 150 | 125 | 25 | 25 | 55 | 275 | 70 | 25 | 30 | 225 | 20 | 20 |
| Zr | ppm | 16.5 | 1.5 | 1.5 | 5 | 13.5 | 8 | 21 | 5.5 | 4 | 4.5 | 5 | 3 | 14.5 | 87.5 | 2 | 4.5 | 0.5 | 1.5 |
| $Al_2O_3$ | % XRF | 3.83 | 0.19 | 0.37 | 1.68 | 1.17 | 0.8 | 1.21 | 0.51 | 0.53 | 0.79 | 0.95 | 0.63 | 1.25 | 1.7 | 0.45 | 0.48 | 0.47 | 0.46 |
| CaO | % XRF | 40.14 | 54.91 | 53.81 | 52.89 | 45.48 | 45.85 | 45.32 | 37.57 | 44.98 | 45.57 | 45.53 | 46.24 | 45.83 | 45.36 | 45.85 | 47.41 | 46.19 | 47.55 |
| $Cr_2O_3$ | % XRF | <0.01 | <0.01 | <0.01 | <0.01 | <0.01 | <0.01 | <0.01 | <0.01 | <0.01 | <0.01 | <0.01 | <0.01 | <0.01 | <0.01 | <0.01 | <0.01 | <0.01 | <0.01 |
| $Fe_2O_3$ | % XRF | 1.68 | 0.07 | 0.13 | 0.19 | 1.04 | 0.57 | 0.97 | 1.57 | 0.31 | 0.46 | 0.33 | 0.37 | 0.6 | 0.23 | 0.26 | 0.28 | 0.12 | 0.22 |
| $K_2O$ | % XRF | 0.53 | 0.02 | 0.03 | 0.02 | 0.01 | 0.02 | 0.02 | 0.03 | 0.22 | 0.02 | 0.02 | 0.02 | 0.05 | 0.02 | 0.04 | 0.05 | 0.03 | 0.03 |
| MgO | % XRF | 10.72 | 0.53 | 0.24 | 0.63 | 0.44 | 0.38 | 0.46 | 4.31 | 0.98 | 0.24 | 0.86 | 0.28 | 0.43 | 0.23 | 0.21 | 0.26 | 0.22 | 0.27 |
| MnO | % XRF | 0.03 | 0.02 | 0.03 | 0.04 | 0.11 | 0.1 | 0.1 | 0.18 | 0.18 | 0.17 | 0.15 | 0.11 | 0.06 | 0.1 | 0.13 | 0.05 | 0.15 | 0.09 |
| $Na_2O$ | % XRF | <0.01 | <0.01 | <0.01 | <0.01 | <0.01 | <0.01 | <0.01 | <0.01 | <0.01 | <0.01 | <0.01 | <0.01 | <0.01 | <0.01 | <0.01 | <0.01 | <0.01 | <0.01 |
| $P_2O_5$ | % XRF | 0.16 | 0.08 | 0.1 | 0.12 | 0.14 | 0.22 | 0.25 | 0.03 | 0.25 | 0.34 | 0.16 | 0.1 | 1.05 | 0.05 | 0.15 | 0.04 | 0.15 | 0.01 |
| $SiO_2$ | % XRF | 11.81 | 1.75 | 6.17 | 8.17 | 49.34 | 50.94 | 50.51 | 51.17 | 51.52 | 47.87 | 44.34 | 46.87 | 45.52 | 50.66 | 51.1 | 38.05 | 50.54 | 38.71 |
| $TiO_2$ | % XRF | 0.15 | <0.01 | 0.01 | 0.02 | 0.06 | 0.03 | 0.09 | 0.01 | 0.03 | 0.03 | 0.04 | 0.04 | 0.08 | 0.02 | 0.02 | 0.03 | 0.01 | 0.01 |
| LOI | % | 29.86 | 41.83 | 38.37 | 35.42 | 1.41 | 0.18 | 0.41 | 3.8 | 0.16 | 3.77 | 6.83 | 4.56 | 4.29 | 0.83 | 0.85 | 12.61 | 1.23 | 11.86 |
| TOTAL | % | 98.91 | 99.4 | 99.26 | 99.18 | 99.2 | 99.09 | 99.34 | 99.18 | 99.16 | 99.26 | 99.21 | 99.22 | 99.16 | 99.2 | 99.06 | 99.26 | 99.11 | 99.21 |

Table 3.2.

| | Sample lithology | 00-H2-W woll skarn | GM1a(u)-W woll skarn | TB 4F garnet skarn | UB 5E garnet skarn | CZ-1 skarnoid | CZ-3 skarnoid | Detection Limit |
|---|---|---|---|---|---|---|---|---|
| Ba | ppm | 3 | 2 | 7 | <0.5 | 59 | 1585 | 0.5 |
| Ce | ppm | 4 | 3 | 11.5 | 10.5 | 3.5 | 28.5 | 0.5 |
| Cs | ppm | <0.1 | <0.1 | <0.1 | <0.1 | <0.1 | 0.1 | 0.1 |
| Co | ppm | 5 | 5 | 25 | 49 | 86 | 22.5 | 0.5 |
| Cu | ppm | 15 | <5 | <5 | 15 | 20 | 30 | 5 |
| Dy | ppm | 0.8 | 0.7 | 4 | 3.1 | 0.6 | 4.3 | 0.1 |
| Er | ppm | 0.6 | 0.6 | 2.5 | 2 | 0.4 | 2.2 | 0.1 |
| Eu | ppm | 0.1 | 0.1 | 0.7 | 0.8 | 0.1 | 1.1 | 0.1 |
| Gd | ppm | 0.8 | 0.8 | 3.6 | 3 | 0.6 | 4.9 | 0.1 |
| Ga | ppm | <1 | 1 | 13 | 11 | 2 | 10 | 1 |
| Hf | ppm | <1 | <1 | 5 | <1 | <1 | <1 | 1 |
| Ho | ppm | 0.2 | 0.1 | 0.8 | 0.7 | 0.1 | 0.9 | 0.1 |
| La | ppm | 3.5 | 1.5 | 6 | 7.5 | 3 | 14.5 | 0.5 |
| Pb | ppm | <5 | <5 | 5 | <5 | <5 | <5 | 5 |
| Lu | ppm | <0.1 | <0.1 | 0.3 | 0.3 | <0.1 | 0.3 | 0.1 |
| Nd | ppm | 3.5 | 2.5 | 10 | 8 | 3 | 17.5 | 0.5 |
| Ni | ppm | <5 | 30 | 35 | 75 | 20 | 15 | 5 |
| Nb | ppm | <1 | <1 | 7 | 1 | 1 | 2 | 1 |
| Pr | ppm | 0.8 | 0.5 | 2.1 | 1.8 | 0.8 | 4.1 | 0.1 |
| Rb | ppm | 0.4 | <0.2 | 1.2 | 0.6 | 3.8 | 28.4 | 0.2 |
| Sm | ppm | 0.7 | 0.5 | 3.3 | 2.7 | 0.7 | 4.2 | 0.1 |
| Ag | ppm | <1 | <1 | <1 | <1 | <1 | <1 | 1 |
| Sr | ppm | 54.7 | 47.3 | 13.6 | 5.1 | 24.9 | 517 | 0.1 |
| Ta | ppm | 0.5 | <0.5 | 0.5 | <0.5 | <0.5 | <0.5 | 0.5 |
| Tb | ppm | 0.1 | 0.1 | 0.6 | 0.5 | <0.1 | 0.7 | 0.1 |
| Tl | ppm | <0.5 | <0.5 | <0.5 | <0.5 | 0.5 | 0.5 | 0.5 |
| Th | ppm | <1 | <1 | 1 | <1 | <1 | <1 | 1 |
| Tm | ppm | <0.1 | <0.1 | 0.4 | 0.3 | <0.1 | 0.2 | 0.1 |
| Sn | ppm | <1 | <1 | 3 | 1 | 1 | 1 | 1 |
| W | ppm | 57 | 57 | 222 | 327 | 1150 | 196 | 1 |
| U | ppm | 4 | 1.5 | 5 | 3 | 3 | 0.5 | 0.5 |
| V | ppm | 60 | 105 | 290 | 315 | 85 | 185 | 5 |
| Yb | ppm | 0.4 | 0.6 | 2.8 | 2.1 | 0.3 | 2.3 | 0.1 |
| Y | ppm | 10 | 9 | 28.5 | 24.5 | 7 | 25.5 | 0.5 |
| Zn | ppm | 25 | 35 | 130 | 1875 | 30 | 150 | 5 |
| Zr | ppm | 1.5 | 0.5 | 198.5 | 45.5 | 15.5 | 15.5 | 0.5 |
| $Al_2O_3$ | % XRF | 0.29 | 0.67 | 10.43 | 9 | 1.89 | 14.73 | 0.01 |
| CaO | % XRF | 46.02 | 45.8 | 37.05 | 28.21 | 0.57 | 8.79 | 0.01 |
| $Cr_2O_3$ | % XRF | <0.01 | <0.01 | <0.01 | <0.01 | <0.01 | <0.01 | 0.01 |
| $Fe_2O_3$ | % XRF | 0.22 | 0.46 | 6.03 | 8.17 | 0.66 | 6.04 | 0.01 |
| $K_2O$ | % XRF | 0.04 | 0.03 | 0.05 | 0.03 | 0.23 | 2.02 | 0.01 |
| MgO | % XRF | 0.31 | 0.33 | 1.39 | 3.72 | <0.01 | 5.02 | 0.01 |
| MnO | % XRF | 0.13 | 0.11 | 0.24 | 0.88 | <0.01 | 0.23 | 0.01 |
| $Na_2O$ | % XRF | <0.01 | <0.01 | <0.01 | 0.09 | 0.31 | 4.4 | 0.01 |
| $P_2O_5$ | % XRF | 0.15 | 0.04 | 0.27 | 0.35 | 0.04 | 0.64 | 0.01 |
| $SiO_2$ | % XRF | 51.38 | 50.94 | 43.02 | 47.96 | 94.86 | 54.74 | 0.01 |
| $TiO_2$ | % XRF | 0.03 | 0.03 | 0.41 | 0.32 | 0.09 | 0.99 | 0.01 |
| LOI | % | 0.6 | 0.7 | 0.29 | 0.21 | 0.26 | 0.97 | 0.01 |
| TOTAL | % | 99.17 | 99.11 | 99.18 | 98.94 | 98.91 | 98.57 | 0.01 |

Table 3.3. Selected igneous major-element whole-rock analyses from Mineral Hill from *Ray and Kilby* [1996]. Data reported in grams.

| Sample | GR94-84 | GR94-85 | GR95-12 | GR95-14 | GR95-60 | GR95-92 | GR95-37 | GR95-40 | R95-42A | GR95-51 | GR95-54 | GR95-29 | GR95-38 | GR95-42 | GR95-43 | GR95-53 | GR95-59 |
|---|---|---|---|---|---|---|---|---|---|---|---|---|---|---|---|---|---|
| lithology | gabbro | gabbro | gabbro | gabbro | gabbro | gabbro | tonalite | tonalite | tonalite | tonalite | tonalite | basalt | basalt | basalt | basalt | basalt | basalt |
| $SiO_2$ | 58.2 | 58.08 | 49.34 | 50.94 | 51.08 | 44.72 | 65.12 | 65.35 | 65.31 | 64.93 | 64.42 | 51.83 | 50.36 | 51.8 | 49.56 | 50.57 | 56.37 |
| $TiO_2$ | 0.63 | 0.62 | 0.91 | 0.86 | 1.49 | 1.78 | 0.28 | 0.25 | 0.28 | 0.25 | 0.26 | 0.67 | 0.76 | 0.66 | 0.68 | 0.65 | 0.65 |
| $Al_2O_3$ | 17.73 | 17.62 | 19 | 18.94 | 17.08 | 16.44 | 17.52 | 17.02 | 17.39 | 17.48 | 17.36 | 17.07 | 18.32 | 17.04 | 18.26 | 17.87 | 18.37 |
| $Fe_2O_3$ | < d/l | < d/l | 3.36 | 2.93 | 2.57 | 4.54 | 2.34 | 1.2 | 1.05 | 1.22 | 0.88 | 2.35 | 2.42 | 2.42 | 1.3 | 1.32 | 3.41 |
| FeO | 3.07 | 4.16 | 5.4 | 5.25 | 6.78 | 7.57 | 1 | 1.95 | 2.36 | 1.76 | 2.28 | 4.29 | 5.43 | 4.35 | 5.57 | 5.13 | 3.81 |
| MnO | 0.12 | 0.14 | 0.15 | 0.16 | 0.17 | 0.15 | 0.05 | 0.11 | 0.14 | 0.1 | 0.12 | 0.13 | 0.16 | 0.12 | 0.16 | 0.13 | 0.1 |
| MgO | 3.41 | 3.41 | 6.06 | 5.75 | 5.11 | 7.8 | 1.12 | 1.11 | 1.14 | 1.08 | 1.23 | 5.91 | 5.76 | 5.91 | 6.29 | 6.21 | 3.24 |
| CaO | 6.85 | 6.83 | 11.2 | 10.27 | 8.93 | 11.45 | 4.48 | 4.81 | 4.6 | 4.64 | 4.71 | 10.95 | 7.47 | 10.84 | 11.13 | 10.02 | 7.38 |
| $Na_2O$ | 3.77 | 3.7 | 3.04 | 3.09 | 3.59 | 2.33 | 4.78 | 4.9 | 4.84 | 4.73 | 4.71 | 2.76 | 3.94 | 2.82 | 3.02 | 3.08 | 3.57 |
| $K_2O$ | 1.1 | 1.19 | 0.013 | 0.2 | 0.6 | 0.61 | 1.75 | 1.42 | 0.97 | 1.53 | 1.77 | 1.63 | 0.72 | 1.61 | 0.6 | 0.57 | 0.58 |
| $P_2O_5$ | 0.15 | 0.2 | 0.24 | 0.1 | 0.58 | 0.18 | 0.22 | 0.22 | 0.21 | 0.22 | 0.22 | 0.18 | 0.17 | 0.18 | 0.19 | 0.18 | 0.22 |
| L.O.I. | 0.9 | 0.93 | 1.17 | 0.89 | 1.46 | 2.09 | 0.98 | 1.2 | 1.3 | 1.08 | 0.97 | 1.78 | 3.79 | 1.97 | 2.86 | 2.35 | 1.53 |

$Al_2O_3$, $Fe_2O_3$, MnO, MgO, CaO, $Na_2O$, $K_2O$ and $P_2O_5$. Nine major oxides (minus $TiO_2$) were reduced to a four component system to allow visual analysis of bulk compositional trends. Silica was projected from alkali feldspar ($Na_2O$ and $K_2O$), aluminium and ferric iron were projected from alkali feldspar, calcium was projected from apatite, and ferrous iron, magnesium and manganese were combined. These were calculated by

$S' = [SiO_2] - 3/2([Na_2O]+[K_2O])$

$A' = [Al_2O_3]+[Fe_2O_3] - ([Na_2O]+[K_2O])$

$C' = [CaO] - 3.3[P_2O_5]$

$F' = [MgO] + [FeO] + [MnO]$

and projected onto the ASC, ASF, ACF, and SFC ternary diagrams [*Winkler*, 1976 ; *Bucher and Frey*, 1994].

All meta-sedimentary and skarn samples were calculated for total iron as $Fe_2O_3$ ($Fe_2O_{3\,T}$, large symbols; Figs. 3.1-3.8) and total iron as FeO ($FeO_T$, small symbols; Figs. 3.1-3.8). Total iron calculated as $Fe_2O_3$ increases abundance of andradite garnet and epidote, whereas total iron calculated as FeO overpredicts almandine garnet and calcic-clinopyroxene abundance. Rocks from Mineral Hill probably contain a combination of FeO and $Fe_2O_3$ mineral compositions and therefore realistically fall along a line between the two extremes ($Fe_2O_{3T}$ and $FeO_T$). The data was normalized and plotted using Sigma Plot [*SPSS Inc.*, 1997].

Major element whole-rock analyses of the seventy-three samples are presented in Table 3.1 and 3.2. In order to interpret possible protolith compositions for the meta-sedimentary and skarn rocks, the data are compared to the compositions of seven meta-sedimentary rock types from the literature [*Ferry*,1988, 1989 and 1994]. These are discussed in a later section. The chemical compositions of twelve common sedimentary rocks from *Brownlow* [1996] were also included. These are presented in Table 3.4. Moreover, end-member chemical compositions of six minerals were projected. These include garnet (grossular, andradite, spessartine, pyrope, and

Fig 3.1. ASC ternary diagrams for a) meta-sedimentary rocks (compiled data converted to $Fe_2O_3$). Possible protolith fields were constructed from whole-rock analyses from sandstone, pelite, limestone/marble, and calcareous hornfels from *Ferry* [1988, 1989, 1994]. Light green= micaceous, carbonate-bearing sandstones from the Vassalboro/ Sangerville Formation [*Ferry*, 1988]; bright green= calcareous hornfels from roof pendants at Hope Valley, CA [*Ferry*, 1989], orange= marble from roof pendants at Hope Valley, CA [*Ferry*, 1989]; light pink= limestone from Giles Mountain Formation and Waits River Formation [*Ferry*, 1994], light blue= sandstone from Giles Mountain Formation and Waits River Formation [*Ferry*, 1994], red= pelites from Giles Mountain Formation and Waits River Formation [*Ferry*, 1994], light purple= meta-carbonate rocks from the Waterville Formation [*Ferry*, 1994]. Common sedimentary rock compositions from *Brownlow* [1996] denoted by blue circles; 1. Orthoquartzite, 2. Arkose, 3. Graywacke, 4. Sub-graywacke, 5. Lithographic limestone, 6. Fossiliferous limestone, 7. Oolitic limestone, 8. Dolomite, 9. Si-shale, 10. K-shale, 11. Calcareous shale, 12. Carbonaceous shale. b) Marble samples ($FeO_T$ and $Fe_2O_{3T}$) denoted by blue triangles (small) and blue triangles (large), respectively. c) Skarn samples ($FeO_T$ and $Fe_2O_{3T}$). Wollastonite skarn denoted as yellow triangles (large-$Fe_2O_3$) and blue triangles (small- FeO); Garnet-wollastonite skarn denoted as red triangles (large-$Fe_2O_3$; small-FeO); Garnet skarn denoted as red circles (large-$Fe_2O_3$; small-FeO); Garnetite denoted as red squares (large-$Fe_2O_3$; small-FeO); Clinopyroxene skarn denoted as green circles (large-$Fe_2O_3$; small-FeO). d) Skarnoid and quartzite samples ($FeO_T$ and $Fe_2O_{3T}$). Skarnoid denoted as green hexagons (large-$Fe_2O_3$; small-FeO); Quartzite denoted as yellow circle (large-$Fe_2O_3$) and blue circle (small-FeO). Small black circles for all ternaries represent end-member mineral compositions; an= anorthite, qtz= quartz, cc=calcite, woll= wollastonite, pyr= pyrope garnet, alm= almandine garnet, spe= spessartine garnet, andr= andradite garnet, gross= grossular, hed= hedenbergite, di= diopside.

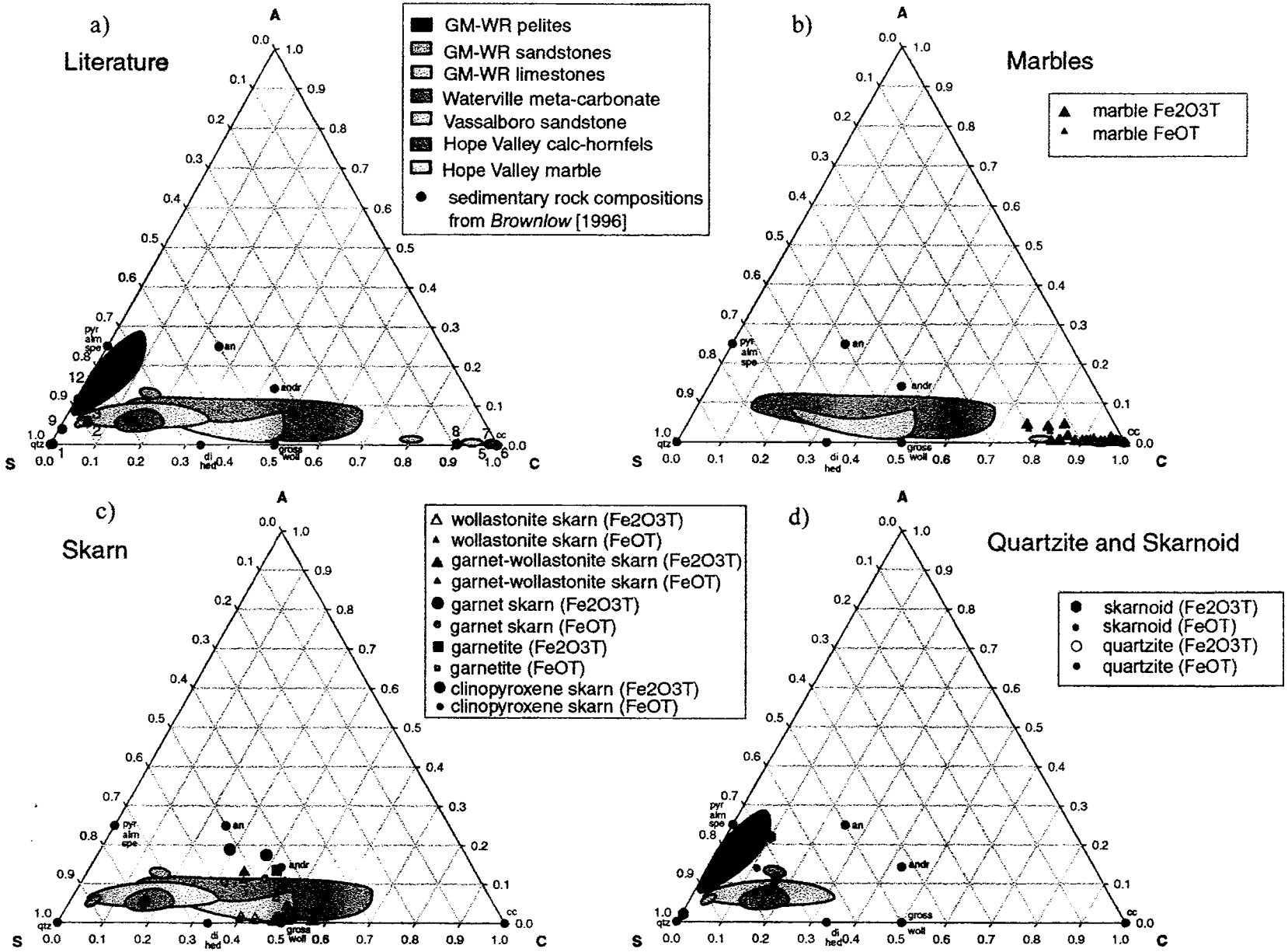


Fig 3.1. ASC ternary diagram (all iron in compiled data converted to Fe2O3)

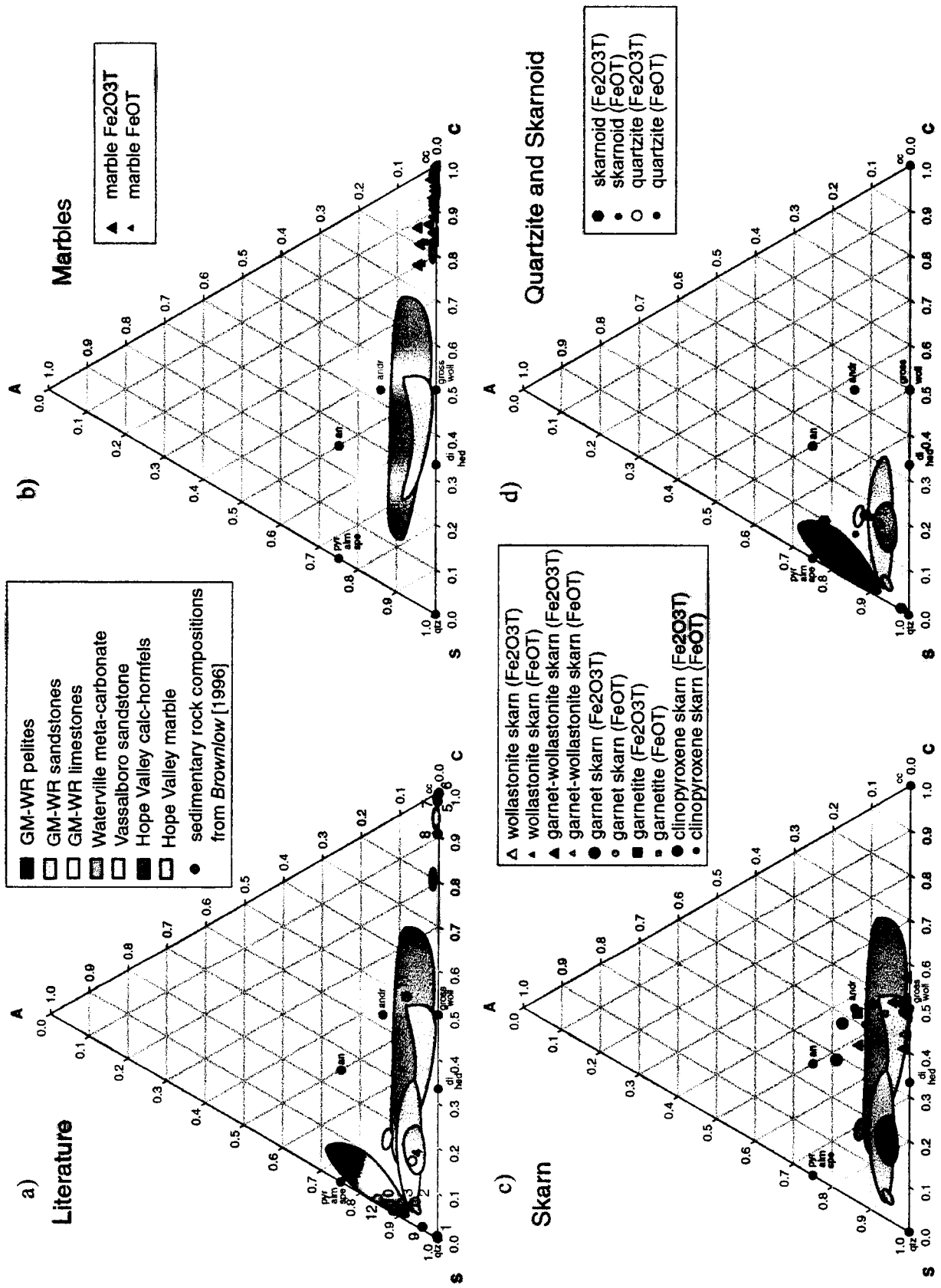


Fig 3.1. ASC ternary diagram (all iron in compiled data converted to Fe2O3)

Fig 3.2. ASF ternary diagrams for a) meta-sedimentary rocks (compiled data converted to $Fe_2O_3$). Possible protolith fields were constructed from whole-rock analyses from sandstone, pelite, limestone/marble, and calcareous hornfels from *Ferry* [1988, 1989, 1994]. Light green= micaceous, carbonate-bearing sandstones from the Vassalboro/ Sangerville Formation [*Ferry*, 1988]; bright green= calcareous hornfels from roof pendants at Hope Valley, CA [*Ferry*, 1989], orange= marble from roof pendants at Hope Valley, CA [*Ferry*, 1989]; light pink= limestone from Giles Mountain Formation and Waits River Formation [*Ferry*, 1994], light blue= sandstone from Giles Mountain Formation and Waits River Formation [*Ferry*, 1994], red= pelites from Giles Mountain Formation and Waits River Formation [*Ferry*, 1994], light purple= meta-carbonate rocks from the Waterville Formation [*Ferry*, 1994]. Common sedimentary rock compositions from *Brownlow* [1996] denoted by blue circles; 1. Orthoquartzite, 2. Arkose, 3. Graywacke, 4. Sub-graywacke, 5. Lithographic limestone, 6. Fossiliferous limestone, 7. Oolitic limestone, 8. Dolomite, 9. Si-shale, 10. K-shale, 11. Calcareous shale, 12. Carbonaceous shale. b) Marble samples ($FeO_T$ and $Fe_2O_{3T}$) denoted by blue triangles (small) and blue triangles (large), respectively. c) Skarn samples ($FeO_T$ and $Fe_2O_{3T}$). Wollastonite skarn denoted as yellow triangles (large-$Fe_2O_3$) and blue triangles (small- FeO); Garnet-wollastonite skarn denoted as red triangles (large-$Fe_2O_3$; small-FeO); Garnet skarn denoted as red circles (large-$Fe_2O_3$; small-FeO); Garnetite denoted as red squares (large-$Fe_2O_3$; small-FeO); Clinopyroxene skarn denoted as green circles (large-$Fe_2O_3$; small-FeO). d) Skarnoid and quartzite samples ($FeO_T$ and $Fe_2O_{3T}$). Skarnoid denoted as green hexagons (large-$Fe_2O_3$; small-FeO); Quartzite denoted as yellow circle (large-$Fe_2O_3$) and blue circle (small-FeO). Small black circles for all ternaries represent end-member mineral compositions; an= anorthite, qtz= quartz, cc=calcite, woll= wollastonite, pyr= pyrope garnet, alm= almandine garnet, spe= spessartine garnet, andr= andradite garnet, gross= grossular, hed= hedenbergite, di= diopside.

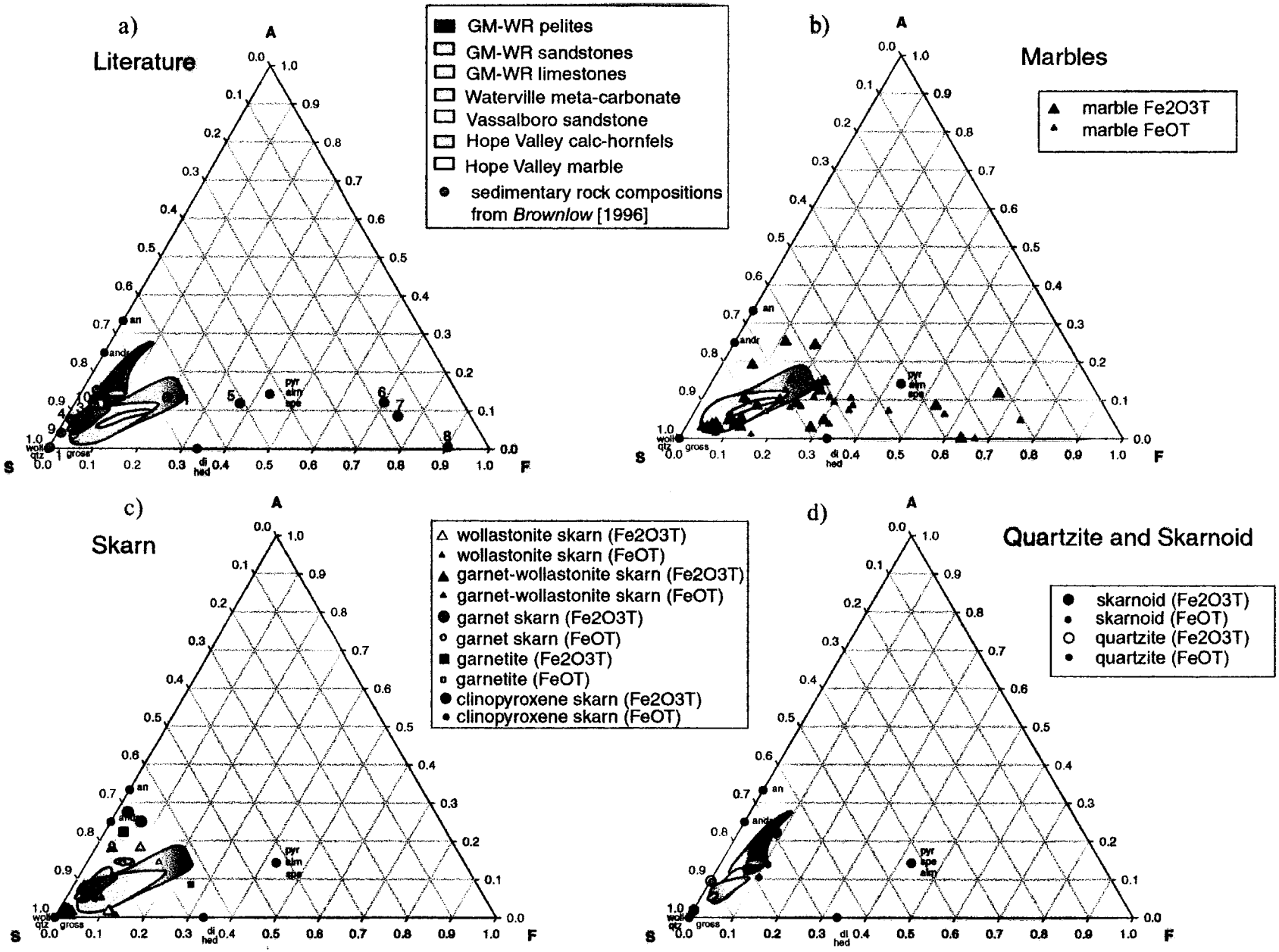


Fig 3.2. ASF ternary diagram (all iron in compiled data converted to Fe2O3)

Fig 3.3. SFC ternary diagrams for a) meta-sedimentary rocks (compiled data converted to $Fe_2O_3$). Possible protolith fields were constructed from whole-rock analyses from sandstone, pelite, limestone/marble, and calcareous hornfels from *Ferry* [1988, 1989, 1994]. Light green= micaceous, carbonate-bearing sandstones from the Vassalboro/ Sangerville Formation [*Ferry*, 1988]; bright green= calcareous hornfels from roof pendants at Hope Valley, CA [*Ferry*, 1989], orange= marble from roof pendants at Hope Valley, CA [*Ferry*, 1989]; light pink= limestone from Giles Mountain Formation and Waits River Formation [*Ferry*, 1994], light blue= sandstone from Giles Mountain Formation and Waits River Formation [*Ferry*, 1994], red= pelites from Giles Mountain Formation and Waits River Formation [*Ferry*, 1994], light purple= meta-carbonate rocks from the Waterville Formation [*Ferry*, 1994]. Common sedimentary rock compositions from *Brownlow* [1996] denoted by blue circles; 1. Orthoquartzite, 2. Arkose, 3. Graywacke, 4. Sub-graywacke, 5. Lithographic limestone, 6. Fossiliferous limestone, 7. Oolitic limestone, 8. Dolomite, 9. Si-shale, 10. K-shale, 11. Calcareous shale, 12. Carbonaceous shale. b) Marble samples ($FeO_T$ and $Fe_2O_{3T}$) denoted by blue triangles (small) and blue triangles (large), respectively. c) Skarn samples ($FeO_T$ and $Fe_2O_{3T}$). Wollastonite skarn denoted as yellow triangles (large-$Fe_2O_3$) and blue triangles (small- FeO); Garnet-wollastonite skarn denoted as red triangles (large-$Fe_2O_3$; small-FeO); Garnet skarn denoted as red circles (large-$Fe_2O_3$; small-FeO); Garnetite denoted as red squares (large-$Fe_2O_3$; small-FeO); Clinopyroxene skarn denoted as green circles (large-$Fe_2O_3$; small-FeO). d) Skarnoid and quartzite samples ($FeO_T$ and $Fe_2O_{3T}$). Skarnoid denoted as green hexagons (large-$Fe_2O_3$; small-FeO); Quartzite denoted as yellow circle (large-$Fe_2O_3$) and blue circle (small-FeO). Small black circles for all ternaries represent end-member mineral compositions; an= anorthite, qtz= quartz, cc=calcite, woll= wollastonite, pyr= pyrope garnet, alm= almandine garnet, spe= spessartine garnet, andr= andradite garnet, gross= grossular, hed= hedenbergite, di= diopside.

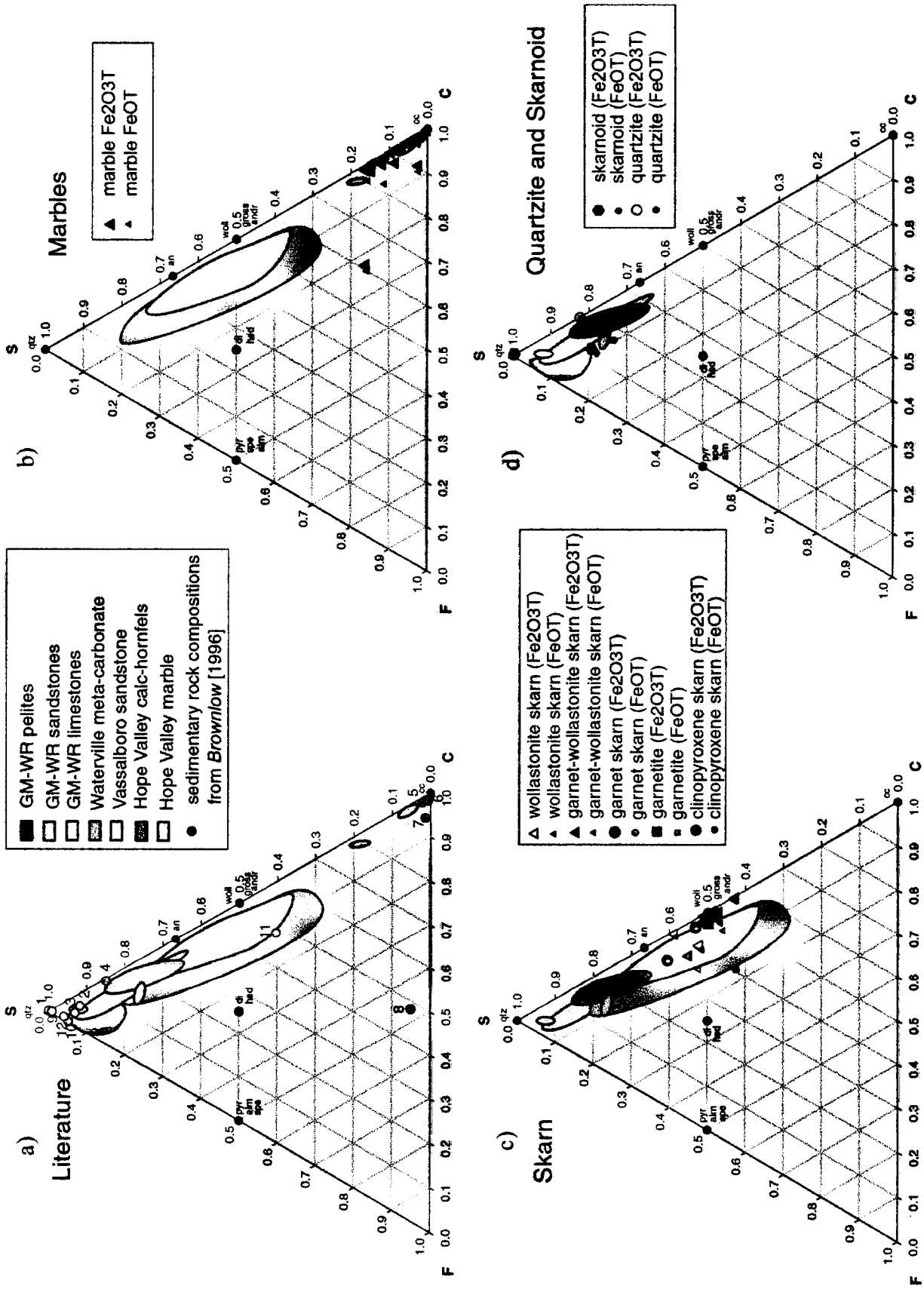


Fig 3.3. SFC ternary diagram (all iron in compiled data converted to Fe2O3)

Fig 3.4. ACF ternary diagrams for a) meta-sedimentary rocks (compiled data converted to $Fe_2O_3$). Possible protolith fields were constructed from whole-rock analyses from sandstone, pelite, limestone/marble, and calcareous hornfels from *Ferry* [1988, 1989, 1994]. Light green= micaceous, carbonate-bearing sandstones from the Vassalboro/ Sangerville Formation [*Ferry*, 1988]; bright green= calcareous hornfels from roof pendants at Hope Valley, CA [*Ferry*, 1989], orange= marble from roof pendants at Hope Valley, CA [*Ferry*, 1989]; light pink= limestone from Giles Mountain Formation and Waits River Formation [*Ferry*, 1994], light blue= sandstone from Giles Mountain Formation and Waits River Formation [*Ferry*, 1994], red= pelites from Giles Mountain Formation and Waits River Formation [*Ferry*, 1994], light purple= meta-carbonate rocks from the Waterville Formation [*Ferry*, 1994]. Common sedimentary rock compositions from *Brownlow* [1996] denoted by blue circles; 1. Orthoquartzite, 2. Arkose, 3. Graywacke, 4. Sub-graywacke, 5. Lithographic limestone, 6. Fossiliferous limestone, 7. Oolitic limestone, 8. Dolomite, 9. Si-shale, 10. K-shale, 11. Calcareous shale, 12. Carbonaceous shale. b) Marble samples ($FeO_T$ and $Fe_2O_{3T}$) denoted by blue triangles (small) and blue triangles (large), respectively. c) Skarn samples ($FeO_T$ and $Fe_2O_{3T}$). Wollastonite skarn denoted as yellow triangles (large-$Fe_2O_3$) and blue triangles (small- FeO); Garnet-wollastonite skarn denoted as red triangles (large-$Fe_2O_3$; small-FeO); Garnet skarn denoted as red circles (large-$Fe_2O_3$; small-FeO); Garnetite denoted as red squares (large-$Fe_2O_3$; small-FeO); Clinopyroxene skarn denoted as green circles (large-$Fe_2O_3$; small-FeO). d) Skarnoid and quartzite samples ($FeO_T$ and $Fe_2O_{3T}$). Skarnoid denoted as green hexagons (large-$Fe_2O_3$; small-FeO); Quartzite denoted as yellow circle (large-$Fe_2O_3$) and blue circle (small-FeO). Small black circles for all ternaries represent end-member mineral compositions; an= anorthite, qtz= quartz, cc=calcite, woll= wollastonite, pyr= pyrope garnet, alm= almandine garnet, spe= spessartine garnet, andr= andradite garnet, gross= grossular, hed= hedenbergite, di= diopside.

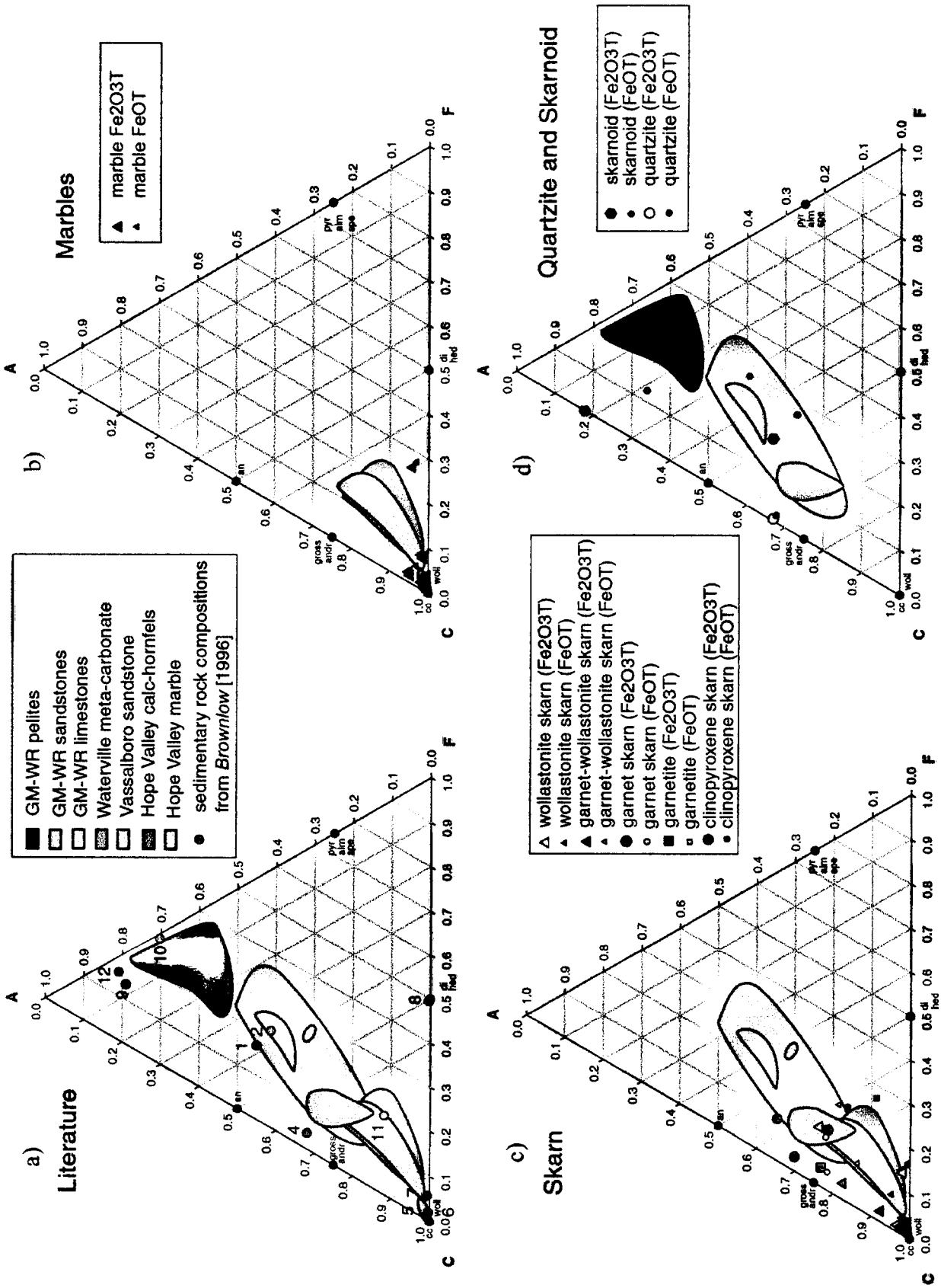


Fig 3.4. ACF ternary diagram (all iron in compiled data converted to Fe2O3)

Fig 3.5. ASC ternary diagrams for a) meta-sedimentary rocks (compiled data converted to FeO). Possible protolith fields were constructed from whole-rock analyses from sandstone, pelite, limestone/marble, and calcareous hornfels from *Ferry* [1988, 1989, 1994]. Light green= micaceous, carbonate-bearing sandstones from the Vassalboro/ Sangerville Formation [*Ferry*, 1988]; bright green= calcareous hornfels from roof pendants at Hope Valley, CA [*Ferry*, 1989], orange= marble from roof pendants at Hope Valley, CA [*Ferry*, 1989]; light pink= limestone from Giles Mountain Formation and Waits River Formation [*Ferry*, 1994], light blue= sandstone from Giles Mountain Formation and Waits River Formation [*Ferry*, 1994], red= pelites from Giles Mountain Formation and Waits River Formation [*Ferry*, 1994], light purple= meta-carbonate rocks from the Waterville Formation [*Ferry*, 1994]. Common sedimentary rock compositions from *Brownlow* [1996] denoted by blue circles; 1. Orthoquartzite, 2. Arkose, 3. Graywacke, 4. Sub-graywacke, 5. Lithographic limestone, 6. Fossiliferous limestone, 7. Oolitic limestone, 8. Dolomite, 9. Si-shale, 10. K-shale, 11. Calcareous shale, 12. Carbonaceous shale. b) Marble samples ($FeO_T$ and $Fe_2O_{3T}$) denoted by blue triangles (small) and blue triangles (large), respectively. c) Skarn samples ($FeO_T$ and $Fe_2O_{3T}$). Wollastonite skarn denoted as yellow triangles (large-$Fe_2O_3$) and blue triangles (small- FeO); Garnet-wollastonite skarn denoted as red triangles (large-$Fe_2O_3$; small-FeO); Garnet skarn denoted as red circles (large-$Fe_2O_3$; small-FeO); Garnetite denoted as red squares (large-$Fe_2O_3$; small-FeO); Clinopyroxene skarn denoted as green circles (large-$Fe_2O_3$; small-FeO). d) Skarnoid and quartzite samples ($FeO_T$ and $Fe_2O_{3T}$). Skarnoid denoted as green hexagons (large-$Fe_2O_3$; small-FeO); Quartzite denoted as yellow circle (large-$Fe_2O_3$) and blue circle (small-FeO). Small black circles for all ternaries represent end-member mineral compositions; an= anorthite, qtz= quartz, cc=calcite, woll= wollastonite, pyr= pyrope garnet, alm= almandine garnet, spe= spessartine garnet, andr= andradite garnet, gross= grossular, hed= hedenbergite, di= diopside.

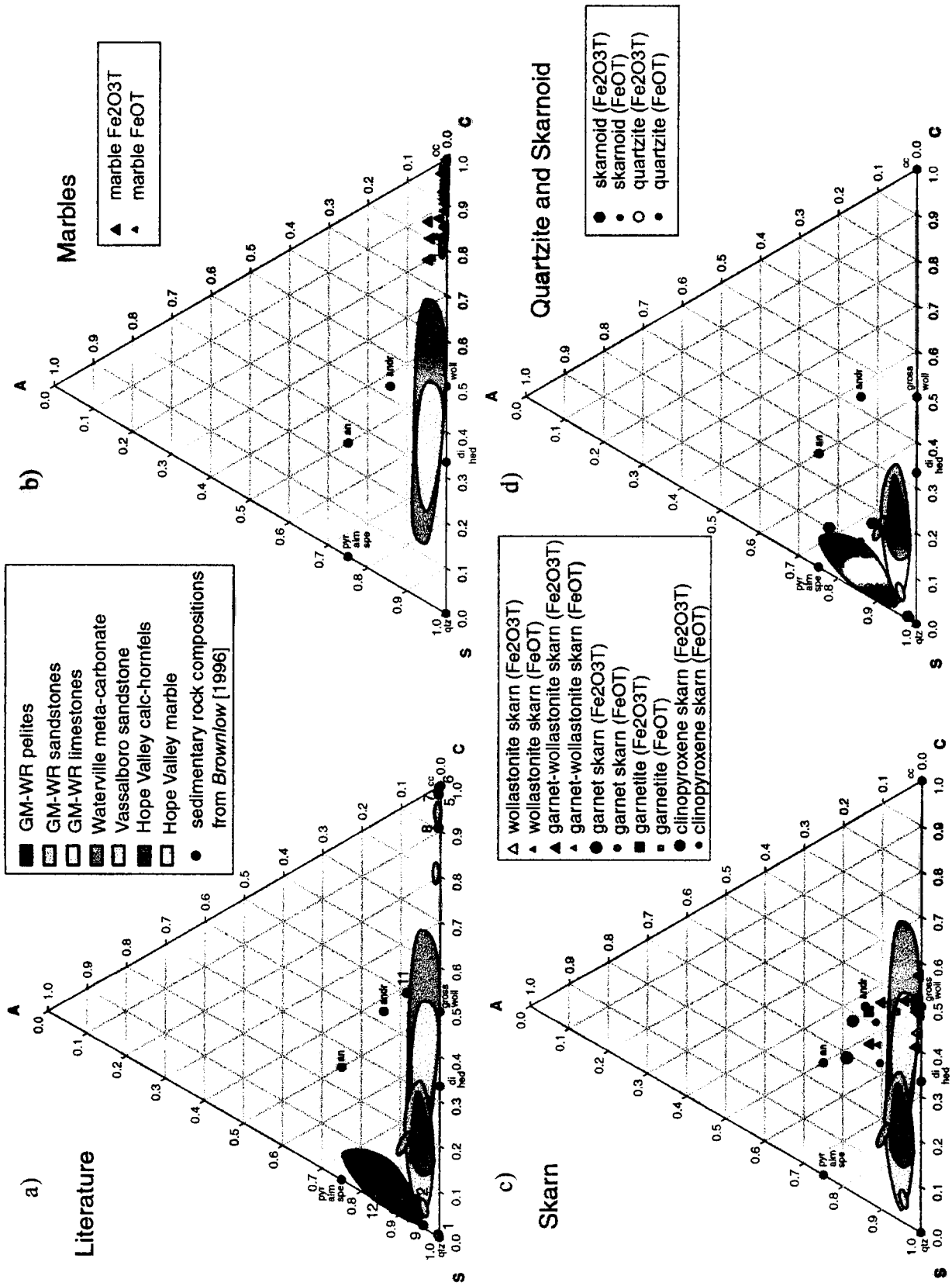


Fig 3.5. ASC ternary diagram (all iron in compiled data converted to FeO)

Fig 3.6. ASF ternary diagrams for a) meta-sedimentary rocks (compiled data converted to FeO). Possible protolith fields were constructed from whole-rock analyses from sandstone, pelite, limestone/marble, and calcareous hornfels from *Ferry* [1988, 1989, 1994]. Light green= micaceous, carbonate-bearing sandstones from the Vassalboro/ Sangerville Formation [*Ferry*, 1988]; bright green= calcareous hornfels from roof pendants at Hope Valley, CA [*Ferry*, 1989], orange= marble from roof pendants at Hope Valley, CA [*Ferry*, 1989]; light pink= limestone from Giles Mountain Formation and Waits River Formation [*Ferry*, 1994], light blue= sandstone from Giles Mountain Formation and Waits River Formation [*Ferry*, 1994], red= pelites from Giles Mountain Formation and Waits River Formation [*Ferry*, 1994], light purple= meta-carbonate rocks from the Waterville Formation [*Ferry*, 1994]. Common sedimentary rock compositions from *Brownlow* [1996] denoted by blue circles; 1. Orthoquartzite, 2. Arkose, 3. Graywacke, 4. Sub-graywacke, 5. Lithographic limestone, 6. Fossiliferous limestone, 7. Oolitic limestone, 8. Dolomite, 9. Si-shale, 10. K-shale, 11. Calcareous shale, 12. Carbonaceous shale. b) Marble samples ($FeO_T$ and $Fe_2O_{3T}$) denoted by blue triangles (small) and blue triangles (large), respectively. c) Skarn samples ($FeO_T$ and $Fe_2O_{3T}$). Wollastonite skarn denoted as yellow triangles (large-$Fe_2O_3$) and blue triangles (small- FeO); Garnet-wollastonite skarn denoted as red triangles (large-$Fe_2O_3$; small-FeO); Garnet skarn denoted as red circles (large-$Fe_2O_3$; small-FeO); Garnetite denoted as red squares (large-$Fe_2O_3$; small-FeO); Clinopyroxene skarn denoted as green circles (large-$Fe_2O_3$; small-FeO). d) Skarnoid and quartzite samples ($FeO_T$ and $Fe_2O_{3T}$). Skarnoid denoted as green hexagons (large-$Fe_2O_3$; small-FeO); Quartzite denoted as yellow circle (large-$Fe_2O_3$) and blue circle (small-FeO). Small black circles for all ternaries represent end-member mineral compositions; an= anorthite, qtz= quartz, cc=calcite, woll= wollastonite, pyr= pyrope garnet, alm= almandine garnet, spe= spessartine garnet, andr= andradite garnet, gross= grossular, hed= hedenbergite, di= diopside.

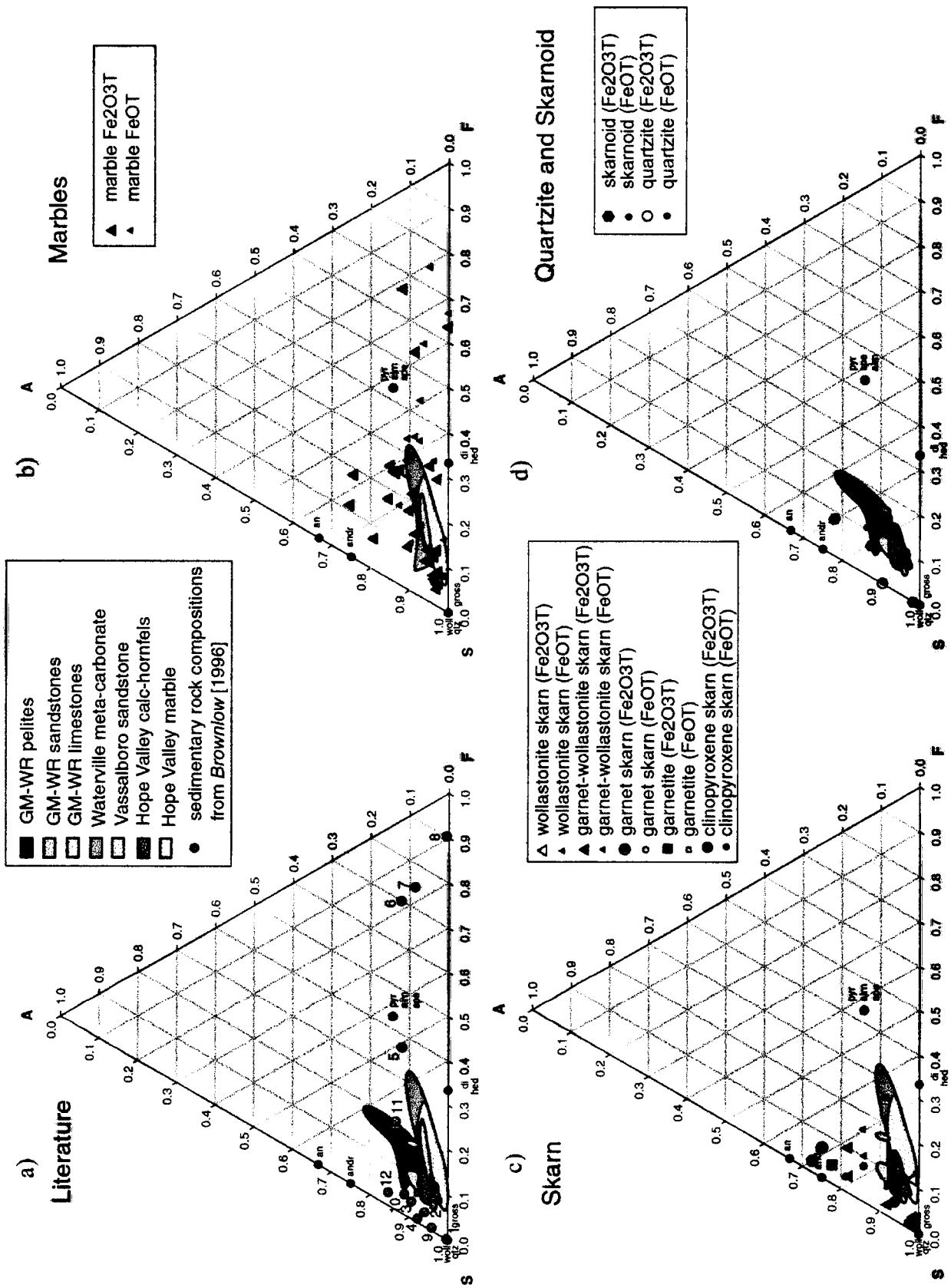


Fig 3.6. ASF ternary diagram (all iron in compiled data converted to FeO)

Fig 3.7. SFC ternary diagrams for a) meta-sedimentary rocks (compiled data converted to FeO). Possible protolith fields were constructed from whole-rock analyses from sandstone, pelite, limestone/marble, and calcareous hornfels from *Ferry* [1988, 1989, 1994]. Light green= micaceous, carbonate-bearing sandstones from the Vassalboro/ Sangerville Formation [*Ferry*, 1988]; bright green= calcareous hornfels from roof pendants at Hope Valley, CA [*Ferry*, 1989], orange= marble from roof pendants at Hope Valley, CA [*Ferry*, 1989]; light pink= limestone from Giles Mountain Formation and Waits River Formation [*Ferry*, 1994], light blue= sandstone from Giles Mountain Formation and Waits River Formation [*Ferry*, 1994], red= pelites from Giles Mountain Formation and Waits River Formation [*Ferry*, 1994], light purple= meta-carbonate rocks from the Waterville Formation [*Ferry*, 1994]. Common sedimentary rock compositions from *Brownlow* [1996] denoted by blue circles; 1. Orthoquartzite, 2. Arkose, 3. Graywacke, 4. Sub-graywacke, 5. Lithographic limestone, 6. Fossiliferous limestone, 7. Oolitic limestone, 8. Dolomite, 9. Si-shale, 10. K-shale, 11. Calcareous shale, 12. Carbonaceous shale. b) Marble samples ($FeO_T$ and $Fe_2O_{3T}$) denoted by blue triangles (small) and blue triangles (large), respectively. c) Skarn samples ($FeO_T$ and $Fe_2O_{3T}$). Wollastonite skarn denoted as yellow triangles (large-$Fe_2O_3$) and blue triangles (small- FeO); Garnet-wollastonite skarn denoted as red triangles (large-$Fe_2O_3$; small-FeO); Garnet skarn denoted as red circles (large-$Fe_2O_3$; small-FeO); Garnetite denoted as red squares (large-$Fe_2O_3$; small-FeO); Clinopyroxene skarn denoted as green circles (large-$Fe_2O_3$; small-FeO). d) Skarnoid and quartzite samples ($FeO_T$ and $Fe_2O_{3T}$). Skarnoid denoted as green hexagons (large-$Fe_2O_3$; small-FeO); Quartzite denoted as yellow circle (large-$Fe_2O_3$) and blue circle (small-FeO). Small black circles for all ternaries represent end-member mineral compositions; an= anorthite, qtz= quartz, cc=calcite, woll= wollastonite, pyr= pyrope garnet, alm= almandine garnet, spe= spessartine garnet, andr= andradite garnet, gross= grossular, hed= hedenbergite, di= diopside.

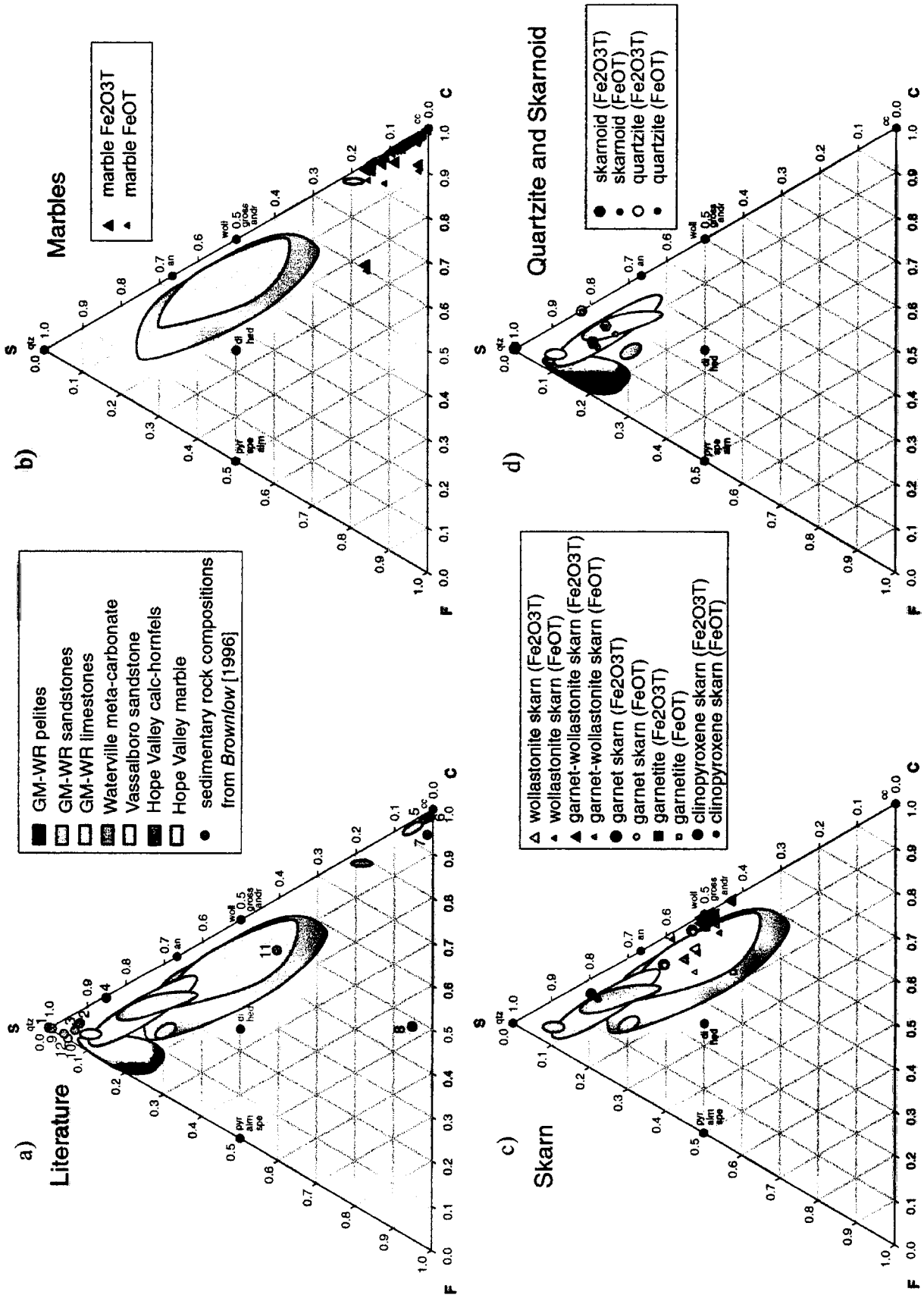


Fig 3.7. SFC ternary diagram (all iron in compiled data converted to FeO)

Fig 3.8. ACF ternary diagrams for a) meta-sedimentary rocks (compiled data converted to FeO). Possible protolith fields were constructed from whole-rock analyses from sandstone, pelite, limestone/marble, and calcareous hornfels from *Ferry* [1988, 1989, 1994]. Light green= micaceous, carbonate-bearing sandstones from the Vassalboro/ Sangerville Formation [*Ferry*, 1988]; bright green= calcareous hornfels from roof pendants at Hope Valley, CA [*Ferry*, 1989], orange= marble from roof pendants at Hope Valley, CA [*Ferry*, 1989]; light pink= limestone from Giles Mountain Formation and Waits River Formation [*Ferry*, 1994], light blue= sandstone from Giles Mountain Formation and Waits River Formation [*Ferry*, 1994], red= pelites from Giles Mountain Formation and Waits River Formation [*Ferry*, 1994], light purple= meta-carbonate rocks from the Waterville Formation [*Ferry*, 1994]. Common sedimentary rock compositions from *Brownlow* [1996] denoted by blue circles; 1. Orthoquartzite, 2. Arkose, 3. Graywacke, 4. Sub-graywacke, 5. Lithographic limestone, 6. Fossiliferous limestone, 7. Oolitic limestone, 8. Dolomite, 9. Si-shale, 10. K-shale, 11. Calcareous shale, 12. Carbonaceous shale. b) Marble samples ($FeO_T$ and $Fe_2O_{3T}$) denoted by blue triangles (small) and blue triangles (large), respectively. c) Skarn samples ($FeO_T$ and $Fe_2O_{3T}$). Wollastonite skarn denoted as yellow triangles (large-$Fe_2O_3$) and blue triangles (small- FeO); Garnet-wollastonite skarn denoted as red triangles (large-$Fe_2O_3$; small-FeO); Garnet skarn denoted as red circles (large-$Fe_2O_3$; small-FeO); Garnetite denoted as red squares (large-$Fe_2O_3$; small-FeO); Clinopyroxene skarn denoted as green circles (large-$Fe_2O_3$; small-FeO). d) Skarnoid and quartzite samples ($FeO_T$ and $Fe_2O_{3T}$). Skarnoid denoted as green hexagons (large-$Fe_2O_3$; small-FeO); Quartzite denoted as yellow circle (large-$Fe_2O_3$) and blue circle (small-FeO). Small black circles for all ternaries represent end-member mineral compositions; an= anorthite, qtz= quartz, cc=calcite, woll= wollastonite, pyr= pyrope garnet, alm= almandine garnet, spe= spessartine garnet, andr= andradite garnet, gross= grossular, hed= hedenbergite, di= diopside.

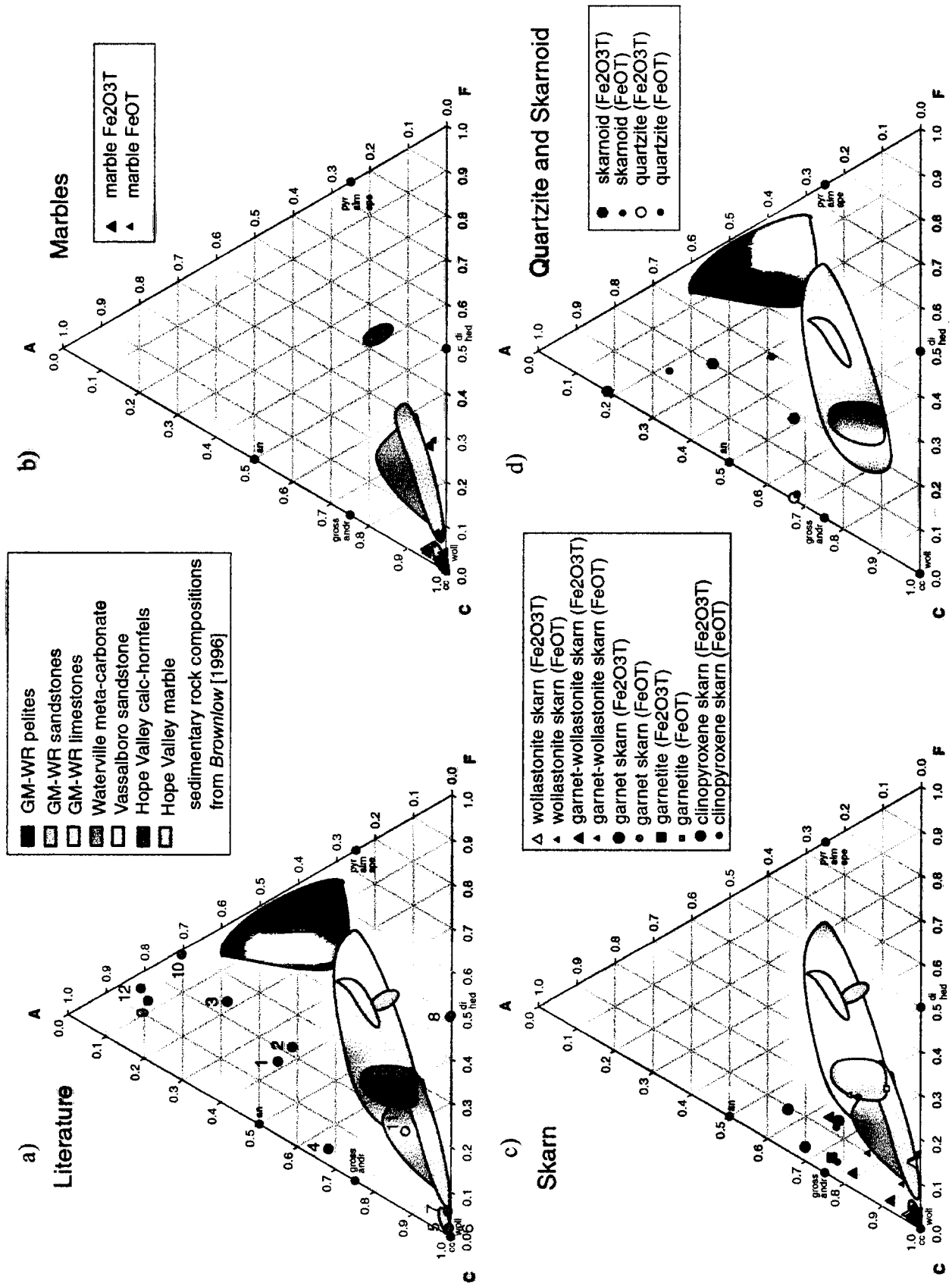


Fig 3.8. ACF ternary diagram (all iron in compiled data converted to FeO)

Table 3.4. Chemical compositions of common sedimentary rocks [*Brownlow*, 1996]. Data reported in grams.

| Lithology abbreviation | orthoquartzite 1 | arkose 2 | graywacke 3 | sub-graywacke 4 | lithographic limestone 5 | fossiliferous limestone 6 | oolitic limestone 7 | dolomite 8 | Si-shale 9 | K-shale 10 | calcareous shale 11 | carbonaceous shale 12 |
|---|---|---|---|---|---|---|---|---|---|---|---|---|
| $SiO_2$ | 99.54 | 72.21 | 68.84 | 65 | 1.15 | 0.29 | 0.75 | 3.24 | 84.14 | 56.29 | 25.05 | 51.03 |
| $TiO_2$ | 0.03 | 0.22 | 0.25 | - | - | - | 0.03 | - | 0.22 | 0.64 | - | - |
| $Al_2O_3$ | 0.35 | 10.69 | 14.54 | 9.57 | 0.45 | 0.26 | 0.25 | 0.17 | 5.79 | 19.22 | 8.28 | 13.47 |
| $Fe_2O_3$ | 0.09 | 0.8 | 0.62 | 1.59 | - | 0.11 | 0.64 | 0.17 | 1.21 | 4.39 | 0.27 | 8.06 |
| FeO | - | 0.72 | 2.47 | 1.08 | 0.26 | - | - | 0.06 | - | - | 2.41 | - |
| MnO | - | 0.22 | - | - | - | 0.01 | - | - | - | - | 4.11 | - |
| MgO | 0.06 | 1.47 | 1.94 | 0.4 | 0.56 | 0.7 | 2.14 | 20.84 | 0.41 | 1.65 | 2.61 | 1.15 |
| CaO | 0.19 | 3.85 | 2.23 | 10.1 | 53.8 | 55.53 | 52.3 | 29.58 | 0.31 | 0.09 | 27.87 | 0.78 |
| $Na_2O$ | - | 2.3 | 3.88 | 2.14 | 0.07 (tot) | 0.07 | 0.01 | - | 0.99 | 0.19 | - | 0.41 |
| $K_2O$ | - | 3.32 | 2.68 | 1.43 | ---- | 0.02 | 0.04 | - | 0.5 | 10.85 | - | 3.16 |
| $P_2O_5$ | - | 0.1 | 0.15 | - | - | 0.05 | - | - | - | - | 0.08 | 0.31 |
| H2O+ | 0.25 | 1.46 | 1.6 | 0.82 | 0.69 | - | 0.5 (tot) | 0.3 (tot) | 5.56 (tot | 2.04 | 2.86 | 0.81(tot) |
| H2O- | - | 0.08 | 0.35 | 0.23 | 0.23 | - | ---- | ---- | ---- | 3.54 | 1.44 | - |
| CO2 | - | 2.66 | 0.14 | 6.9 | 42.69 | 43.42 | 43.54 | 45.54 | - | - | 24.2 | - |
| SO3 | - | - | 0.15 | 0.04 | - | 0.15 | - | - | - | 0.72 | - | - |

almandine), calcic-clinopyroxene (diopside and hedenbergite), wollastonite, anorthite, calcite, and quartz. End-member compositions are listed in Table 3.5.

### 3.2.1 Inter-laboratory comparison

Thirty-one rock powders were sent to Geochemical Laboratories at McGill University and forty-two rock powders were sent to ALS Chemex in North Vancouver, British Columbia for whole-rock geochemical analysis. Repeated analyses of blind samples were submitted to ALS Chemex in order to compare the results reported by each laboratory. These samples included two marble samples, W1d(mb) and UBM1a, and five wollastonite skarn samples, W1a, W1b, W1c, W1d(w), and UB4e.

Inter-laboratory comparisons of absolute abundances, relative abundances and relative abundances in respect to the detection limit between ALS Chemex and McGill University were examined. ALS Chemex gives systematically lower abundances of $TiO_2$, $Fe_2O_3$, MnO, and MgO and systematically higher abundances of $Al_2O_3$ and V than McGill University (Figs. 3.9-3.11). Mean variability and standard deviation of each comparable element is presented in Table 3.6. The evaluations reveal that analyses between labs should not be compared when looking at element ratios because inter-laboratory variation would introduce significant error, especially since relatively immobile elements (i.e. $TiO_2$ and $Al_2O_3$) occur in such low abundance. On the other hand, these variable element oxides are low enough in abundance that analyses between labs can be compared in ternary projections in order to distinguish between the geochemistry of different unit types (Figs. 3.12-3.15).

## 3.3 Intrusive rocks

The chemical components of eleven samples of intrusive rocks were examined in order to classify their composition. Three rock powders from the Crowston Lake Pluton were analyzed

Table 3.5. End member chemical formulas for selected minerals

**Garnet Group**

| | |
|---|---|
| grossular | $Ca_3Al_2Si_3O_{12}$ |
| andradite | $Ca_3Fe_2Si_3O_{12}$ |
| pyrope | $Mg_3Al_2Si_3O_{12}$ |
| almandine | $Fe_3Al_2Si_3O_{12}$ |
| spessartine | $Mn_3Al_2Si_3O_{12}$ |

**Calcic-clinopyroxene**

| | |
|---|---|
| diopside | $CaMgSi_2O_6$ |
| hedenbergite | $CaFeSi_2O_6$ |

**Other minerals**

| | |
|---|---|
| wollastonite | $CaSiO_3$ |
| anorthite | $CaAlSi_2O_8$ |
| calcite | $CaCO_3$ |
| quartz | $SiO_2$ |

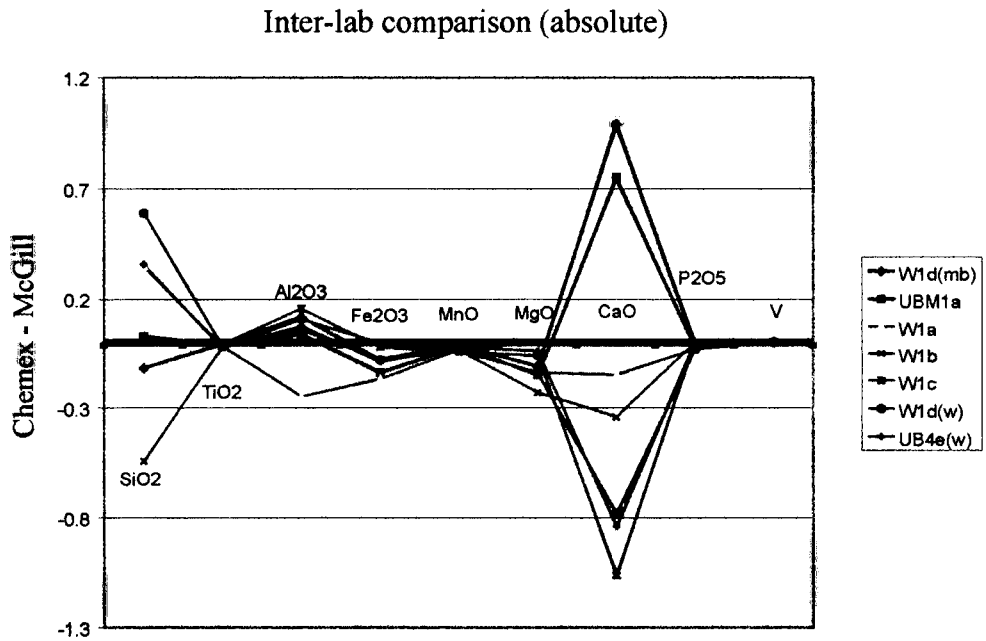


Fig 3.9. Inter-laboratory comparison of absolute abundances from data reported by McGill University and ALS Chemex. Red lines denote wollastonite skarn; blue lines denote marble.

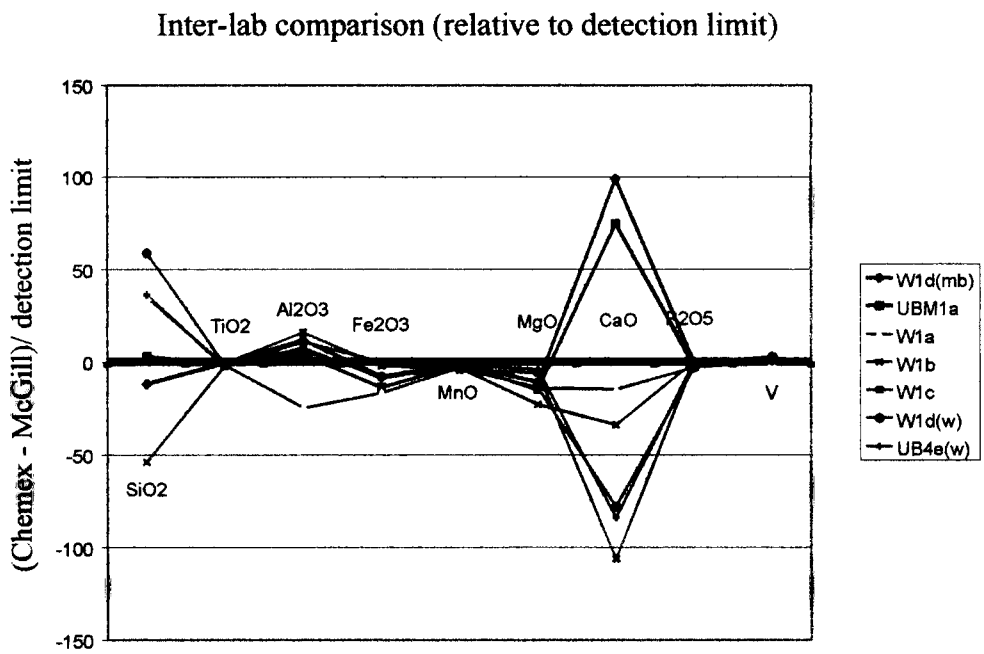


Fig 3.10. Inter-laboratory comparison of relative abundances in respect to detection limit from data analyzed by McGill University and ALS Chemex. Red lines denote wollastonite skarn; blue lines denote marble.

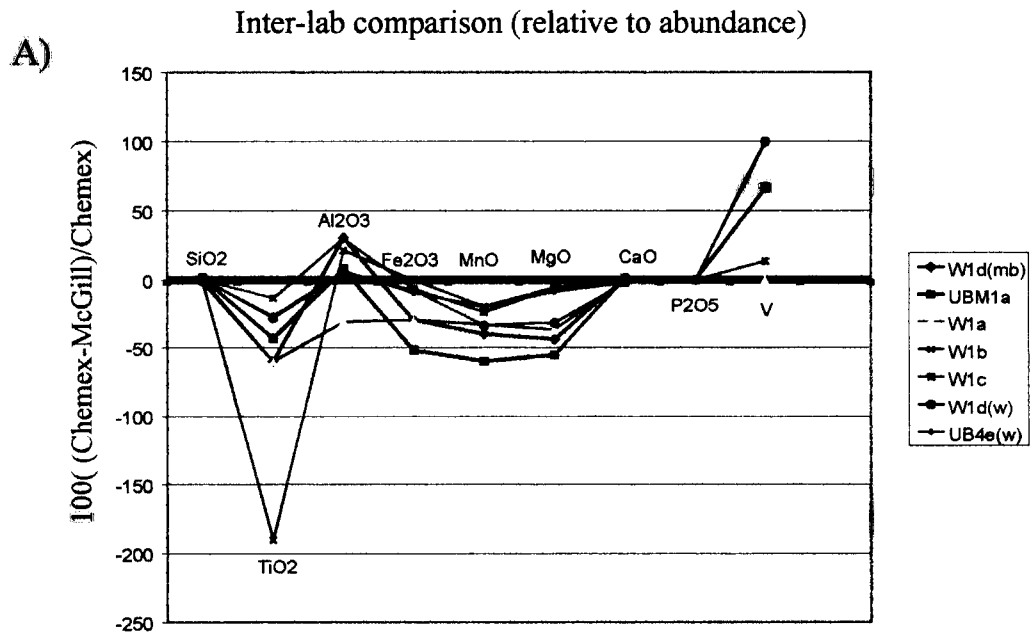


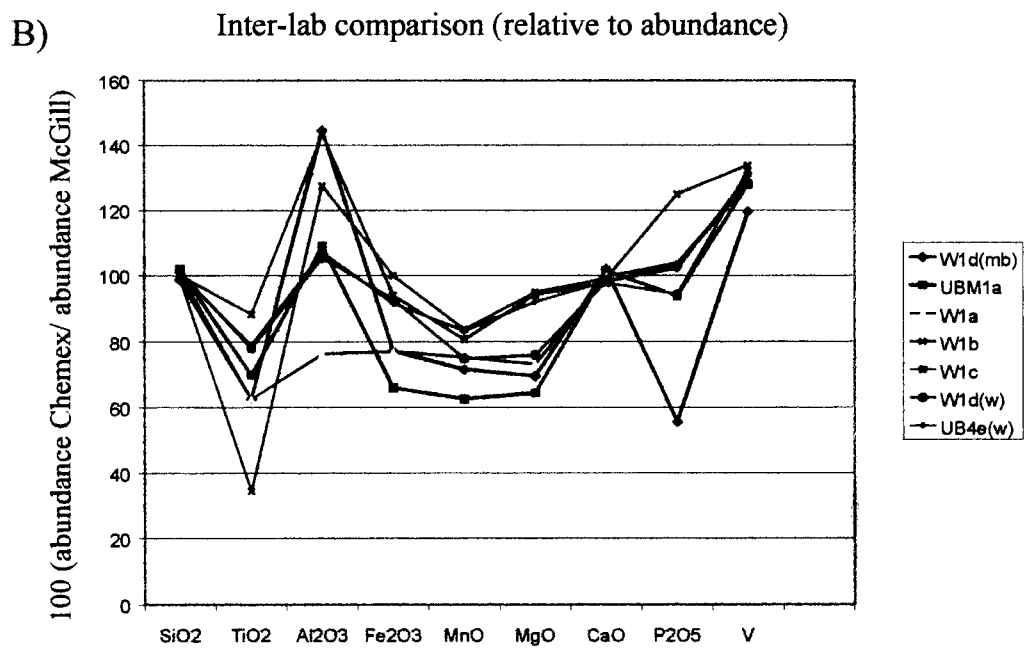


Fig. 3.11. A) Inter-laboratory comparison of relative abundances from data reported by McGill University and ALS Chemex. Red lines denote wollastonite skarn; blue lines denote marble. B) Inter-laboratory comparison of relative abundances from data reported by McGill University and ALS Chemex. Red lines denote wollastonite skarn; blue lines denote marble.

Table 3.6. Mean variability of compared inter-laboratory elements and cooresponding standard deviation (bold).

| | $SiO_2$ | | $TiO_2$ | | $Al_2O_3$ | | $Fe_2O_3$ | | MnO | | MgO | | CaO | | $P_2O_5$ | | V | |
|---|---|---|---|---|---|---|---|---|---|---|---|---|---|---|---|---|---|---|
| absolute | 0.10 | **0.37** | -0.01 | **0.01** | 0.05 | **0.14** | -0.08 | **0.06** | -0.03 | **0.01** | -0.12 | **0.06** | -0.20 | **0.80** | -0.01 | **0.01** | 0.00 | **0.01** |
| relative to detection limit | 9.71 | **0.40** | -1.44 | **0.01** | 4.57 | **0.15** | -8.29 | **0.07** | -2.83 | **0.01** | -12.43 | **0.07** | -20.43 | **0.66** | -1.14 | **0.02** | 2.00 | **0.01** |
| relative to abundance (a) | 0.31 | **0.44** | -60.24 | **0.01** | 10.17 | **0.16** | -19.25 | **0.07** | -32.85 | **0.01** | -26.91 | **0.08** | -0.56 | **0.38** | 0.00 | **0.00** | 68.61 | **0.01** |
| relative to abundance (b) | 100.32 | **0.49** | 67.76 | **0.01** | 116.11 | **0.04** | 85.48 | **0.04** | 75.96 | **0.01** | 80.55 | **0.09** | 99.46 | **0.30** | 96.77 | **0.02** | 128.65 | **0.01** |

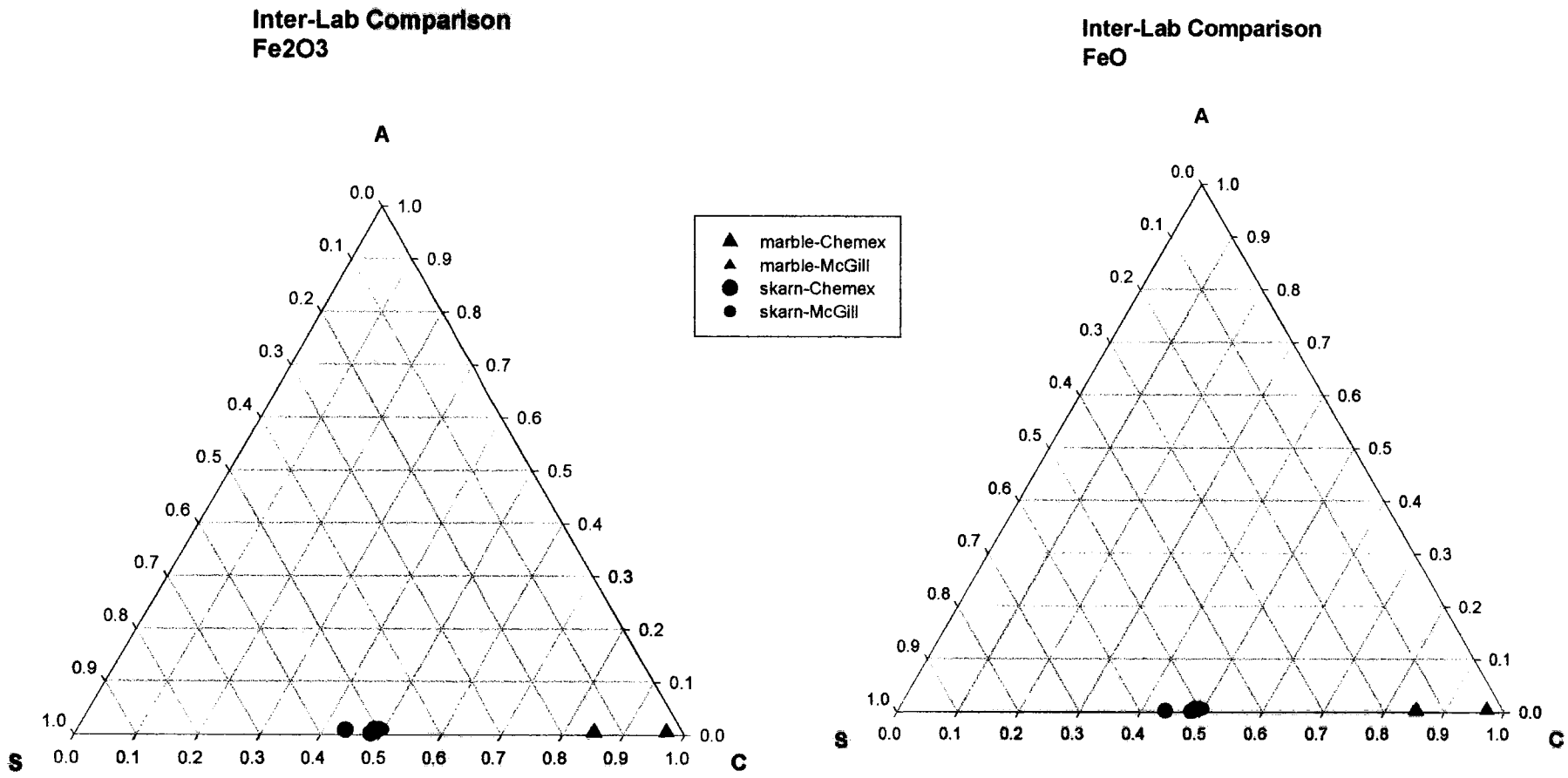


Fig 3.12. ASC ternary projections for samples submitted to McGill University and ALS Chemex for geochemical analysis.

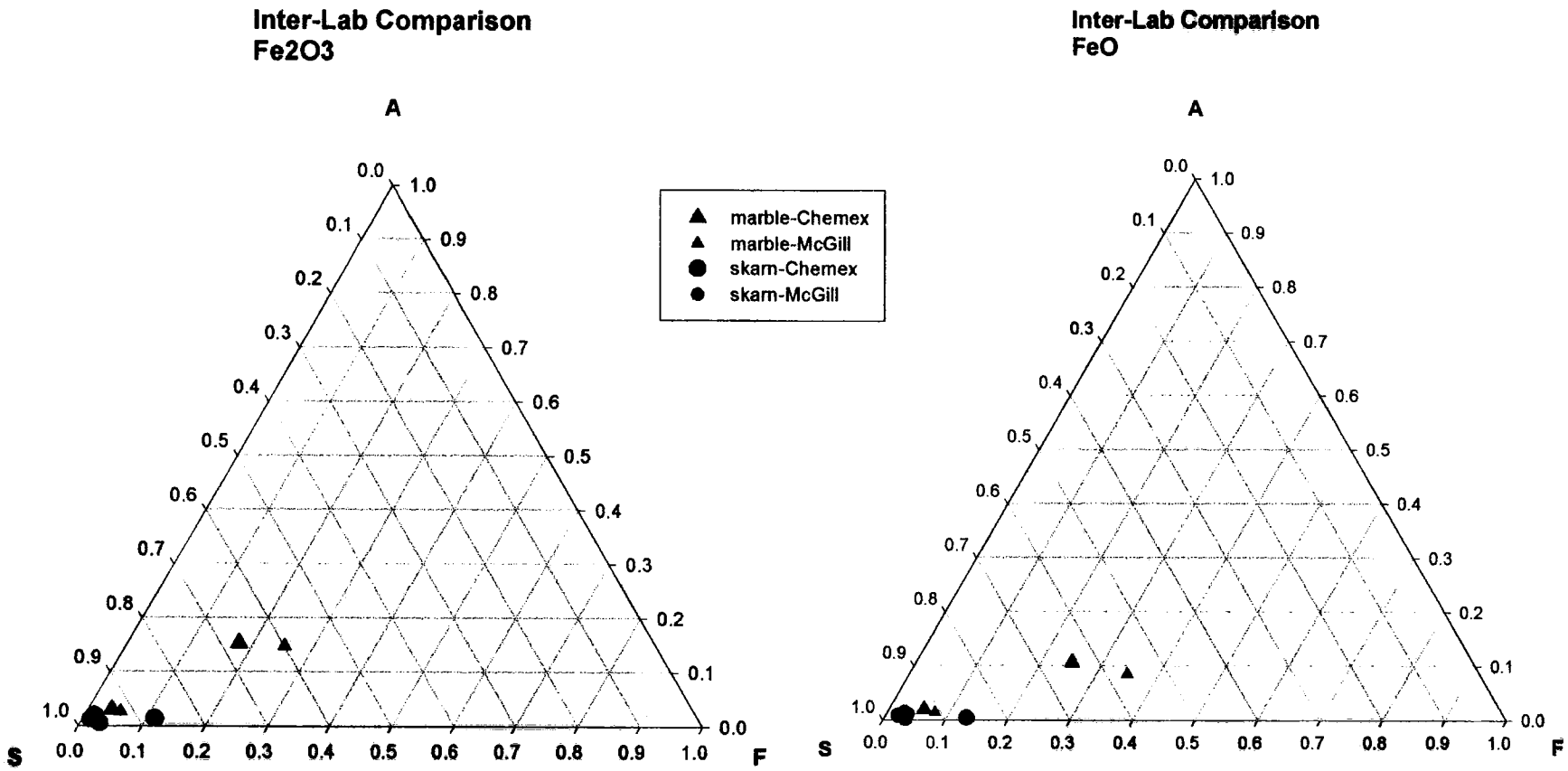


Fig 3.13. ASF ternary projections for samples submitted to McGill University and ALS Chemex for geochemical analysis.

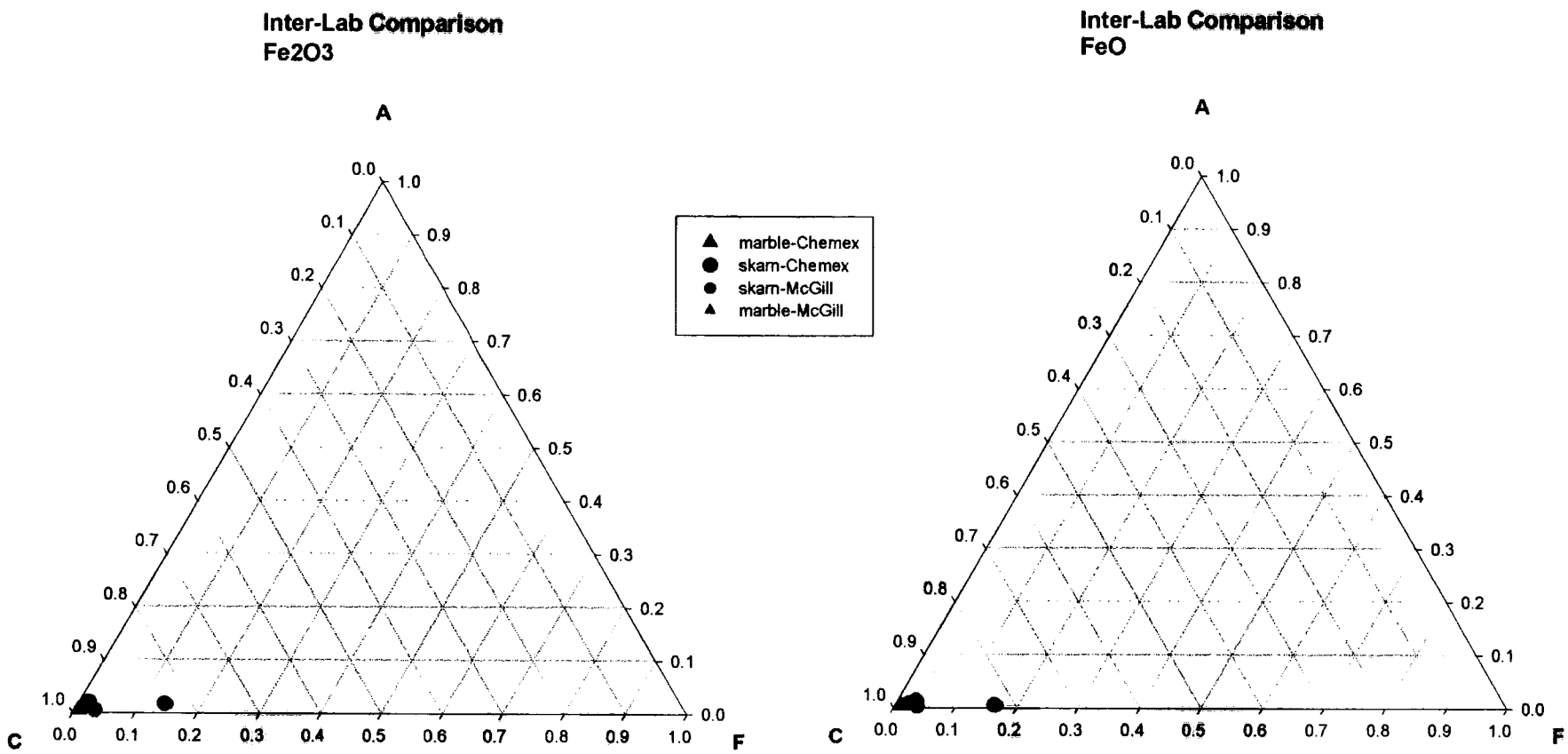


Fig 3.14. ACF ternary projections for samples submitted to McGill University and ALS Chemex for geochemical analysis.

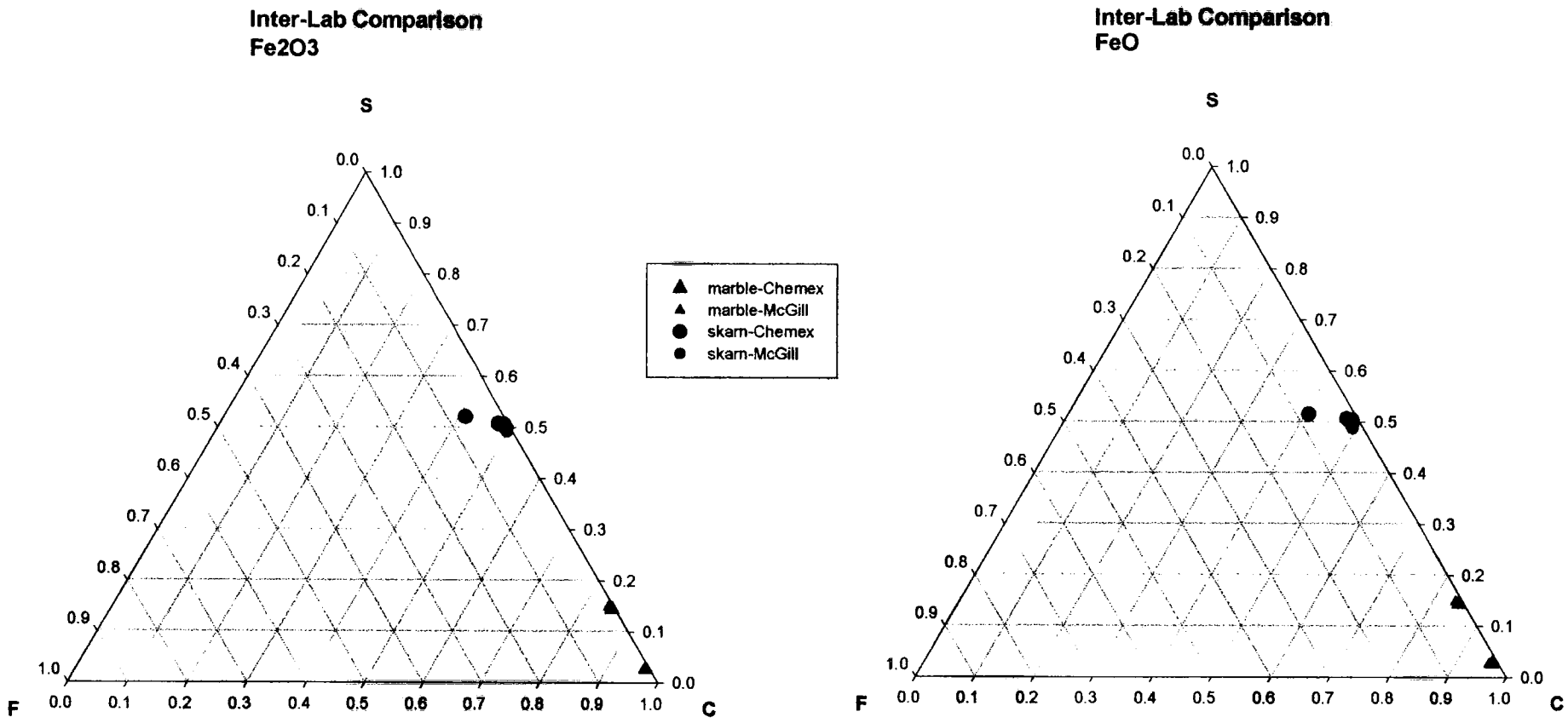


Fig 3.15. SFC ternary projections for samples submitted to McGill University and ALS Chemex for geochemical analysis.

for major element oxides plus $Cr_2O_3$, Sc, V, and Zn by XRF. Whole rock analyses are graphically represented by plots created in NEWPET. The data collected in the course of this study (open symbols) is augmented with the data of *Ray and Kilby* [1996] (closed symbols). Their data is tabulated in Table 3.3. The Crowston Lake Pluton is calc-alkaline (with the exception of sample MB1b) and sub-alkaline (Fig. 3.16(a,b)). The Crowston Lake Pluton is a gabbro (Fig. 3.16c), however data from *Ray and Kilby* [1996] indicate a variation from gabbro to quartz diorite. The samples analyzed by *Ray and Kilby* [1996] derive, in part, from localities outside of the map area and therefore may be more representative of the pluton as a whole. This study sampled no further than 20 meters from the pluton-wall rock contact, and might represent a mafic part of the pluton. The mafic character of pluton rocks within the study area might reflect an early phase of crystallization or interaction with carbonate wall rocks [cf. *Westphal et al.*, 1999]. The pluton is metaluminous (Fig. 3.17), thus $K_2O + Na_2O < Al_2O_3 < K_2O + Na_2O + CaO$ [*Hess*, 1989].

The first dike and sill generation (D1), which is temporally and genetically related to the Crowston Lake Pluton [*Ray and Kilby*, 1996] is gabbro in composition (Fig. 3.16c). It has a similar composition to the Crowston Lake Pluton, however is slightly enriched in $SiO_2$, $Na_2O$, and $K_2O$ and is slightly depleted in $Al_2O_3$, $Fe_2O_3$, MgO, and CaO.

The second dike and sill generation (D2) is dominant in the axis of a regional fold interpreted as a result of field mapping (Fig. 1.8). The second dike and sill generation is chemically, mineralogically and texturally distinct from the gabbroic dikes and sills related to the Crowston Lake Pluton, however it is uncertain if the two are related as no isotopic dating has been done on the intrusives at Mineral Hill. Three rock powders were analyzed for ten major element oxides plus $Cr_2O_3$, Sc, V, Zn by XRF. Whole-rock analyses are graphically represented by plots created in NEWPET. The D2 dikes and sills are calc-alkaline and sub-alkaline (Fig. 3.18(a, b)). Compositionally, the D2 dikes and sills are tonalitic and metaluminous (Figs. 3.18c

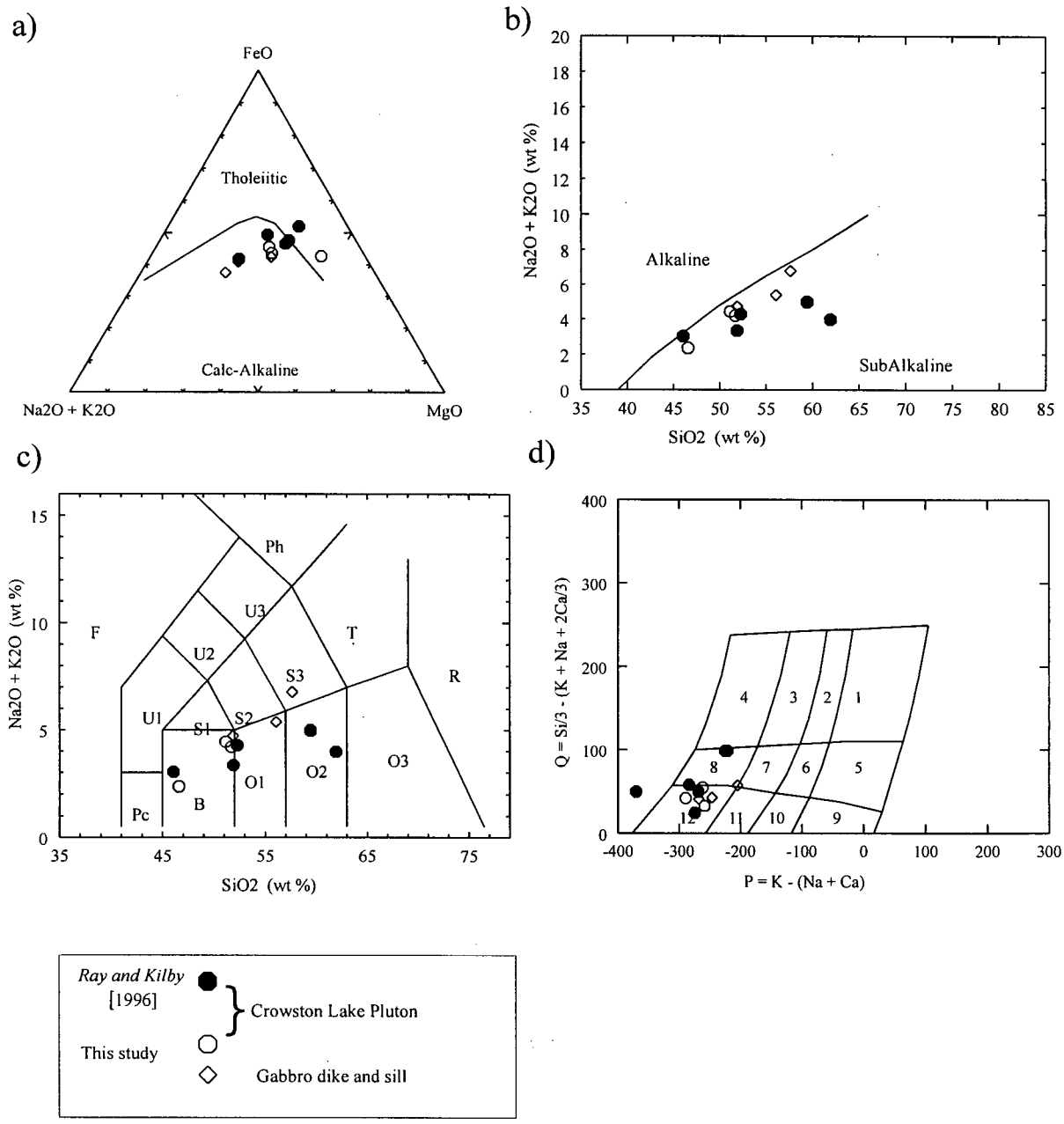


Fig. 3.16. a) AFM diagram for Crowston Lake pluton and gabbroic dike and sill compositions after *Irvine and Baragar* [1971]. b)Alkali vs. Silica for Crowston Lake pluton and gabbroic dike and sill compositions after *Irvine and Baragar* [1971]. c) Na2O vs. SiO2 composition diagram for Crowston Lake pluton and gabbroic dikes and sills after *Le Maitre* [1989]; Rock Compositions: F= foidite, Pc= picrobasalt, B= basalt, O1= basaltic andesite, O2= andesite, O3= dacite, R= rhyolite, S1= trachybasalt, S2= basaltic trachyandesite, S3= trachyandesite, T= trachyte, U1= tephrite basanite, U2= phonotephrite, U3= tephriphonolite, Ph= phonolite. D) Q vs. P composition diagram for Crowston Lake pluton and gabbroic dikes and sills after *Debon and Le Fort* [1983]; Rock compositions: 1. Granite, 2. Adamellite, 3. Granodiorite 4. Tonalite, 5. Quartz syenite, 6. Quartz monzonite, 7. Quartz monzodiorite, 8. Quartz diorite, 9. Syenite, 10. Monzonite, 11. Monzogabbro, 12. Gabbro.

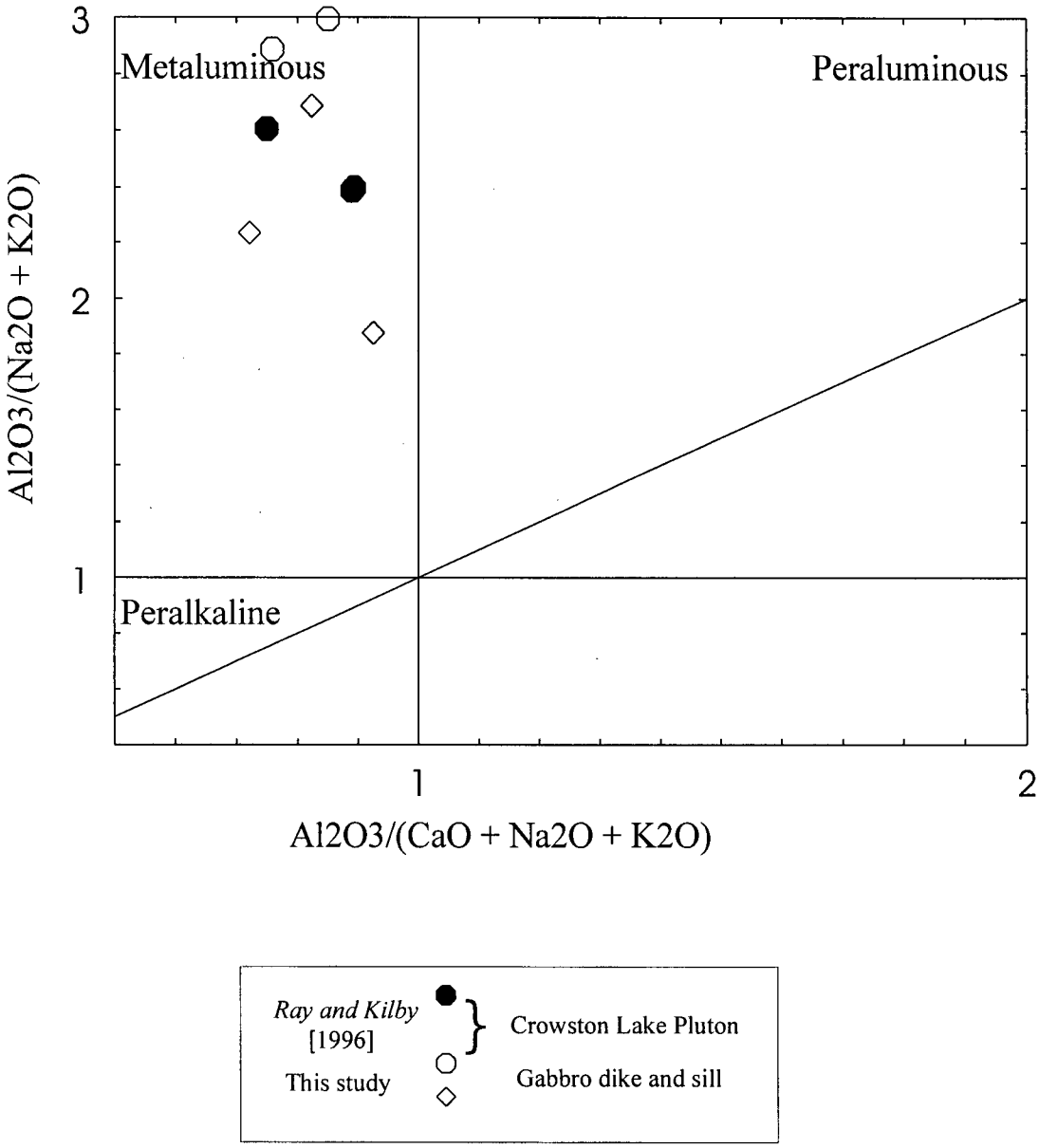


Fig. 3.17. Metaluminous compositions for Crowston Lake pluton and gabbroic dikes after *Maniar & Piccoli* [1989].

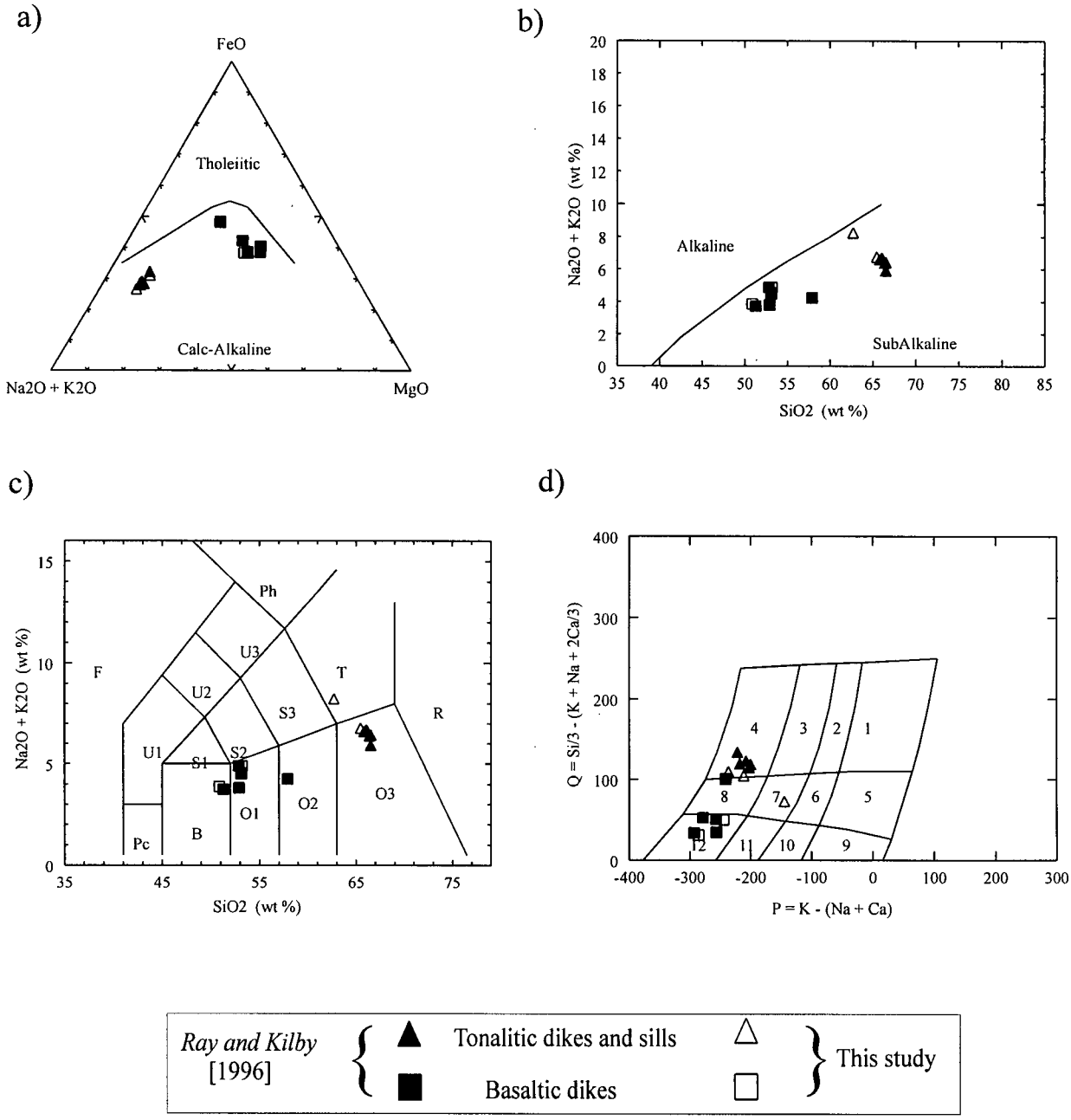


Fig. 3.18. a) AFM diagram for tonalitic and basaltic dike compositions after *Irvine and Baragar* [1971]. b)Alkali vs. Silica for tonalitic and basaltic dike compositions after *Irvine and Baragar* [1971]. C) Na2O vs. SiO2 composition diagram for tonalitic and basaltic dikes after *Le Maitre* [1989]; Rock Compositions: F= foidite, Pc= picrobasalt, B= basalt, O1= basaltic andesite, O2= andesite, O3= dacite, R= rhyolite, S1= trachybasalt, S2= basaltic trachyandesite, S3= trachyandesite, T= trachyte, U1= tephrite basanite, U2= phonotephrite, U3= tephriphonolite, Ph= phonolite. d) Q vs. P composition diagram for tonalitic and basaltic dikes after *Debon and Le Fort* [1983]; Rock compositions: 1. granite, 2. adamellite, 3. granodiorite 4. Tonalite, 5. quartz syenite, 6. quartz monzonite, 7. quartz monzodiorite, 8. quartz diorite, 9. syenite, 10. monzonite, 11. monzogabbro, 12. gabbro.

and 3.19). The data suggests that the tonalitic dikes and sills could be silica enriched counterparts to the gabbroic dikes and sills. However, because their temporal relationship is unclear, their genetic relationship cannot be definitely determined.

Likewise, the third generation dikes (D3) are dominant in the axis of a regional fold interpreted as a result of field mapping (Fig. 1.8). D3 are calc-alkaline and sub-alkaline (Fig. 3.18 (a, b)) and vary from basalt to basaltic-andesites (Fig. 3.18c). The basalt dikes are metaluminous, however are enriched in $Al_2O_3$ as compared to the tonalitic dikes and sills (Fig. 3.19).

### 3.4 Meta-sedimentary and skarn units

Skarn samples (N=11), including garnet-wollastonite skarn, garnetite, clinopyroxene skarn and wollastonite skarn; marble (N=7); calc-silicate skarnoid (N=1) and quartzite (vein?) (N=1) sample(s) were analyzed by XRF at Geochemical Laboratories at McGill University. Additional samples (N=42) were analyzed by XRF and ICP-MS at ALS Chemex Ltd., including marble (N=22), wollastonite skarn (N=16), garnet skarn (N=2), and calc-silicate skarnoid (N=2) samples. Oxide and element abundances were converted to molar quantities, calculated for S', A', C', and F', normalized to 100 percent, and projected onto ternary diagrams. All geochemical data was plotted using total iron as $Fe_2O_{3T}$ (large symbols) and $FeO_T$ (small symbols) in Figs. 3.1-3.8.

Seven meta-sedimentary rocks from geochemical analyses from the literature [*Ferry*, 1988, 1989, and 1994], were also projected onto ASC, ASF, ACF, and SFC ternary diagrams as graphical comparisons to the meta-sedimentary and skarn samples analyzed at Mineral Hill. These fields represent micaceous, carbonate-bearing sandstones from the Sangerville Formation [*Ferry*, 1988], meta-carbonate rocks from the Waterville Formation [*Ferry*, 1994], limestone, sandstone, pelites and their metamorphic equivalents from Giles Mountain and Waits River

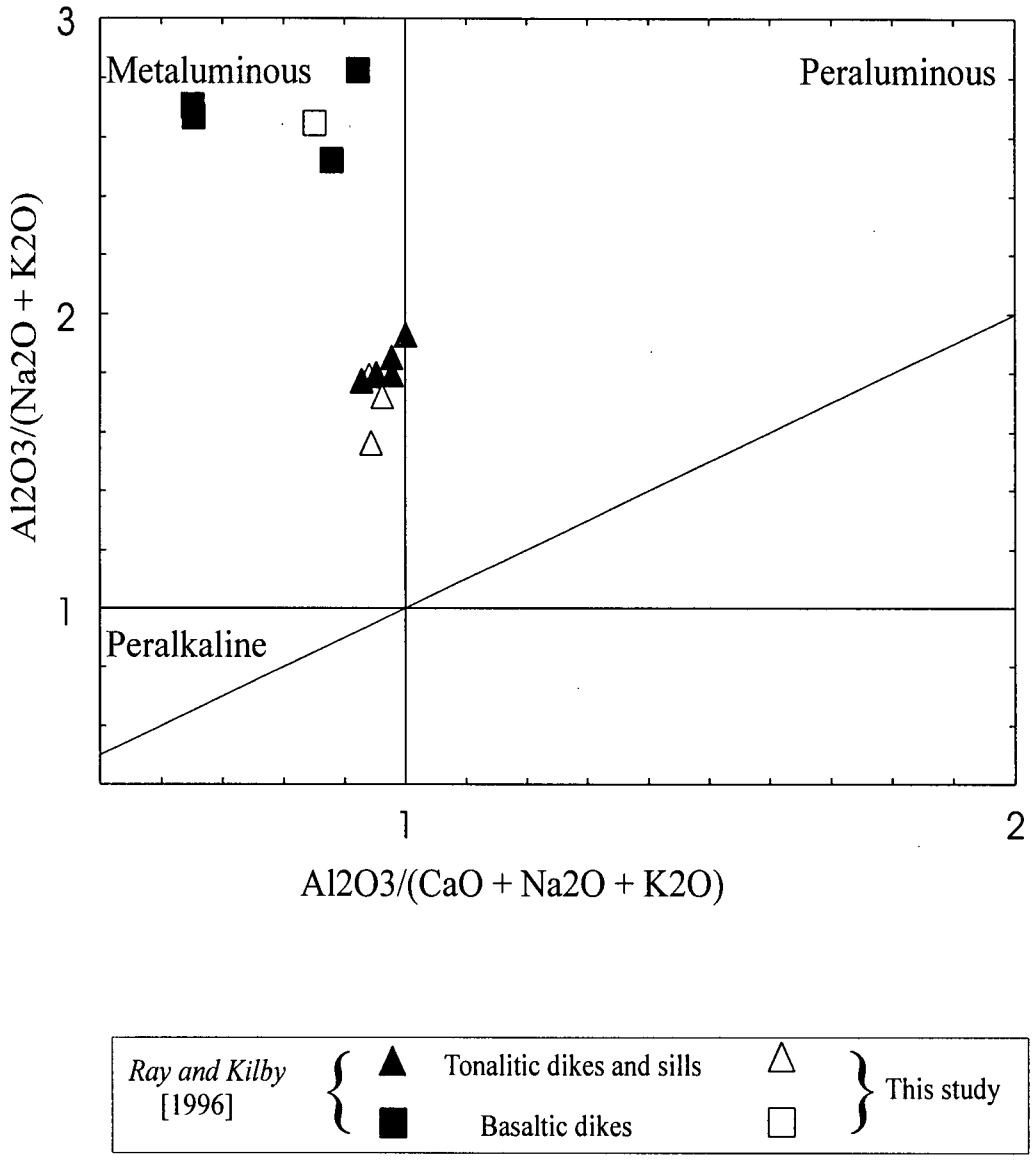


Fig. 3.19. Metaluminous compositions for tonalitic and basaltic dikes after *Maniar & Piccoli* [1989].

Formations [*Ferry*, 1994], and calcareous hornfels and marbles from roof pendants at Hope Valley, CA [*Ferry*, 1989]. Chemical compositions for all meta-sedimentary units were converted to molar quantities, normalized to 100 percent, and projected onto ASC, ASF, ACF, and SFC ternary diagrams (as described in *Method of Investigation*). The range of composition for each type of meta-sediment is represented by a field in Figs. 3.1-3.8. Chemical compositions from twelve common sedimentary rock types compiled by *Brownlow* [1996] were also projected onto the ternary diagrams representing literature fields. These analyses were not added to the plots that project data from Mineral Hill in order to avoid clutter.

Finally, end-member chemical compositions of grossular, andradite, spessartine, pyrope, almandine, diopside, hedenbergite, wollastonite, anorthite, calcite and quartz were projected onto all constructed ternary diagrams.

The following section is two-fold: (1) to describe the geologic setting and mineralogy of each meta-sedimentary field from the literature and significant geochemical trends, and (2) to discuss geochemical trends of meta-sedimentary and skarn units from Mineral Hill observed in ternary diagrams as well as any distinguishing geochemical characteristics between units (as classified petrographically), and relationship to literature fields.

### 3.4.1 Meta-sedimentary Rock Compositions

***Vassalboro/ Sangerville Formation***

Chemical compositions for micaceous, carbonate-bearing sandstones from the Silurian Sangerville (formerly Vassalboro) Formation, south-central Maine are tabulated in *Ferry* [1988, p. 6 ]. The meta-sediments are isoclinally folded by deformation that preceded the peak of metamorphism, both which occurred during the Acadian Orogeny [*Osberg*, 1979, *Dallmeyer and Van Breeman*, 1981; *Ferry*, 1988]. The sandstones are classified under four mineral assemblages which correspond to metamorphism in the amphibolite facies at peak conditions:

**Assemblage A**: calcite + ankerite + muscovite + quartz + albite +/- chlorite
**Assemblage B**: biotite + quartz + plagioclase +/- ankerite +/- calcite +/- chlorite +/- muscovite
**Assemblage C**: calcic-amphibole + biotite + chlorite + calcite + quartz + plagioclase
**Assemblage D**: clinozoisite + diopside + calcic-amphibole + calcite + quartz + plagioclase +/- garnet +/- microcline

### *Waterville Formation*

Chemical compositions of meta-carbonate rocks of the Silurian Waterville Formation, south-central Maine are tabulated in *Ferry* [1994, p. 928]. The meta-sediments were isoclinally folded in the same deformation event as the Sangerville Formation and regionally metamorphosed during the Acadian Orogeny. Two limestones were differentiated and analyzed in the Waterville Formation; folded limestones and thin limestones (interbedded with a sandy-to-pelitic package).

The mineralogy of the folded limestones includes muscovite, biotite, chlorite, ankerite, calcite, plagioclase, quartz, rutile, pyrrohotite, and chalcopyrite. The thin limestones show mineral evolution with increasing metamorphic grade. Zones are based on mineral assemblages in pelites and correspond to greenschist-amphibolite facies conditions:

**chlorite zone**: muscovite + ankerite + albite + quartz + rutile + accessory sulfides + chlorite or calcite (but not both)
**biotite zone**: muscovite + biotite + chlorite + calcite + plagioclase + quartz + ilmenite + accessory sulfides +/- ankerite
**garnet zone**: biotite + chlorite + calcite + plagioclase + quartz + garnet + ilmenite + accessory sulfides +/- calcic-amphibole
**staurolite-andalusite zone**: calcic-amphibole + chlorite + calcite + plagioclase (calcic) + quartz + garnet + ilmenite + accessory sulfides +/- biotite

### *Giles Mountain and Waits River Formations*

Chemical compositions for limestone, sandstone, and pelitic units of the Siluro-Devonian Giles Mountain and Waits River Formations, east-central Vermont are tabulated in *Ferry* [1994, p.930-931]. Stratigraphically, the Waits River Formation is overlain by the Giles Mountain Formation. Similarly to the sediments studied in south-central Maine, these rocks were folded

and regionally metamorphosed during the Acadian Orogeny. Because analogous rock types are found in the Giles Mountain and Waits River Formation, their geochemical analyses were grouped together to represent three fields; limestone, sandstone, and pelite.

The Giles Mountain Formation is composed of interbedded pelites, micaceous sandstones, and minor micaceous carbonate rocks (limestones). The Waits River Formation is composed of interbedded micaceous limestone and pelites (and their metamorphic equivalents). All packages within the Giles Mountain and Waits River Formation show mineral evolution with increasing metamorphic grade. For simplicity, these are compiled in Table 3.7.

Table 3.7. Mineral evolution of Giles Mountain (GM) and Waits River (WR) sediments

| **Formation** | **GM** | **WR** | **GM** | **WR** | **GM** |
|---|---|---|---|---|---|
| **Rock type** | **limestones** | **limestones** | **pelite** | **pelite** | **sandstone** |
| **Chlorite zone** | musc, ank, cc, alb, qtz, rut, sulfides | musc, par, ank, cc, alb, qtz, rut, sulfides +/- chl | musc, chl, ank, alb, qtz, rut, sulfides, +/- siderite | musc, chl, ank, pl, qtz, rut, +/- ilm, +/- par | musc, ank, alb, qtz, rut, sulfides, (chl or cc) |
| **Biotite zone** | musc, ank, cc, qtz, sulfides +/ (rut or ilm), +/- (alb or olig) | musc, ank, cc, olig, qtz, rut, sulfides +/- chl | musc, chl, bt, ilm, olig, qtz, rut, ank, sulfides | n/a | musc, bt, ilm, ank, olig, qtz, rut, sulfides, (chl or cc) |
| **Garnet zone** | musc, gnt, ank, cc, pl, qtz, sulfides, rut a/o ilm, +/- bt | musc, ank, cc, olig, qtz, rut, sulfides +/- chl | musc, bt, chl, gnt, pl, qtz, ilm, sulfides, +/- rut | musc, bt, chl, gnt, ank, pl, qtz, ilm, sulfides | musc, bt, chl, gnt, pl, qtz, ilm, sulfides, (ank or cc), +/- rut |
| **Kyanite zone** | musc, gnt, ank, cc, pl, qtz, sulfides, chl, rut a/o ilm, +/- bt | musc, bt, chl, ank, cc, pl, qtz, rut, sulfides, +/ calc-amph (replacing musc) | n/a | musc, bt, chl, gnt, pl, qtz, ilm, sulfides, rut, cc, st, ky, clz | musc, bt, chl, gnt, pl, qtz, ilm, sulfides, clz a/o calc-amph, (ank or cc), +/- rut |

***Roof pendant at Hope Valley, CA***

Chemical compositions for the calcareous hornfels and marble from a Mesozoic roof pendant at Hope Valley, California are tabulated in *Ferry* [1989, p. 407]. Although the rocks at Hope Valley were originally interbedded limestones, marls, sandstones, tuffs, and other volcanics, the study focused on the carbonate rocks which were contact metamorphosed in the Cretaceous with the emplacement of the calc-alkaline Sierra Nevada batholith. Two fields were created and projected onto ternary diagrams; calcareous hornfels and marble. The mineralogy for both calcareous hornfels and marble includes calcite + K-feldspar + quartz + sphene +/- diopside +/- plagioclase +/- scapolite +/- clinozoisite. Moreover, rocks on one side a fault contain variable amounts of biotite, amphibole, and muscovite while those on the other side contain variable amounts of grossular, wollastonite, and axinite.

### 3.4.2 Geochemical trends in Meta-sedimentary Rocks

Geochemical analyses from each formation was projected onto the ASC, ASF, ACF, and SFC diagrams and fields were constructed separately for geochemical data calculated and projected using total iron as $Fe_2O_3$ and FeO (e.g. Fig. 3.1a vs. Fig. 3.5a). Because all rocks will contain a mix of $Fe_2O_3$ and FeO, these two projections serve as end-members that bound rock composition. For clarity, geochemical trends for the literature are noted below in tabulated format followed by brief descriptions.

***Vassalboro/Sangerville Formation***

| **iron** | | **ASC** | | | **ASF** | | **lithology** |
|---|---|---|---|---|---|---|---|
| | **S'** | **A'** | **C'** | **S'** | **A'** | **F'** | |
| **FeO** | 64-95% | 2-9% | 1-32% | 80-90% | 2-10% | 7-11% | sandstone |
| **$Fe_2O_3$** | 62-93% | 5-11% | 3-34% | 82-92% | 4-12% | 2-8% | sandstone |
| | | **ACF** | | | **SFC** | | |
| | **A'** | **C'** | **F'** | **F'** | **S'** | **C'** | |
| **FeO** | 10-30% | variable | variable | 8-11% | variable | variable | sandstone |
| **$Fe_2O_3$** | 15-50% | variable | variable | 3-8% | variable | variable | sandstone |

The chemical composition of the Vassalboro/Sangerville sandstone is controlled primarily by $SiO_2$ and to a lesser extent CaO. Therefore the Vassalboro/Sangerville field plots near the S' apex with variable CaO (< 34 percent). In projections where the $SiO_2$ component is not represented, the field ranges between the C' and F' apex with no more than 50 percent [$Al_2O_3$ + $Fe_2O_3$], controlled by $Fe_2O_3$ in mineral compositions (Fig. 3.4). Where CaO is not represented (Fig. 3.2, 3.6), the Vassalboro/Sangerville field strongly is restricted and plots near the S' apex.

### *Waterville Formation*

| iron | | ASC | | | ASF | | lithology |
|---|---|---|---|---|---|---|---|
| | S' | A' | C' | S' | A' | F' | |
| FeO | variable | 0-9% | variable | 60-90% | 0-11% | 6-33% | meta-carbonate |
| $Fe_2O_3$ | variable | 1-11% | variable | 62-92% | 1-18% | 4-24% | meta-carbonate |
| | | ACF | | | SFC | | |
| | A' | C' | F' | F' | S' | C' | |
| FeO | 0-20% | variable | variable | 2-20% | variable | variable | meta-carbonate |
| $Fe_2O_3$ | variable | variable | 5-30% | 1-17% | variable | variable | meta-carbonate |

The chemical composition of the Waterville meta-carbonate is dominated by $SiO_2$, CaO, and to a lesser extent FeO and $Fe_2O_3$. In ternary projections where both the primary components ($SiO_2$ and CaO) are represented (Figs. 3.1, 3.3, 3.5, and 3.7), the Waterville field trends linearly between the S' and C' apexes. In projections where one of the primary components is missing (Fig. 3.2, 3.6, 3.4, 3.8) the field trends toward the F' apex.

### *Giles Mountain and Waits River Formation*

*1. limestone*

| iron | | ASC | | | ASF | | lithology |
|---|---|---|---|---|---|---|---|
| | S' | A' | C' | S' | A' | F' | |
| FeO | variable | 0-7% | variable | 67-94% | 0-7% | 7-28% | limestone |
| $Fe_2O_3$ | variable | 1-8% | variable | 70-95% | 1-12% | 3-19% | limestone |

| | | ACF | | | SFC | | |
|---|---|---|---|---|---|---|---|
| | A' | C' | F' | F' | S' | C' | |
| **FeO** | 0-13% | 58-93% | 7-32% | 2-17% | variable | variable | limestone |
| **$Fe_2O_3$** | 1-24% | 63-94% | 5-19% | 1-12% | variable | variable | limestone |

The Giles Mountain and Waits River limestone is consists predominantly of $SiO_2$ and CaO and to a lesser extent FeO or $Fe_2O_3$ and mimics the Waterville trend. The Giles Mountain and Waits River limestone fields are smaller, but this probably reflects a smaller number of analyzed samples.

*1. sandstone*

| **iron** | | **ASC** | | | **ASF** | | **lithology** |
|---|---|---|---|---|---|---|---|
| | S' | A' | C' | S' | A' | F' | |
| **FeO** | 72-93% | 5-11% | 4-20% | 72-91% | 4-11% | 5-18% | sandstone |
| **$Fe_2O_3$** | 69-92% | 5-14% | 5-19% | 2-10% | 75-93% | 5-15% | sandstone |
| | | **ACF** | | | **SFC** | | |
| | A' | C' | F' | F' | S' | C' | |
| **FeO** | 19-30% | 28-45% | 38-45% | 5-18% | 67-92% | 2-27% | sandstone |
| **$Fe_2O_3$** | 35-45% | 30-50% | 16-27% | 2-10% | 76-96% | 2-19% | sandstone |

The chemical composition of the Giles Mountain and Waits River sandstone is controlled primarily by $SiO_2$ and to a lesser degree CaO and mimics the Vassalboro/Sangerville trend.

*2. pelite*

| **iron** | | **ASC** | | | **ASF** | | **lithology** |
|---|---|---|---|---|---|---|---|
| | S' | A' | C' | S' | A' | F' | |
| **FeO** | 69-92% | 6-35% | 0-11% | 60-83% | 7-21% | 7-20% | pelite |
| **$Fe_2O_3$** | 66-91% | 7-28% | 0-9% | 62-87% | 10-28% | 2-10% | pelite |
| | | **ACF** | | | **SFC** | | |
| | A' | C' | F' | F' | S' | C' | |
| **FeO** | variable | 1-24% | variable | 6-23% | 70-92% | 0-10% | pelite |
| **$Fe_2O_3$** | 52-78% | 1-28% | 20-39% | 4-14% | 80-97% | 0-11% | pelite |

The chemical composition of the Giles Mountain and Waits River pelite is controlled primarily by $SiO_2$, $Al_2O_3$, and to a lesser extent FeO or $Fe_2O_3$. In projections where all three of the

aforementioned components are represented, the pelite field strongly favors the S' apex. This trend also holds for projections that do not represent the A' apex.

***Roof pendant at Hope Valley, CA***

*1. calcareous hornfels*

| iron | | ASC | | | ASF | | lithology |
|---|---|---|---|---|---|---|---|
| | S' | A' | C' | S' | A' | F' | |
| FeO | 65-85% | 2-7% | 12-30% | 80-90% | 2-8% | 7-16% | calcareous hornfels |
| $Fe_2O_3$ | 73-83% | 5-9% | 11-21% | 80-94% | 4-10% | 2-10% | calcareous hornfels |
| | | ACF | | | SFC | | |
| | A' | C' | F' | F' | S' | C' | |
| FeO | 1-24% | 52-66% | 21-31% | 7-12% | 60-82% | 12-27% | calcareous hornfels |
| $Fe_2O_3$ | 15-31% | 56-69% | 9-19% | 1-8% | 65-85% | 12-29% | calcareous hornfels |

The chemical composition of the calcareous hornfels at Hope Valley is controlled primarily by $SiO_2$ and to a lesser extent CaO. Calcareous hornfels falls within the Vassalboro/Sangerville field.

*2. marble*

| iron | | ASC | | | ASF | | lithology |
|---|---|---|---|---|---|---|---|
| | S' | A' | C' | S' | A' | F' | |
| FeO | 3-20% | 0-2% | 79-96% | 70-85% | 5-7% | 10-23% | marble |
| $Fe_2O_3$ | 3-21% | 0-2% | 79-97% | 72-86% | 5-10% | 9-17% | marble |
| | | ACF | | | SFC | | |
| | A' | C' | F' | F' | S' | C' | |
| FeO | 0-2% | 93-99% | 1-5% | 1-3% | 3-21% | 88-96% | marble |
| $Fe_2O_3$ | 0-2% | 95-99% | 0-3% | 0-3% | 4-21% | 88-96% | marble |

The chemical composition of marble at Hope Valley is controlled primarily by CaO and to a lesser extent $SiO_2$. The marble field plots near the C' apex. In projections that represent $SiO_2$, the

marble field plots more toward the S' apex, however never exceeds 21 percent S', except where CaO is not projected (Fig. 3.2, 3.6).

### 3.4.3 Meta-sedimentary and Skarn rock compositions at Mineral Hill

***Marble***

Marble outcrops throughout the map area. Twenty-nine samples were analyzed for whole rock chemical composition by XRF (Tables 3.1 and 3.2), including green marble (N=3) from within the main skarn body, grey and bleached marble (N=8) from the upper marble quarry, grey and bleached marble (N=4) from the northern extension, grey and bleached marble (N=12) from Marble Hill and black marble (N=1) (Fig. 1.2).

Most marbles are chemically similar with the notable exception of BM-1-M, a black phlogopite-bearing marble, which plots toward the F' apex due to high magnesium content (10.72 percent; Figs. 3.2b, 3.6b, 3.3b, 3.7b, 3.4b, and 3.8b). Moreover, BM-1-M, is drawn toward the chemical composition of dolomite (8). All other marble analyses plot near the C' apex due to the dominance of CaO content. Some marbles are influenced by a higher $SiO_2$ content coupled with small increases in FeO and MgO, which pull marble composition towards the S' and F' apex, respectively.

In general, Mineral Hill marble compositions coincide most closely with the roof pendant marble composition from Hope Valley, CA. In a few samples, compositions are closer to the fields representing the Waterville meta-carbonates and Giles Mountain/Waits River limestone. Most marble analyses resemble those of fossiliferous, lithographic, and oolitic limestone (5, 6, 7) from *Brownlow* [1996], but are more siliceous (e.g. Fig. 3.2b).

***Skarn***

Geochemical analyses of twenty-nine skarn samples including wollastonite skarn (N=22), clinopyroxene skarn (N=1), garnet-wollastonite skarn (N=3), garnet skarn (N=2), and garnetite (N=1) are presented in Tables 3.1 and 3.2.

*Wollastonite skarn*

Not suprisingly, the composition of wollastonite skarn is primarily controlled by CaO and $SiO_2$ (Figs. 3.1c, 3.5c, 3.3c, and 3.7c). As a consequence, wollastonite skarn analyses plot along the line between the S' and C' apexes (average 50:50). Wollastonite skarn contains very little iron. In the ACF ternary diagram (Figs. 3.4c and 3.8c), projected partially from $SiO_2$, wollastonite skarn plots near the C' apex illustrating the strong influence of CaO within the mineral assemblage. Likewise, in the ASF ternary diagram (Figs. 3.2c and 3.6c), wollastonite skarn plots near the S' apex. One clear exception is sample W1b which has an anomolously high magnesium content. Wollastonite skarn is poor in $Al_2O_3$, (< 2.2 wt. %).

Wollastonite skarn samples do not consistently plot near any single meta-sedimentary protolith field. In general, wollastonite skarn samples coincide mostly closely with Waterville meta-carbonate and Giles Mountain/Waits River limestone, except in ternary diagrams projected from either S' or C' (Figs. 3.2c, 3.6c, 3.4c, and 3.8c). In this case, wollastonite skarn plots within the fields for roof pendant marble from Hope Valley, CA. In those ternary diagrams which include both primary components (i.e. CaO and $SiO_2$; Figs. 3.1c, 3.5c, 3.3c, and 3.7c), wollastonite skarn compositions most commonly resemble a calcareous shale (11) from *Brownlow* [1996].

*Clinopyroxene skarn*

The chemical composition of one sample of clinopyroxene skarn is dominated by $SiO_2$, $Al_2O_3$, and CaO with lesser iron ($Fe_2O_3$ and FeO) and MgO. Clinopyroxene skarn is chemically distinctive from all other skarn types due to very high (~70 percent) $SiO_2$ content.

Clinopyroxene skarn plots within (or near to) compositions of the Vassalboro sandstone and calcareous hornfels from Hope Valley, CA (Figs. 3.1-3.8) and most closely resembles a sub-graywacke (4) from *Brownlow* [1996].

*Garnet-wollastonite skarn*

The chemical composition of garnet-wollastonite skarn is dominated by CaO, $SiO_2$, $Al_2O_3$, iron ($Fe_2O_3$ and FeO), and to a lesser extent MgO. Samples fall on a line between $Fe_2O_3$ and FeO end-members. Garnet-wollastonite skarn plots near garnetite and garnet skarn compositions although typically (except sample UB2c) with lesser [$Al_2O_3$ + $Fe_2O_3$] and greater $SiO_2$ content (see below)( e.g. Figs. 3.2c and 3.6c). They are differentiated from wollastonite skarn by greater [$Al_2O_3$ + $Fe_2O_3$] even among plots where total iron is FeO (e.g. Figs. 3.4c and 3.8c). UB2c has the highest percentages of $SiO_2$, $Al_2O_3$, ($Fe_2O_3$ or FeO), and MgO at the expense of CaO, driving this sample farthest from the C' apex (Figs. 3.1c, 3.5c, 3.3c, 3.7c, 3.4c, and 3.8c).

Garnet-wollastonite skarn compositions plot near the Waterville meta-carbonate and Giles Mountain/ Waits River limestone. One exception is sample UB2c which also plots near to the Vassalboro sandstone and calcareous hornfels from Hope Valley, CA, especially if the mineral composition of garnet dominantly fixed by FeO (e.g. Fig. 3.4c). Garnet-wollastonite skarn compositions most closely resemble that of calcareous shale (11) from *Brownlow* [1996].

*Garnet skarn*

The chemical composition of garnet skarn is dominated by CaO, $SiO_2$, $Al_2O_3$, iron ($Fe_2O_3$ and FeO) and to a lesser extent MgO. Because of the prevalence of grandite garnet, samples fall on a line between $Fe_2O_3$ and FeO end-members. Garnet skarn plots in a similar field as garnet-wollastonite skarn and garnetite samples, however is differentiated by greater [$Al_2O_3$ + $Fe_2O_3$] contents.

In general, garnet skarn compositions coincide most closely with the Waterville meta-carbonate and Giles Mountain/Waits River limestone, although garnet skarn at Mineral Hill has greater [$Al_2O_3$ + $Fe_2O_3$] content (Figs. 3.1c, 3.5c, 3.2c, 3.6c, 3.4c, and 3.8c). In the ACF projection (Figs. 3.4c and 3.8c), garnet skarn plots near the compositions of the Vassalboro/Sangerville sandstone and calcareous hornfels from Hope Valley, CA. Garnet skarn does not consistently plot near any common sedimentary rock type.

*Garnetite*

Garnetite consists of < 80 wt % andraditic garnet and its composition therefore plots near this end-member composition. If garnetite was FeO-rich the bulk composition ($FeO_T$) would plot near pyrope/almandine end-member compositions. The composition of garnetite is primarily controlled by CaO, $SiO_2$, iron ($Fe_2O_3$ [] FeO), and $Al_2O_3$. Garnetite plots near garnet-wollastonite skarn and garnet skarn and is differentiated from garnet-wollastonite skarn by the higher [$Al_2O_3$ +$Fe_2O_3$] content in garnet pulling the composition toward the A' (Figs. 3.1c, 3.5c, 3.2c, 3.6c, 3.4c, and 3.8c).

In general, the Mineral Hill garnetite sample lies spatially close to the Waterville meta-carbonate and Giles Mountain/Waits River limestone fields, however the garnetite always plots closer to the A' apex (Figs. 3.1c, 3.5c, 3.2c, 3.6c, 3.4c, and 3.8c). As with garnet skarn, garnetite does not consistently plot near any common sedimentary rock type.

### *Calc-silicate Skarnoid*

Three skarnoid samples were analyzed by XRF for whole rock chemical composition. The compositions of two of the samples (CZ-3 and UB14c) are primarily controlled by $SiO_2$, $Al_2O_3$, CaO and $Na_2O$ with lesser iron ($Fe_2O_3$ and FeO), MgO and $K_2O$. The greater percentage of $Na_2O$ and $K_2O$ reflect the presence of feldspar and distinguishes these skarnoid samples from all other meta-sedimentary and skarn units at Mineral Hill. The alkali content of these rocks is not reflected in the ternary diagrams which are projected from the alkali feldspars. Samples CZ-1 and UB14c plot near clinopyroxene skarn (cf. Fig. 3.1c and 3.1d). Skarnoid sample CZ-1 is very rich in $SiO_2$ (94.86 wt %) and plots near the S' apex in all ternary projection except ACF (Fig. 3.4d and 3.8d), where it plots near the A' apex.

Skarnoid most closely resembles the chemical composition of a sub-graywacke (CZ-3 and UB14c) (4) and orthoquartzite (CZ-1) (1) from *Brownlow* [1996]. Skarnoid does not plot near any single meta-sedimentary rock type.

### *Quartzite*

The chemical composition of a single sample of quartzite is dominated by $SiO_2$, $Al_2O_3$, and CaO. The rock is of unknown origin and consists predominantly of quartz and epidote.

Quartzite plots near the compositions of the Vassalboro sandstone and calcareous hornfels from Hope Valley, CA and closely resembles the chemical composition of a sub-graywacke (4) from *Brownlow* [1996].

## 3.5 Discussion

By observing geochemical trends of meta-sedimentary rocks formed at or near isochemical conditions [*Ferry*, 1988, 1989, and 1994], and whole-rock geochemistry of common sedimentary rocks [*Brownlow*, 1996] and comparing whole-rock geochemistry of meta-

sedimentary and skarn rocks from Mineral Hill, we can deduce to a certain degree the origin of each unit. In particular, by comparing each in SACF ternary space, whether the chemical composition of the rock unit is primarily controlled by protolith composition or interaction with external material (discussed later) can be inferred.

Both garnet-wollastonite skarn and wollastonite skarn plot near fields for the Waterville meta-carbonate and Giles Mountain/Waits River limestone, however do not fall consistently within these fields. Moreover, garnet-wollastonite plots closer to the A' apex than wollastonite skarn, due to higher concentrations of $Al_2O_3$, probably reflecting the greater garnet abundance. Both garnet-wollastonite skarn and wollastonite skarn also most closely resemble a calcareous shale (11, from *Brownlow*, 1996).

It is unlikely that wollastonite skarn formed isochemically from a calcareous shale since it would reflect higher concentrations of $Al_2O_3$. Wollastonite skarn on average has < 1.5 wt % $Al_2O_3$. Instead, it is likely that wollastonite skarn formed from marble due to the interaction with aqueous silica by the reaction:

$$CaCO3 + SiO_2(aq) = CaSiO_3 + CO_2. \qquad (R1)$$

This is supported by wollastonite skarn compositions consistently plotting on average 50:50 between the S' and C' apex. Moreover, in the field, wollastonite skarn is often proximal to and in contact with marble units.

Even though garnet-wollastonite skarn most closely resembles the chemical composition of a calcareous shale, all samples do not consistently plot near it (e.g. Figs. 3.1, 3.2, 3.3, and 3.4). Instead, it varies in having a greater $SiO_2$, CaO and $Al_2O_3$ abundance than calcareous shale. This probably reflects the varying garnet and wollastonite content in garnet-wollastonite skarn. Therefore, garnet-wollastonite skarn was probably derived from protolith interaction with external material. *Meinert* [1992] argues that a garnet skarn derived from a limestone protolith would be relatively wollastonite-rich (discussed later). Based on his assertion and the proximity

of many garnet-wollastonite skarn sample to green marble in the field, it is probable that this unit derived from a limestone or marble protolith (possibly interbedded with variable amounts of argillaceous or marl material) and external $SiO_2$ and possibly $Al_2O_3$.

Garnet skarn and garnetite plot most closely to meta-sedimentary fields of the Waterville meta-carbonate and Giles Mountain/Waits River limestone however elevated in [$Al_2O_3$ + $Fe_2O_3$] consistently plotting closer to the A' apex. They do not resemble any singular common sedimentary rock [from *Brownlow*, 1996]. Therefore, garnet skarn and garnetite probably originated from a protolith that interacted with an external source.

Because of the dominance of grandite garnet (Ca), in garnet skarn mineral assemblage and relative lack of wollastonite (to garnet-wollastonite skarn), garnet skarn (and clinopyroxene skarn?) probably formed from a mixed sequence of calc-argillaceous, marl and marble material or intensive infiltration of FeO, MgO, $Al_2O_3$, and $SiO_2$. Although we see evidence of infiltration of these elements by the existence of a garnet zone in the study area (zonation discussed later), it is more probable that a mixture of these scenarios produced garnet skarn. However, it should be noted that no calc-silicate protolith is preserved within the field area.

Because garnetite contains >80 percent andraditic garnet, a metasomatic origin from marble is likely due to higher $Al_2O_3$ content from that of marble and garnet skarn geochemistry. In the field, garnetite is observed to be spatially associated with green marble.

Skarnoid is highly variable geochemically. Skarnoid most closely resembles a sub-graywacke and orthoquartzite. This reflects the high $SiO_2$ content in these samples. However, it is unlikely that skarnoid derived from similar sediments because they resemble no members within the Quatsino sequence, and skarnoid outcrops in a large portion of the map area. Skarnoid generally crops out within in an area that is intruded extensively by dikes and likely represents a unit with a complex origin, possibly involving several metasomatic events.

The distribution of minerals in skarn units at Mineral Hill denote a typical zonation pattern found in skarn formed adjacent to plutons. Skarn zonation within the field area and controls of protolith and fluid infiltration are discussed in further detail in the next section.

## 3.6 Distribution of Minerals in Calcic Exoskarn at Mineral Hill

### 3.6.1 Introduction

No skarn unit identified at Mineral Hill falls within a typical geochemical field for meta-carbonate rocks formed at or near to isochemical conditions [from *Ferry*, 1988, 1989, and 1994], nor do they correspond consistently with an chemical composition for common sedimentary rocks [from *Brownlow*, 1996]. Although some protolith control within skarn is evident, metamorphism could not have been purely isochemical to produce the geochemistry and volume loss we see in skarn units.

The distribution of map units at Mineral Hill is attributed to: (1) changes in protolith host rock and (2) the variation in style and intensity of alteration which reflects the propagation rates of alteration fronts, and overprinting of multiple fluid events.

Skarn units (wollastonite and garnet-wollastonite) which most likely formed from marble (1) plot outside of the field for marbles and limestone compositions, more $SiO_2$-and $Al_2O_3$-rich, respectively. (2) Garnet-wollastonite skarn does not plot within approximately constant ratios with marble compositions from Mineral Hill, implying either different protolith or different reactions to produce skarn.

In other skarn units (garnet and clinopyroxene), the protolith composition is uncertain although their percent mineralogy suggests either a mixed parent lithology (such as calc-argillite), or intensive infiltration of FeO, MgO , $Al_2O_3$, and $SiO_2$. Although mobility of these elements is likely, it is more probable that a mixture of these scenarios occurred to form skarn.

Interleaves of garnet and garnet-wollastonite skarn are observed within the main skarn body proximal to the pluton contact. This occurrence suggests that the sedimentary pendant prior to metamorphism was an interbedded limestone, dirty limestone and/or calc-argillitic sequence. This is consistent with descriptions outlined in the Quatsino sequence. Both garnet and garnet-wollastonite skarn are compositionally layered. Garnet infilling clinopyroxene grain boundary porosity suggests that MgO front occurred producing a clinopyroxene zone prior to garnet formation. Most evidence of a clinopyroxene zone has been overprinted by garnet. All units in which brown, greenish-brown and dark red garnets are observed are defined as garnet zone. The extent of garnet zone reaches the contact of wollastonite skarn. Even though some wollastonite skarn contains garnet, these rocks are predominantly monomineralic and garnet presence is attributed to greater concentrations of $Al_2O_3$ and $TiO_2$ in the protolith composition. It can also be suggested that if garnet-wollastonite was produced from a similar protolith, some of the garnet could be controlled by protolith composition, however not all due to lack of abundant $Al_2O_3$ and $TiO_2$ in marble compositions.

### 3.6.2 Skarn Zonation

Zonation at Mineral Hill is observed within a 450 m by 150 m area on the south-eastern flank of a roof pendant enclosed by a dioritic component of the Crowston Lake Pluton (Fig. 3.20). Zones were interpreted on the basis of the presence of minerals dominant in skarn development; garnet, pyroxene, and wollastonite. The deposit is zoned over ~65 m from garnet skarn (with interleaved garnet-wollastonite skarn and garnetite) proximal to the Crowston Lake Pluton, through wollastonite skarn to distal calcite marble. As with most skarn systems, garnet and pyroxene are the dominant minerals and represent the first products of water-rock reactions [*Einaudi and Burt*, 1982]. Zoning during the early stages of skarn formation commonly occurs as garnet-pyroxene-(wollastonite)-marble, proximal to distal from the pluton, respectively [*Einaudi*

*and Burt*, 1982]. Grossular-andradite solid solutions are common garnet phases in calcic exoskarn [*Zharikov*, 1970] with less than 15 mole percent spessartine + almandine [*Einaudi and Burt*, 1982]. Pyroxene phases range within the diopside-hedenbergite and hedenbergite-johannsenite solid solution series, with a notable absence of diopside-johannsenite compositions [*Einaudi and Burt*, 1982]. Other common skarn minerals (calc-silicates) are wollastonite, rhodonite, vesuvianite, epidote, scapolite, plagioclase, and potassium feldspar (Table 3.8). Accessory minerals are titanite and apatite; rare minerals are monticellite, merwinite, spurrite, melinites, cuspidine, and bustamite.

***Garnet zone***

The Mineral Hill skarn deposit has similar zoning characteristics as most skarn systems, however most evidence of a pyroxene zone has now been overprinted. Garnet skarn, garnet-wollastonite skarn, garnetite, and some outcrops of skarnoid are attributed to the garnet zone of the map area based on the presence of garnet (Fig. 3.20). Garnet zone extends at most ~50 m outboard of the Crowston Lake Pluton. Relative mineral abundance differences between skarn units within the garnet zone can be partially attributed to controls of protolith composition. Although the protolith is not always preserved in skarns, the composition of the protolith often defines skarn mineralogy and zonation. For instance, *Meinert* [1992] showed that a garnet skarn derived from a limestone protolith would be wollastonite-rich (approximately >75-80 percent) whereas garnet skarn derived from marl will be relatively wollastonite-poor (< 20 percent), and will be dominated by garnet and clinopyroxene (Fig. 3.21). On this basis, garnet skarn at Mineral Hill is proposed to have been altered from an argillitic or marl sequence and garnet-wollastonite skarn from marble or calcite veins interbedded within the argillite or marl. Extensive isoclinal deformation precludes identification of the calcitic protolith of garnet-wollastonite skarn. The calcitic unit could be interbeds of pinched out marble due to isoclinal folding or boudinaged

Table 3.8. Skarn mineralogy- common minerals, mineral groups and compositions [after *Meinert*,1992]. Minerals identified in Mineral Hill skarn (bold).

| General Group | End Members | Composition |
|---|---|---|
| Garnet | **grossular** | $\mathbf{Ca_3Al_2(SiO_4)_3}$ |
| | **andradite** | $\mathbf{Ca_3Fe_2(SiO_4)_3}$ |
| | spessartine | $Mn_3Al_2(SiO_4)_3$ |
| | almandine | $Fe_3Al_2(SiO_4)_3$ |
| | pyrope | $Mg_3Al_2(SiO_4)_3$ |
| Pyroxene | **diopside** | $\mathbf{CaMgSi_2O_6}$ |
| | hedenbergite | $CaFeSi_2O_6$ |
| | johannsenite | $CaMnSi_2O_6$ |
| | fassaite | $Ca(Mg, Fe, Al)(Si, Al)_2O_6$ |
| Olivine | larnite | $Ca_2SiO_4$ |
| | forsterite | $Mg_2SiO_4$ |
| | fayalite | $Fe_2SiO_4$ |
| | tephroite | $Mn_2SiO_4$ |
| Pyroxenoid | ferrosilite | $FeSiO_3$ |
| | rhodonite | $MnSiO_3$ |
| | **wollastonite** | $\mathbf{CaSiO_3}$ |
| Amphibole | tremolite | $Ca_2Mg_5Si_8O_{22}(OH)_2$ |
| | ferroactinolite | $Ca_2Fe_5Si_8O_{22}(OH)_2$ |
| | manganese actinolite | $Ca_2Mn_5Si_8O_{22}(OH)_2$ |
| | **hornblende** | $\mathbf{Ca_2(Mg, Fe)_4Al_2Si_7O_{22}(OH)_2}$ |
| | pargasite | $NaCa_2(Mg, Fe)_4Al_3Si_6O_{22}(OH)_2$ |
| | cummingtonite | $Mg_2(Mg, Fe)_5Si_8O_{22}(OH)_2$ |
| | dannemorite | $Mn_2(Fe, Mg)5Si_8O_{22}(OH)_2$ |
| | grunerite | $Fe_2(Fe, Mg)_5Si_8O_{22}(OH)_2$ |
| Epidote | piemontite | $Ca_2(Mn, Fe, Al)_3(SiO_4)_3(OH)$ |
| | allanite | $(Ca, REE)_2(Fe,Al)_3(SiO_4)_3(OH)$ |
| | **epidote** | $\mathbf{Ca_2(Fe, Al)_3(SiO_4)_3(OH)}$ |
| | **clinozoisite** | $\mathbf{Ca_2Al_3(SiO_4)_3(OH)}$ |
| Plagioclase | **anorthite** | $\mathbf{CaAl_2Si_2O_8}$ |
| Scapolite | marialite | $Na_4Al_3Si_9O_{24}(Cl, CO_3, OH, SO_4)$ |
| | meionite | $Ca_4Al_6Si_6O_{24}(CO_3, Cl, OH, SO_4)$ |
| Axinite | | $(Ca, Mn, Fe, Mg)_3Al_2BSi_4O_{15}(OH)$ |
| Other | vesuvianite | $Ca_{10}(Mg, Fe, Mn)_2Al_4Si_9O_{34}(OH, Cl, F)_4$ |
| | prehnite | $Ca_2Al_2Si_3O_{10}(OH)_2$ |

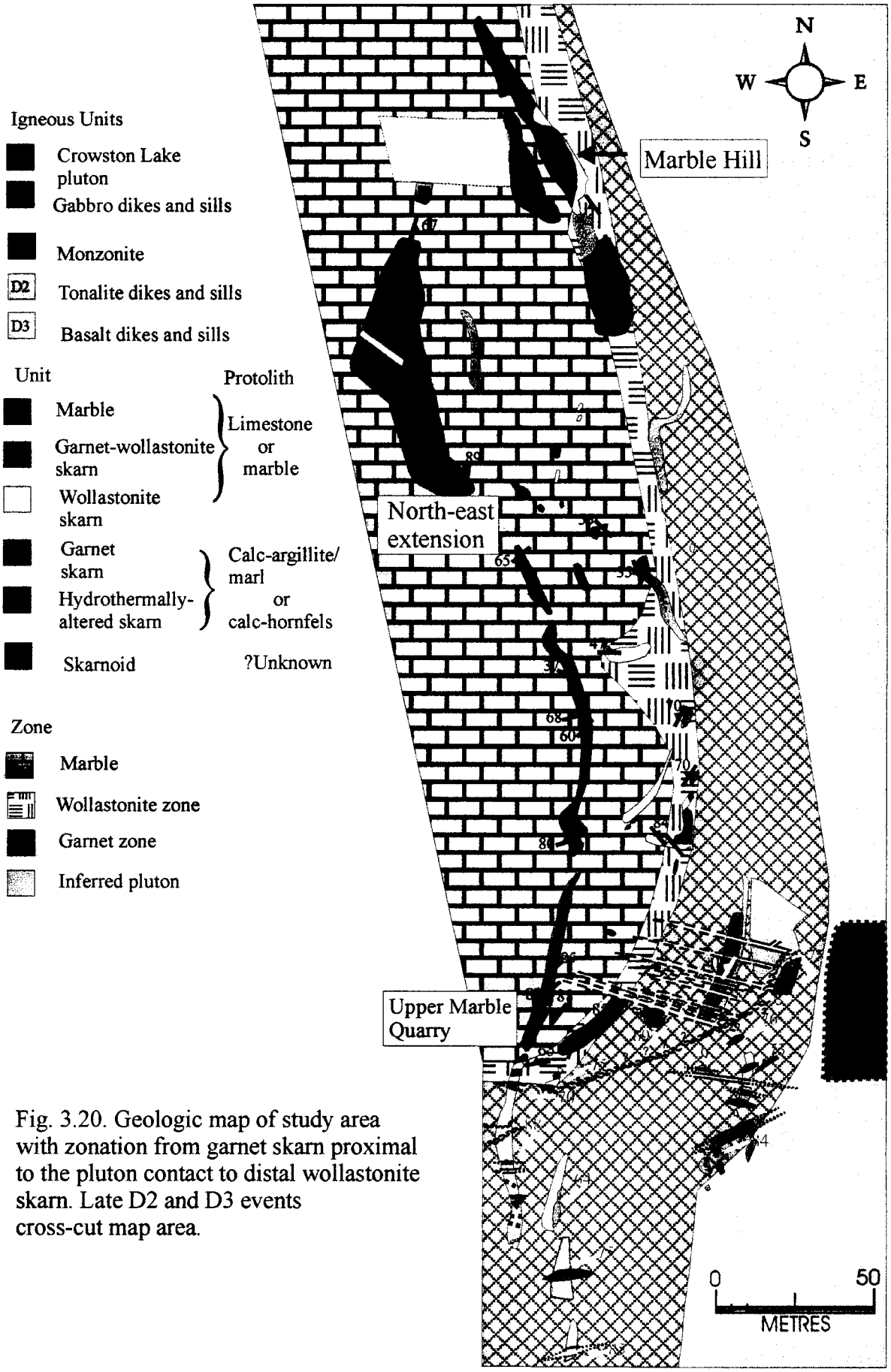


Fig. 3.20. Geologic map of study area with zonation from garnet skarn proximal to the pluton contact to distal wollastonite skarn. Late D2 and D3 events cross-cut map area.

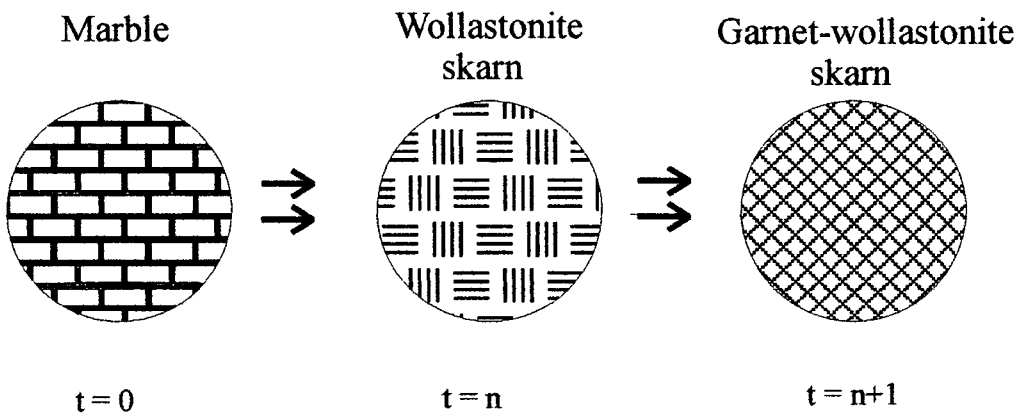


Fig. 3.21. Schematic illustrating the rock history of a marble infiltrated by magmatic fluid carrying aqueous Fe, Al and $SiO_2$. At t = 0, marble; t = n, $SiO_2$ has reacted with marble to form wollastonite skarn; at t = n+1, Fe and Al have reacted to form garnet.

calcite vein material within garnet skarn and garnetite units. The protolith was probably contaminated with clastic sediment due to garnet abundance up to but not exceeding 35 percent. Due to its green color, the calcite marble spatially associated to garnet-wollastonite skarn is differentiated from other marble units.

Although protolith composition can partially control the mineralogy and zonation in skarn, infiltration of reactive fluid can also define spatial distribution of skarn mineralogy and zoning; often both controls work in tandem. Fluid composition influences reactions producing skarn. If an exotic fluid is out of equilibrium with the rock it infiltrates, reaction will occur in order to maintain chemical equilibrium. As reaction continues, the composition of the rock and fluid changes. Several studies have determined that different reactions propagate at different rates [*Korzhinskii*, 1970; *Bickle and Baker*,1990; *Dipple and Gerdes,* 1998]. They observed that although the reactions may start at the same interface, the reaction fronts spread farther apart as infiltration continues (Fig. 3.22). Such geometries are distinctive of infiltration-driven reaction and allow mapping of fluid flow paths. This sort of phenomena could have partial control over mineral zone distribution in skarn. Moreover, reaction caused by infiltration of fluid can have a tremendous impact on skarn development due to reaction-infiltration feedback (discussed later).

Parts of skarnoid is attributed to the garnet zone due to the presence of garnet observed in field and identified petrographically in samples TB14B, CZ-1, and CZ-2. However, skarnoid is distinguished from typical skarn since this unit appears to have a complex origin, probably involving multiple metasomatic events and/or overprinting of skarn-like assemblages onto a hornfels or reaction skarn. This is inferred due to high $SiO_2$ content and spatial relationships with extensive tonalite and basalt diking events.

Quartzite outcrops within the garnet zone, however no garnet is present in these samples. This unit might represent altered dike or skarn material, vein or $SiO_2$ infiltration into brecciated

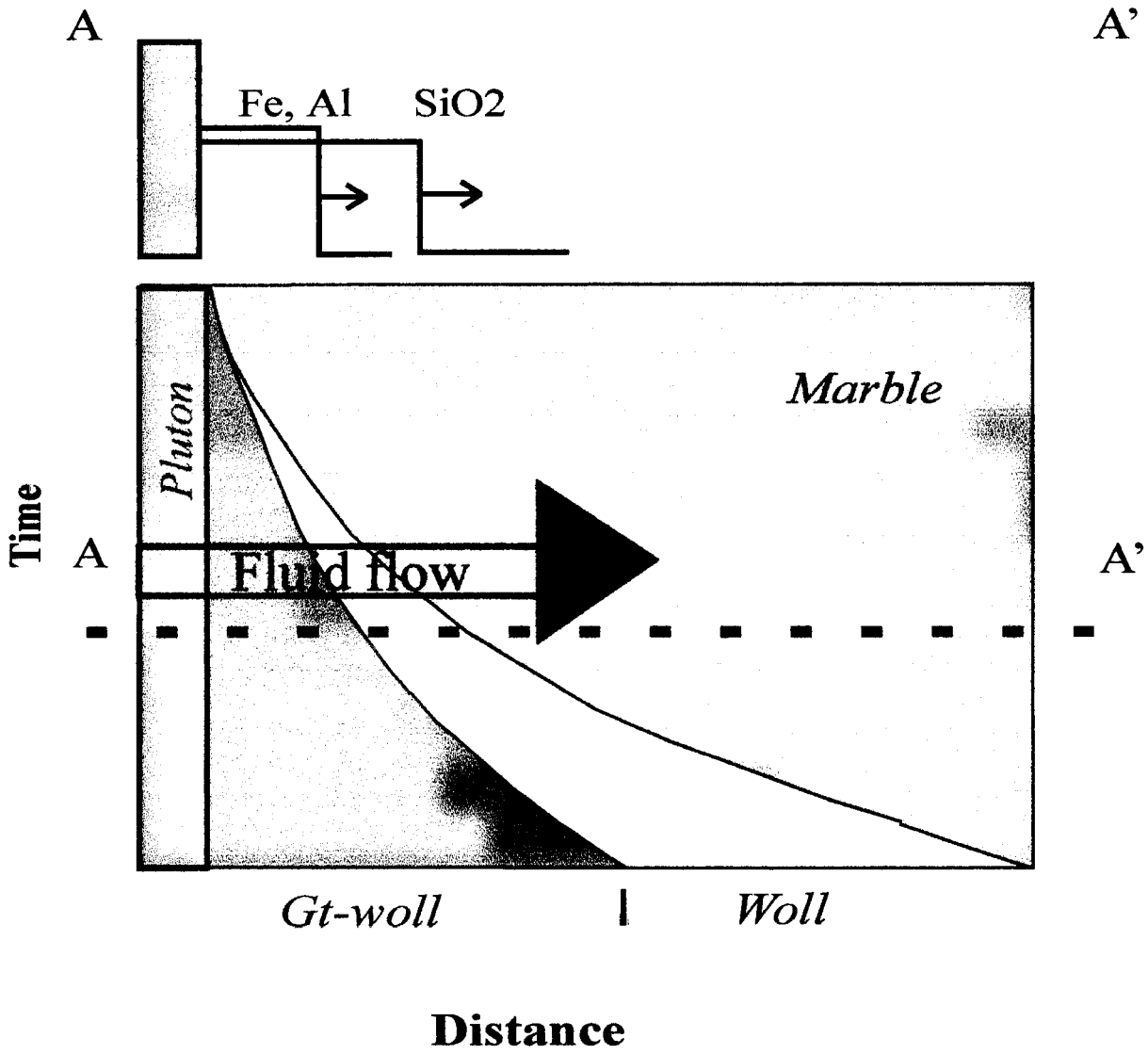


Fig. 3.22. Time versus distance schematic showing that two reactions that start at the same interface (t=0), propagate at different rates. The result is a spatial distribution or zoning of metasomatized sediments in respect to the magmatic fluid source (i.e. pluton) from distal marble to wollastonite skarn to proximal garnet-wollastonite skarn. Cross section AA' illustrates fluid migration of mobile elements at t =n.

garnet skarn related or emplaced with the skarn forming event, but was not altered by it (with the possible exception of late epidotization).

### *Clinopyroxene zone*

One sample MB3b is identified as a clinopyroxene skarn, however no other clinopyroxene skarn samples were observed. Some garnet skarn samples do show compositionally layering with mineralogy from high garnet abundance to zones of high clinopyroxene abundance. Nevertheless, evidence of a clinopyroxene zone is preserved as garnet infilling porosity around clinopyroxene grains, although no 'classic' clinopyroxene zone exists in the map area.

### *Wollastonite zone*

Wollastonite skarn is attributed to the wollastonite zone. Where exposed, wollastonite skarn interfingers into grey and bleached marble (Plate 2.8, Figs. 1.9-1.11). This boundary marks the extent of aqueous silica infiltration.

Even though garnet is present in many samples, wollastonite skarn is essentially monomineralic. Garnet production in these samples cannot be exclusively contributed to the infiltration of an elemental front (metasomatism) since the marble protolith probably varies in $Al_2O_3$ and $TiO_2$ (i.e. type A skarn). Moreover, wollastonite skarn does not plot near the A' or F' apex in ternary diagrams, therefore the composition is not primarily controlled by the presence of grossular or andradite.

### *Hydrothermally altered skarn*

Often zoning will occur due to overprinting of the initial skarn event by either a single fluid event or multiple fluid events. Since calcic exoskarn is dominated by mostly anhydrous

minerals (e.g. garnet, pyroxene and wollastonite phases) formed by infiltration of magmatic fluids, it represents the highest temperature metasomatic alteration, which often introduces silica, iron and alumina while removing large amounts of volatiles from the system [*Barton et al.*, 1991]. This is often the first skarn forming event, especially when the alteration is related to the emplacement of a pluton. It is not uncommon, however, that subsequent lower temperature hydrothermal activity will result in production of hydrous calc-silicates (e.g. epidote), and deposition of oxides and sulfides referred to as hydrous skarn or retrograde skarn [*Barton et al.*, 1991]. This fluid event can overprint anhydrous skarn, and the anhydrous phases may retrograde to their lower temperature equivalents.

At Mineral Hill, hydrous skarn overprinting is observed within garnet zone and wollastonite zone units. Extensive hydrous skarn is always spatially related to late brittle faults and/or the pluton contact. The areas of intense retrograde mineralization are shown as hydrothermally altered garnet skarn on the map (Fig. 1.2) and are characterized by the abundance of chlorite, epidote and sulfide minerals overprinting anhydrous assemblages (e.g. garnet and pyroxene). However, in places where the hydrous alteration occurs near the pluton is not always clear if the outcrop is hydrothermally altered garnet skarn or hydrothermally altered pluton. Less extensive hydrous alteration occurs throughout the map area in all units to some extent (sometimes in trace amounts) typically as epidote or pyrite mineralization.

## 3.7 Marble to Wollastonite Skarn Transformation- Quantification of transient syn-metamorphic permeability

### 3.7.1 Introduction

Early researchers recognized skarn formation as a dynamic process [*Lindgren*, 1902; *Barrell*, 1902; *Lawson*, 1914; *Korzhinskii*, 1936]. Since, it has been shown that metasomatism is

a much more complex process to quantify than isochemical metamorphism. In general, metasomatism can be defined as a type of metamorphism that occurs when the chemical composition of a rock changes due to the introduction of material from an external source. Although the primary control on the chemical composition of a metamorphic rock is the composition of the protolith, often fluid dynamics during metamorphism drive reaction causing changes in composition and can produce infiltration skarn. This type of skarn formation generally occurs at high temperature by metasomatic reaction with magmatic fluids where advective mass transfer is the main mechanism driving the alteration event. Although fluid composition controls much of the reaction producing skarn mineralogy and zoning, many factors are integral in influencing and driving reaction (e.g. permeability and fluid pressure gradients). Moreover, when quantifying a skarn system , there are several assumptions that must be evaluated based on geologic field and analytical evidence. First, the alteration event must be defined as open or closed. An open system involves the exchange of mass and energy between the system and surroundings whereas if the system remained closed the exchange of energy can occur but no mass change between the system and surroundings. Therefore, if gain and losses of species accompanies alteration, the geologic process must be defined as a geochemically open.

Once the skarn system is defined, other assumptions must be considered: (1) volume change, (2) immobile components, and (3) protolith. It is not necessary to make all of these assumptions simultaneously as one assumption may lead the researcher to conclusions about the others. Nevertheless, an accurate initial assumption when attempting to quantify skarn formation is essential. Textural relationships can often reveal the nature of volume change during an alteration event. On the outcrop scale, drastic volume losses (e.g. ~60-70 percent) may be seen in the field as extensive collapse features and vuggy textures. However, often these textures are not observed especially when volume losses are only on the scale of ~10 percent. Constant volume has been observed by measuring beds between protolith and altered rock and finding no

difference in thickness [*Lindgren*, 1924]. However, thickness differences usually cannot be measured due to extensive deformation and/or lack of protolith.

Likewise, immobility of one or more element can be an unreliable assumption. Many studies have assumed the immobility of $Al_2O_3$ and/or $TiO_2$ [*Ague*, 1994; *Lentz*, 1995; *this study*]. However, other authors contend that few to no elements remain immobile during this scale of metasomatic alteration in skarn [*Rae et. al.*, 1996; *Lentz*, 2000].

Moreover, protolith assumptions can be difficult in cases where no true (unaltered) protolith is preserved. This is especially evident in some roof pendants in the Coast Plutonic Complex of British Columbia (e.g. Mineral Hill) especially when reaction between units effectively creates a "new" rock type. Furthermore, metamorphism is frequently accompanied by deformation. Consequently, there may be tectonic interleaving of different protolith compositions, which gives rise to a metamorphic rock of mixed parentage.

The following section integrates geochemistry (e.g. XRF, ICP-MS) and mass balance to attempt to quantify complex geologic processes forming the Mineral Hill skarn deposit. In particular, volume change due to the reaction of marble to form wollastonite skarn is assessed.

### 3.7.2 Mass Balance

***Background***

Because changes in modes of minerals and bulk chemical composition is the essence of metasomatism, mass balance approaches were used to quantify gains and losses of components during wollastonite skarn petrogenesis at Mineral Hill. *Gresens'* [1967] introduced composition-volume relationships that calculate gains and losses using the chemical compositions and specific gravities of unaltered and metasomatically altered rocks or minerals. For the reaction:

100 grams of rock A + added species = X grams of rock B + removed species (R2)

he derived a set of equations to assess gains or losses of species in solution denoted as $x_n$ (in grams):

$$100[\, f_v\, (g^B/g^A)C_n^{\,B} - C_n^{\,A}] = x_n \qquad (1)$$

where $f_v$ is the volume factor, $g^B/g^A$ is the ratio of specific gravity of rock B to rock A, $C_n^{\,B}$ is the weight fraction of chemical species in rock B, $C_n^{\,A}$ is the weight fraction of chemical species in rock A (notation is also defined in Table 3.9).

To use *Gresens'* equations when comparing two rocks, it is necessary to know the chemical composition of the protolith (sometimes the "least-altered" sample is considered), and either the nature of volume change (reference frame) or the mobility/immobility of at least one component [*Gresens*, 1967; *Grant*, 1986]. *Gresens'* [1967] argued that some components will be immobile during alteration, therefore they can be used to define the volume change. Assuming that this volume factor is common to all components in the system, gains and losses of each component can be calculated.

*Grant* [1986] simplified *Gresens'* equations to mass relationships rather than volume and derived the equation:

$$\Delta M_n = [(M^B/M^A)C_n^{\,B} - C_n^{\,A}]M^A \qquad (2)$$

where $M_n$ is the mass of component *n* in rock A, $M^A$ is the total mass of rock A ($M^A = 100$ grams, dictated by eq. 1), $M^B$ is the total mass in rock B, $C_n^{\,A}$ is $M_n^{\,A}/M^A$ and $C_n^{\,B}$ is $M_n^{\,B}/M^B$. If the mass factor, $f_m$, is known ($M^B/M^A$) then a simple solution to the equation:

$$M^A[C_n^{\,B} f_m - C_n^{\,A}] = \Delta M_n \qquad (3)$$

will yield gains and losses of each component in the metasomatic system.

However, if $f_m$ is unknown, as is common in most metasomatic systems, then $\Delta M_n = 0$ for known or inferred immobile components. In this case, the mass factor can be resolved by:

$$f_m = f_v\, (g^B/g^A) = C_n^{\,A}/\, C_n^{\,B} \qquad (4)$$

Table 3.9. Notation for equations in Chapter 3.

| Definition | Symbol |
|---|---|
| Superscript for unaltered sample | A |
| Superscript for altered sample | B |
| Subscript for component (species) | $n$ |
| Specific gravity | g |
| Volume factor | $f_v$ |
| Mass factor | $f_m$ |
| Mass of sample | M |
| Mass of component $n$ | $M_n$ |
| Gain or loss of component relative To reference mass | $\Delta M_n$ |
| Gain or loss of component relative To reference volume | $x_n$ |
| Concentration of species $n$ | $C_n$ |
| time-integrated fluid flux | $q_v$ |
| time-integrated molar flux | $q_m$ |
| distance coordinate | z |
| fluid-rock ratio | F/R |

if $n$ = an immobile element. The mass factor can be graphically estimated by plotting $C_n^A$ against $C_n^B$. The concentration ratios of the immobile elements create an "isocon" through the origin that represents a linear array ($M^B/M^A$). This slope is taken as the mass factor value (considered a constant for the whole chemical system), consequently the volume change due to alteration. If $f_m = 1$ then there was no mass change; $f_m > 1$ a gain in mass; $f_m < 1$ a loss in mass [*Gresens*, 1967; *Grant*, 1986]. Moreover, the relative gains and losses for the mobile elements are graphically displayed above and below this isocon, respectively. It is crucial to note that the validity of an isocon choice increases when it is based on several geochemically unrelated species [*Grant*, 1986]. Grant's method was not used in this study even though it is easy to implement, since it is only convenient for small sample populations.

In this study, element ratio diagrams were utilized to assess immobile components since they easily accommodate large sample sets. This method plots the concentration of two immobile elements against each other (e.g. $Al_2O_3$ vs. $TiO_2$). The samples should plot along a straight line (or close to) that intercepts at the origin. The sample population experiencing a mass gain plots on the line below (closer to the origin) protolith samples; those experiencing a mass loss plot on the line above the protolith samples [*Russell and Nicholls*, 1988; *Russell and Stanley*, 1990].

In order to accurately evaluate mass transport in this method (as with any of the aforementioned methods), multiple analyses of altered and unaltered rocks were included in order to evaluate the uncertainties associated with analytical procedures and the degree of variation within the sample population. Moreover, it is important to note that when using a mass-balance approach to quantify a metasomatic process, the gains and losses calculated address only time-integrated effects, not changes at any moment in time [*Baumgartner and Olsen*, 1995].

Few studies have been done that use *Gresens'* approach to mass balance calculations in order to quantify skarn-forming processes. Most studies have compared unaltered mineralogy and microprobe data to altered equivalents [*Lindgren*, 1924; *James*, 1976; *Kwak*, 1978; *Kwak*

*and Askin*, 1981]. There is uncertainty in their results where no assumptions on volume change or immobility were made. Since detailed field mapping showing skarn mineral phases and their distribution, combined with geochemistry, can provide much of the information in order to make the appropriate assumptions involved in mass balance calculation, the gains and losses of components in a specific skarn can be quantified.

### 3.7.3 Results

***Element Ratios***

Element ratio diagrams were constructed in order to identify immobile components during skarn formation at Mineral Hill. Inter-laboratory comparisons revealed that geochemical analyses between ALS Chemex and McGill labs should not be compared when looking at element ratios because inter-laboratory variation would introduce significant error (see section 3.2.1). Therefore, only geochemical analyses from ALS Chemex were examined for the following reasons: (1) A more extensive suite of elements was analyzed, and (2) abundant spatially related wollastonite skarn and marbles were analyzed.

Approximately constant ratios between Al, Ti, Zr, V, Yb, and Y in marble and wollastonite skarn suggest that they were relatively immobile during skarn formation (Fig. 3.23). Marble whole rock major, minor and trace element abundances are relatively homogeneous. Most marble compositions fall within fields for marble from Hope Valley, CA and common limestone chemical compositions. However, wollastonite skarn whole rock compositions vary markedly. Wollastonite skarn samples have been divided into two groups based on the abundance of Al, Ti, Zr, V, Yb, and Y. Although there is some overlap, in type B skarn these components are slightly elevated over those in the marble while in type A skarn these elements are much more abundant. However, there are no obvious, systematic textural or mineralogical

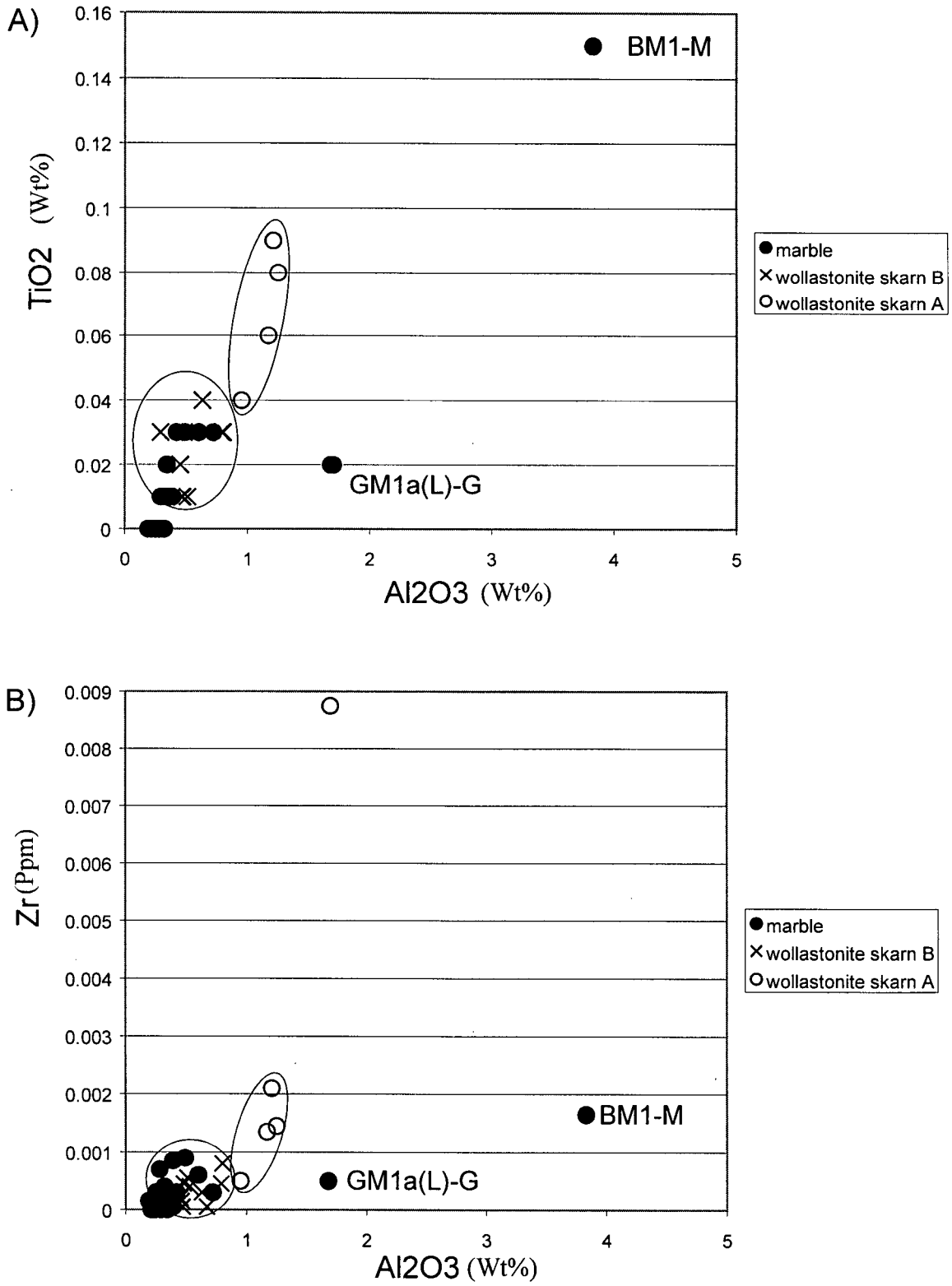


Fig 3.23. A) Element Ratio plot of $TiO_2$ vs. $Al_2O_3$. B) Element Ratio plot of Zr vs. $Al_2O_3$. Ovals represent fields for type A skarn or type B skarn based on concentrations of $Al_2O_3$ greater (A) or less than (B) ~1 wt%.

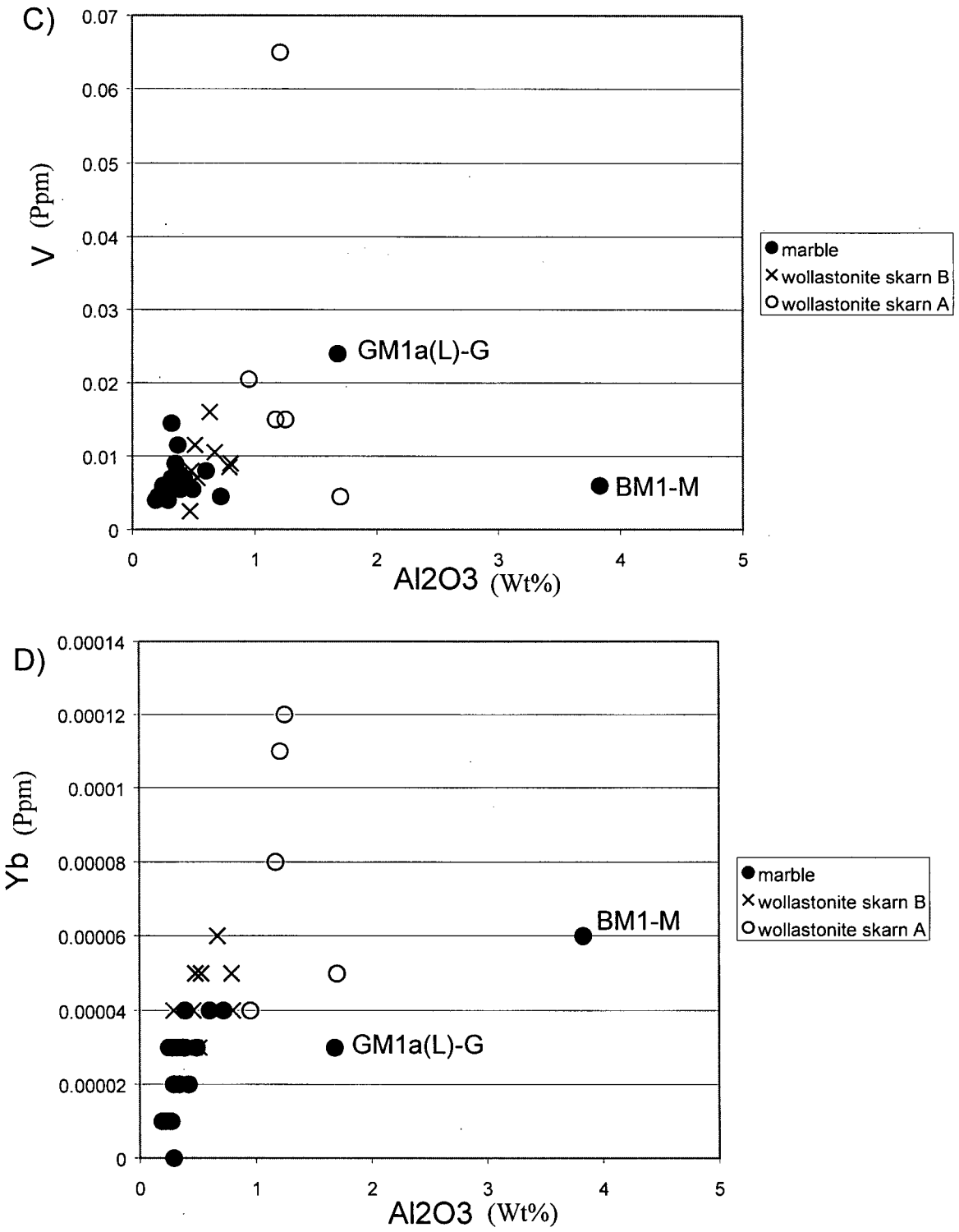


Fig 3.23. C) Element Ratio plot of V vs. Al2O3. D) Element Ratio plot of Yb vs. Al2O3. Relatively constant ratios suggest immobility during wollastonite skarn formation.

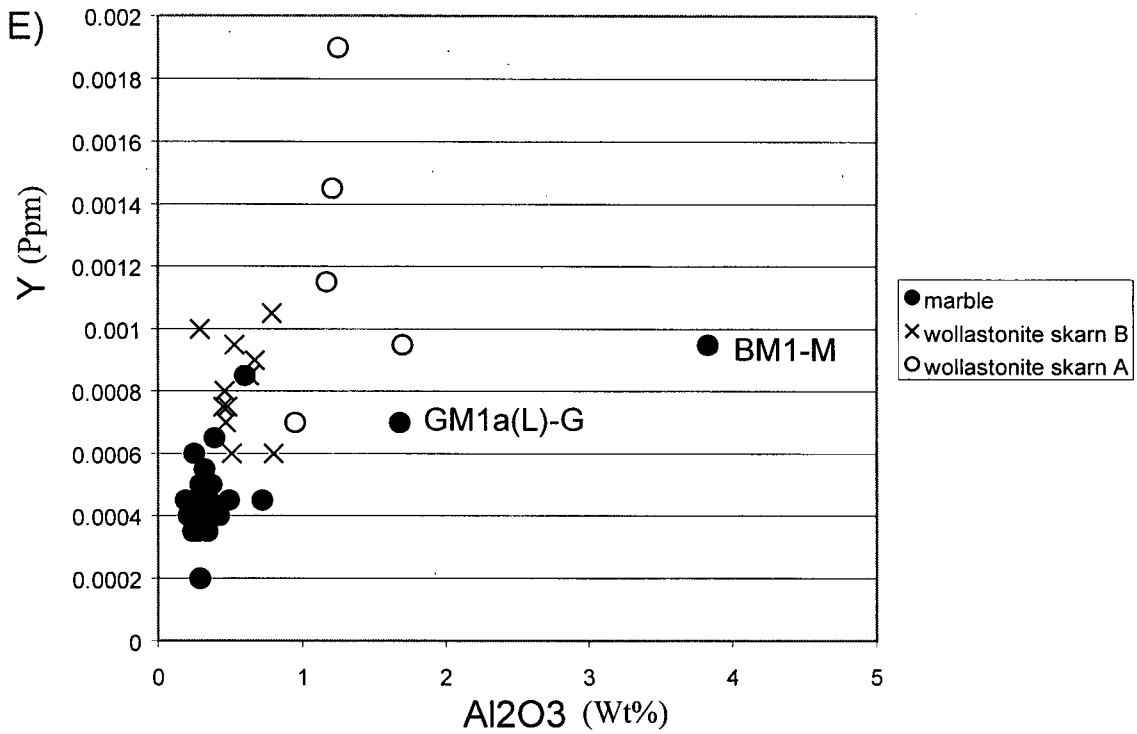


Fig. 3.23. E) Element Ratio plot of Y vs. Al2O3. Relatively constant ratios suggest immobility during wollastonite skarn formation.

differences between skarn types. Geochemistry of type A skarn, type B skarn, and marble are presented in Table 3.10.

Elemental differences between type A and type B skarn can be interpreted in one of two ways: (1) the two wollastonite skarn types developed from different protoliths, or (2) they shared a common protolith but developed by different reactions.

The volume change from marble samples to type A skarn and from marble to type B skarn was calculated from eq. 4, chemical analyses, and densities of calcite and wollastonite (Table 3.11). Since $\Delta M_n = 0$ for inferred immobile components (i.e. $Al_2O_3$), then the mass factor can be resolved by $f_m = C_n^A/C_n^B$. Volume losses of ~50-70% were calculated for the formation of type A skarn from marble (Table 3.11). Volume losses of ~20% were calculated for the formation of skarn B from marbles (Table 3.11). Volume losses of 50-70 % are considered unlikely along the delicately fingered skarn-marble interface because of the lack of collapse features to accommodate a large volume change. Therefore, it is suggested that the two wollastonite skarn types developed from different protoliths, since Type A skarn probably formed by reaction between limestone and other rock types that contained these elements in greater abundance. Type A skarn also contains greater abundances of Ni, La, Lu, and $Fe_2O_3$ although constant ratios are not observed among these elements insinuating their possible mobility. Type B skarn appears to have formed by reaction of calcite marble with $SiO_2$-bearing, $H_2O$-rich fluids. The large volume loss (~20%) associated with this reaction must have led to a substantial local increase in permeability.

***Fluid-rock ratios and time-integrated fluid fluxes for silica metasomatism***

Gains and losses of species from average marble to wollastonite type B, type A, and type ? (borderline A or B) were calculated assuming the immobility of $Al_2O_3$ and V, and respective mass factors (Table 3.11a, b). These values are presented in Table 3.12. Wollastonite skarn at

Table 3.10. Geochemistry of type A skarn (A), type B skarn (B), and marble. All analyses from ALS Chemex

| Sample | | | W1d (w) | UB4e(w) | 00-H8-W | 00-H11-W | M1h- | W1b | W1c | 00H13-W | 00H1-W |
|---|---|---|---|---|---|---|---|---|---|---|---|
| lithology | | | A | A | A | A | A? | B | B | B | B |
| | Ba | ICP-MS | 6.5 | 16.5 | 16.5 | 4.5 | 4.5 | 2.5 | 201 | 23 | 12.5 |
| | Ce | ICP-MS | 4.5 | 8 | 8 | 2.5 | 2 | 2 | 5 | 2 | 21.5 |
| | Cs | ICP-MS | <0.1 | <0.1 | <0.1 | <0.1 | <0.1 | <0.1 | <0.1 | <0.1 | <0.1 |
| | Co | ICP-MS | 8 | 17 | 10 | 3 | 13 | 12 | 6 | 4 | 14 |
| | Cu | ICP-MS | 30 | 5 | <5 | 5 | 5 | 5 | 5 | 5 | 5 |
| | Dy | ICP-MS | 1 | 1.5 | 1.7 | 0.8 | 0.5 | 0.5 | 0.8 | 0.7 | 0.8 |
| | Er | ICP-MS | 0.8 | 1 | 1.3 | 0.7 | 0.5 | 0.4 | 0.7 | 0.5 | 0.5 |
| | Eu | ICP-MS | 0.2 | 0.3 | 0.4 | 0.2 | 0.1 | 0.1 | 0.1 | 0.1 | 0.2 |
| | Gd | ICP-MS | 0.9 | 1.8 | 1.8 | 0.7 | 0.7 | 0.5 | 0.9 | 0.9 | 0.9 |
| | Ga | ICP-MS | 2 | 3 | 1 | 2 | 1 | 1 | 1 | 1 | 1 |
| | Hf | ICP-MS | <1 | <1 | <1 | 1 | <1 | <1 | <1 | <1 | <1 |
| | Ho | ICP-MS | 0.2 | 0.3 | 0.4 | 0.1 | 0.1 | 0.1 | 0.2 | 0.1 | 0.1 |
| | La | ICP-MS | 4.5 | 8.5 | 9.5 | 2.5 | 2.5 | 2 | 5 | 2.5 | 22 |
| | Pb | ICP-MS | <5 | <5 | 5 | 5 | <5 | 10 | <5 | 5 | <5 |
| | Lu | ICP-MS | 0.1 | 0.1 | 0.2 | <0.1 | <0.1 | <0.1 | <0.1 | <0.1 | <0.1 |
| | Nd | ICP-MS | 3.5 | 8 | 7.5 | 2.5 | 2 | 1.5 | 4 | 2.5 | 6.5 |
| | Ni | ICP-MS | 10 | 50 | 25 | <5 | 25 | <5 | <5 | 5 | <5 |
| | Nb | ICP-MS | 1 | 4 | 1 | 1 | <1 | <1 | <1 | <1 | 1 |
| | Pr | ICP-MS | 1 | 1.8 | 1.8 | 0.6 | 0.5 | 0.4 | 0.9 | 0.5 | 2 |
| | Rb | ICP-MS | 0.2 | 2.2 | 1.2 | 1 | 0.4 | 0.6 | 6.2 | 0.8 | 1.4 |
| | Sm | ICP-MS | 0.7 | 1.5 | 1.3 | 0.6 | 0.5 | 0.4 | 0.6 | 0.5 | 0.9 |
| | Ag | ICP-MS | <1 | 2 | <1 | <1 | <1 | <1 | <1 | <1 | <1 |
| | Sr | ICP-MS | 69.1 | 102.5 | 99.4 | 44.4 | 92.2 | 94.5 | 33 | 68.5 | 104 |
| | Ta | ICP-MS | <0.5 | <0.5 | <0.5 | <0.5 | <0.5 | <0.5 | <0.5 | <0.5 | 0.5 |
| | Tb | ICP-MS | 0.1 | 0.2 | 0.3 | 0.1 | 0.1 | <0.1 | 0.1 | 0.1 | 0.1 |
| | Tl | ICP-MS | <0.5 | <0.5 | <0.5 | <0.5 | <0.5 | <0.5 | <0.5 | <0.5 | <0.5 |
| | Th | ICP-MS | <1 | <1 | <1 | 1 | <1 | <1 | <1 | <1 | <1 |
| | Tm | ICP-MS | 0.1 | 0.1 | 0.1 | <0.1 | <0.1 | <0.1 | <0.1 | <0.1 | <0.1 |
| | Sn | ICP-MS | <1 | <1 | <1 | <1 | <1 | <1 | <1 | <1 | <1 |
| | W | ICP-MS | 21 | 70 | 66 | 35 | 135 | 69 | 29 | 40 | 75 |
| | U | ICP-MS | 6.5 | 16 | 6.5 | 25.5 | 5 | 1.5 | 12.5 | 4.5 | 5 |
| | V | ICP-MS | 150 | 650 | 150 | 45 | 205 | 115 | 70 | 160 | 75 |
| | Yb | ICP-MS | 0.8 | 1.1 | 1.2 | 0.5 | 0.4 | 0.3 | 0.5 | 0.4 | 0.3 |
| | Y | ICP-MS | 11.5 | 14.5 | 19 | 9.5 | 7 | 6 | 9.5 | 8.5 | 7.5 |
| | Zn | ICP-MS | 95 | 150 | 70 | 25 | 55 | 125 | 25 | 275 | 30 |
| | Zr | ICP-MS | 13.5 | 21 | 14.5 | 87.5 | 5 | 5.5 | 4 | 3 | 2 |
| | Al2O3 | XRF | 1.17 | 1.21 | 1.25 | 1.7 | 0.95 | 0.51 | 0.53 | 0.63 | 0.45 |
| | CaO | XRF | 45.48 | 45.32 | 45.83 | 45.36 | 45.53 | 37.57 | 44.98 | 46.24 | 45.85 |
| | Cr2O3 | XRF | <0.01 | <0.01 | <0.01 | <0.01 | <0.01 | <0.01 | <0.01 | <0.01 | <0.01 |
| | Fe2O3 | XRF | 1.04 | 0.97 | 0.6 | 0.23 | 0.33 | 1.57 | 0.31 | 0.37 | 0.26 |
| | K2O | XRF | 0.01 | 0.02 | 0.05 | 0.02 | 0.02 | 0.03 | 0.22 | 0.02 | 0.04 |
| | MgO | XRF | 0.44 | 0.46 | 0.43 | 0.23 | 0.86 | 4.31 | 0.98 | 0.28 | 0.21 |
| | MnO | XRF | 0.11 | 0.1 | 0.06 | 0.1 | 0.15 | 0.18 | 0.18 | 0.11 | 0.13 |
| | Na2O | XRF | <0.01 | <0.01 | <0.01 | <0.01 | <0.01 | <0.01 | <0.01 | <0.01 | <0.01 |
| | P2O5 | XRF | 0.14 | 0.25 | 1.05 | 0.05 | 0.16 | 0.03 | 0.25 | 0.1 | 0.15 |
| | SiO2 | XRF | 49.34 | 50.51 | 45.52 | 50.66 | 44.34 | 51.17 | 51.52 | 46.87 | 51.1 |
| | TiO2 | XRF | 0.06 | 0.09 | 0.08 | 0.02 | 0.04 | 0.01 | 0.03 | 0.04 | 0.02 |
| | LOI | XRF | 1.41 | 0.41 | 4.29 | 0.83 | 6.83 | 3.8 | 0.16 | 4.56 | 0.85 |

Table 3.10.

| Sample lithology | | | 00H7-W B | 00H4-W B | 00H3-W B | 00-H2-W B | 1a(u B | W1a B? | 00H10-W B? | W1d (mb marble | UBM1a marble |
|---|---|---|---|---|---|---|---|---|---|---|---|
| | Ba | ICP-MS | 9.5 | 20.5 | 5 | 3 | 2 | 6 | 4 | 8 | 7 |
| | Ce | ICP-MS | 5 | 1.5 | 2 | 4 | 3 | 5 | 2 | 4 | 4 |
| | Cs | ICP-MS | <0.1 | <0.1 | <0.1 | <0.1 | <0.1 | <0.1 | <0.1 | <0.1 | <0.1 |
| | Co | ICP-MS | 6 | 4 | 5 | 5 | 5 | 9 | 13 | 9 | 7 |
| | Cu | ICP-MS | 10 | 5 | 5 | 15 | <5 | 15 | 5 | 10 | 10 |
| | Dy | ICP-MS | 0.7 | 0.6 | 0.5 | 0.8 | 0.7 | 0.4 | 0.8 | 0.5 | 0.4 |
| | Er | ICP-MS | 0.5 | 0.5 | 0.5 | 0.6 | 0.6 | 0.4 | 0.7 | 0.4 | 0.3 |
| | Eu | ICP-MS | 0.1 | <0.1 | 0.1 | 0.1 | 0.1 | 0.1 | 0.1 | 0.1 | 0.1 |
| | Gd | ICP-MS | 0.8 | 0.6 | 0.7 | 0.8 | 0.8 | 0.7 | 0.7 | 0.6 | 0.5 |
| | Ga | ICP-MS | <1 | <1 | <1 | <1 | 1 | 1 | 1 | <1 | <1 |
| | Hf | ICP-MS | <1 | <1 | <1 | <1 | <1 | <1 | <1 | <1 | <1 |
| | Ho | ICP-MS | 0.1 | 0.1 | 0.1 | 0.2 | 0.1 | 0.1 | 0.2 | 0.1 | 0.1 |
| | La | ICP-MS | 5 | 2 | 2.5 | 3.5 | 1.5 | 5.5 | 2.5 | 5 | 4 |
| | Pb | ICP-MS | <5 | <5 | <5 | <5 | <5 | <5 | <5 | <5 | <5 |
| | Lu | ICP-MS | <0.1 | <0.1 | <0.1 | <0.1 | <0.1 | <0.1 | <0.1 | <0.1 | <0.1 |
| | Nd | ICP-MS | 5 | 2 | 2 | 3.5 | 2.5 | 4 | 2.5 | 4 | 2.5 |
| | Ni | ICP-MS | <5 | <5 | 15 | <5 | 30 | <5 | 5 | <5 | <5 |
| | Nb | ICP-MS | <1 | <1 | <1 | <1 | <1 | <1 | <1 | <1 | <1 |
| | Pr | ICP-MS | 1.1 | 0.4 | 0.5 | 0.8 | 0.5 | 1 | 0.6 | 1.2 | 0.7 |
| | Rb | ICP-MS | 1.6 | 0.2 | 0.6 | 0.4 | <0.2 | 1.2 | 0.8 | 0.2 | 3 |
| | Sm | ICP-MS | 1 | 0.4 | 0.4 | 0.7 | 0.5 | 0.7 | 0.5 | 0.5 | 0.5 |
| | Ag | ICP-MS | <1 | <1 | 4 | <1 | <1 | <1 | 11 | <1 | <1 |
| | Sr | ICP-MS | 207 | 479 | 228 | 54.7 | 47.3 | 55.1 | 55.4 | 790 | 340 |
| | Ta | ICP-MS | 0.5 | <0.5 | <0.5 | 0.5 | <0.5 | <0.5 | <0.5 | <0.5 | <0.5 |
| | Tb | ICP-MS | 0.1 | <0.1 | 0.1 | 0.1 | 0.1 | <0.1 | 0.1 | <0.1 | <0.1 |
| | Tl | ICP-MS | <0.5 | <0.5 | <0.5 | <0.5 | <0.5 | <0.5 | <0.5 | <0.5 | <0.5 |
| | Th | ICP-MS | <1 | <1 | <1 | <1 | <1 | <1 | <1 | <1 | <1 |
| | Tm | ICP-MS | <0.1 | <0.1 | <0.1 | <0.1 | <0.1 | <0.1 | 0.1 | <0.1 | <0.1 |
| | Sn | ICP-MS | <1 | <1 | <1 | <1 | <1 | <1 | 1 | <1 | <1 |
| | W | ICP-MS | 56 | 37 | 57 | 57 | 57 | 41 | 53 | 25 | 14 |
| | U | ICP-MS | 1.5 | 4 | 1.5 | 4 | 1.5 | 7 | 10.5 | 1 | 4 |
| | V | ICP-MS | 80 | 25 | 60 | 60 | 105 | 90 | 85 | 55 | 55 |
| | Yb | ICP-MS | 0.5 | 0.3 | 0.4 | 0.4 | 0.6 | 0.4 | 0.5 | 0.3 | 0.3 |
| | Y | ICP-MS | 7.5 | 7 | 8 | 10 | 9 | 6 | 10.5 | 6.5 | 4.5 |
| | Zn | ICP-MS | 225 | 20 | 20 | 25 | 35 | 35 | 25 | 25 | 5 |
| | Zr | ICP-MS | 4.5 | 0.5 | 1.5 | 1.5 | 0.5 | 8 | 4.5 | 8.5 | 9 |
| | Al2O3 | XRF | 0.48 | 0.47 | 0.46 | 0.29 | 0.67 | 0.8 | 0.79 | 0.39 | 0.49 |
| | CaO | XRF | 47.41 | 46.19 | 47.55 | 46.02 | 45.8 | 45.85 | 45.57 | 53.68 | 54.95 |
| | Cr2O3 | XRF | <0.01 | <0.01 | <0.01 | <0.01 | <0.01 | <0.01 | <0.01 | <0.01 | <0.01 |
| | Fe2O3 | XRF | 0.28 | 0.12 | 0.22 | 0.22 | 0.46 | 0.57 | 0.46 | 0.27 | 0.27 |
| | K2O | XRF | 0.05 | 0.03 | 0.03 | 0.04 | 0.03 | 0.02 | 0.02 | 0.03 | 0.03 |
| | MgO | XRF | 0.26 | 0.22 | 0.27 | 0.31 | 0.33 | 0.38 | 0.24 | 0.25 | 0.27 |
| | MnO | XRF | 0.05 | 0.15 | 0.09 | 0.13 | 0.11 | 0.1 | 0.17 | 0.03 | 0.03 |
| | Na2O | XRF | <0.01 | <0.01 | <0.01 | <0.01 | <0.01 | <0.01 | <0.01 | <0.01 | <0.01 |
| | P2O5 | XRF | 0.04 | 0.15 | 0.01 | 0.15 | 0.04 | 0.22 | 0.34 | 0.01 | 0.09 |
| | SiO2 | XRF | 38.05 | 50.54 | 38.71 | 51.38 | 50.94 | 50.94 | 47.87 | 9.86 | 1.65 |
| | TiO2 | XRF | 0.03 | 0.01 | 0.01 | 0.03 | 0.03 | 0.03 | 0.03 | 0.01 | 0.03 |
| | LOI | XRF | 12.61 | 1.23 | 11.86 | 0.6 | 0.7 | 0.18 | 3.77 | 34.71 | 41.41 |

Table 3.10.

| Sample lithology | | | 00H3-M marble | 00NE-3a-marble | 0-NE-2-M marble | 00UMQ-2-M marble | 0UMQ-1-marble | 00H4-M marble | 00H10-marble |
|---|---|---|---|---|---|---|---|---|---|
| | Ba | ICP-MS | 12 | 17 | 13 | 21 | 42.5 | 259 | 10 |
| | Ce | ICP-MS | 7 | 3 | 2 | 4 | 7 | 2.5 | 3 |
| | Cs | ICP-MS | <0.1 | 0.1 | <0.1 | <0.1 | <0.1 | <0.1 | <0.1 |
| | Co | ICP-MS | 3 | 2 | 3 | 3 | 2 | 3 | 3 |
| | Cu | ICP-MS | 10 | 5 | 5 | 10 | 5 | 5 | 10 |
| | Dy | ICP-MS | 0.4 | 0.2 | 0.3 | 0.3 | 0.3 | 0.2 | 0.4 |
| | Er | ICP-MS | 0.5 | 0.2 | 0.2 | 0.2 | 0.3 | 0.1 | 0.4 |
| | Eu | ICP-MS | 0.1 | <0.1 | <0.1 | 0.1 | 0.1 | 0.1 | 0.1 |
| | Gd | ICP-MS | 0.6 | 0.3 | 0.4 | 0.4 | 0.5 | 0.5 | 0.6 |
| | Ga | ICP-MS | <1 | <1 | <1 | <1 | <1 | <1 | <1 |
| | Hf | ICP-MS | <1 | <1 | <1 | <1 | <1 | <1 | <1 |
| | Ho | ICP-MS | 0.1 | <0.1 | <0.1 | <0.1 | 0.1 | <0.1 | 0.1 |
| | La | ICP-MS | 9 | 3.5 | 2.5 | 4 | 7 | 3.5 | 3.5 |
| | Pb | ICP-MS | 5 | <5 | 5 | <5 | <5 | 5 | <5 |
| | Lu | ICP-MS | <0.1 | <0.1 | <0.1 | <0.1 | <0.1 | <0.1 | <0.1 |
| | Nd | ICP-MS | 4 | 1.5 | 1.5 | 2.5 | 3 | 2 | 3 |
| | Ni | ICP-MS | <5 | <5 | <5 | <5 | <5 | <5 | <5 |
| | Nb | ICP-MS | <1 | <1 | <1 | <1 | <1 | <1 | <1 |
| | Pr | ICP-MS | 1.1 | 0.5 | 0.4 | 0.6 | 0.8 | 0.5 | 0.6 |
| | Rb | ICP-MS | 1.2 | 3 | 1.8 | 1 | 3.4 | 0.6 | 0.2 |
| | Sm | ICP-MS | 0.6 | 0.3 | 0.3 | 0.3 | 0.4 | 0.3 | 0.6 |
| | Ag | ICP-MS | <1 | <1 | <1 | <1 | <1 | <1 | <1 |
| | Sr | ICP-MS | 696 | 240 | 302 | 361 | 369 | 356 | 402 |
| | Ta | ICP-MS | <0.5 | <0.5 | <0.5 | <0.5 | <0.5 | <0.5 | <0.5 |
| | Tb | ICP-MS | <0.1 | <0.1 | <0.1 | <0.1 | <0.1 | <0.1 | <0.1 |
| | Tl | ICP-MS | <0.5 | <0.5 | <0.5 | <0.5 | <0.5 | <0.5 | <0.5 |
| | Th | ICP-MS | <1 | <1 | <1 | <1 | <1 | <1 | <1 |
| | Tm | ICP-MS | <0.1 | <0.1 | <0.1 | <0.1 | <0.1 | <0.1 | <0.1 |
| | Sn | ICP-MS | <1 | <1 | <1 | <1 | <1 | <1 | <1 |
| | W | ICP-MS | 14 | 10 | 9 | 5 | 7 | 12 | 16 |
| | U | ICP-MS | 3.5 | 3 | 3 | 5 | 3 | 3 | 2.5 |
| | V | ICP-MS | 60 | 55 | 55 | 70 | 60 | 50 | 70 |
| | Yb | ICP-MS | 0.3 | 0.1 | 0.2 | 0.2 | 0.3 | 0.1 | 0.3 |
| | Y | ICP-MS | 6 | 3.5 | 4 | 4 | 4.5 | 3.5 | 5.5 |
| | Zn | ICP-MS | 125 | 105 | 25 | 5 | <5 | 15 | 125 |
| | Zr | ICP-MS | 3 | 3 | <0.5 | 3 | 7 | <0.5 | 4 |
| | Al2O3 | XRF | 0.25 | 0.27 | 0.29 | 0.42 | 0.28 | 0.24 | 0.32 |
| | CaO | XRF | 54.68 | 55.08 | 54.72 | 55.22 | 55.16 | 54.91 | 53.79 |
| | Cr2O3 | XRF | <0.01 | <0.01 | <0.01 | <0.01 | <0.01 | <0.01 | <0.01 |
| | Fe2O3 | XRF | 0.05 | 0.1 | 0.09 | 1.18 | 0.31 | 0.03 | 0.23 |
| | K2O | XRF | 0.03 | 0.04 | 0.03 | 0.03 | 0.03 | 0.03 | 0.02 |
| | MgO | XRF | 0.16 | 0.23 | 0.22 | 0.31 | 0.28 | 0.21 | 0.32 |
| | MnO | XRF | 0.01 | 0.01 | 0.01 | 0.06 | 0.05 | 0.01 | 0.03 |
| | Na2O | XRF | <0.01 | <0.01 | <0.01 | <0.01 | <0.01 | <0.01 | <0.01 |
| | P2O5 | XRF | 0.13 | 0.05 | 0.06 | 0.07 | 0.03 | 0.07 | 0.08 |
| | SiO2 | XRF | 3.45 | 0.89 | 0.89 | 1.61 | 1.19 | 1.04 | 4.91 |
| | TiO2 | XRF | <0.01 | <0.01 | <0.01 | 0.03 | <0.01 | <0.01 | 0.01 |
| | LOI | XRF | 40.41 | 42.54 | 42.83 | 40.11 | 41.99 | 42.72 | 39.56 |

Table 3.10.

| Sample lithology | | | 00H6-M marble | 00NE-1-marble | GM1h-M marble | 0UMQ-3-marble | 00H15-M marble | 00NE-3b-marble | 00H12-marble | 00H9-M marble |
|---|---|---|---|---|---|---|---|---|---|---|
| | Ba | ICP-MS | 8.5 | 24 | 13 | 11 | 12.5 | 19 | 11.5 | 10 |
| | Ce | ICP-MS | 4.5 | 3 | 4.5 | 4.5 | 3 | 2.5 | 4.5 | 4.5 |
| | Cs | ICP-MS | <0.1 | <0.1 | <0.1 | 0.1 | <0.1 | <0.1 | <0.1 | <0.1 |
| | Co | ICP-MS | 3 | 2 | 3 | 4 | 3 | 3 | 4 | 3 |
| | Cu | ICP-MS | 5 | 5 | 20 | 10 | 5 | <5 | 25 | 15 |
| | Dy | ICP-MS | 0.2 | <0.1 | 0.4 | 0.7 | 0.3 | 0.2 | 0.4 | 0.3 |
| | Er | ICP-MS | 0.3 | 0.1 | 0.3 | 0.5 | 0.3 | 0.3 | 0.3 | 0.4 |
| | Eu | ICP-MS | 0.1 | <0.1 | 0.1 | 0.2 | 0.1 | 0.1 | 0.1 | 0.1 |
| | Gd | ICP-MS | 0.4 | 0.2 | 0.5 | 0.9 | 0.5 | 0.4 | 0.5 | 0.7 |
| | Ga | ICP-MS | <1 | <1 | <1 | <1 | <1 | <1 | <1 | <1 |
| | Hf | ICP-MS | <1 | <1 | <1 | <1 | <1 | <1 | <1 | <1 |
| | Ho | ICP-MS | <0.1 | <0.1 | 0.1 | 0.1 | 0.1 | <0.1 | <0.1 | 0.1 |
| | La | ICP-MS | 5 | 2 | 3.5 | 4.5 | 3 | 2.5 | 2.5 | 3.5 |
| | Pb | ICP-MS | <5 | <5 | <5 | <5 | <5 | <5 | <5 | <5 |
| | Lu | ICP-MS | <0.1 | <0.1 | <0.1 | <0.1 | <0.1 | <0.1 | <0.1 | <0.1 |
| | Nd | ICP-MS | 2.5 | 1.5 | 2.5 | 4 | 2 | 1.5 | 2 | 3 |
| | Ni | ICP-MS | <5 | <5 | 25 | 5 | <5 | <5 | 15 | <5 |
| | Nb | ICP-MS | <1 | <1 | <1 | 1 | <1 | <1 | <1 | <1 |
| | Pr | ICP-MS | 0.7 | 0.4 | 0.6 | 0.9 | 0.5 | 0.4 | 0.5 | 0.6 |
| | Rb | ICP-MS | <0.2 | 2.6 | <0.2 | 0.6 | 0.4 | 0.8 | 1.4 | 1 |
| | Sm | ICP-MS | 0.4 | 0.2 | 0.4 | 0.7 | 0.3 | 0.3 | 0.4 | 0.5 |
| | Ag | ICP-MS | <1 | <1 | <1 | <1 | <1 | 25 | <1 | <1 |
| | Sr | ICP-MS | 544 | 531 | 454 | 316 | 357 | 253 | 369 | 457 |
| | Ta | ICP-MS | <0.5 | <0.5 | <0.5 | <0.5 | <0.5 | <0.5 | <0.5 | <0.5 |
| | Tb | ICP-MS | <0.1 | <0.1 | <0.1 | 0.1 | <0.1 | <0.1 | <0.1 | <0.1 |
| | Tl | ICP-MS | <0.5 | <0.5 | <0.5 | <0.5 | <0.5 | <0.5 | <0.5 | <0.5 |
| | Th | ICP-MS | <1 | <1 | <1 | <1 | <1 | <1 | <1 | <1 |
| | Tm | ICP-MS | <0.1 | <0.1 | <0.1 | <0.1 | <0.1 | <0.1 | <0.1 | <0.1 |
| | Sn | ICP-MS | <1 | <1 | <1 | <1 | <1 | <1 | <1 | <1 |
| | W | ICP-MS | 14 | 8 | 9 | 18 | 13 | 8 | 16 | 9 |
| | U | ICP-MS | 2 | 2 | 2 | 5 | 2 | 2 | 3 | 2 |
| | V | ICP-MS | 45 | 40 | 145 | 80 | 90 | 60 | 45 | 75 |
| | Yb | ICP-MS | 0.1 | <0.1 | 0.3 | 0.4 | 0.3 | 0.2 | 0.4 | 0.4 |
| | Y | ICP-MS | 4 | 2 | 5.5 | 8.5 | 4.5 | 3.5 | 4.5 | 6.5 |
| | Zn | ICP-MS | 35 | 5 | 25 | 20 | 25 | 35 | 10 | 285 |
| | Zr | ICP-MS | <0.5 | <0.5 | 3.5 | 6 | 1.5 | <0.5 | 3 | 0.5 |
| | Al2O3 | XRF | 0.21 | 0.29 | 0.32 | 0.6 | 0.35 | 0.34 | 0.72 | 0.39 |
| | CaO | XRF | 55.59 | 54.49 | 53.92 | 52.45 | 52.68 | 54.85 | 53.11 | 53.6 |
| | Cr2O3 | XRF | <0.01 | <0.01 | <0.01 | <0.01 | <0.01 | <0.01 | <0.01 | <0.01 |
| | Fe2O3 | XRF | 0.01 | 0.01 | 0.19 | 1.18 | 0.09 | 0.1 | 0.21 | 0.22 |
| | K2O | XRF | 0.01 | 0.09 | 0.02 | 0.03 | 0.03 | 0.05 | 0.07 | 0.05 |
| | MgO | XRF | 0.17 | 0.23 | 0.36 | 2.93 | 1.46 | 0.24 | 0.46 | 0.28 |
| | MnO | XRF | 0.01 | 0.01 | 0.03 | 0.06 | 0.06 | 0.01 | 0.04 | 0.02 |
| | Na2O | XRF | <0.01 | <0.01 | <0.01 | <0.01 | <0.01 | <0.01 | <0.01 | <0.01 |
| | P2O5 | XRF | 0.07 | 0.04 | 0.06 | 0.09 | 0.07 | 0.03 | 0.07 | 0.08 |
| | SiO2 | XRF | 1.92 | 2.89 | 7.37 | 1.51 | 5.47 | 1.54 | 4.29 | 4.3 |
| | TiO2 | XRF | <0.01 | <0.01 | <0.01 | 0.03 | 0.01 | 0.02 | 0.03 | 0.01 |
| | LOI | XRF | 41.21 | 41.08 | 36.99 | 40.22 | 39.05 | 42.17 | 40.28 | 40.27 |

Table 3.10.

| Sample lithology | | | 00H13-M marble | BM-1-M marble | 00H14-M marble | GM1e (R)-G marble |
|---|---|---|---|---|---|---|
| | Ba | ICP-MS | 15 | 88.5 | 14.5 | 14.5 |
| | Ce | ICP-MS | 4 | 10.5 | 4.5 | 6 |
| | Cs | ICP-MS | <0.1 | 1.1 | <0.1 | <0.1 |
| | Co | ICP-MS | 2 | 10 | 4 | 3 |
| | Cu | ICP-MS | <5 | 5 | 5 | 15 |
| | Dy | ICP-MS | 0.4 | 1.2 | 0.3 | 0.4 |
| | Er | ICP-MS | 0.3 | 0.7 | 0.3 | 0.4 |
| | Eu | ICP-MS | 0.1 | 0.4 | 0.1 | 0.2 |
| | Gd | ICP-MS | 0.6 | 1.4 | 0.4 | 0.8 |
| | Ga | ICP-MS | <1 | 3 | <1 | <1 |
| | Hf | ICP-MS | <1 | <1 | <1 | <1 |
| | Ho | ICP-MS | 0.1 | 0.2 | 0.1 | 0.1 |
| | La | ICP-MS | 3 | 5 | 2.5 | 5 |
| | Pb | ICP-MS | <5 | <5 | <5 | <5 |
| | Lu | ICP-MS | <0.1 | 0.1 | <0.1 | <0.1 |
| | Nd | ICP-MS | 2 | 6 | 2 | 3.5 |
| | Ni | ICP-MS | <5 | 15 | <5 | 20 |
| | Nb | ICP-MS | <1 | 3 | <1 | <1 |
| | Pr | ICP-MS | 0.5 | 1.3 | 0.5 | 0.9 |
| | Rb | ICP-MS | 0.6 | 10.8 | <0.2 | <0.2 |
| | Sm | ICP-MS | 0.4 | 1.2 | 0.4 | 0.6 |
| | Ag | ICP-MS | <1 | <1 | <1 | <1 |
| | Sr | ICP-MS | 416 | 264 | 348 | 474 |
| | Ta | ICP-MS | <0.5 | <0.5 | <0.5 | <0.5 |
| | Tb | ICP-MS | <0.1 | 0.2 | <0.1 | <0.1 |
| | Tl | ICP-MS | <0.5 | <0.5 | <0.5 | <0.5 |
| | Th | ICP-MS | <1 | <1 | <1 | <1 |
| | Tm | ICP-MS | <0.1 | 0.1 | <0.1 | <0.1 |
| | Sn | ICP-MS | <1 | <1 | <1 | <1 |
| | W | ICP-MS | 8 | 13 | 16 | 9 |
| | U | ICP-MS | 3 | 14.5 | 1.5 | 3.5 |
| | V | ICP-MS | 50 | 60 | 40 | 115 |
| | Yb | ICP-MS | 0.2 | 0.6 | 0.1 | 0.3 |
| | Y | ICP-MS | 5 | 9.5 | 4.5 | 5 |
| | Zn | ICP-MS | 25 | 10 | 10 | 80 |
| | Zr | ICP-MS | <0.5 | 16.5 | 1.5 | 1.5 |
| | Al2O3 | XRF | 0.29 | 3.83 | 0.19 | 0.37 |
| | CaO | XRF | 54.25 | 40.14 | 54.91 | 53.81 |
| | Cr2O3 | XRF | <0.01 | <0.01 | <0.01 | <0.01 |
| | Fe2O3 | XRF | 0.09 | 1.68 | 0.07 | 0.13 |
| | K2O | XRF | 0.05 | 0.53 | 0.02 | 0.03 |
| | MgO | XRF | 0.18 | 10.72 | 0.53 | 0.24 |
| | MnO | XRF | 0.03 | 0.03 | 0.02 | 0.03 |
| | Na2O | XRF | <0.01 | <0.01 | <0.01 | <0.01 |
| | P2O5 | XRF | 0.11 | 0.16 | 0.08 | 0.1 |
| | SiO2 | XRF | 5.55 | 11.81 | 1.75 | 6.17 |
| | TiO2 | XRF | 0.01 | 0.15 | <0.01 | 0.01 |
| | LOI | XRF | 38.78 | 29.86 | 41.83 | 38.37 |

Table 3.11a. Mass factors and volume factors

| mass factor | Al2O3 | TiO2 | Y | V | Zr | Yb |
|---|---|---|---|---|---|---|
| average marble to type B skarn | 0.840 | 0.471 | 0.598 | 0.846 | 1.105 | 0.584 |
| average marble to type A skarn | 0.314 | 0.176 | 0.356 | 0.283 | 0.083 | 0.267 |
| average marble to ? Skarn | 0.495 | 0.330 | 0.619 | 0.557 | 0.484 | 0.554 |
| volume factor | | | | | | |
| average marble to type B skarn | 0.799 | 0.448 | 0.569 | 0.804 | 1.051 | 0.555 |
| average marble to type A skarn | 0.299 | 0.167 | 0.338 | 0.269 | 0.079 | 0.254 |
| average marble to ? Skarn | 0.471 | 0.314 | 0.589 | 0.529 | 0.460 | 0.527 |

Table 3.11b. Mass factor values for transformation of average marble to wollastonite skarn samples based on the immobility of Al2O3 and V.

| | W1b skarn B | W1c skarn B | 00H13-W skarn B | 00H1-W skarn B | 00H7-W skarn B | 00H4-W skarn B | 00H3-W skarn B | 00-H2-W skarn B | GM1a(u)-W skarn B | W1d (W011) skarn A |
|---|---|---|---|---|---|---|---|---|---|---|
| Al2O3 | 0.82 | 0.79 | 0.67 | 0.93 | 0.87 | 0.89 | 0.91 | 1.44 | 0.63 | 0.36 |
| V | 0.61 | 1.01 | 0.44 | 0.94 | 0.88 | 2.82 | 1.18 | 1.18 | 0.67 | 0.47 |

Table 3.11b

| | UB4e(w) skarn A | 00-H8-W skarn A | 00-H11-W skarn A | GM1h-W skarn ? | W1a skarn ? | 00H10-W skarn ? |
|---|---|---|---|---|---|---|
| Al2O3 | 0.35 | 0.34 | 0.25 | 0.44 | 0.52 | 0.53 |
| V | 0.11 | 0.47 | 1.57 | 0.34 | 0.78 | 0.83 |

Table 3.12. Gains/losses of components from average marble to skarn B based on the immobility of Al2O3

| | | W1b | W1c | 00H13-W | 00H1-W | 00H7-W |
|---|---|---|---|---|---|---|
| Ba | ppm | -24.95 | 131.90 | -11.70 | -15.36 | -18.71 |
| Ce | ppm | -2.51 | -0.20 | -2.82 | 15.87 | 0.21 |
| Cs | ppm | -0.01 | -0.01 | -0.01 | -0.01 | -0.01 |
| Co | ppm | 6.41 | 1.29 | -0.79 | 9.59 | 1.79 |
| Cu | ppm | -3.64 | -3.80 | -4.42 | -3.09 | 0.98 |
| Dy | ppm | 0.07 | 0.29 | 0.13 | 0.40 | 0.27 |
| Er | ppm | 0.01 | 0.24 | 0.02 | 0.15 | 0.12 |
| Eu | ppm | -0.01 | -0.02 | -0.03 | 0.09 | -0.01 |
| Gd | ppm | -0.12 | 0.18 | 0.07 | 0.31 | 0.17 |
| Ga | ppm | 0.72 | 0.69 | 0.57 | 0.83 | -0.10 |
| Hf | ppm | 0.00 | 0.00 | 0.00 | 0.00 | 0.00 |
| Ho | ppm | 0.02 | 0.10 | 0.01 | 0.03 | 0.03 |
| La | ppm | -2.38 | -0.07 | -2.36 | 16.46 | 0.34 |
| Pb | ppm | 7.47 | -0.75 | 2.58 | -0.75 | -0.75 |
| Lu | ppm | 0.00 | 0.00 | 0.00 | 0.00 | 0.00 |
| Nd | ppm | -1.34 | 0.59 | -0.91 | 3.48 | 1.79 |
| Ni | ppm | -3.50 | -3.50 | -0.17 | -3.50 | -3.50 |
| Nb | ppm | -0.05 | -0.05 | -0.05 | 0.88 | -0.05 |
| Pr | ppm | -0.33 | 0.06 | -0.32 | 1.21 | 0.31 |
| Rb | ppm | -0.60 | 3.81 | -0.56 | 0.21 | 0.31 |
| Sm | ppm | -0.11 | 0.04 | -0.10 | 0.40 | 0.44 |
| Ag | ppm | -1.25 | -1.25 | -1.25 | -1.25 | -1.25 |
| Sr | ppm | -340.71 | -392.26 | -372.79 | -321.51 | -237.66 |
| Ta | ppm | 0.00 | 0.00 | 0.00 | 0.47 | 0.44 |
| Tb | ppm | -0.01 | 0.07 | 0.06 | 0.08 | 0.08 |
| Tl | ppm | 0.00 | 0.00 | 0.00 | 0.00 | 0.00 |
| Th | ppm | 0.00 | 0.00 | 0.00 | 0.00 | 0.00 |
| Tm | ppm | 0.00 | 0.00 | 0.00 | 0.00 | 0.00 |
| Sn | ppm | 0.00 | 0.00 | 0.00 | 0.00 | 0.00 |
| W | ppm | 44.69 | 10.93 | 14.60 | 57.83 | 36.88 |
| U | ppm | -1.67 | 6.98 | 0.09 | 1.76 | -1.59 |
| V | ppm | 23.98 | -15.16 | 35.91 | -0.67 | -0.67 |
| Yb | ppm | 0.01 | 0.16 | 0.03 | 0.04 | 0.20 |
| Y | ppm | 0.08 | 2.66 | 0.80 | 2.13 | 1.70 |
| Zn | ppm | 52.95 | -29.99 | 133.15 | -21.82 | 146.66 |
| Zr | ppm | 1.69 | 0.34 | -0.83 | -0.96 | 1.10 |
| Al2O3 | XRF(%) | 0.00 | 0.00 | 0.00 | 0.00 | 0.00 |
| CaO | XRF(%) | -23.37 | -18.68 | -23.49 | -11.55 | -12.86 |
| Cr2O3 | XRF(%) | 0.00 | 0.00 | 0.00 | 0.00 | 0.00 |
| Fe2O3 | XRF(%) | 1.05 | 0.00 | 0.00 | 0.00 | 0.00 |
| K2O | XRF(%) | -0.01 | 0.14 | -0.02 | 0.00 | 0.01 |
| MgO | XRF(%) | 3.06 | 0.29 | -0.29 | -0.28 | -0.25 |
| MnO | XRF(%) | 0.12 | 0.11 | 0.04 | 0.09 | 0.02 |
| Na2O | XRF(%) | 0.00 | 0.00 | 0.00 | 0.00 | 0.00 |
| P2O5 | XRF(%) | -0.05 | 0.13 | -0.01 | 0.07 | -0.04 |
| SiO2 | XRF(%) | 38.59 | 37.28 | 27.72 | 44.13 | 29.76 |
| TiO2 | XRF(%) | 0.00 | 0.01 | 0.02 | 0.01 | 0.02 |
| LOI | XRF(%) | -37.13 | -40.12 | -37.22 | -39.46 | -29.24 |

Table 3.12.

| | | 00H4-W | 00H3-W | 00-H2-W | GM1a(u)-W | ave skarn B |
|---|---|---|---|---|---|---|
| Ba | ppm | -8.72 | -22.45 | -22.67 | -25.75 | -0.96 |
| Ce | ppm | -2.81 | -2.33 | 1.63 | -2.27 | 0.14 |
| Cs | ppm | -0.01 | -0.01 | -0.01 | -0.01 | -0.01 |
| Co | ppm | 0.12 | 1.10 | 3.77 | -0.32 | 2.24 |
| Cu | ppm | -3.29 | -3.20 | 13.92 | -7.75 | -2.62 |
| Dy | ppm | 0.19 | 0.12 | 0.82 | 0.10 | 0.23 |
| Er | ppm | 0.13 | 0.14 | 0.55 | 0.06 | 0.13 |
| Eu | ppm | -0.10 | 0.00 | 0.05 | -0.03 | -0.01 |
| Gd | ppm | 0.00 | 0.11 | 0.63 | -0.03 | 0.11 |
| Ga | ppm | -0.10 | -0.10 | -0.10 | 0.53 | 0.37 |
| Hf | ppm | 0.00 | 0.00 | 0.00 | 0.00 | 0.00 |
| Ho | ppm | 0.03 | 0.03 | 0.23 | 0.00 | 0.04 |
| La | ppm | -2.24 | -1.75 | 1.03 | -3.09 | 0.27 |
| Pb | ppm | -0.75 | -0.75 | -0.75 | -0.75 | 0.65 |
| Lu | ppm | 0.00 | 0.00 | 0.00 | 0.00 | 0.00 |
| Nd | ppm | -0.79 | -0.75 | 2.48 | -1.01 | 0.18 |
| Ni | ppm | -3.50 | 10.16 | -3.50 | 15.26 | 1.17 |
| Nb | ppm | -0.05 | -0.05 | -0.05 | -0.05 | 0.04 |
| Pr | ppm | -0.30 | -0.20 | 0.50 | -0.34 | 0.01 |
| Rb | ppm | -0.91 | -0.54 | -0.51 | -1.09 | 0.01 |
| Sm | ppm | -0.08 | -0.07 | 0.58 | -0.12 | 0.07 |
| Ag | ppm | -1.25 | 2.39 | -1.25 | -1.25 | -0.88 |
| Sr | ppm | 8.67 | -210.67 | -339.32 | -388.77 | -295.54 |
| Ta | ppm | 0.00 | 0.00 | 0.72 | 0.00 | 0.14 |
| Tb | ppm | -0.01 | 0.08 | 0.13 | 0.05 | 0.06 |
| Tl | ppm | 0.00 | 0.00 | 0.00 | 0.00 | 0.00 |
| Th | ppm | 0.00 | 0.00 | 0.00 | 0.00 | 0.00 |
| Tm | ppm | 0.00 | 0.00 | 0.00 | 0.00 | 0.00 |
| Sn | ppm | 0.00 | 0.00 | 0.00 | 0.00 | 0.00 |
| W | ppm | 20.99 | 39.92 | 70.36 | 23.65 | 32.51 |
| U | ppm | 0.67 | -1.53 | 2.88 | -1.96 | 0.46 |
| V | ppm | -48.21 | -15.85 | 16.19 | -4.84 | -0.51 |
| Yb | ppm | 0.03 | 0.12 | 0.34 | 0.14 | 0.11 |
| Y | ppm | 1.39 | 2.44 | 9.60 | 0.78 | 1.96 |
| Zn | ppm | -31.92 | -31.53 | -13.63 | -27.86 | 23.04 |
| Zr | ppm | -2.38 | -1.46 | -0.66 | -2.51 | -0.68 |
| Al2O3 | XRF(%) | 0.00 | 0.00 | 0.00 | 0.00 | 0.00 |
| CaO | XRF(%) | -13.06 | -10.93 | 12.25 | -25.60 | -16.20 |
| Cr2O3 | XRF(%) | 0.00 | 0.00 | 0.00 | 0.00 | 0.00 |
| Fe2O3 | XRF(%) | -0.13 | -0.04 | 0.08 | 0.05 | 0.11 |
| K2O | XRF(%) | -0.01 | -0.01 | 0.02 | -0.02 | 0.01 |
| MgO | XRF(%) | -0.28 | -0.23 | -0.03 | -0.27 | 0.19 |
| MnO | XRF(%) | 0.11 | 0.05 | 0.16 | 0.04 | 0.08 |
| Na2O | XRF(%) | 0.00 | 0.00 | 0.00 | 0.00 | 0.00 |
| P2O5 | XRF(%) | 0.06 | -0.06 | 0.14 | -0.05 | 0.01 |
| SiO2 | XRF(%) | 41.60 | 31.81 | 70.78 | 28.40 | 36.70 |
| TiO2 | XRF(%) | 0.00 | 0.00 | 0.03 | 0.01 | 0.01 |
| LOI | XRF(%) | -39.15 | -29.45 | -39.38 | -39.81 | -36.85 |

Table 3.12. Gains/losses of components from average marble to skarn A based on the immobility of Al2O3

| | | W1d (W011) | UB4e(w) | 00-H8-W | 00-H11-W | ave skarn A |
|---|---|---|---|---|---|---|
| Ba | ppm | -24.67 | -21.29 | -21.47 | -25.89 | -23.54 |
| Ce | ppm | -2.54 | -1.38 | -1.47 | -3.53 | -2.34 |
| Cs | ppm | -0.01 | -0.01 | -0.01 | -0.01 | -0.01 |
| Co | ppm | -0.59 | 2.44 | -0.10 | -2.71 | -0.46 |
| Cu | ppm | 2.99 | -6.02 | -7.75 | -6.52 | -4.61 |
| Dy | ppm | 0.02 | 0.18 | 0.23 | -0.14 | 0.05 |
| Er | ppm | -0.03 | 0.03 | 0.12 | -0.14 | -0.02 |
| Eu | ppm | -0.02 | 0.01 | 0.04 | -0.05 | -0.01 |
| Gd | ppm | -0.21 | 0.09 | 0.07 | -0.36 | -0.12 |
| Ga | ppm | 0.62 | 0.94 | 0.24 | 0.39 | 0.53 |
| Hf | ppm | 0.00 | 0.00 | 0.00 | 0.25 | 0.08 |
| Ho | ppm | 0.01 | 0.04 | 0.07 | -0.04 | 0.02 |
| La | ppm | -2.41 | -1.08 | -0.84 | -3.41 | -2.06 |
| Pb | ppm | -0.75 | -0.75 | 0.93 | 0.48 | 0.04 |
| Lu | ppm | 0.04 | 0.03 | 0.07 | 0.00 | 0.03 |
| Nd | ppm | -1.32 | 0.20 | -0.06 | -1.96 | -0.88 |
| Ni | ppm | 0.08 | 13.81 | 4.88 | -3.50 | 3.18 |
| Nb | ppm | 0.31 | 1.34 | 0.29 | 0.20 | 0.50 |
| Pr | ppm | -0.30 | -0.03 | -0.05 | -0.51 | -0.25 |
| Rb | ppm | -1.02 | -0.33 | -0.69 | -0.84 | -0.73 |
| Sm | ppm | -0.18 | 0.08 | 0.00 | -0.29 | -0.11 |
| Ag | ppm | -1.25 | -0.56 | -1.25 | -1.25 | -1.09 |
| Sr | ppm | -393.60 | -382.86 | -385.03 | -407.41 | -393.56 |
| Ta | ppm | 0.00 | 0.00 | 0.00 | 0.00 | 0.00 |
| Tb | ppm | 0.03 | 0.06 | 0.09 | 0.01 | 0.05 |
| Tl | ppm | 0.00 | 0.00 | 0.00 | 0.00 | 0.00 |
| Th | ppm | 0.00 | 0.00 | 0.00 | 0.25 | 0.08 |
| Tm | ppm | 0.04 | 0.03 | 0.03 | 0.00 | 0.02 |
| Sn | ppm | 0.00 | 0.00 | 0.00 | 0.00 | 0.00 |
| W | ppm | -4.48 | 12.24 | 10.12 | -3.37 | 3.09 |
| U | ppm | -0.57 | 2.64 | -0.72 | 3.39 | 1.38 |
| V | ppm | -16.78 | 154.58 | -20.22 | -59.41 | 7.72 |
| Yb | ppm | 0.05 | 0.14 | 0.16 | -0.12 | 0.04 |
| Y | ppm | -0.73 | 0.17 | 1.52 | -2.51 | -0.57 |
| Zn | ppm | -15.73 | 2.19 | -26.29 | -43.59 | -23.02 |
| Zr | ppm | 2.01 | 4.45 | 2.04 | 18.74 | 7.91 |
| Al2O3 | XRF(%) | 0.00 | 0.00 | 0.00 | 0.00 | 0.00 |
| CaO | XRF(%) | -37.95 | -38.55 | -38.88 | -43.06 | -39.93 |
| Cr2O3 | XRF(%) | 0.00 | 0.00 | 0.00 | 0.00 | 0.00 |
| Fe2O3 | XRF(%) | 0.13 | 0.09 | -0.04 | -0.18 | -0.02 |
| K2O | XRF(%) | -0.03 | -0.03 | -0.02 | -0.03 | -0.03 |
| MgO | XRF(%) | -0.32 | -0.32 | -0.34 | -0.42 | -0.36 |
| MnO | XRF(%) | 0.01 | 0.01 | -0.01 | 0.00 | 0.00 |
| Na2O | XRF(%) | 0.00 | 0.00 | 0.00 | 0.00 | 0.00 |
| P2O5 | XRF(%) | -0.02 | 0.01 | 0.28 | -0.06 | 0.04 |
| SiO2 | XRF(%) | 14.22 | 14.04 | 11.81 | 9.03 | 11.96 |
| TiO2 | XRF(%) | 0.01 | 0.02 | 0.02 | -0.01 | 0.01 |
| LOI | XRF(%) | -39.74 | -40.11 | -38.81 | -40.04 | -39.70 |

Table 3.12. Gains/losses of components from average marble to skarn ? based on the immobility of Al2O3

| | | GM1h-W | W1a | 00H10-W | ave skarn ? |
|---|---|---|---|---|---|
| Ba | ppm | -25.02 | -23.86 | -24.88 | -24.61 |
| Ce | ppm | -3.27 | -1.53 | -3.09 | -2.67 |
| Cs | ppm | -0.01 | -0.01 | -0.01 | -0.01 |
| Co | ppm | 2.28 | 1.26 | 3.44 | 2.32 |
| Cu | ppm | -5.54 | 0.11 | -5.10 | -3.63 |
| Dy | ppm | -0.12 | -0.13 | 0.08 | -0.06 |
| Er | ppm | -0.09 | -0.11 | 0.06 | -0.05 |
| Eu | ppm | -0.05 | -0.04 | -0.04 | -0.05 |
| Gd | ppm | -0.22 | -0.16 | -0.16 | -0.18 |
| Ga | ppm | 0.34 | 0.42 | 0.43 | 0.39 |
| Hf | ppm | 0.00 | 0.00 | 0.00 | 0.00 |
| Ho | ppm | -0.02 | -0.01 | 0.05 | 0.01 |
| La | ppm | -2.92 | -1.14 | -2.70 | -2.29 |
| Pb | ppm | -0.75 | -0.75 | -0.75 | -0.75 |
| Lu | ppm | 0.00 | 0.00 | 0.00 | 0.00 |
| Nd | ppm | -1.69 | -0.48 | -1.25 | -1.17 |
| Ni | ppm | 7.53 | -3.50 | -0.85 | 1.45 |
| Nb | ppm | -0.05 | -0.05 | -0.05 | -0.05 |
| Pr | ppm | -0.43 | -0.13 | -0.34 | -0.31 |
| Rb | ppm | -0.91 | -0.46 | -0.67 | -0.69 |
| Sm | ppm | -0.21 | -0.07 | -0.17 | -0.15 |
| Ag | ppm | -1.25 | -1.25 | 4.58 | 0.56 |
| Sr | ppm | -377.68 | -389.49 | -388.97 | -384.91 |
| Ta | ppm | 0.00 | 0.00 | 0.00 | 0.00 |
| Tb | ppm | 0.03 | -0.01 | 0.04 | 0.02 |
| Tl | ppm | 0.00 | 0.00 | 0.00 | 0.00 |
| Th | ppm | 0.00 | 0.00 | 0.00 | 0.00 |
| Tm | ppm | 0.00 | 0.00 | 0.05 | 0.02 |
| Sn | ppm | 0.00 | 0.00 | 0.53 | 0.16 |
| W | ppm | 47.54 | 9.47 | 16.11 | 25.78 |
| U | ppm | -0.69 | 0.77 | 2.67 | 0.81 |
| V | ppm | 19.92 | -23.36 | -25.42 | -7.81 |
| Yb | ppm | -0.06 | -0.03 | 0.03 | -0.03 |
| Y | ppm | -1.76 | -1.71 | 0.72 | -0.97 |
| Zn | ppm | -25.49 | -31.42 | -36.49 | -30.78 |
| Zr | ppm | -0.62 | 1.37 | -0.44 | 0.06 |
| Al2O3 | XRF(%) | 0.00 | 0.00 | 0.00 | 0.00 |
| CaO | XRF(%) | -34.16 | -30.23 | -30.07 | -31.65 |
| Cr2O3 | XRF(%) | 0.00 | 0.00 | 0.00 | 0.00 |
| Fe2O3 | XRF(%) | -0.10 | 0.06 | 0.00 | -0.02 |
| K2O | XRF(%) | -0.03 | -0.03 | -0.03 | -0.03 |
| MgO | XRF(%) | -0.10 | -0.28 | -0.35 | -0.24 |
| MnO | XRF(%) | 0.04 | 0.02 | 0.06 | 0.04 |
| Na2O | XRF(%) | 0.00 | 0.00 | 0.00 | 0.00 |
| P2O5 | XRF(%) | 0.00 | 0.04 | 0.11 | 0.05 |
| SiO2 | XRF(%) | 16.10 | 23.23 | 21.94 | 20.16 |
| TiO2 | XRF(%) | 0.01 | 0.00 | 0.00 | 0.01 |
| LOI | XRF(%) | -37.24 | -40.15 | -38.25 | -38.47 |

Table 3.12. Gains/losses of components from average marble to skarn B based on the immobility of V

| | | W1b | W1c | 00H13-W | 00H1-W | 00H7-W | 00H4-W |
|---|---|---|---|---|---|---|---|
| Ba | ppm | -25.47 | 175.44 | -16.87 | -15.25 | -18.63 | 30.81 |
| Ce | ppm | -2.92 | 0.89 | -3.27 | 16.06 | 0.26 | 0.08 |
| Cs | ppm | -0.01 | -0.01 | -0.01 | -0.01 | -0.01 | -0.01 |
| Co | ppm | 3.91 | 2.59 | -1.69 | 9.71 | 1.84 | 7.83 |
| Cu | ppm | -4.68 | -2.71 | -5.55 | -3.05 | 1.06 | 6.35 |
| Dy | ppm | -0.03 | 0.47 | -0.03 | 0.41 | 0.28 | 1.35 |
| Er | ppm | -0.07 | 0.39 | -0.09 | 0.16 | 0.13 | 1.10 |
| Eu | ppm | -0.03 | 0.01 | -0.05 | 0.09 | -0.01 | -0.10 |
| Gd | ppm | -0.22 | 0.38 | -0.13 | 0.32 | 0.18 | 1.16 |
| Ga | ppm | 0.51 | 0.91 | 0.34 | 0.84 | -0.10 | -0.10 |
| Hf | ppm | 0.00 | 0.00 | 0.00 | 0.00 | 0.00 | 0.00 |
| Ho | ppm | 0.00 | 0.14 | -0.02 | 0.03 | 0.03 | 0.22 |
| La | ppm | -2.80 | 1.01 | -2.92 | 16.66 | 0.38 | 1.62 |
| Pb | ppm | 5.38 | -0.75 | 1.45 | -0.75 | -0.75 | -0.75 |
| Lu | ppm | 0.00 | 0.00 | 0.00 | 0.00 | 0.00 | 0.00 |
| Nd | ppm | -1.66 | 1.45 | -1.47 | 3.54 | 1.83 | 3.07 |
| Ni | ppm | -3.50 | -3.50 | -1.30 | -3.50 | -3.50 | -3.50 |
| Nb | ppm | -0.05 | -0.05 | -0.05 | 0.89 | -0.05 | -0.05 |
| Pr | ppm | -0.41 | 0.25 | -0.43 | 1.23 | 0.31 | 0.47 |
| Rb | ppm | -0.72 | 5.15 | -0.74 | 0.23 | 0.32 | -0.53 |
| Sm | ppm | -0.19 | 0.17 | -0.21 | 0.41 | 0.45 | 0.69 |
| Ag | ppm | -1.25 | -1.25 | -1.25 | -1.25 | -1.25 | -1.25 |
| Sr | ppm | -360.42 | -385.11 | -388.17 | -320.59 | -235.93 | 932.43 |
| Ta | ppm | 0.00 | 0.00 | 0.00 | 0.47 | 0.44 | 0.00 |
| Tb | ppm | -0.01 | 0.09 | 0.03 | 0.08 | 0.08 | -0.01 |
| Tl | ppm | 0.00 | 0.00 | 0.00 | 0.00 | 0.00 | 0.00 |
| Th | ppm | 0.00 | 0.00 | 0.00 | 0.00 | 0.00 | 0.00 |
| Tm | ppm | 0.00 | 0.00 | 0.00 | 0.00 | 0.00 | 0.00 |
| Sn | ppm | 0.00 | 0.00 | 0.00 | 0.00 | 0.00 | 0.00 |
| W | ppm | 30.30 | 17.21 | 5.63 | 58.50 | 37.35 | 92.34 |
| U | ppm | -1.98 | 9.69 | -0.92 | 1.80 | -1.58 | 8.38 |
| V | ppm | 0.00 | 0.00 | 0.00 | 0.00 | 0.00 | 0.00 |
| Yb | ppm | -0.06 | 0.26 | -0.06 | 0.04 | 0.20 | 0.61 |
| Y | ppm | -1.17 | 4.72 | -1.10 | 2.20 | 1.76 | 14.89 |
| Zn | ppm | 26.88 | -24.57 | 71.42 | -21.55 | 148.53 | 6.65 |
| Zr | ppm | 0.55 | 1.20 | -1.50 | -0.95 | 1.14 | -1.42 |
| Al2O3 | XRF(%) | -0.11 | 0.11 | -0.14 | 0.00 | 0.00 | 0.91 |
| CaO | XRF(%) | -31.21 | -8.94 | -33.87 | -11.14 | -12.46 | 76.01 |
| Cr2O3 | XRF(%) | 0.00 | 0.00 | 0.00 | 0.00 | 0.00 | 0.00 |
| Fe2O3 | XRF(%) | 0.72 | 0.07 | -0.08 | 0.00 | 0.01 | 0.10 |
| K2O | XRF(%) | -0.02 | 0.19 | -0.03 | 0.00 | 0.01 | 0.05 |
| MgO | XRF(%) | 2.16 | 0.51 | -0.36 | -0.28 | -0.25 | 0.14 |
| MnO | XRF(%) | 0.08 | 0.15 | 0.02 | 0.09 | 0.02 | 0.39 |
| Na2O | XRF(%) | 0.00 | 0.00 | 0.00 | 0.00 | 0.00 | 0.00 |
| P2O5 | XRF(%) | -0.05 | 0.18 | -0.03 | 0.07 | -0.04 | 0.35 |
| SiO2 | XRF(%) | 27.92 | 48.44 | 17.20 | 44.58 | 30.08 | 139.07 |
| TiO2 | XRF(%) | 0.00 | 0.02 | 0.01 | 0.01 | 0.02 | 0.02 |
| LOI | XRF(%) | -37.92 | -40.09 | -38.24 | -39.45 | -29.14 | -36.78 |

Table 3.12.

| | | 00H3-W | 00-H2-W | GM1a(u)-W | ave skarn B |
|---|---|---|---|---|---|
| Ba | ppm | -21.13 | -23.48 | -25.66 | -0.77 |
| Ce | ppm | -1.80 | 0.55 | -2.14 | 0.17 |
| Cs | ppm | -0.01 | -0.01 | -0.01 | -0.01 |
| Co | ppm | 2.43 | 2.43 | -0.09 | 2.28 |
| Cu | ppm | -1.88 | 9.88 | -7.75 | -2.58 |
| Dy | ppm | 0.25 | 0.60 | 0.13 | 0.23 |
| Er | ppm | 0.27 | 0.39 | 0.09 | 0.14 |
| Eu | ppm | 0.02 | 0.02 | -0.03 | -0.01 |
| Gd | ppm | 0.29 | 0.41 | 0.01 | 0.12 |
| Ga | ppm | -0.10 | -0.10 | 0.57 | 0.37 |
| Hf | ppm | 0.00 | 0.00 | 0.00 | 0.00 |
| Ho | ppm | 0.06 | 0.18 | 0.01 | 0.04 |
| La | ppm | -1.09 | 0.09 | -3.02 | 0.30 |
| Pb | ppm | -0.75 | -0.75 | -0.75 | 0.66 |
| Lu | ppm | 0.00 | 0.00 | 0.00 | 0.00 |
| Nd | ppm | -0.23 | 1.54 | -0.90 | 0.20 |
| Ni | ppm | 14.13 | -3.50 | 16.64 | 1.20 |
| Nb | ppm | -0.05 | -0.05 | -0.05 | 0.04 |
| Pr | ppm | -0.07 | 0.29 | -0.32 | 0.01 |
| Rb | ppm | -0.39 | -0.62 | -1.09 | 0.02 |
| Sm | ppm | 0.04 | 0.39 | -0.10 | 0.07 |
| Ag | ppm | 3.45 | -1.25 | -1.25 | -0.87 |
| Sr | ppm | -150.45 | -354.08 | -386.59 | -294.65 |
| Ta | ppm | 0.00 | 0.59 | 0.00 | 0.14 |
| Tb | ppm | 0.11 | 0.11 | 0.06 | 0.06 |
| Tl | ppm | 0.00 | 0.00 | 0.00 | 0.00 |
| Th | ppm | 0.00 | 0.00 | 0.00 | 0.00 |
| Tm | ppm | 0.00 | 0.00 | 0.00 | 0.00 |
| Sn | ppm | 0.00 | 0.00 | 0.00 | 0.00 |
| W | ppm | 54.98 | 54.98 | 26.27 | 32.84 |
| U | ppm | -1.14 | 1.80 | -1.89 | 0.48 |
| V | ppm | 0.00 | 0.00 | 0.00 | 0.00 |
| Yb | ppm | 0.23 | 0.23 | 0.16 | 0.11 |
| Y | ppm | 4.55 | 6.90 | 1.19 | 2.01 |
| Zn | ppm | -26.25 | -20.38 | -26.25 | 23.57 |
| Zr | ppm | -1.06 | -1.06 | -2.49 | -0.66 |
| Al2O3 | XRF(%) | 0.12 | -0.08 | 0.03 | 0.00 |
| CaO | XRF(%) | 1.63 | -0.17 | -23.49 | -15.93 |
| Cr2O3 | XRF(%) | 0.00 | 0.00 | 0.00 | 0.00 |
| Fe2O3 | XRF(%) | 0.02 | 0.02 | 0.07 | 0.12 |
| K2O | XRF(%) | 0.00 | 0.01 | -0.02 | 0.01 |
| MgO | XRF(%) | -0.16 | -0.12 | -0.26 | 0.19 |
| MnO | XRF(%) | 0.08 | 0.12 | 0.05 | 0.08 |
| Na2O | XRF(%) | 0.00 | 0.00 | 0.00 | 0.00 |
| P2O5 | XRF(%) | -0.06 | 0.10 | -0.05 | 0.01 |
| SiO2 | XRF(%) | 42.03 | 56.92 | 30.75 | 36.99 |
| TiO2 | XRF(%) | 0.00 | 0.02 | 0.01 | 0.01 |
| LOI | XRF(%) | -26.31 | -39.54 | -39.78 | -36.83 |

Table 3.12. Gains/losses of components from average marble to skarn A based on the immobility of V

| | | W1d (W011) | UB4e(w) | 00-H8-W | 00-H11-W | ave skarnA |
|---|---|---|---|---|---|---|
| Ba | ppm | -23.95 | -25.21 | -19.25 | -19.95 | -23.88 |
| Ce | ppm | -2.04 | -3.28 | -0.39 | -0.23 | -2.52 |
| Cs | ppm | -0.01 | -0.01 | -0.01 | -0.01 | -0.01 |
| Co | ppm | 0.31 | -1.61 | 1.25 | 1.25 | -0.76 |
| Cu | ppm | 6.35 | -7.21 | -7.75 | 0.08 | -4.92 |
| Dy | ppm | 0.13 | -0.18 | 0.46 | 0.91 | 0.01 |
| Er | ppm | 0.06 | -0.21 | 0.30 | 0.78 | -0.05 |
| Eu | ppm | 0.00 | -0.06 | 0.09 | 0.22 | -0.02 |
| Gd | ppm | -0.11 | -0.33 | 0.32 | 0.57 | -0.16 |
| Ga | ppm | 0.84 | 0.23 | 0.37 | 3.03 | 0.47 |
| Hf | ppm | 0.00 | 0.00 | 0.00 | 1.57 | 0.07 |
| Ho | ppm | 0.03 | -0.03 | 0.13 | 0.10 | 0.01 |
| La | ppm | -1.91 | -3.10 | 0.44 | -0.11 | -2.25 |
| Pb | ppm | -0.75 | -0.75 | 1.60 | 7.08 | -0.04 |
| Lu | ppm | 0.05 | 0.01 | 0.09 | 0.00 | 0.03 |
| Nd | ppm | -0.93 | -1.71 | 0.95 | 1.34 | -1.05 |
| Ni | ppm | 1.20 | 1.92 | 8.25 | -3.50 | 2.52 |
| Nb | ppm | 0.42 | 0.38 | 0.42 | 1.52 | 0.45 |
| Pr | ppm | -0.19 | -0.46 | 0.19 | 0.29 | -0.29 |
| Rb | ppm | -1.00 | -0.85 | -0.53 | 0.48 | -0.76 |
| Sm | ppm | -0.11 | -0.27 | 0.18 | 0.51 | -0.14 |
| Ag | ppm | -1.25 | -1.03 | -1.25 | -1.25 | -1.11 |
| Sr | ppm | -385.87 | -407.23 | -371.63 | -348.79 | -396.00 |
| Ta | ppm | 0.00 | 0.00 | 0.00 | 0.00 | 0.00 |
| Tb | ppm | 0.04 | 0.01 | 0.13 | 0.15 | 0.04 |
| Tl | ppm | 0.00 | 0.00 | 0.00 | 0.00 | 0.00 |
| Th | ppm | 0.00 | 0.00 | 0.00 | 1.57 | 0.07 |
| Tm | ppm | 0.05 | 0.01 | 0.05 | 0.00 | 0.02 |
| Sn | ppm | 0.00 | 0.00 | 0.00 | 0.00 | 0.00 |
| W | ppm | -2.13 | -4.41 | 19.02 | 42.83 | 1.60 |
| U | ppm | 0.16 | -1.16 | 0.16 | 37.05 | 0.96 |
| V | ppm | 0.00 | 0.00 | 0.00 | 0.00 | 0.00 |
| Yb | ppm | 0.14 | -0.12 | 0.32 | 0.54 | 0.02 |
| Y | ppm | 0.56 | -3.28 | 4.08 | 10.03 | -0.99 |
| Zn | ppm | -5.10 | -33.48 | -16.85 | -10.58 | -25.66 |
| Zr | ppm | 3.52 | -0.55 | 3.99 | 134.26 | 6.85 |
| Al2O3 | XRF(%) | 0.13 | -0.29 | 0.17 | 2.24 | -0.04 |
| CaO | XRF(%) | -32.87 | -49.33 | -32.70 | 16.82 | -41.35 |
| Cr2O3 | XRF(%) | 0.00 | 0.00 | 0.00 | 0.00 | 0.00 |
| Fe2O3 | XRF(%) | 0.25 | -0.14 | 0.04 | 0.12 | -0.04 |
| K2O | XRF(%) | -0.03 | -0.03 | -0.01 | 0.00 | -0.03 |
| MgO | XRF(%) | -0.27 | -0.43 | -0.28 | -0.12 | -0.37 |
| MnO | XRF(%) | 0.02 | -0.02 | 0.00 | 0.13 | 0.00 |
| Na2O | XRF(%) | 0.00 | 0.00 | 0.00 | 0.00 | 0.00 |
| P2O5 | XRF(%) | -0.01 | -0.05 | 0.42 | 0.01 | 0.03 |
| SiO2 | XRF(%) | 19.74 | 2.03 | 17.94 | 75.91 | 10.44 |
| TiO2 | XRF(%) | 0.02 | 0.00 | 0.03 | 0.02 | 0.01 |
| LOI | XRF(%) | -39.59 | -40.20 | -38.23 | -38.95 | -39.76 |

Table 3.12. Gains/losses of components from average marble to skarn ? based on the immobility of V

| | | GM1h-W | W1a | 00H10-W | av e skarn ? |
|---|---|---|---|---|---|
| Ba | ppm | -25.45 | -22.30 | -23.68 | -24.31 |
| Ce | ppm | -3.46 | -0.23 | -2.49 | -2.48 |
| Cs | ppm | -0.01 | -0.01 | -0.01 | -0.01 |
| Co | ppm | 1.02 | 3.60 | 7.33 | 3.04 |
| Cu | ppm | -6.03 | 4.00 | -3.60 | -3.11 |
| Dy | ppm | -0.17 | -0.03 | 0.32 | -0.02 |
| Er | ppm | -0.14 | 0.00 | 0.27 | -0.02 |
| Eu | ppm | -0.06 | -0.02 | -0.01 | -0.04 |
| Gd | ppm | -0.29 | 0.02 | 0.05 | -0.14 |
| Ga | ppm | 0.24 | 0.68 | 0.73 | 0.46 |
| Hf | ppm | 0.00 | 0.00 | 0.00 | 0.00 |
| Ho | ppm | -0.03 | 0.02 | 0.11 | 0.01 |
| La | ppm | -3.17 | 0.28 | -1.95 | -2.08 |
| Pb | ppm | -0.75 | -0.75 | -0.75 | -0.75 |
| Lu | ppm | 0.00 | 0.00 | 0.00 | 0.00 |
| Nd | ppm | -1.89 | 0.56 | -0.50 | -1.00 |
| Ni | ppm | 5.10 | -3.50 | 0.65 | 2.07 |
| Nb | ppm | -0.05 | -0.05 | -0.05 | -0.05 |
| Pr | ppm | -0.48 | 0.13 | -0.16 | -0.27 |
| Rb | ppm | -0.95 | -0.15 | -0.43 | -0.64 |
| Sm | ppm | -0.26 | 0.11 | -0.02 | -0.12 |
| Ag | ppm | -1.25 | -1.25 | 7.87 | 0.79 |
| Sr | ppm | -386.64 | -375.19 | -372.40 | -380.74 |
| Ta | ppm | 0.00 | 0.00 | 0.00 | 0.00 |
| Tb | ppm | 0.02 | -0.01 | 0.07 | 0.03 |
| Tl | ppm | 0.00 | 0.00 | 0.00 | 0.00 |
| Th | ppm | 0.00 | 0.00 | 0.00 | 0.00 |
| Tm | ppm | 0.00 | 0.00 | 0.08 | 0.02 |
| Sn | ppm | 0.00 | 0.00 | 0.83 | 0.19 |
| W | ppm | 34.43 | 20.12 | 31.96 | 30.49 |
| U | ppm | -1.18 | 2.58 | 5.81 | 1.27 |
| V | ppm | 0.00 | 0.00 | 0.00 | 0.00 |
| Yb | ppm | -0.10 | 0.07 | 0.17 | 0.00 |
| Y | ppm | -2.44 | -0.15 | 3.86 | -0.49 |
| Zn | ppm | -30.84 | -22.33 | -29.01 | -28.41 |
| Zr | ppm | -1.11 | 3.44 | 0.91 | 0.42 |
| Al2O3 | XRF(%) | -0.09 | 0.21 | 0.24 | 0.05 |
| CaO | XRF(%) | -38.58 | -18.33 | -16.44 | -28.83 |
| Cr2O3 | XRF(%) | 0.00 | 0.00 | 0.00 | 0.00 |
| Fe2O3 | XRF(%) | -0.13 | 0.21 | 0.14 | 0.01 |
| K2O | XRF(%) | -0.03 | -0.02 | -0.02 | -0.02 |
| MgO | XRF(%) | -0.18 | -0.18 | -0.28 | -0.21 |
| MnO | XRF(%) | 0.02 | 0.05 | 0.11 | 0.05 |
| Na2O | XRF(%) | 0.00 | 0.00 | 0.00 | 0.00 |
| P2O5 | XRF(%) | -0.02 | 0.10 | 0.21 | 0.06 |
| SiO2 | XRF(%) | 11.80 | 36.45 | 36.25 | 23.11 |
| TiO2 | XRF(%) | 0.00 | 0.01 | 0.01 | 0.01 |
| LOI | XRF(%) | -37.90 | -40.11 | -37.12 | -38.25 |

Mineral Hill probably formed by R1 by the influx of an $H_2O$-rich, $SiO_2$-bearing fluid. Reaction transport theory can be used to assess the time-integrated fluid flux (TIFF) over a maximum wollastonite skarn extent of 65 meters at Mineral Hill. Three scenarios were evaluated: (1) $TIFF_{(max)}$ required to form wollastonite skarn type B from average marble compositions, (2) $TIFF_{(max)}$ required to form wollastonite skarn type A from average marble compositions, and (3) $TIFF_{(max)}$ required to form borderline wollastonite skarn type ? (A or B) from average marble compositions. The values and parameters for fluid/rock ratios and TIFF are presented in Table 3.13. Notation is presented in Table 3.9.

R2 dictates silica addition to calcite marble to form wollastonite skarn. On average wollastonite skarn B formed from the addition of 37 grams of $SiO_2$ to marble. A maximum of 2.4 grams of $SiO_2$ can be added to the system from each kilogram of $H_2O$ that infiltrates under conditions of 550°C, 1 kbar [from *Dipple and Gerdes*, 1998]. These P-T conditions are reasonable for wollastonite skarn formation at Mineral Hill. Calculations result in a fluid/rock ratio of ~413 to 417 and a TIFF of $\sim 2.7 \times 10^6$ $cm^3/cm^2$ for (1) (Table 3.13a,b). On average wollastonite skarn A formed from the addition of 10 to 12 grams of $SiO_2$ to marble. A fluid/rock ratio of ~118 to 135 and a TIFF of $\sim 7.6 \times 10^5$ to $8.7 \times 10^5$ $cm^3/cm^2$ was calculated for (2) (Table 3.13c,d). Average transitional wollastonite skarn ? formed from the addition of 20 to 23 grams of $SiO_2$ to marble. Calculations result in a fluid/rock ratio of 227 to 260 and a TIFF of $1.5 \times 10^5$ to $1.7 \times 10^5$ $cm^3/cm^2$ (Table 3.13e,f).

For a molar volume of $H_2O$= 22 $cm^3$, the Darcy flux can be related to a molar flux ($q_m$) of $\sim 10^4$ - $10^5$ moles/$cm^2$ (Table 3.13). This time-integrated molar flux is consistent with fluxes integrated over the duration of contact and regional metamorphic events interpreted from measured reaction progress [*Dipple and Ferry*, 1992]. Moreover, this value is comparable to fluxes calculated for metasomatism in ductile fault zones [*Dipple and Ferry*, 1992].

Table 3.13a. Fluid/rock ratios (F/R) and time-integrated fluid flux calculations during duration of $SiO_2$ infiltration forming wollastonite skarn B from average composition of marble samples (55O C, 1kbar). SiO2 gains (x SiO2) based on the immobility of Al2O3.

| | W1b | W1c | 00H13-W | 00H1-W | 00H7-W | 00H4-W | 00H3-W | 00-H2-W | GM1a(u)-W | ave skarnB |
|---|---|---|---|---|---|---|---|---|---|---|
| x *SiO2* | 38.587 | 37.277 | 27.720 | 44.127 | 29.762 | 41.603 | 31.807 | 70.783 | 28.404 | 36.701 |
| grams SiO2/kg solution (max) | 2.4 | 2.4 | 2.4 | 2.4 | 2.4 | 2.4 | 2.4 | 2.4 | 2.4 | 2.4 |
| litres of H2O (max) | 16.1 | 15.5 | 11.5 | 18.4 | 12.4 | 17.3 | 13.3 | 29.5 | 11.8 | 15.3 |
| litres of rock ($cm^3$) | 0.037 | 0.037 | 0.037 | 0.037 | 0.037 | 0.037 | 0.037 | 0.037 | 0.037 | 0.037 |
| F/R | 435 | 420 | 312 | 497 | 335 | 469 | 358 | 797 | 320 | 413 |
| z in centimeters (max) | 6.5E+03 | 6.5E+03 | 6.5E+03 | 6.5E+03 | 6.5E+03 | 6.5E+03 | 6.5E+03 | 6.5E+03 | 6.5E+03 | 6.5E+03 |
| $q_v$ ($cm^3/cm^2$) | 2.82E+06 | 2.73E+06 | 2.03E+06 | 3.23E+06 | 2.18E+06 | 3.05E+06 | 2.33E+06 | 5.18E+06 | 2.08E+06 | 2.69E+06 |
| $q_m$ (moles $H_2O$/ $cm^2$ rock) | 1.28E+05 | 1.24E+05 | 9.22E+04 | 1.47E+05 | 9.90E+04 | 1.38E+05 | 1.06E+05 | 2.36E+05 | 9.45E+04 | 1.22E+05 |

Table 3.13b. Fluid/rock ratios (F/R) and time-integrated fluid flux calculations during duration of $SiO_2$ infiltration forming wollastonite skarn B from average composition of marble samples (55O C, 1kbar). SiO2 gains (x SiO2) based on the immobility of V.

| | W1b | W1c | 00H13-W | 00H1-W | 00H7-W | 00H4-W | 00H3-W | 00-H2-W | GM1a(u)-W | ave skarnB |
|---|---|---|---|---|---|---|---|---|---|---|
| x *SiO2* | 27.917 | 48.436 | 17.200 | 44.582 | 30.079 | 139.070 | 42.032 | 56.919 | 30.750 | 36.994 |
| grams SiO2/kg solution (max) | 2.4 | 2.4 | 2.4 | 2.4 | 2.4 | 2.4 | 2.4 | 2.4 | 2.4 | 2.4 |
| litres of H2O (max) | 11.6 | 20.2 | 7.2 | 18.6 | 12.5 | 57.9 | 17.5 | 23.7 | 12.8 | 15.4 |
| litres of rock ($cm^3$) | 0.037 | 0.037 | 0.037 | 0.037 | 0.037 | 0.037 | 0.037 | 0.037 | 0.037 | 0.037 |
| F/R | 314.380 | 545.445 | 193.689 | 502.044 | 338.728 | 1566.107 | 473.331 | 640.980 | 346.285 | 416.597 |
| z in centimeters (max) | 6.5E+03 | 6.5E+03 | 6.5E+03 | 6.5E+03 | 6.5E+03 | 6.5E+03 | 6.5E+03 | 6.5E+03 | 6.5E+03 | 6.5E+03 |
| $q_v$ ($cm^3/cm^2$) | 2.04E+06 | 3.55E+06 | 1.26E+06 | 3.26E+06 | 2.20E+06 | 1.02E+07 | 3.08E+06 | 4.17E+06 | 2.25E+06 | 2.71E+06 |
| $q_m$ (moles $H_2O$/ $cm^2$ rock) | 9.29E+04 | 1.61E+05 | 5.72E+04 | 1.48E+05 | 1.00E+05 | 4.63E+05 | 1.40E+05 | 1.89E+05 | 1.02E+05 | 1.23E+05 |

Table 3.13c. Fluid/rock ratios (F/R) and time-integrated fluid flux calculations during duration of $SiO_2$ infiltration forming wollastonite skarn A from average composition of marble samples (55O C, 1kbar). SiO2 gains (x SiO2) based on the immobility of Al2O3.

| | W1d (W011) | UB4e(w) | 00-H8-W | 00-H11-W | ave skarnA |
|---|---|---|---|---|---|
| x *SiO2* | 14.217 | 14.038 | 11.806 | 9.034 | 11.958 |
| grams SiO2/kg solution (max) | 2.4 | 2.4 | 2.4 | 2.4 | 2.4 |
| litres of H2O (max) | 5.9 | 5.8 | 4.9 | 3.8 | 5.0 |
| litres of rock ($cm^3$) | 0.037 | 0.037 | 0.037 | 0.037 | 0.037 |
| F/R | 160.103 | 158.087 | 132.948 | 101.731 | 134.659 |
| z in centimeters (max) | 6.5E+03 | 6.5E+03 | 6.5E+03 | 6.5E+03 | 6.5E+03 |
| $q_v$ ($cm^3/cm^2$) | 1.04E+06 | 1.03E+06 | 8.64E+05 | 6.61E+05 | 8.75E+05 |
| $q_m$ (moles $H_2O$/ $cm^2$ rock) | 4.73E+04 | 4.67E+04 | 3.93E+04 | 3.01E+04 | 3.98E+04 |

Table 3.13d. Fluid/rock ratios (F/R) and time-integrated fluid flux calculations during duration of $SiO_2$ infiltration forming wollastonite skarn A from average composition of marble samples (55O C, 1kbar). SiO2 gains (x SiO2) based on the immobility of V.

| | W1d (W011) | UB4e(w) | 00-H8-W | 00-H11-W | ave skarnA |
|---|---|---|---|---|---|
| x *SiO2* | 19.737 | 2.026 | 17.942 | 75.915 | 10.437 |
| grams SiO2/kg solution (max) | 2.4 | 2.4 | 2.4 | 2.4 | 2.4 |
| litres of H2O (max) | 8.2 | 0.8 | 7.5 | 31.6 | 4.3 |
| litres of rock ($cm^3$) | 0.037 | 0.037 | 0.037 | 0.037 | 0.037 |
| F/R | 222.267 | 22.814 | 202.048 | 854.897 | 117.534 |
| z in centimeters (max) | 6.5E+03 | 6.5E+03 | 6.5E+03 | 6.5E+03 | 6.5E+03 |
| $q_v$ ($cm^3/cm^2$) | 1.44E+06 | 1.48E+05 | 1.31E+06 | 5.56E+06 | 7.64E+05 |
| $q_m$ (moles $H_2O$/ $cm^2$ rock) | 6.57E+04 | 6.74E+03 | 5.97E+04 | 2.53E+05 | 3.47E+04 |

Table 3.13e. Fluid/rock ratios (F/R) and time-integrated fluid flux calculations during duration of $SiO_2$ infiltration forming wollastonite skarn ? from average composition of marble samples (55O C, 1kbar). SiO2 gains (x SiO2) based on the immobility of Al2O3.

| | GM1h-W | W1a | 00H10-W | ave skarn? |
|---|---|---|---|---|
| x *SiO2* | 16.104 | 23.227 | 21.937 | 20.162 |
| grams SiO2/kg solution (max) | 2.4 | 2.4 | 2.4 | 2.4 |
| litres of H2O (max) | 6.7 | 9.7 | 9.1 | 8.4 |
| litres of rock ($cm^3$) | 0.037 | 0.037 | 0.037 | 0.037 |
| F/R | 181.349 | 261.569 | 247.036 | 227.045 |
| z in centimeters (max) | 6.5E+03 | 6.5E+03 | 6.5E+03 | 6.5E+03 |
| $q_v$ ($cm^3/cm^2$) | 1.18E+06 | 1.70E+06 | 1.61E+06 | 1.48E+06 |
| $q_m$ (moles $H_2O$/ $cm^2$ rock) | 5.36E+04 | 7.73E+04 | 7.30E+04 | 6.71E+04 |

Table 3.13f. Fluid/rock ratios (F/R) and time-integrated fluid flux calculations during duration of $SiO_2$ infiltration forming wollastonite skarn ? from average composition of marble samples (55O C, 1kbar). SiO2 gains (x SiO2) based on the immobility of V.

| | GM1h-W | W1a | 00H10-W | ave skarn? |
|---|---|---|---|---|
| x *SiO2* | 11.796 | 36.451 | 36.251 | 23.106 |
| grams SiO2/kg solution (max) | 2.4 | 2.4 | 2.4 | 2.4 |
| litres of H2O (max) | 4.915 | 15.188 | 15.105 | 9.627 |
| litres of rock (1000 $cm^3$) | 0.037 | 0.037 | 0.037 | 0.037 |
| F/R | 132.839 | 410.479 | 408.237 | 260.198 |
| z in centimeters (max) | 6.5E+03 | 6.5E+03 | 6.5E+03 | 6.5E+03 |
| $q_v$ ($cm^3/cm^2$) | 8.63E+05 | 2.67E+06 | 2.65E+06 | 1.69E+06 |
| $q_m$ (moles $H_2O$/ $cm^2$ rock) | 3.92E+04 | 1.21E+05 | 1.21E+05 | 7.69E+04 |

***Rare Earth Element patterns***

Forty samples were analyzed for rare-earth elements (REE) by ALS Chemex. REE's have atomic numbers (Z) from 57 to 71 and decrease in radius with increasing atomic number. Elements with Z = 57 to 62 (i.e. La, Ce, Pr, Nd, and Sm) are referred to as light rare earth elements (LREE); elements with Z> 63 (europium) (i.e. Gd, Tb, Dy, Ho, Er, Tm, Yb, and Lu)are the heavy rare-earth elements (HREE) [*Brownlow*, 1996]. To study REE distribution, we calculated a chondrite-normalized ratio in which the concentration of REE in the samples were divided by chondrite values; representatives of unfractionated original solar system meteorites [*Brownlow*, 1996].

REE plots were constructed for marble, wollastonite skarn type A, wollastonite skarn type B and garnet skarn to observe if their respective concentrations produce distinguishable trends. REE normalized to chondrite values [Table 3.14; *McDonough and Sun*, 1995] show a negative Ce anomaly indicative of seawater deposition of marble (Fig. 3.24a). A negative Eu anomaly in seawater may reflect either aolian or hydrothermal input [*Whitney and Olmsted*, 1998; *Boulais et al.*, 2000]. Generally, the marble trend is enriched in LREE's and depleted in HREE's. Although there is some overlap, wollastonite skarn shows a similar but slightly elevated REE pattern (Fig. 3.24b and Fig. 3.25). This is consistent with other studies in which REE concentrations in skarn are enriched over protolith concentrations due to isotopic equilibration with magmatic volatiles from adjacent igneous intrusions [*Vander Auwera and Andre*, 1991]. Moreover, the patterns suggest that some LREEs may be mobile (i.e. enrichment in La; Fig. 3.24b). Several authors contend that REE systematics are not significantly affected unless intense infiltration metasomatism has occurred [*Bau*, 1991; *Whitney and Olmsted*, 1998; *Boulais et al.*, 2000.] Garnet skarn is enriched in HREE's indicating garnet take-up of the REE's [*Whitney and Olmsted*, 1998] but still reflects a negative Eu anomaly (Fig. 3.24c).

Table 3.14. REE concentrations in marble and wollastonite samples normalized to chondrite values

| | Detection Limit | CHONDRITE Sun and McDonough, 1989 | ROCK/CHONDRITE W1d (mb) marble | UBM1a marble | 00H3-M marble | 00NE-3a-M marble | 0-NE-2-M marble | 00UMQ-2-M marble | 00UMQ-1-M marble | 00H4-M marble |
|---|---|---|---|---|---|---|---|---|---|---|
| La | 0.5 | 0.237 | 21.097 | 16.878 | 37.975 | 14.768 | 10.549 | 16.878 | 29.536 | 14.768 |
| Ce | 0.5 | 0.612 | 6.525 | 6.525 | 11.419 | 4.894 | 3.263 | 6.525 | 11.419 | 4.078 |
| Pr | 0.1 | 0.095 | 12.931 | 7.543 | 11.853 | 5.388 | 4.310 | 6.466 | 8.621 | 5.388 |
| Nd | 0.5 | 0.467 | 8.753 | 5.470 | 8.753 | 3.282 | 3.282 | 5.470 | 6.565 | 4.376 |
| Sm | 0.1 | 0.153 | 3.378 | 3.378 | 4.054 | 2.027 | 2.027 | 2.027 | 2.703 | 2.027 |
| Eu | 0.1 | 0.058 | 1.776 | 1.776 | 1.776 | 0.000 | 0.000 | 1.776 | 1.776 | 1.776 |
| Gd | 0.1 | 0.2055 | 3.015 | 2.513 | 3.015 | 1.508 | 2.010 | 2.010 | 2.513 | 2.513 |
| Tb | 0.1 | 0.0374 | 0.000 | 0.000 | 0.000 | 0.000 | 0.000 | 0.000 | 0.000 | 0.000 |
| Dy | 0.1 | 0.254 | 2.033 | 1.626 | 1.626 | 0.813 | 1.220 | 1.220 | 1.220 | 0.813 |
| Ho | 0.1 | 0.0566 | 1.832 | 1.832 | 1.832 | 0.000 | 0.000 | 0.000 | 1.832 | 0.000 |
| Er | 0.1 | 0.1655 | 2.500 | 1.875 | 3.125 | 1.250 | 1.250 | 1.250 | 1.875 | 0.625 |
| Tm | 0.1 | 0.0255 | 0.000 | 0.000 | 0.000 | 0.000 | 0.000 | 0.000 | 0.000 | 0.000 |
| Yb | 0.1 | 0.17 | 1.863 | 1.863 | 1.863 | 0.621 | 1.242 | 1.242 | 1.863 | 0.621 |
| Lu | 0.1 | 0.0254 | 0.000 | 0.000 | 0.000 | 0.000 | 0.000 | 0.000 | 0.000 | 0.000 |

Table 3.14.

| | 00H10-M marble | 00H6-M marble | 00NE-1-M marble | GM1h-M marble | 00UMQ-3-M marble | 00H15-M marble | 00NE-3b-M marble | 00H12-M marble | 00H9-M marble | 00H13-M marble | BM-1-M marble |
|---|---|---|---|---|---|---|---|---|---|---|---|
| La | 14.768 | 21.097 | 8.439 | 14.768 | 18.987 | 12.658 | 10.549 | 10.549 | 14.768 | 12.658 | 21.097 |
| Ce | 4.894 | 7.341 | 4.894 | 7.341 | 7.341 | 4.894 | 4.078 | 7.341 | 7.341 | 6.525 | 17.129 |
| Pr | 6.466 | 7.543 | 4.310 | 6.466 | 9.698 | 5.388 | 4.310 | 5.388 | 6.466 | 5.388 | 14.009 |
| Nd | 6.565 | 5.470 | 3.282 | 5.470 | 8.753 | 4.376 | 3.282 | 4.376 | 6.565 | 4.376 | 13.129 |
| Sm | 4.054 | 2.703 | 1.351 | 2.703 | 4.730 | 2.027 | 2.027 | 2.703 | 3.378 | 2.703 | 8.108 |
| Eu | 1.776 | 1.776 | 0.000 | 1.776 | 3.552 | 1.776 | 1.776 | 1.776 | 1.776 | 1.776 | 7.105 |
| Gd | 3.015 | 2.010 | 1.005 | 2.513 | 4.523 | 2.513 | 2.010 | 2.513 | 3.518 | 3.015 | 7.035 |
| Tb | 0.000 | 0.000 | 0.000 | 0.000 | 2.770 | 0.000 | 0.000 | 0.000 | 0.000 | 0.000 | 5.540 |
| Dy | 1.626 | 0.813 | 0.000 | 1.626 | 2.846 | 1.220 | 0.813 | 1.626 | 1.220 | 1.626 | 4.878 |
| Ho | 1.832 | 0.000 | 0.000 | 1.832 | 1.832 | 1.832 | 0.000 | 0.000 | 1.832 | 1.832 | 3.663 |
| Er | 2.500 | 1.875 | 0.625 | 1.875 | 3.125 | 1.875 | 1.875 | 1.875 | 2.500 | 1.875 | 4.375 |
| Tm | 0.000 | 0.000 | 0.000 | 0.000 | 0.000 | 0.000 | 0.000 | 0.000 | 0.000 | 0.000 | 4.049 |
| Yb | 1.863 | 0.621 | 0.000 | 1.863 | 2.484 | 1.863 | 1.242 | 2.484 | 2.484 | 1.242 | 3.727 |
| Lu | 0.000 | 0.000 | 0.000 | 0.000 | 0.000 | 0.000 | 0.000 | 0.000 | 0.000 | 0.000 | 4.065 |

Table 3.14.

| | 00H14-M marble | GM1e (R)-G marble | GM1a (L)-G marble | W1d (W011) skarn A | UB4e(w) skarn A | 00-H8-W skarn A | 00-H11-W skarn A | GM1h-W skarn A? | 00H1-W skarnB | 00H7-W skarnB | 00H4-W skarnB |
|---|---|---|---|---|---|---|---|---|---|---|---|
| La | 10.549 | 21.097 | 21.097 | 18.987 | 35.865 | 40.084 | 10.549 | 10.549 | 92.827 | 21.097 | 8.439 |
| Ce | 7.341 | 9.788 | 8.972 | 7.341 | 13.051 | 13.051 | 4.078 | 3.263 | 35.073 | 8.157 | 2.447 |
| Pr | 5.388 | 9.698 | 8.621 | 10.776 | 19.397 | 19.397 | 6.466 | 5.388 | 21.552 | 11.853 | 4.310 |
| Nd | 4.376 | 7.659 | 7.659 | 7.659 | 17.505 | 16.411 | 5.470 | 4.376 | 14.223 | 10.941 | 4.376 |
| Sm | 2.703 | 4.054 | 4.730 | 4.730 | 10.135 | 8.784 | 4.054 | 3.378 | 6.081 | 6.757 | 2.703 |
| Eu | 1.776 | 3.552 | 1.776 | 3.552 | 5.329 | 7.105 | 3.552 | 1.776 | 3.552 | 1.776 | 0.000 |
| Gd | 2.010 | 4.020 | 4.020 | 4.523 | 9.045 | 9.045 | 3.518 | 3.518 | 4.523 | 4.020 | 3.015 |
| Tb | 0.000 | 0.000 | 2.770 | 2.770 | 5.540 | 8.310 | 2.770 | 2.770 | 2.770 | 2.770 | 0.000 |
| Dy | 1.220 | 1.626 | 2.439 | 4.065 | 6.098 | 6.911 | 3.252 | 2.033 | 3.252 | 2.846 | 2.439 |
| Ho | 1.832 | 1.832 | 1.832 | 3.663 | 5.495 | 7.326 | 1.832 | 1.832 | 1.832 | 1.832 | 1.832 |
| Er | 1.875 | 2.500 | 3.125 | 5.000 | 6.250 | 8.125 | 4.375 | 3.125 | 3.125 | 3.125 | 3.125 |
| Tm | 0.000 | 0.000 | 0.000 | 4.049 | 4.049 | 4.049 | 0.000 | 0.000 | 0.000 | 0.000 | 0.000 |
| Yb | 0.621 | 1.863 | 1.863 | 4.969 | 6.832 | 7.453 | 3.106 | 2.484 | 1.863 | 3.106 | 1.863 |
| Lu | 0.000 | 0.000 | 0.000 | 4.065 | 4.065 | 8.130 | 0.000 | 0.000 | 0.000 | 0.000 | 0.000 |

Table 3.14.

| | 00H3-W skarnB | 00-H2-W skarnB | GM1a(u)-W skarnB | 00H13-W skarnB | W1b skarnB | W1c skarnB | W1a skarnB? | 00H10-W skarnB? | TB 4F garnet skarn | UB 5E garnet skarn |
|---|---|---|---|---|---|---|---|---|---|---|
| La | 10.549 | 14.768 | 6.329 | 10.549 | 8.439 | 21.097 | 23.207 | 10.549 | 25.316 | 31.646 |
| Ce | 3.263 | 6.525 | 4.894 | 3.263 | 3.263 | 8.157 | 8.157 | 3.263 | 18.760 | 17.129 |
| Pr | 5.388 | 8.621 | 5.388 | 5.388 | 4.310 | 9.698 | 10.776 | 6.466 | 22.629 | 19.397 |
| Nd | 4.376 | 7.659 | 5.470 | 5.470 | 3.282 | 8.753 | 8.753 | 5.470 | 21.882 | 17.505 |
| Sm | 2.703 | 4.730 | 3.378 | 3.378 | 2.703 | 4.054 | 4.730 | 3.378 | 22.297 | 18.243 |
| Eu | 1.776 | 1.776 | 1.776 | 1.776 | 1.776 | 1.776 | 1.776 | 1.776 | 12.433 | 14.210 |
| Gd | 3.518 | 4.020 | 4.020 | 4.523 | 2.513 | 4.523 | 3.518 | 3.518 | 18.090 | 15.075 |
| Tb | 2.770 | 2.770 | 2.770 | 2.770 | 0.000 | 2.770 | 0.000 | 2.770 | 16.620 | 13.850 |
| Dy | 2.033 | 3.252 | 2.846 | 2.846 | 2.033 | 3.252 | 1.626 | 3.252 | 16.260 | 12.602 |
| Ho | 1.832 | 3.663 | 1.832 | 1.832 | 1.832 | 3.663 | 1.832 | 3.663 | 14.652 | 12.821 |
| Er | 3.125 | 3.750 | 3.750 | 3.125 | 2.500 | 4.375 | 2.500 | 4.375 | 15.625 | 12.500 |
| Tm | 0.000 | 0.000 | 0.000 | 0.000 | 0.000 | 0.000 | 0.000 | 4.049 | 16.194 | 12.146 |
| Yb | 2.484 | 2.484 | 3.727 | 2.484 | 1.863 | 3.106 | 2.484 | 3.106 | 17.391 | 13.043 |
| Lu | 0.000 | 0.000 | 0.000 | 0.000 | 0.000 | 0.000 | 0.000 | 0.000 | 12.195 | 12.195 |

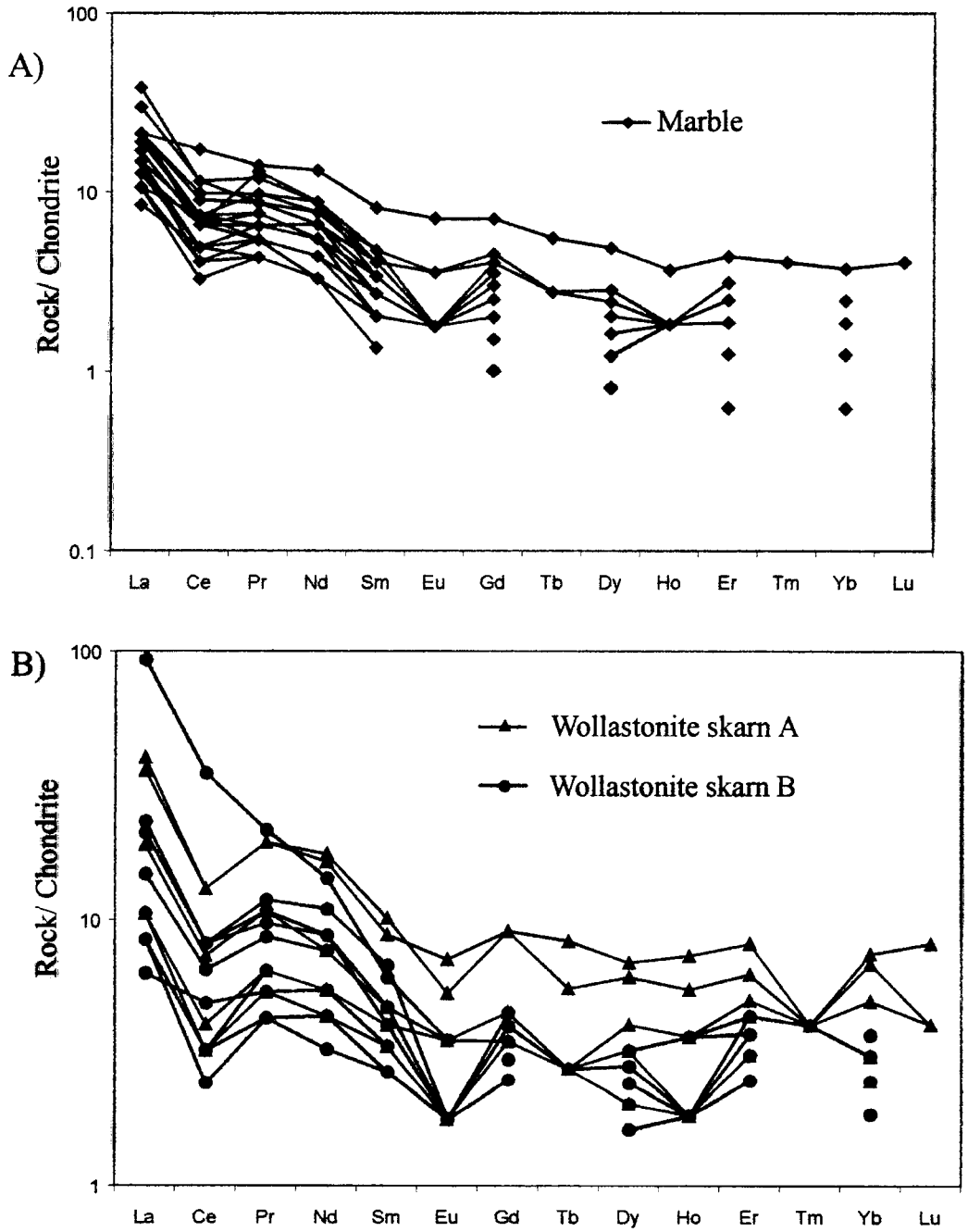


Fig 3.24. A) REE pattern for marble samples (red diamonds) and B) wollastonite skarn A (black triangles) and wollastonite skarn B (blue circles) samples. Generally, wollastonite skarn A is enriched in HREEs relative to wollastonite skarn B. All patterns are in log scale and show negative Ce and Eu anomalies and LREE enrichment. Values below detection limit were not included.

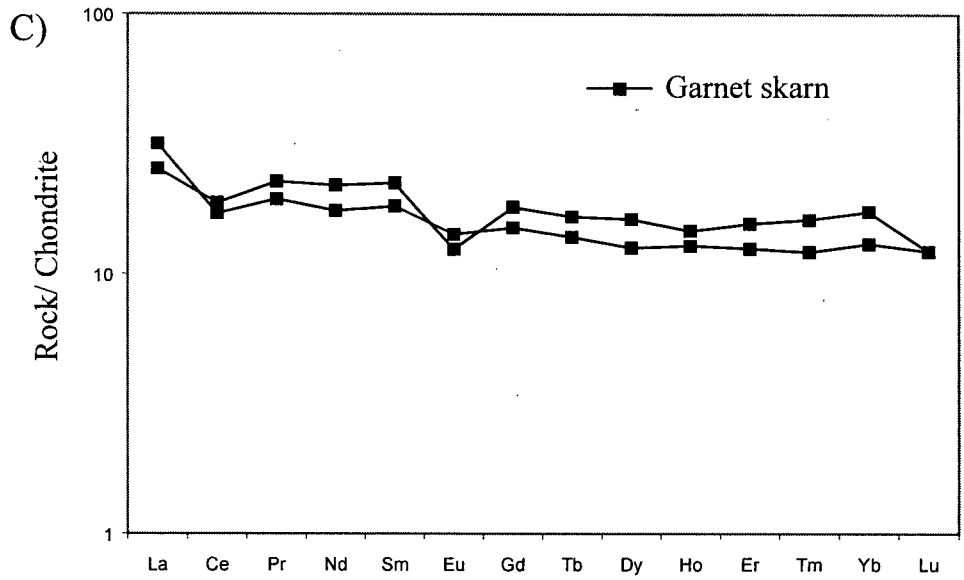


Fig 3.24. C) REE pattern for garnet skarn samples (black squares). Enriched pattern suggests garnet takeup of HREEs. All patterns are in log scale.

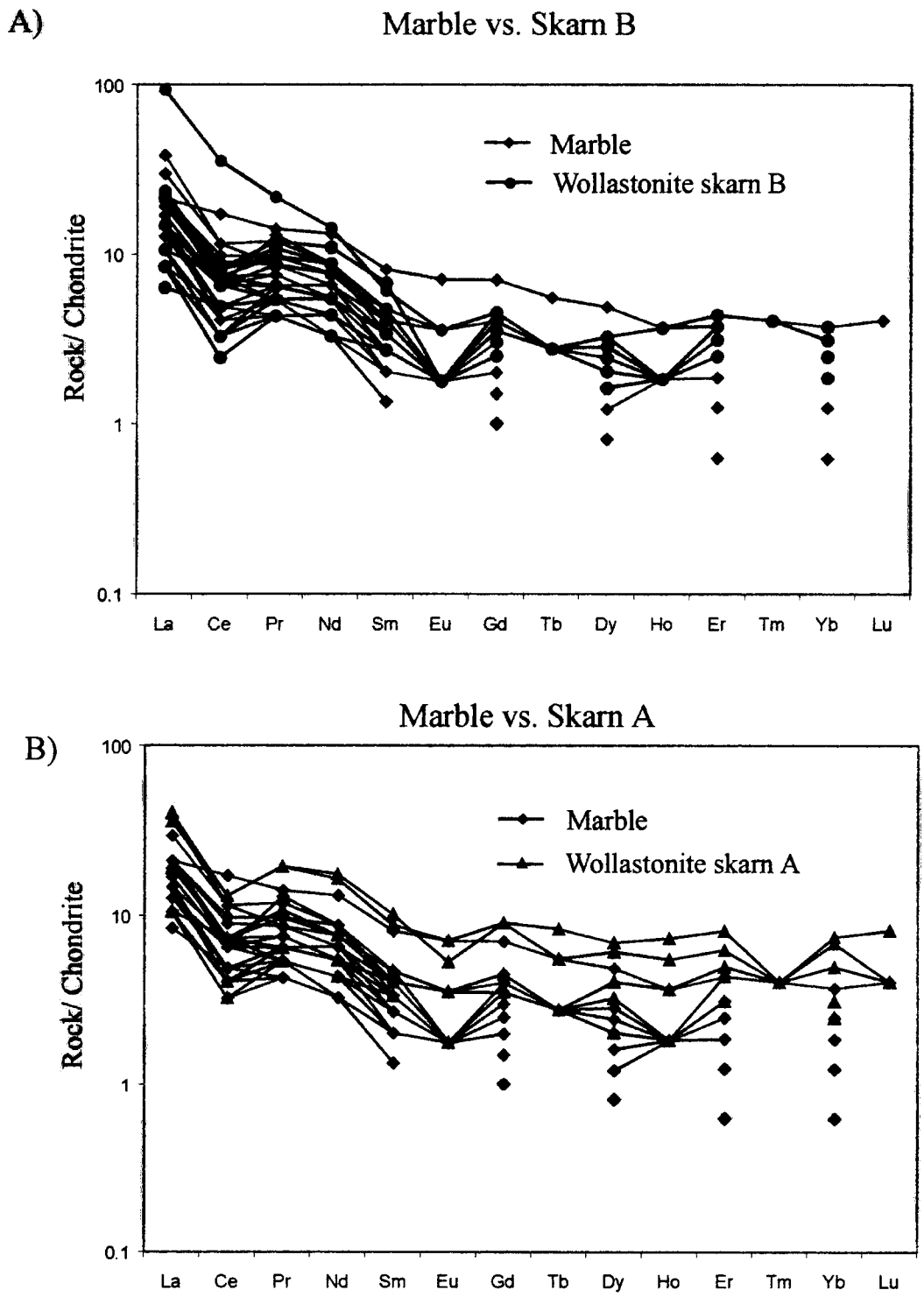


Fig 3.25. A) REE concentrations of marble samples (red) compared to wollastonite skarn B samples (blue). Reveals that marble and skarn B have similar REE concentrations. B) REE concentrations of marble samples (red) compared to wollastonite skarn A (black). Wollastonite skarn A has higher concentrations of REEs than marble. All patterns are in log scale; values below detection limit were not included.

Two marble protoliths for wollastonite skarn are delineated from REE and element ratios for wollastonite skarn consistent with whole rock major, minor and trace interpretations. Type B skarn is likely derived from a relatively pure marble since its REE distribution pattern is similar yet slightly elevated (Fig. 3.25a). However type A skarn appears to have been derived from a marble protolith enriched in REE's, since the REE distribution pattern mimics that of pure marble samples but it elevated over Type B skarn ( Fig. 3.25b and Fig. 3.26a, b). These patterns are especially evident in HREE concentrations.

### 3.7.4 Discussion

Element ratios between marble and wollastonite skarn suggest two skarn types. It is improbable that the divergent elemental abundances in type A and type B skarn were produced by different reactions; instead they probably reflect variances in protolith composition. It is plausible that both wollastonite skarn types have a marble precursor, however that which proceeded type A skarn had greater abundance of Al, Ti, Zr, V, Yb, and Y. Moreover, type A skarn has greater abundance of HREE's. If type A skarn formed from a different protolith, Gresen's [1967] mass balance (gains and losses of species) calculations for wollastonite skarn A formed from average marble compositions have no physical relevance. However, in this case, gains and losses calculated for type B skarn formed from average marble are still valid. A volume loss of ~20% estimated from the conversion of marble to type B skarn must have led to a substantial local increase in permeability and may have resulted in reaction-flow focusing.

Wollastonite skarn at Mineral Hill probably formed by R1 by the influx of an $H_2O$-rich, $SiO_2$-bearing fluid. Mass balance calculations support large increases of $SiO_2$ to produce wollastonite skarn. Type B skarn has the largest $SiO_2$ addition probably facilitated by the associated volume loss. Type A skarn and borderline (?) skarn gained less silica indicating more calcite dissolution associated with skarn formation, although this cannot be confidently

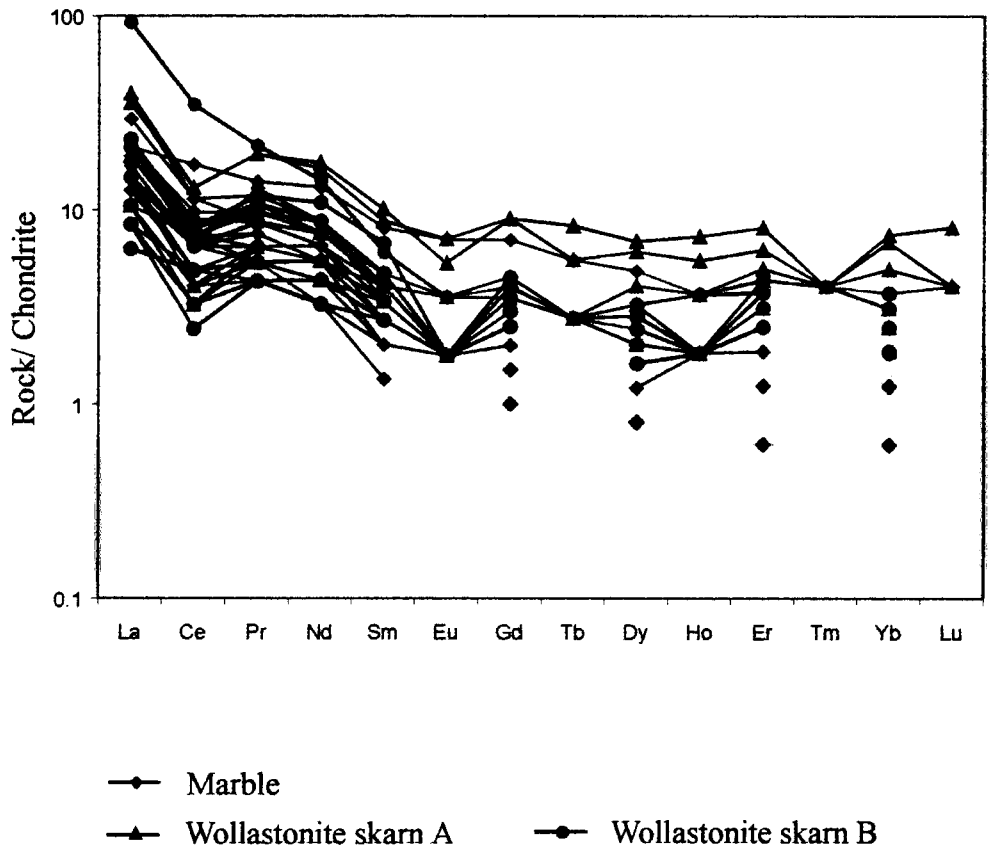


Fig. 3.26. REE pattern for marble, wollastonite skarn B, and wollastonite skarn A samples showing passive enrichment of HREEs in wollastonite skarn A and B over marble HREE concentrations. All patterns are in log scale; values below detection limit are not included.

determined since it is improbable that skarn B derived from a relatively pure marble. That is, volume losses on the order of 50-70 % estimated during skarn A formation are not supported by major collapse features as evidence of a large porosity gain.

Time-integrated molar fluxes between $3 \times 10^4$ and $1 \times 10^5$ moles/cm$^2$ are calculated over the duration of wollastonite skarn formation. However, the lower flux (i.e. ~$3 \times 10^4$ moles/cm$^2$) assessed for skarn A and borderline ? skarn formation are probably misleading if their respective mass balance calculations are invalid. REE patterns suggest LREE mobility during the alteration event. Large time-integrated molar fluxes, such as those calculated for Mineral Hill samples, might have facilitated not only spatially extensive skarn formation but LREE systematics [*Bau*, 1991; *Whitney and Olmsted*, 1998; *Boulais et al.*, 2000].

# CHAPTER 4: STABLE ISOTOPIC AND PETROLOGIC EVIDENCE FOR PERMEABILITY EVOLUTION AND TIMING OF INFILTRATION EVENTS

## 4.1 Introduction

It is well established that the oxygen isotopic composition of igneous rocks is distinctly different from that of sedimentary rocks. As such, studies of the isotope variations around intrusive contacts allow the role of fluids interacting with rocks around cooling plutons to be investigated. Although this study area is not a classic "aureole", but rather a raft of meta-sedimentary rock enclosed in a pluton, the system can be defined in one of two ways : (1) a "closed" aureole where fluids are derived internal to the defined system (i.e. pluton or the wall-rock) or (2) an "open" aureole which part of the metamorphic history involves infiltration by fluids external to the defined system [*Nabelek*, 1991]. The first scenario will be dominated by magmatic or metamorphic fluids, whereas the isotopically "open" system are dominated by surface-derived fluids [*Hoefs*, 1997]. Combined petrologic and isotope studies in many contact aureoles have provided evidence that fluids were primarily locally derived. For example, several studies have concluded that oxygen isotope composition of calc-silicates from various contact aureoles approach those of the respective intrusions. They conclude that magmatic fluids are often dominant during contact metamorphism [*Taylor and O'Neil*, 1977; *Nabelek et al.*, 1984; *Bowman*, 1985; *Valley*, 1986]. Moreover, stable isotopic studies have been important in documenting the multiple fluids present in skarn systems [e.g. *Taylor and O'Neil*, 1977]. Although it is suggested magmatic fluids controlled skarn formation at Mineral Hill, we see isotopic signatures in skarn and marble that are indicative of exchange with externally-derived fluids (i.e. meteoric). We conclude therefore that skarn genesis occurred within an open system.

Oxygen isotope data have been used in mineral deposit studies where the distribution of mineral alteration is irregular and where mineral assemblages have been obliterated by

subsequent metamorphism [*Beaty and Taylor*, 1982; *Green et al.*, 1983; in *Hoefs*, 1997]. Moreover, spatial correlation between low $\delta^{18}O$-values (see Table 4.1 for $\delta$-notation) and economic mineralization have been documented [*Criss et al.*,1985, 1991]. Consequently, regions that show anomalously low $^{18}O$ contents may be a valuable analytical tool for exploration of hydrothermal ore deposits.

Interaction between water and rock or mineral may result in a shift of the oxygen isotope ratios of the rock and/or the water away from their initial values. Three possible exchange mechanisms for water/rock interaction are discussed by *Hoefs* [1997]. These include: (1) *Solution-precipitation* where larger grains grow at the expense of smaller grains, decreasing the surface area and lowering the surface energy of the system. Isotopic exchange with the fluid occurs while the material is in solution. (2) *Chemical reaction* occurs when the chemical activity of one component of both fluid and solid is out of equilibrium in the two phases. The breakdown of the original crystal and the formation of new crystals is inferred as they form at or near isotopic equilibrium with the fluid. (3) During d*iffusion*, isotopic exchange occurs along grain boundaries between the crystal and the fluid with little to no change in shape of the reactant grains. The driving force is the random thermal motion of the ions with net movement along an activity gradient [*Hoefs*, 1997].

In this chapter mineralogic and isotopic alteration in Mineral Hill samples are examined in order to evaluate the nature of fluid flow during the first and most spatially extensive skarn-forming event. The timing and source of fluid infiltration can be constrained from the extent and type of alteration of peak mineral assemblages. In order to interpret flow geometry based on mineralogic and isotopic data we must first answer two questions: (1) What is the timing of isotopic alteration? (2) In which samples can isotopic shifts be attributed to devolatilization reactions? This chapter not only documents isotopic alteration in Mineral Hill samples, but interprets the timing of isotopic alteration in these from mineralogic evidence, especially those

Table 4.1. Notation for oxygen and carbon isotopes.

| Standard | Ratio | Notation | measurement (ratio) |
|---|---|---|---|
| SMOW | $^{18}O/^{16}O$ | $\delta^{18}O$ | permil |
| PDB | $^{13}C/^{12}C$ | $\delta^{13}C$ | permil |

Superscripts (i.e. 18, 16 in O) represent mass numbers (A). A= proton number (Z) – neutron number (N). (A)-variation results in fractionation during geologic processes.

Example:

The isotopic ratio in qtz:

$$R^{18}O_{qtz} = {}^{18}O_{qtz}/{}^{16}O_{qtz}$$

are reported relative to Standard Mean Ocean Water (SMOW), as:

$$\delta^{18}O_{qtz} = [(R^{18}O_{qtz}/ R^{18}O_{std}) - 1] \times 1000$$

These values are reported in permil which is already a ratio, therefore compositions can be directly compared.

with low $^{18}O/^{16}O$ ratios. In order to determine if oxygen isotopic shifts are solely a result of fractionation due to devolatilization reactions, $\delta^{18}O$ variation of wollastonite skarn and marble samples is evaluated. Those samples in which changes in $\delta^{18}O$ can be attributed entirely to devolitilization reactions are excluded from further consideration. From this suite, we can confidently image flow geometry and interpret an infiltration history for the study area.

## 4.2 Method of Investigation

One hundred and twelve rock powders from Mineral Hill were analyzed for $\delta^{18}O$ at Queen's University Geochemistry Lab (Dr. T.K. Kyser, dir.) (Table 4.2). Silicate whole rock powders (N=53) were analyzed using $BrF_5$ procedure described in *Clayton and Mayeda* [1963]. Carbonates (N=59) were also analyzed for $\delta^{13}C$ and $\delta^{18}O$ using the techniques outlined in *McCrea* [1950] for liberation of $CO_2$ by reaction with $H_3PO_4$. Values are reported relative to VSMOW($\delta^{18}O$) and VPDB($\delta^{13}C$). Analyzed samples include green marble, bleached marble, grey marble, black marble, augen material, calcite vein material, wollastonite skarn, clinopyroxene skarn, calc-silicate skarnoid, quartzite, garnet-wollastonite skarn, garnetite, diorite, tonalite, and basalt. Blind duplicate analyses yielded a $1\sigma$ of 0.07 permil for $\delta^{18}O$ and $\delta^{13}C$ (Table 4.3). $\delta^{18}O$ and $\delta^{13}C$ data are listed in Table 4.2.

Forty-six whole-rock silicate and twenty-seven whole-rock carbonate analyses derive from the same powders that were used for whole-rock chemical analyses (see Chapter 3). An additional seven silicate analyses of wollastonite pods were crushed and powdered from ~3cm$^3$ slabs in a steel mortar and pestle. Thirty-two additional carbonate powders were drilled from slabs using a diamond-impregnated drill bit in a Dremel tool. Powders constituted no more than 4mm$^3$ of sample material.

Table 4.2. O and C stable isotope data (in permil) for samples from Mineral Hill. Distance measurements are relative to the wollastonite skarn/marble interface where the contact = 0 cm.

| Sample | lithology | del 18O (SMOW) | del 13C (PDB) | distance (cm) |
|---|---|---|---|---|
| KM-MB4c | green marble | 15.6 | 0.3 | |
| KM-UB4e(mb) | green marble | 2.3 | -5 | |
| KM-TB4e | green marble | 4 | -4.6 | |
| KM-TB4f | green marble | 2.8 | -2.6 | |
| KM-W1d(mb) | bleached marble | 3 | -4.2 | |
| GM1a(U)-B | bleached marble | 3.8 | -2.9 | 1.13 |
| GM1a(U)-B2 | bleached marble | 3.4 | -2.5 | 0.53 |
| GM1a(L)-B1 | bleached marble | 3.3 | -2.5 | 0.39 |
| GM1a(L)-B2 | bleached marble | 3.1 | -3.2 | 6.09 |
| GM1a(L)-B3 | bleached marble | 3.1 | -2 | 1.16 |
| GM1a(UR)-B | bleached marble | 3.5 | -2.3 | 0.36 |
| GM1e(L)-B1 | bleached marble | 2.7 | -3.4 | 0.62 |
| GM1f-B | bleached marble | 2.9 | -3.5 | 3.05 |
| BM-1-B | bleached marble | 12.4 | -1.9 | |
| MH5a-B | bleached marble | 4.2 | -0.8 | |
| KM-UBM1a | grey marble | 15.9 | -0.2 | 600 |
| KM-FRM2c | grey marble | 12.3 | -2 | |
| GM 1h-M | grey marble | 3 | -3.5 | |
| 00H3-M | grey marble | 3.9 | -1.3 | 100 |
| 00H4-M | grey marble | 6.5 | -3.1 | 200 |
| 00H5-M | grey marble | 4.7 | -6.2 | 300 |
| 00H6-M | grey marble | 3.6 | -0.6 | 200 |
| 00H9-M | grey marble | 3.4 | -2.6 | 200 |
| 00H10-M | grey marble | 3.6 | -1.9 | 200 |
| 00H12-M | grey marble | 4.2 | -1.1 | 100 |
| 00H13-M | grey marble | 2.9 | -1.6 | 400 |
| 00H14-M | grey marble | 3.6 | -0.9 | 400 |
| 00H15-M | grey marble | 3.1 | -1 | 1000 |
| 00H16-M | grey marble | 3.4 | -1.6 | 500 |
| 00NE-1-M | grey marble | 6.2 | 0.2 | 5500 |
| 00NE-2-M | grey marble | 8.5 | -4.7 | 5700 |
| 00NE-3a-M | grey marble | 9.6 | -3.1 | 3500 |
| 00NE-3b-M | grey marble | 8.9 | -5.1 | 3500 |
| OOUMQ-1-M | grey marble | 13 | -1.1 | 1000 |
| OOUMQ-2-M | grey marble | 12.2 | -1.1 | 1000 |
| OOUMQ-3-M | grey marble | 10 | -2.1 | 1000 |
| GM1e(R)-G | grey marble | 3 | -3.2 | |
| GM1a(L)-G | grey marble | 3.2 | -3.6 | |
| GM1a(U)-G | grey marble | 3.6 | -2.6 | 1.65 |
| GM1a(L)-G1 | grey marble | 3.4 | -2.7 | 2.13 |
| GM1a(L)-G2 | grey marble | 3.3 | -3.1 | 5.61 |
| GM1a(L)-G3 | grey marble | 3.3 | -1.4 | 1.45 |
| GM1a(UR)-G | grey marble | 3.4 | -2.7 | 3.91 |
| GM1e(L)-G1 | grey marble | 3.7 | -3.1 | 3.55 |
| GM1e(L)-G2 | grey marble | 3.2 | -3.4 | 1.68 |
| GM1e(L)-G3 | grey marble | 3 | -3.4 | 0.44 |

| Sample | lithology | del 18O (SMOW) | del 13C (PDB) | distance (cm) |
|---|---|---|---|---|
| GM1e(L)-G4 | grey marble | 3.2 | -3.3 | 1.24 |
| GM1e(R)-G1 | grey marble | 3.7 | -3.5 | 4.47 |
| GM1e(R)-G2 | grey marble | 3.5 | -2.9 | 1.38 |
| GM1f-G1 | grey marble | 3.4 | -3.2 | 0.77 |
| GM1f-G2 | grey marble | 3 | -4 | 2.59 |
| BM-1-G1 | grey marble | 10.7 | -2.9 | |
| MH5a-G | grey marble | 4.1 | -0.6 | |
| BM-1-M | grey marble | 14.4 | -2.2 | |
| BM-1-D1 | black marble | 12.1 | -3.6 | |
| BM-1-D2 | black marble | 12 | -3.7 | |
| BM-1-D3 | black marble | 16.3 | -1.3 | |
| GM1g-V1 | calcite vein | 2.1 | -4.1 | |
| GM1g-V2 | calcite vein | 2.4 | -3.1 | |
| KM-W1d(w) | woll skarn | 3.6 | | |
| KM-W1a | woll skarn | 6.1 | | |
| KM-W1c | woll skarn | 10.2 | | |
| KM-UB4e(w) | woll skarn | 6.4 | | |
| KM-W1b | woll skarn | 7.1 | | |
| 00NE-2-WP | woll skarn | 12.1 | | |
| 00NE-3a-WP | woll skarn | 19.8 | | |
| 00UMQ-2-WP | woll skarn | 9.6 | | |
| GM-1h-W | woll skarn | 17.5 | | |
| 00H1-W | woll skarn | 12 | | -300 |
| 00H2-W | woll skarn | 11.5 | | -200 |
| 00H3-W | woll skarn | 11.3 | | |
| 00H4-WP | woll skarn | 7.6 | | |
| 00H5-WP | woll skarn | 10.1 | | |
| 00H7-W | woll skarn | 17.4 | | -50 |
| 00H8-W | woll skarn | 18.6 | | -100 |
| 00H10-W | woll skarn | 9.4 | | |
| 00H11-W | woll skarn | 7.6 | | -100 |
| 00H13-W | woll skarn | 17.7 | | |
| 00H14-WP | woll skarn | 10.8 | | |
| 00H16-WP | woll skarn | 8 | | |
| GM1a(UR)-W | woll skarn | 13.5 | | -0.89 |
| GM1e(L)-W | woll skarn | 10.6 | | -1.33 |
| GM1e(R)-W | woll skarn | 6 | | -1.03 |
| MH5a-W | woll skarn | 8.4 | | |
| GM1a(L)-W1 | woll skarn | 9 | | -0.97 |
| GM1a(L)-W3 | woll skarn | 12.9 | | -1.45 |
| GM1a(U)-W1 | woll skarn | 6.6 | | -0.60 |
| GM1a(U)-W2 | woll skarn | 8.9 | | -5.85 |
| GM1g-W | woll skarn | 3.3 | | |
| 00H4-W | woll skarn | 12.8 | | |
| GM1a(U)-W | woll skarn | 13.9 | | |
| GM1f-W | woll skarn | 9.2 | | -0.77 |
| KM-TB9a | g-w skarn | 1.5 | | |
| KM-UB2c | g-w skarn | 1 | | |
| KM-MB5b | g-w skarn | 9.4 | | |
| KM-MB4b | g-w skarn | 8.4 | | |
| KM-TB13a | garnetite | 0.6 | | |

| Sample | lithology | del 18O (SMOW) | del 13C (PDB) | distance (cm) |
|---|---|---|---|---|
| KM-MB3b | cpx skarn | 1.9 | | |
| KM-UB14c | skarnoid | 2.6 | | |
| BM-1-A | augen | 7.1 | | |
| KM-MB7a | quartzite | 3.1 | | |
| KM-LB1d | diorite | 4.3 | | |
| KM-MB1a | diorite | 1.1 | | |
| KM-MB1b | diorite | 5.4 | | |
| KM-d1a | diorite dike | 1.4 | | |
| KM-d1b | diorite dike | 3.1 | | |
| KM-d1f | diorite dike | 2.3 | | |
| KM-d2a | tonalitic dike | 2.9 | | |
| KM-UBFRd2 | tonalitic dike | 4.7 | | |
| KM-MBFRd2 | tonalitic dike | 3.5 | | |
| KM-UBd3a | basaltic dike | 1.8 | | |
| KM-FRd3a | basaltic dike | 0.8 | | |

Table 4.3. Mean and standard deviation (sd) for blind duplicate analyses d-13C and d-18O compositions.

| | d-13C(PDB) | mean d-13C | sd d-13C | d-O18(SMOW) | mean d-18O | sd d-18O |
|---|---|---|---|---|---|---|
| BN(mb)-1 | 1.9 | 1.95 | 0.07 | 13.6 | 13.65 | 0.07 |
| BN(mb)-2 | 2 | | | 13.7 | | |

## 4.3 Carbonates

Carbonates analyzed for $\delta^{18}O$ and $\delta^{13}C$ included green marble (N=4), bleached marble (N=11), grey marble (N=17), grey and bleached marble (N=22), black marble (N=3), and calcite vein (N=2). Localities and values presented in Fig. 4.1, 4.2, 4.3, and 4.4.

Fig. 4.5 plots $\delta^{18}O$ of carbonate versus sampling method (bulk vs. micro drill). The similar spread for both sampling methods suggests that the two data sets can be directly compared. A similar analysis for $\delta^{13}C$ (Fig. 4.6) illustrates that drilled samples have a more restricted range in composition than bulk crushed samples. Below, these trends are analyzed as a function of the rock type sampled.

$\delta^{18}O$ isotope compositions for all marbles range from 2.3 to 16.3 permil and are depleted relative to marine limestone even though $\delta^{18}O$ values for limestone vary through geologic time (~27 to 35 permil in Upper Triassic)[*Veizer et al.*, 1999]. These compositions therefore likely record the interaction between marble and a low $^{18}O$ fluid such as meteoric and/or magmatic water. Marble from Mineral Hill is also depleted in $^{18}O$ relative to the Waterville limestone ($\delta^{18}O$=18.2 to 19.8 permil) [*Bickle et al.*, 1997]. $\delta^{18}O$-values for green marble range between 2.3 to 15.6 permil, bleached marble range between 2.7 to 12.4 permil, grey marble range between 2.9 to 15.9 permil, black marble range between 12.0 to 16.3 permil and calcite vein range between 2.1 to 2.4 permil (Fig. 4.7). Among spatially related grey and bleached marble samples (i.e. grid map samples from Marble Hill), bleached marble tends to have between 0.1 to 0.5 permil lower $^{18}O$-content (Fig. 4.8).

Marbles from Mineral Hill are depleted relative to $\delta^{13}C$-values for Upper Triassic marine carbonates (2 to 4 permil) [Veizer et al., 1999]. $\delta^{13}C$-values for green marble range between –5.0 to 0.3 permil, bleached marble range between –4.2 to –0.8 permil, grey marble range between –6.2 to 0.2 permil, black marble range between –3.7 to –1.3 permil and calcite vein range between

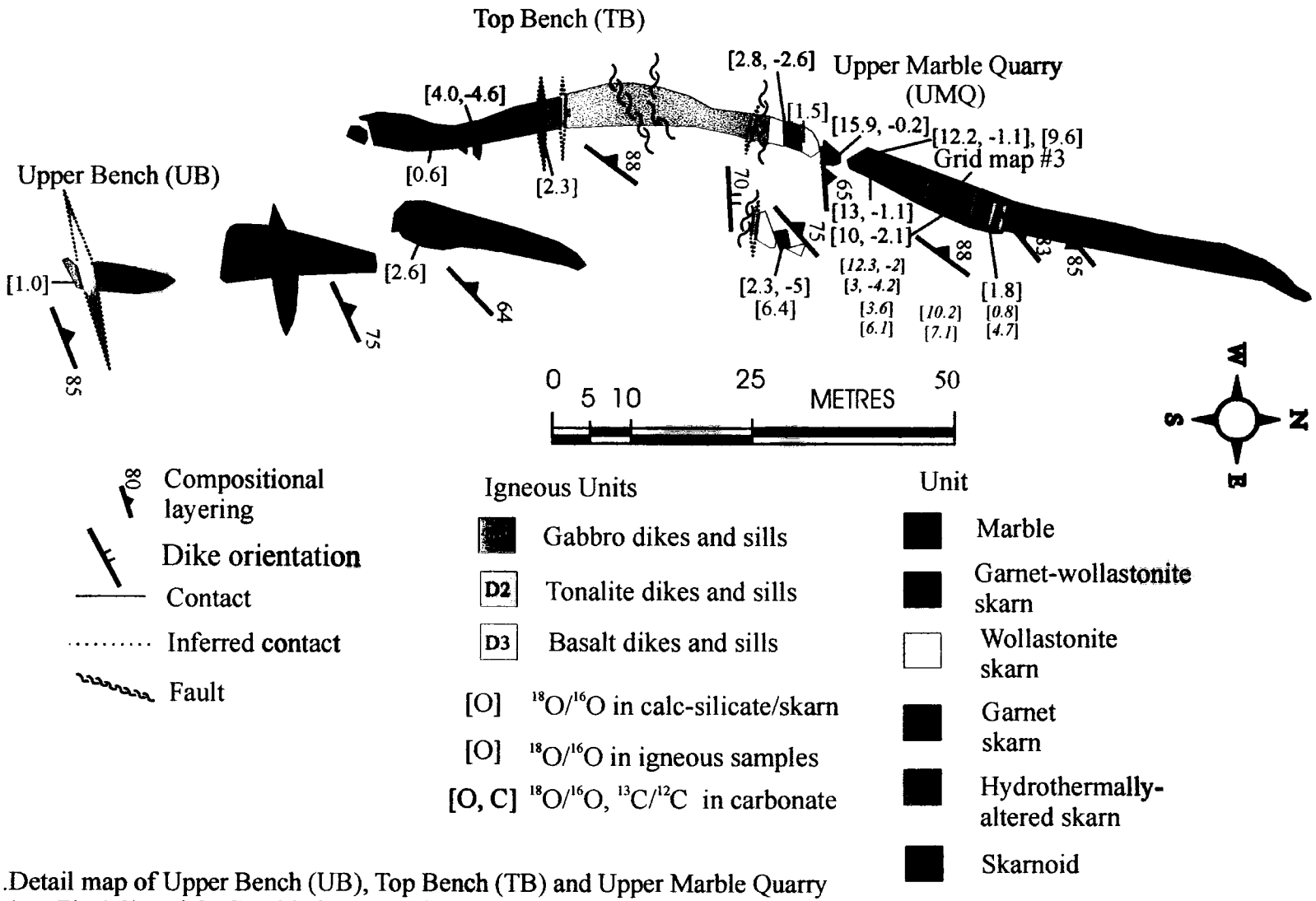


Fig. 4.1.Detail map of Upper Bench (UB), Top Bench (TB) and Upper Marble Quarry (UMQ) (see Fig.1.2) and O, C stable isotope values and locality. Smaller *italizied* values indicate fall rock sample.

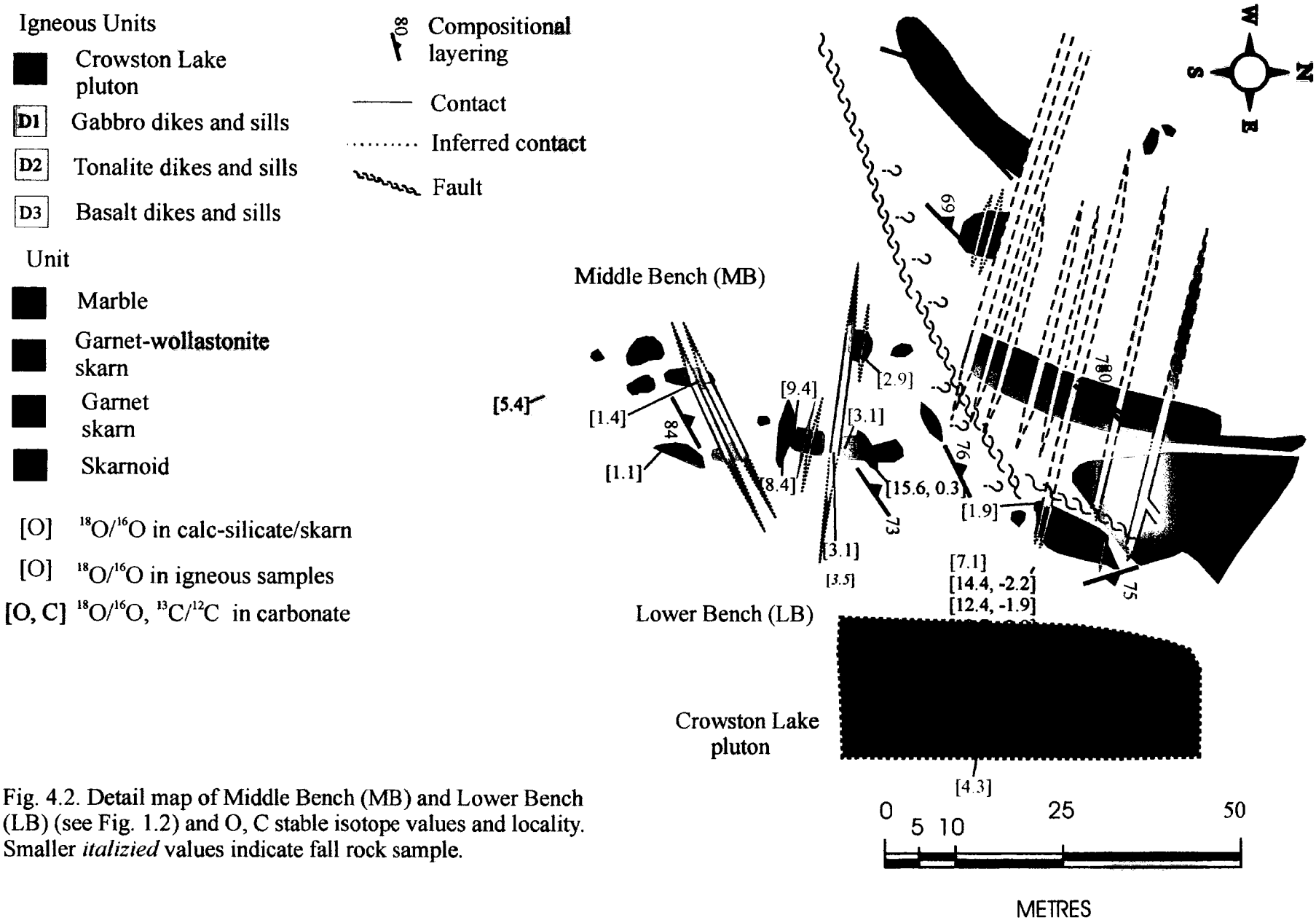


Fig. 4.2. Detail map of Middle Bench (MB) and Lower Bench (LB) (see Fig. 1.2) and O, C stable isotope values and locality. Smaller *italizied* values indicate fall rock sample.

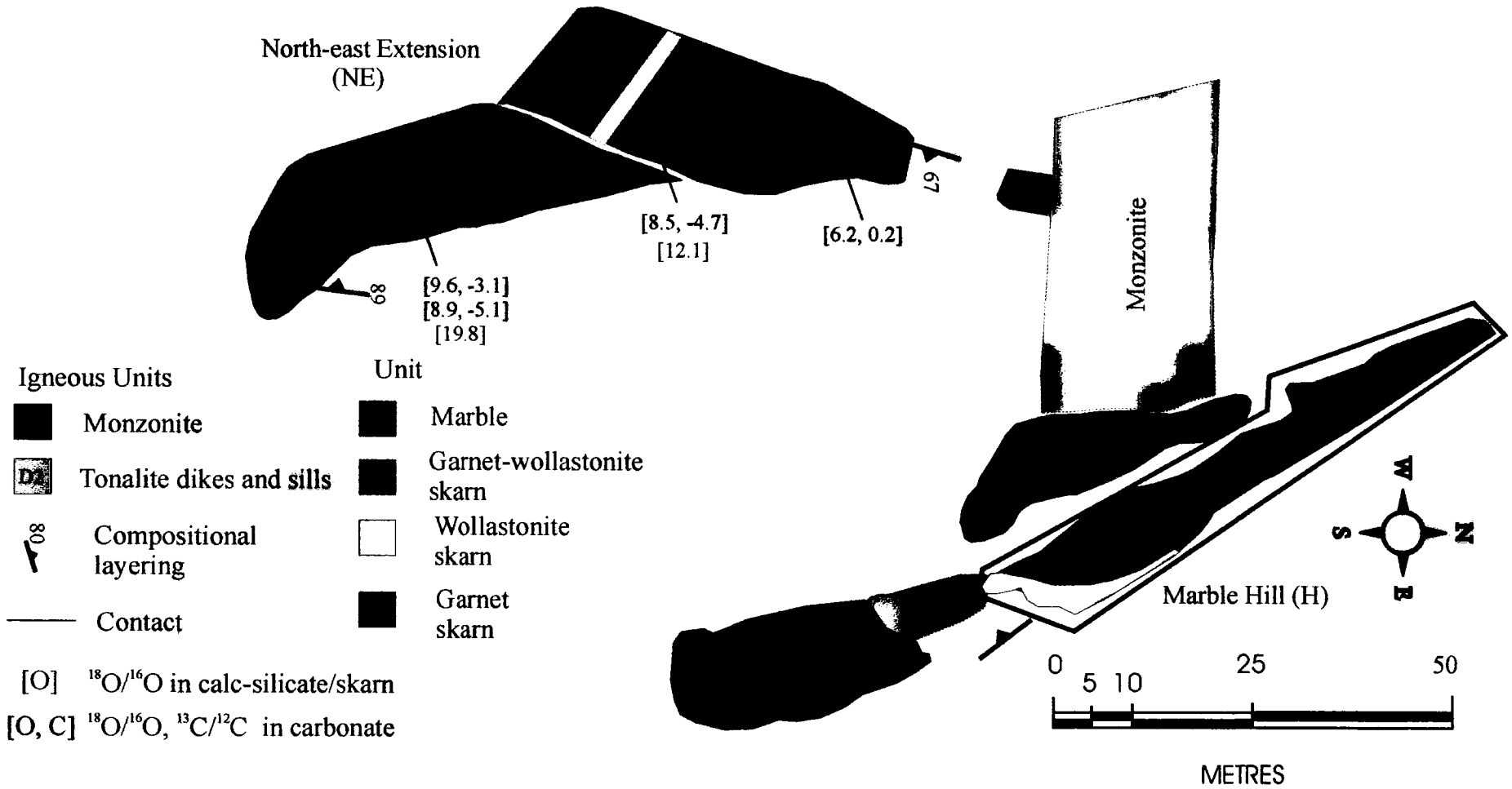


Fig. 4.3. Detail map of North-east Extension (NE) and Marble Hill (H) (see Fig. 1.2) and O, C stable isotope values and locality for samples from NE. See Fig. 4.4 for O, C stable isotope values and locality from H (inset area).

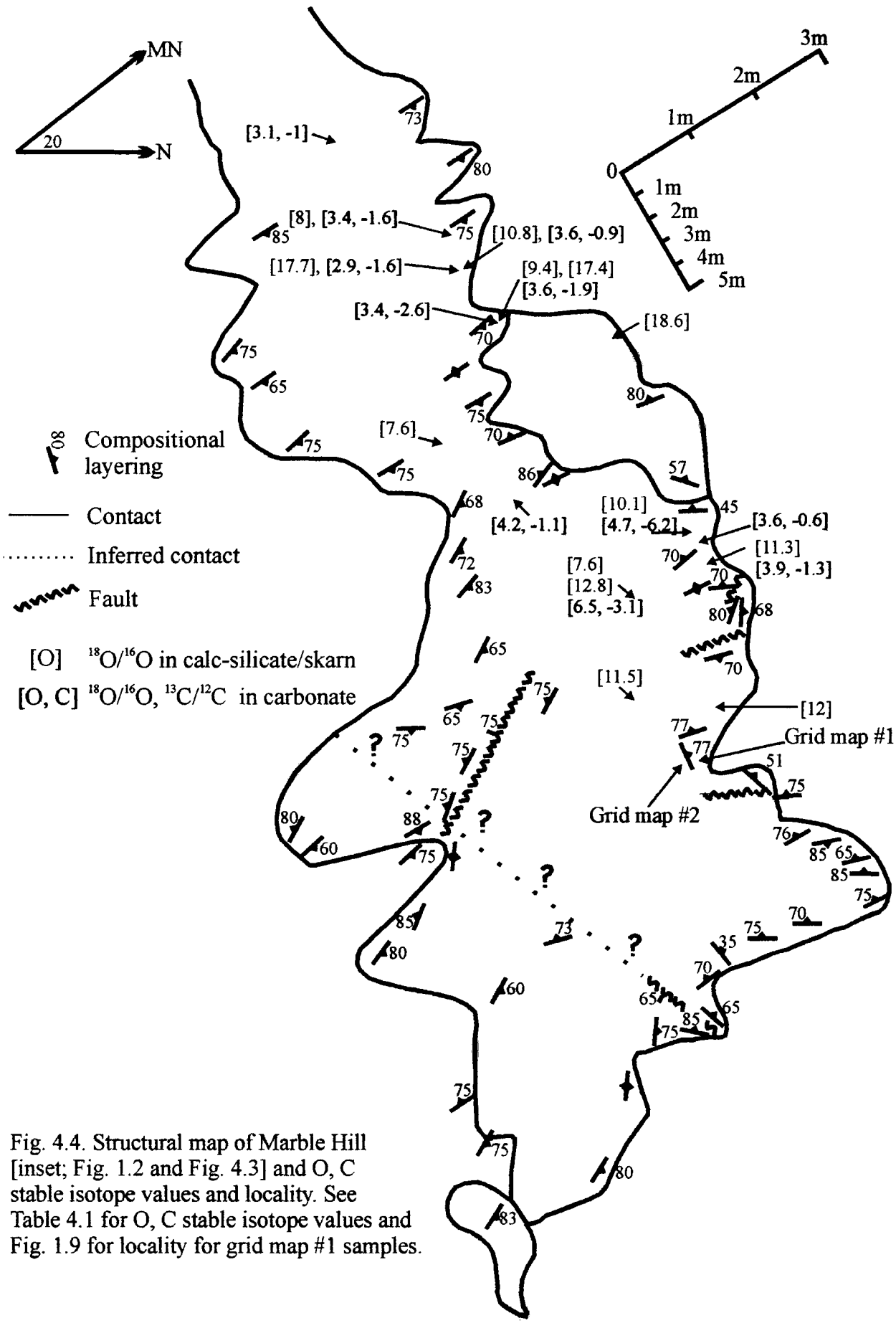


Fig. 4.4. Structural map of Marble Hill [inset; Fig. 1.2 and Fig. 4.3] and O, C stable isotope values and locality. See Table 4.1 for O, C stable isotope values and Fig. 1.9 for locality for grid map #1 samples.

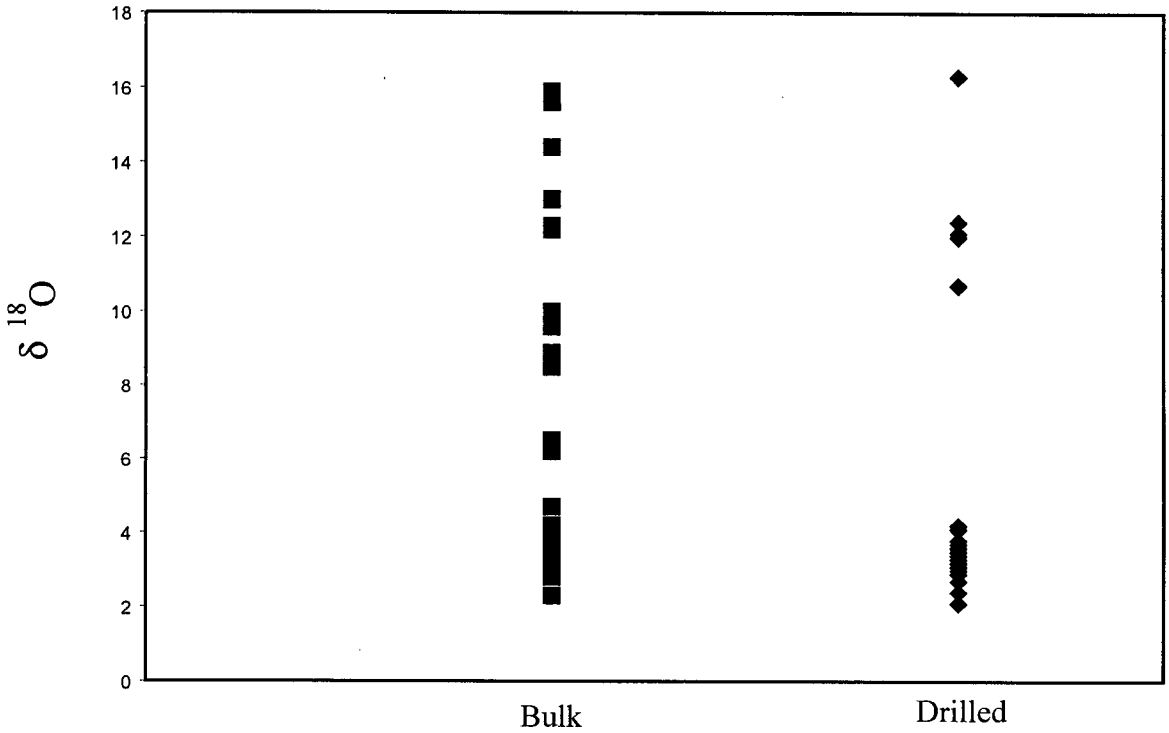


Fig.4.5. $\delta^{18}O$ vs. powder type for marble samples from Mineral Hill.

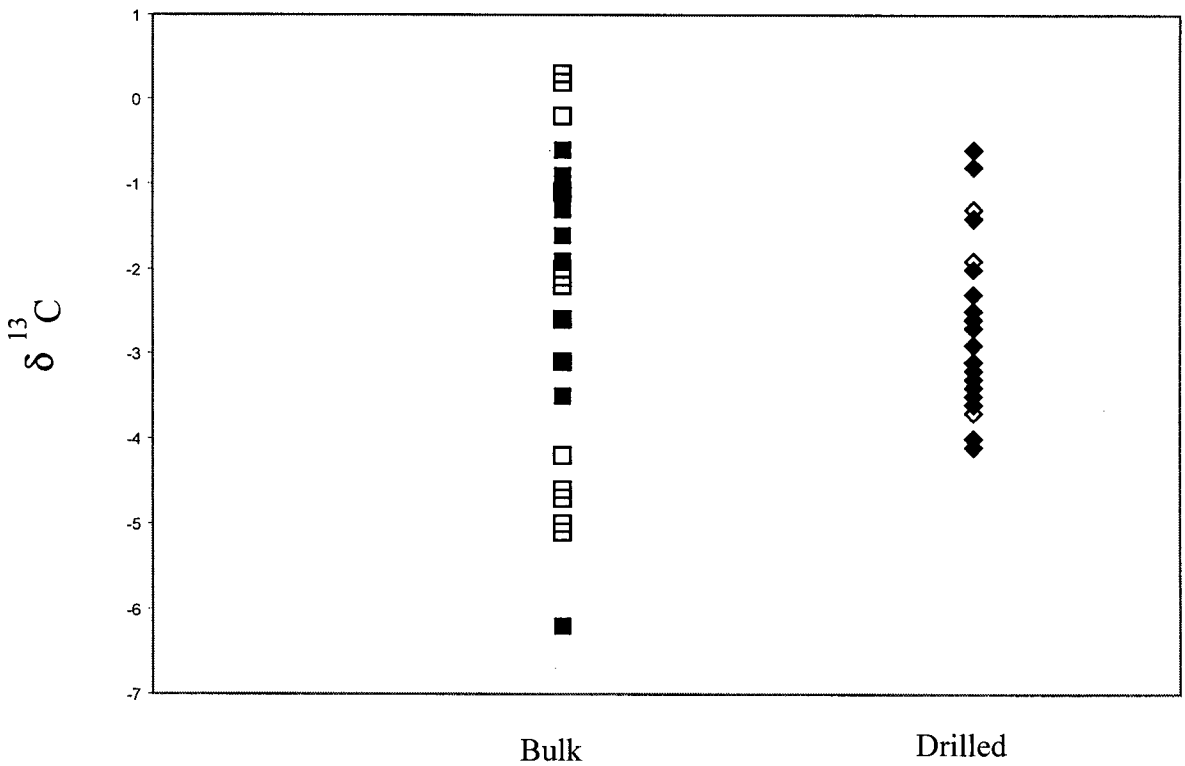


Fig. 4.6. $\delta^{13}C$ vs. powder type for marble samples from Mineral Hill. Closed symbols from Marble Hill samples; open symbols from Upper Marble Quarry and North-east extension.

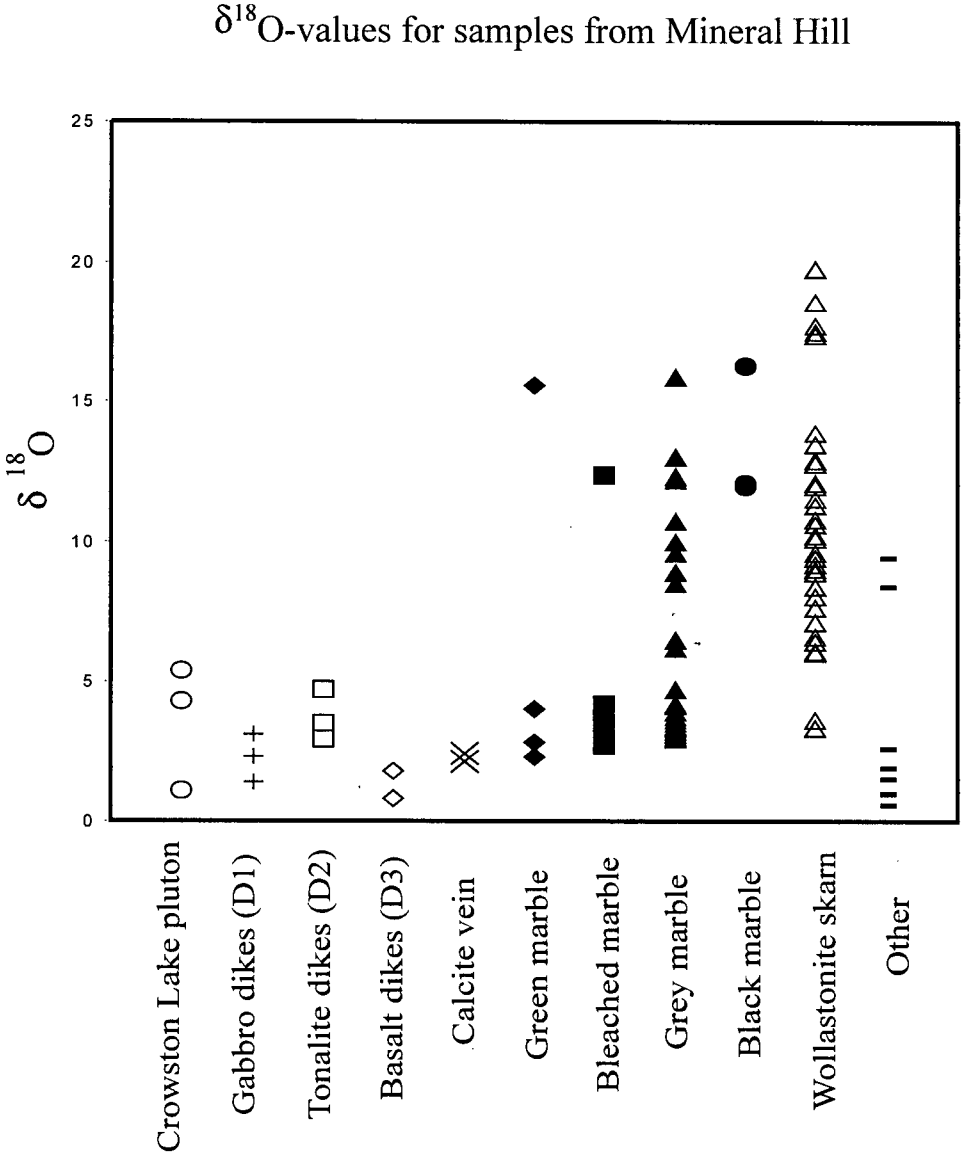


Fig. 4.7. $\delta^{18}O$ compositions of Mineral Hill samples.

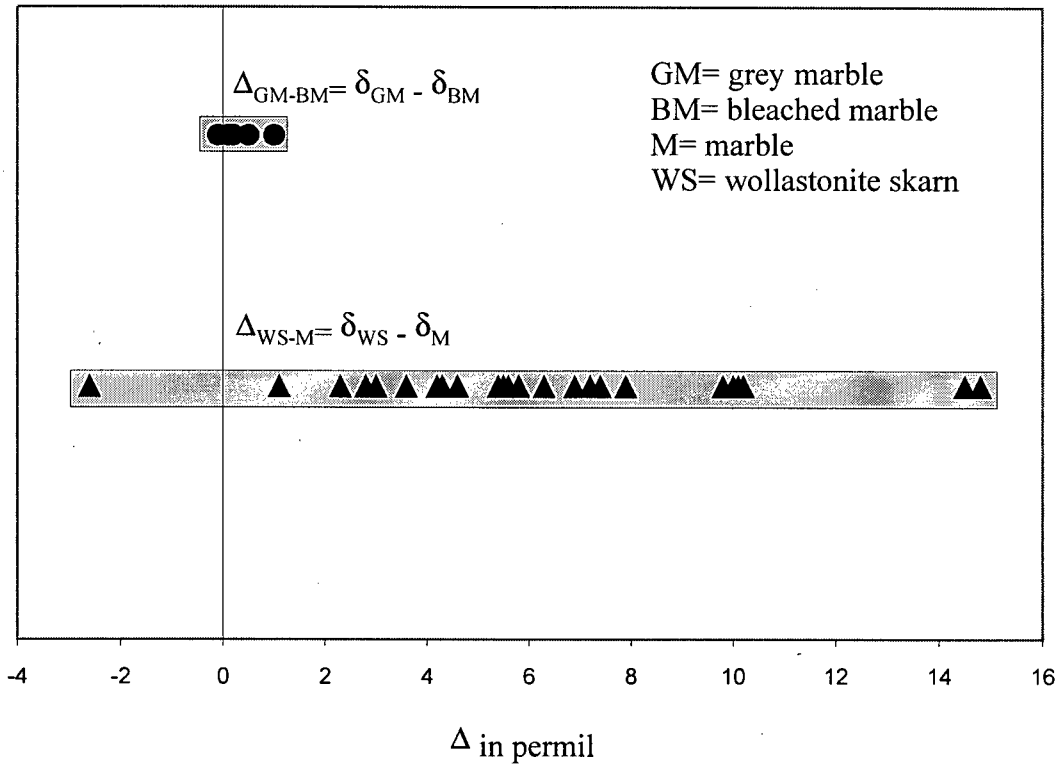


Fig. 4.8. $\delta^{18}O$ isotopic differences between spatially related grey and bleached marble (solid circles) and wollastonite skarn and marble (solid triangles). Differences in grey and bleached marble were derived from $\Delta_{GM-BM} = \delta_{GM} - \delta_{BM}$. Differences in wollastonite skarn and marble (both GM and BM) were derived from $\Delta_{WS-M} = \delta_{WS} - \delta_{M}$. Note the dominance of positive values (see text for explanation).

–4.1 to –3.1 permil (Fig. 4.9). The variation in $\delta^{13}C$ values in calcite could be due to progressive reaction of magmatic fluids with carbonate wall rocks. The $\delta^{13}C$-values for powders derived from drilled samples have a more restricted range than bulk samples (Fig. 4.6). Samples MB4c, UBM1a, and NE-1 have higher 13C-content (0.3 to –0.2 permil) than drilled samples. No powders from these samples where derived from drilling. Higher values might reflect bulk sampling methodology, differences in lithology (i.e. green marble; sample MB4c) or geographic location (i.e. no samples from Marble Hill). Samples NE-2, NE-3b, 00H5, TB4e, W1b, and UB4e have lower $^{13}C$-content (-4.2 to –6.2 permil) than drilled samples. Lower values might also reflect bulk sampling methodology, differences in lithology (i.e. green marble; sample TB4e and UB4e) or geographic location (i.e. only one sample from Marble Hill). The lowest value (-6.2 permil; sample H5) occurs in close proximity to the Crowston Lake Pluton at Marble Hill, however, other samples near this sample locality have $\delta^{13}C$ values that range between -0.6 to -3.6 permil, suggesting heterogeneity in carbon isotopic alteration on outcrop scale.

To conclude, there is no direct evidence to suggest that sampling by microdrill contaminates the isotopic composition of carbonate rocks. The only systematic differences between bulk samples and drilled samples is in $\delta^{13}C$, but the drilled samples show a more restricted range of composition; a trend opposite of what would be expected through contamination. The observed variation in $\delta^{13}C$ likely reflects heterogeneous $\delta^{13}C$ compositions between various rock types and on an outcrop scale.

## 4.4 Silicates

Analyzed silicates powders derive from diorite, tonalite, basalt, wollastonite skarn, garnet-wollastonite skarn, garnetite, clinopyroxene skarn, calc-silicate skarnoid, clinozoisite augen (in black marble), and quartzite. Values are reported relative to VSMOW. $\delta^{18}O$

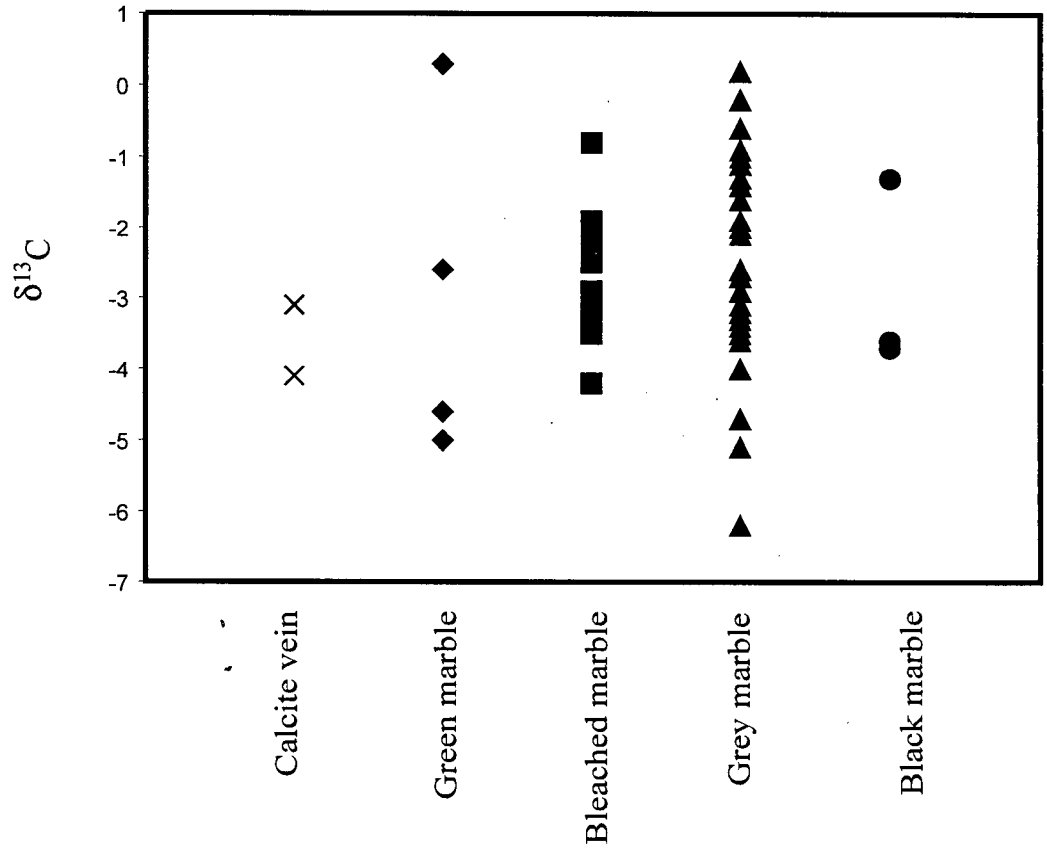


Fig. 4.9. $\delta^{13}C$ compositions of Mineral Hill marble samples.

compositions for all samples from Mineral Hill are compared in Fig 4.10. Localities and values are presented in Figs. 4.1, 4.2, and 4.4.

### 4.4.1 Intrusive rocks

Igneous rocks from Mineral Hill analyzed for $^{18}O$ content include diorite (N=3), D1 diorite dike (N=3), D2 tonalite dike (N=3) and D3 basalt dike (N=2). Values reported for diorite ranges between 1.1 to 5.4 permil, D1 ranges between 1.4 to 3.1 permil, D2 ranges between 2.9 to 4.7 permil and D3 ranges between 0.8 to 1.8 permil. The data indicate that the igneous rocks are depleted in $^{18}O$-content compared to standard $^{18}O$-values reported for mafic igneous rocks (Fig. 4.11). Igneous rocks must have also interacted with an isotopically light oxygen reservoir. An alteration index for diorite, D2 and D3, based on petrographical observation and estimation of alteration minerals, was developed in order to determine whether isotopically low oxygen values decreased relative to alteration of the sample (Fig. 4.12). Generally, the least altered samples have higher $^{18}O$ compositions than the most altered samples, however there is significant overlap. Overall, retrograde minerals and textures are observed in igneous samples (see Chapter 2). Therefore, it is likely that depleted $^{18}O$-values are a result of subsolidus isotopic exchange of dike rocks with a low $\delta^{18}O$ fluid (e.g. meteoric water).

### 4.4.2 Skarn

***Wollastonite skarn***

Wollastonite skarn from the Upper Marble Quarry (N=5), the North-east Extension (N=2), Marble Hill (N=1) and in green marble (N=1) range in $\delta^{18}O$ composition from 3.6 to 19.8 permil. Wollastonite skarn (N=24) was also sampled on a centimeter scale at Marble Hill along the wollastonite skarn-marble contact as a part of a detailed isotopic study. $\delta^{18}O$ values range

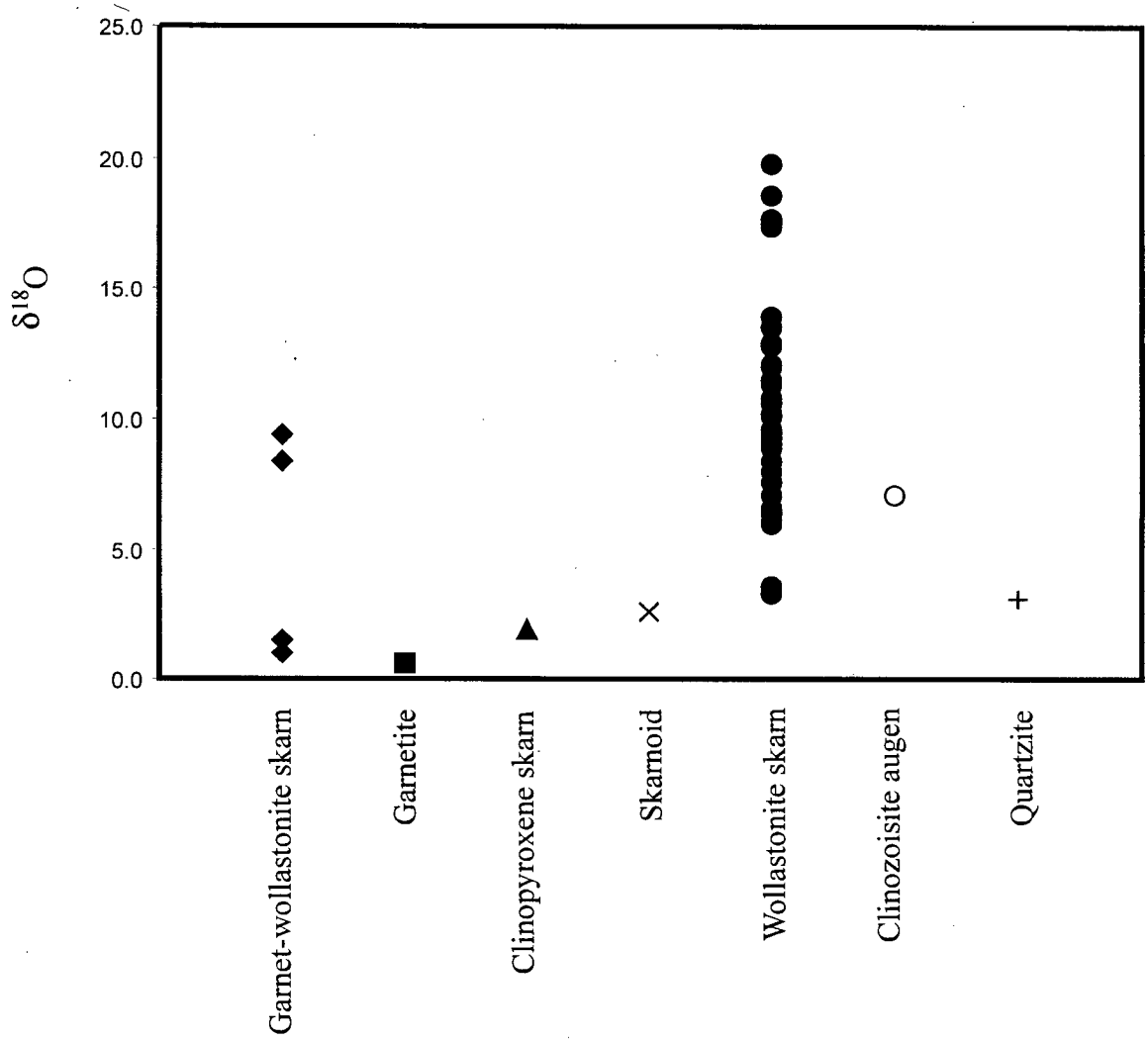


Fig. 4.10. Silicate $\delta^{18}O$ compositions of meta-sedimentary and skarn rock samples.

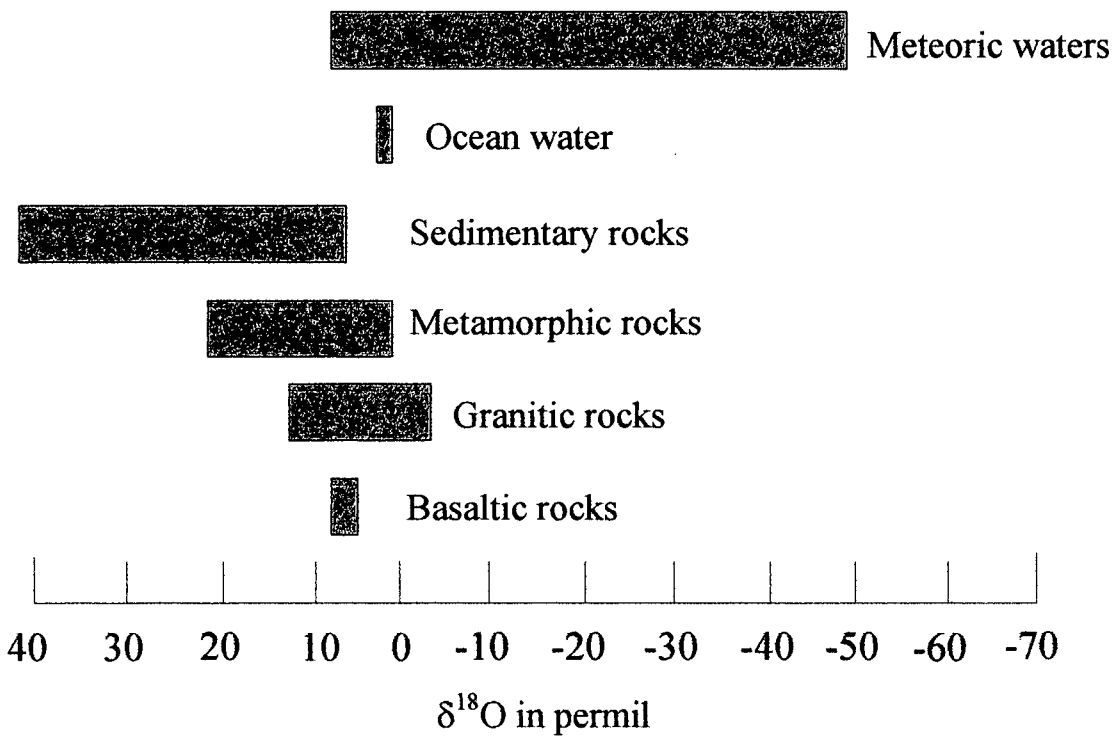


Fig. 4.11. $\delta^{18}O$-values of important geological reservoirs [modified from *Hoefs*, 1997].

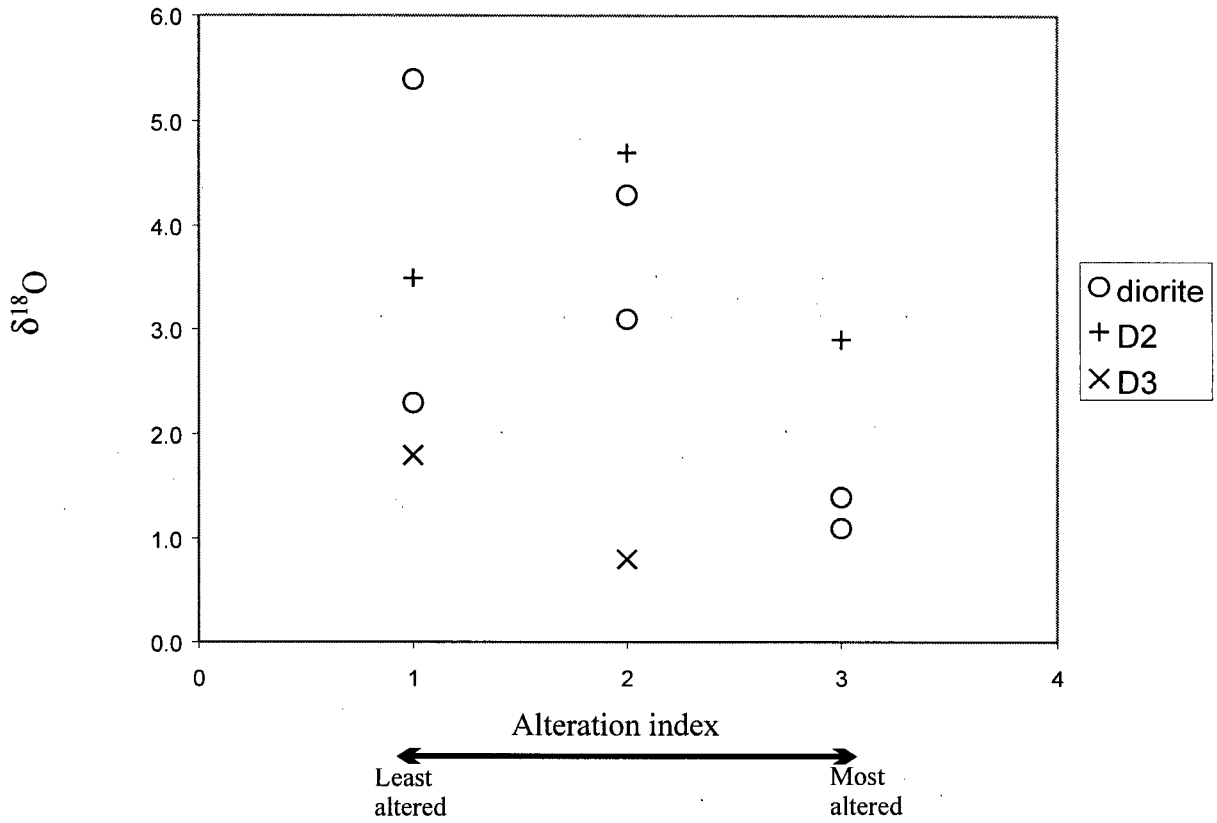


Fig. 4.12. $\delta^{18}O$ compositions vs. alteration index for igneous rocks from Mineral Hill. 1. Least altered, 2. Moderately altered, 3. Most altered. Alteration index based on petrographical observation and estimation of alteration minerals.

between 3.3 to 18.6 permil. The $\delta^{18}O$ compositions of wollastonite skarn along this contact and in wollastonite pods within grey and bleached marble are systematically higher than $\delta^{18}O$ compositions reported for marble (Fig 4.7). Trace amounts of late opaque mineralization and calcite veins were observed in thin section for samples with reported $\delta^{18}O$ compositions less than 5 permil. This carbonate was removed by reaction with HCl prior to $\delta^{18}O$ analysis, but the veins may record incursion of exotic fluids that altered skarn after skarn formation. Two wollastonite skarn samples, which yield a $\delta^{18}O$-value less than 5 permil, include GM1g-W and W1d(w), at 3.3 and 3.6 permil, respectively. Upon petrographic examination, GM1g-W ranges from non-foliated to strongly foliated, has optically-unidentifiable fine-grained alteration along cleavage planes (~15% by volume) whereas most wollastonite skarn samples examined show minor to no alteration. Calcite veins are common at Mineral Hill. In contrast, W1d (w) is weakly foliated and shows no retrograde alteration of peak minerals (woll) although trace amounts of opaque minerals are present. However, many wollastonite samples that contain opaque minerals yield magmatic $\delta^{18}O$ signatures.

***Garnet-wollastonite skarn***

Garnet-wollastonite skarn (N=4) was sampled in the Upper Bench and Middle Bench. The $\delta^{18}O$ values range between 1.0 to 9.4 permil. Late opaque and epidote mineralization, veins and moderately-altered skarn minerals were observed in samples with $\delta^{18}O$ compositions less than 5 permil. The alteration and depleted isotopic signatures probably reflect interaction with a low $^{18}O$ fluid after skarn formation.

*Garnetite*

A sample of garnetite from the Top Bench has a $\delta^{18}O$ value of 0.6 permil. In thin section, extensive wollastonite, quartz and calcite veins are observed within garnetite.

*Clinopyroxene skarn*

One sample of clinopyroxene skarn from the Middle Bench has a $\delta^{18}O$ -value of 1.9 permil. Late opaque and epidote mineralization, veins and moderately-altered skarn minerals are present in thin section.

### 4.4.3 Skarnoid

One sample of calc-silicate skarnoid from the Upper Bench has a $\delta^{18}O$ value of 2.6 permil. Late opaque and epidote mineralization, veins and moderately-altered skarn minerals are present in thin section.

### 4.4.4 Quartzite

A sample of quartzite from the Middle Bench has a $\delta^{18}O$ value of 3.1 permil. The sample contains very high amounts of moderately-altered epidote, some late opaque mineralization, and veins.

### 4.4.5 Clinozoisite Augen (in Black Marble)

A sample of an augen (BM-1; see Table 2.2) from a black marble from the Middle Bench has a $\delta^{18}O$ value of 7.1 permil. This value is lower than the $\delta^{18}O$ values reported from the adjacent black marble, grey marble and bleached marble.

## 4.5 Wollastonite skarn-marble interface

Variation in $\delta^{18}O$ across skarn-marble contacts was examined closely in seven places (centimeter-scale). Six contacts between wollastonite skarn and marble were in samples collected from Grid Map #1 (Fig. 1.9) at Marble Hill (Fig. 4.13 a-g). In general, there are sharp isotopic shifts (< 2 centimeters) across the contact from marble to wollastonite skarn. Moreover, wollastonite skarn samples are enriched in $^{18}O$ relative to marble samples, ranging from 6 to 13.9 permil, indicating $^{18}O$ exchange equilibrium with the pluton. Calcite marble is observed directly outboard of wollastonite skarn as proximal bleached marble to distal grey marble (Fig. 1.9). Bleached marble has depleted $\delta^{18}O$ compositions that range between 2.7 and 3.8 permil. Generally, grey marble is slightly higher in $^{18}O$ and ranges between 3 to 3.7 permil. Only grey marble in sample GM1a(U) has a lower $\delta^{18}O$ composition than the spatially related bleached marble (Fig. 4.13a). One wollastonite skarn sample (GM1g-W) has a significantly lower signature ($\delta^{18}O$ = 3.3 permil), however this sample is in very close proximity to large calcite veins with $\delta^{18}O$ compositions of 2.1 and 2.4 (Fig. 4.13f). Because of the presence of veins in this sample, the isotope alteration in sample GM1g-W is probably due to influx of exotic fluids that equilibrated with skarn after skarn formation.

In the last sample (BM-1), I examined isotopic variations between black marble, grey marble, bleached marble, and a clinozoisite augen (Fig. 4.13h). In sample BM-1, the $\delta^{18}O$ compositions in marbles are significantly higher than those in the previous contacts. grey marble has the lowest $^{18}O$-content (10.7 permil), bleached marble has 12.4 permil, and black marble ranges between 12 to 16.3 permil. Spatially, sample BM-1 is located proximal to the Crowston Lake Pluton and unlike other marble samples does not seem to have equilibrated with a meteoric fluid. However, marble is depleted from "pristine" values for marble (~20-25 permil), and likely

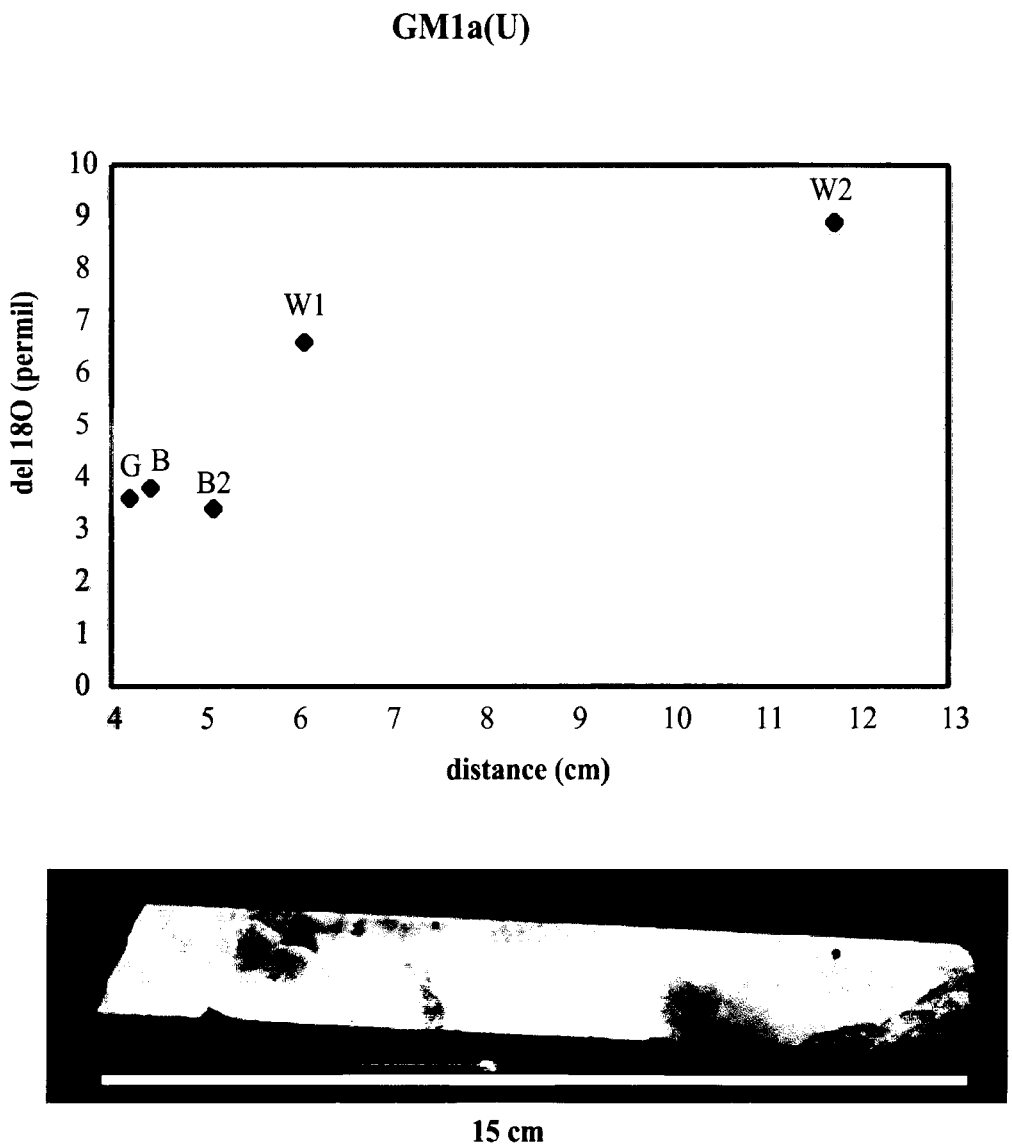


Fig. 4.13. a) Centimeter-scale oxygen isotopic shifts in grid map sample GM1a(U). All analyses derive from drilled powders from slabs (photo). G= grey marble, B= bleached marble, W= wollastonite skarn; numbers indicate sample number (see Table 4.1).

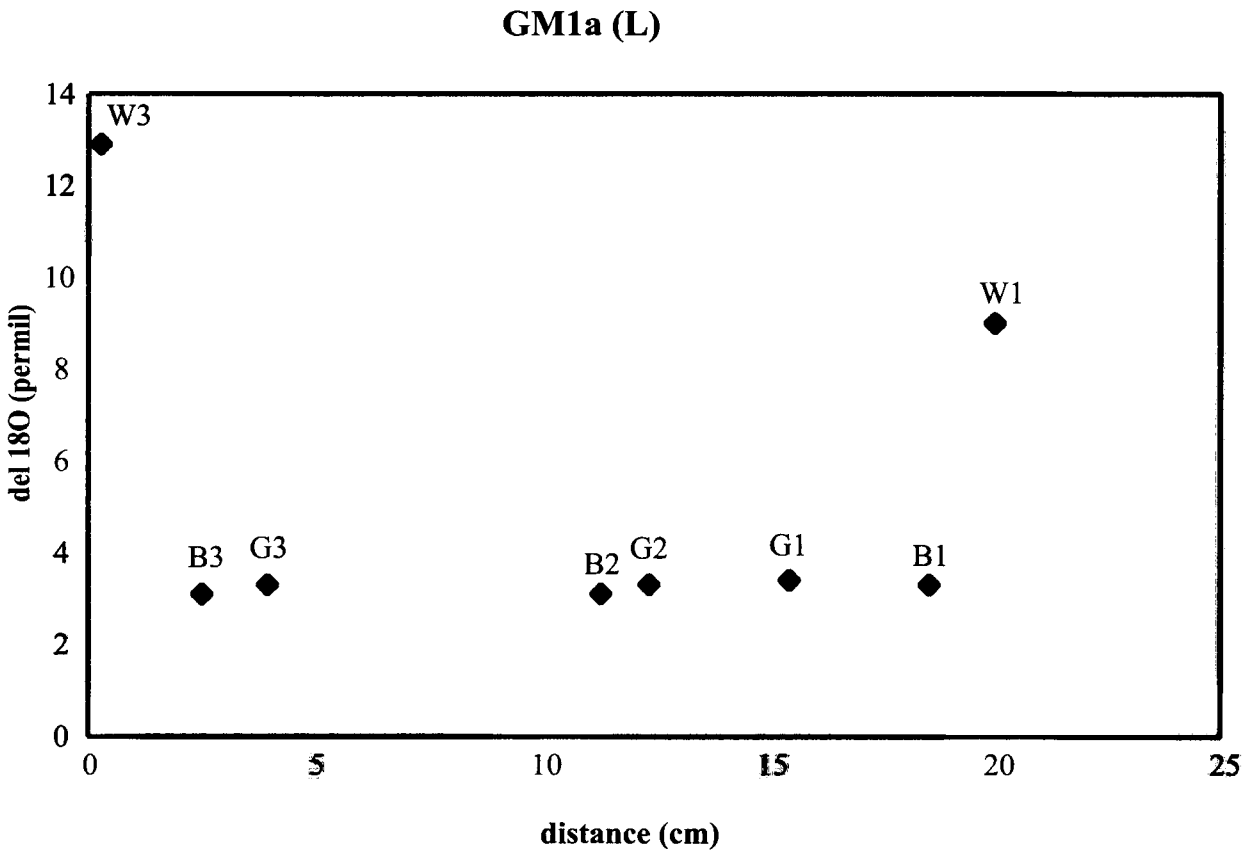


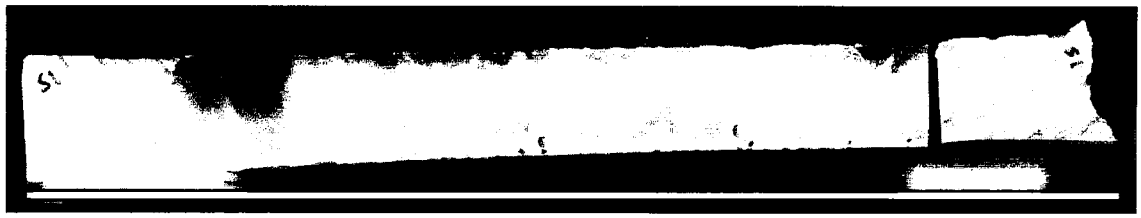

23.5 cm

Fig. 4.13. b) Centimeter-scale oxygen isotopic shifts in grid map sample GM1a(L). All analyses derive from drilled powders from slabs (photo). G= grey marble, B= bleached marble, W= wollastonite skarn; numbers indicate sample number (see Table 4.1).

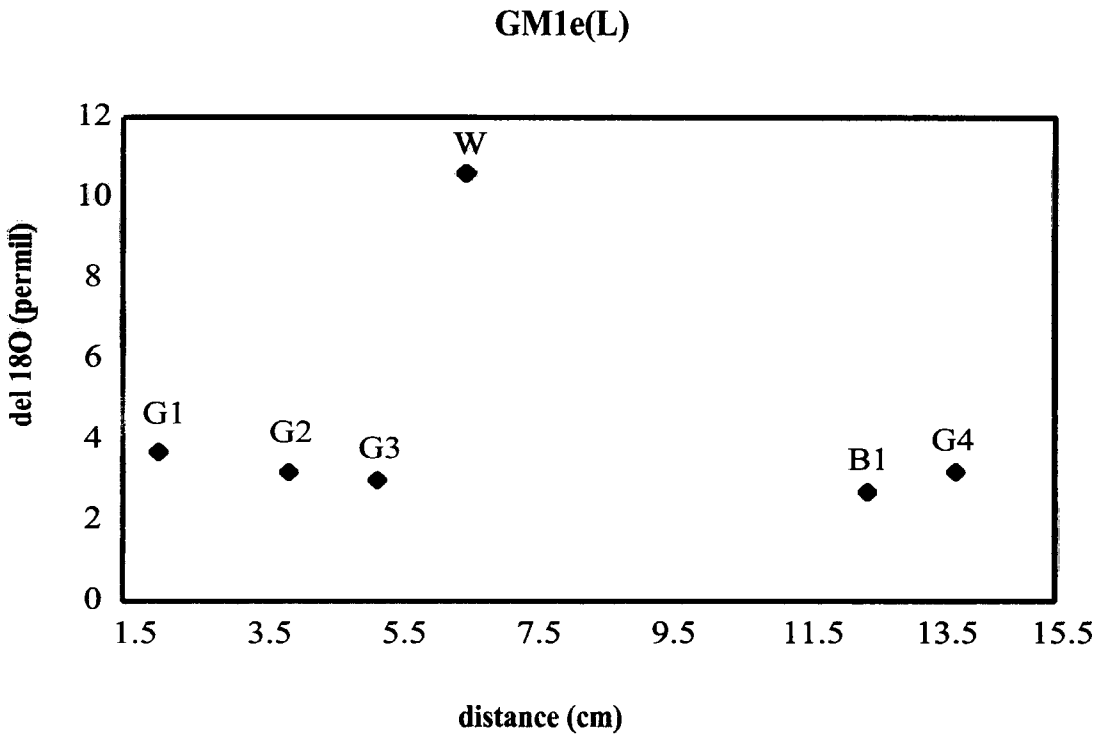


18 cm

Fig. 4.13. c) Centimeter-scale oxygen isotopic shifts in grid map sample GM1e(L). All analyses derive from drilled powders from slabs (photo). G= grey marble, B= bleached marble, W= wollastonite skarn; numbers indicate sample number (see Table 4.1).

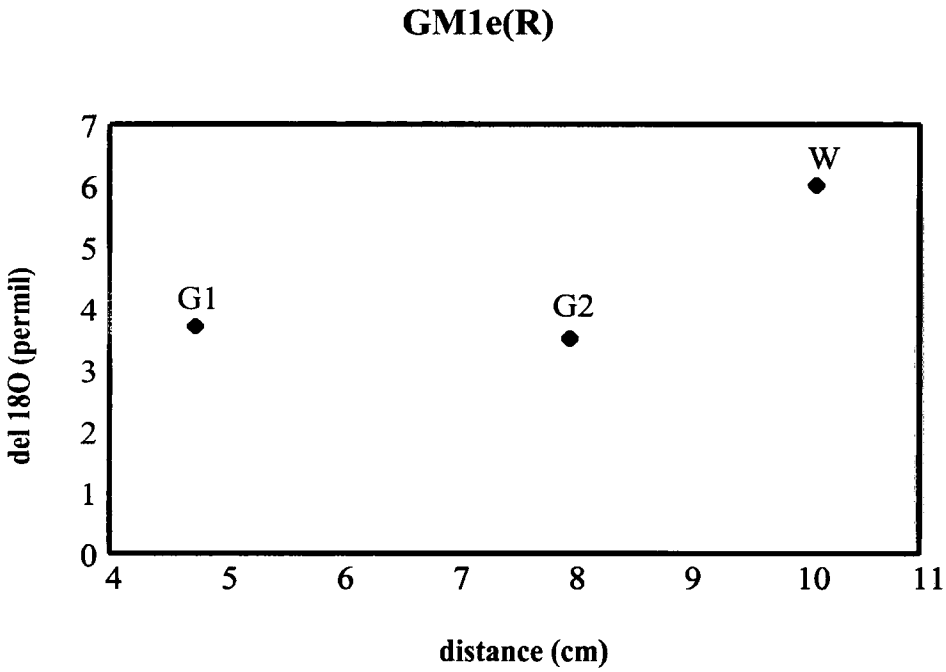


16.5 cm

Fig. 4.13. d) Centimeter-scale oxygen isotopic shifts in grid map sample GM1e(R). All analyses derive from drilled powders from slabs (photo). G= grey marble, B= bleached marble, W= wollastonite skarn; numbers indicate sample number (see Table 4.1).

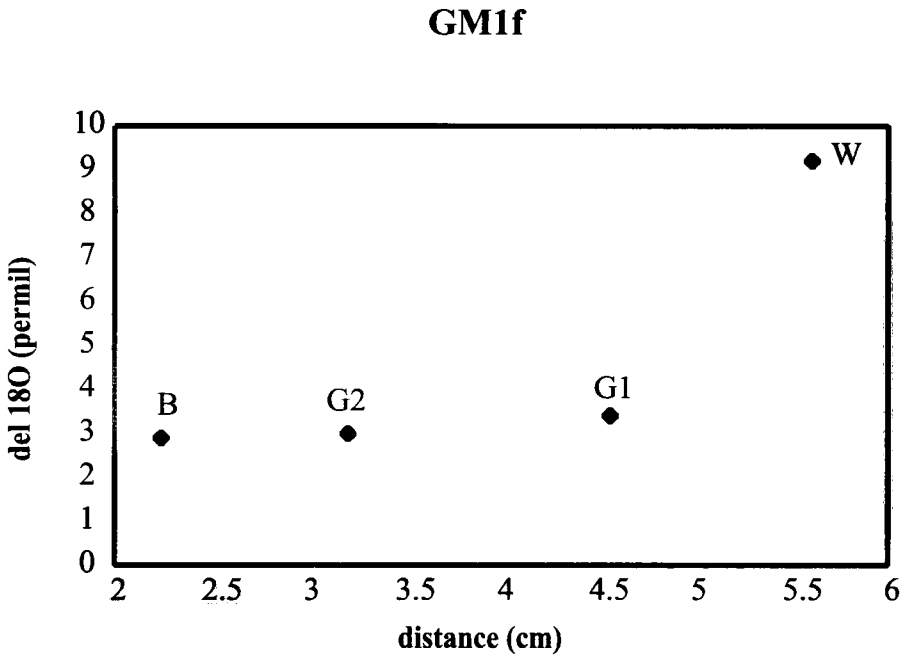


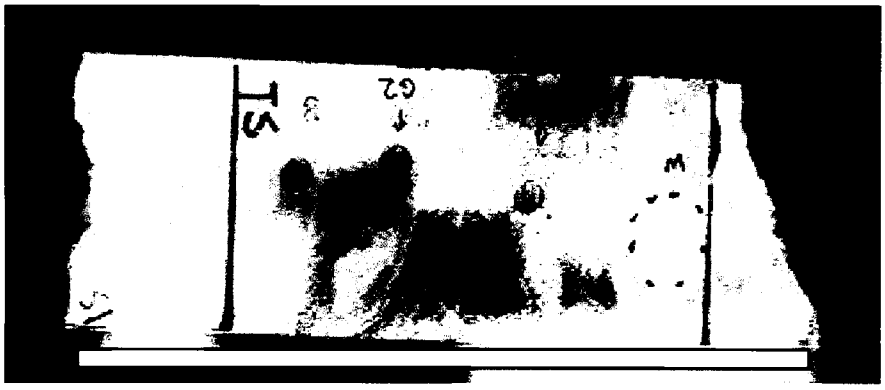

7.5 cm

Fig. 4.13. e) Centimeter-scale oxygen isotopic shifts in grid map sample GM1f. All analyses derive from drilled powders from slabs (photo). G= grey marble, B= bleached marble, W= wollastonite skarn; numbers indicate sample number (see Table 4.1).

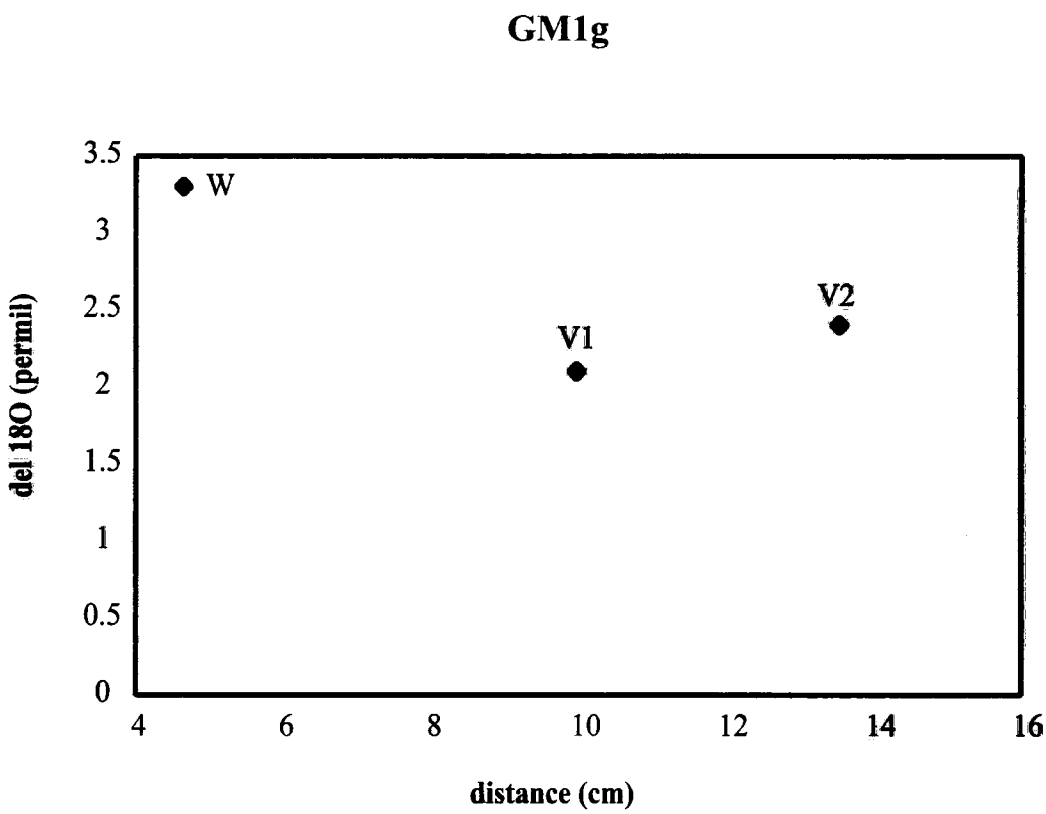


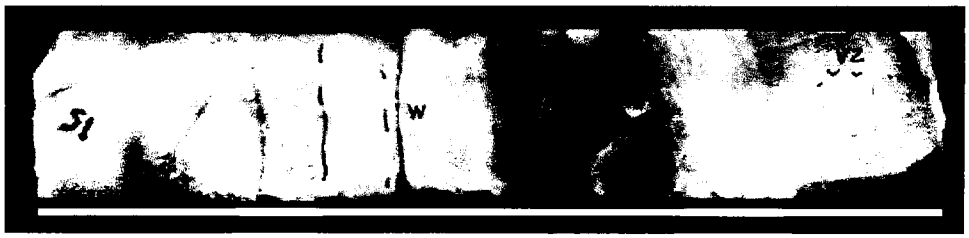


15.1 cm

Fig. 4.13. f) Centimeter-scale oxygen isotopic shifts in grid map sample GM1g. All analyses derive from drilled powders from slabs (photo). V= calcite vein, W= wollastonite skarn; numbers indicate sample number (see Table 4.1).

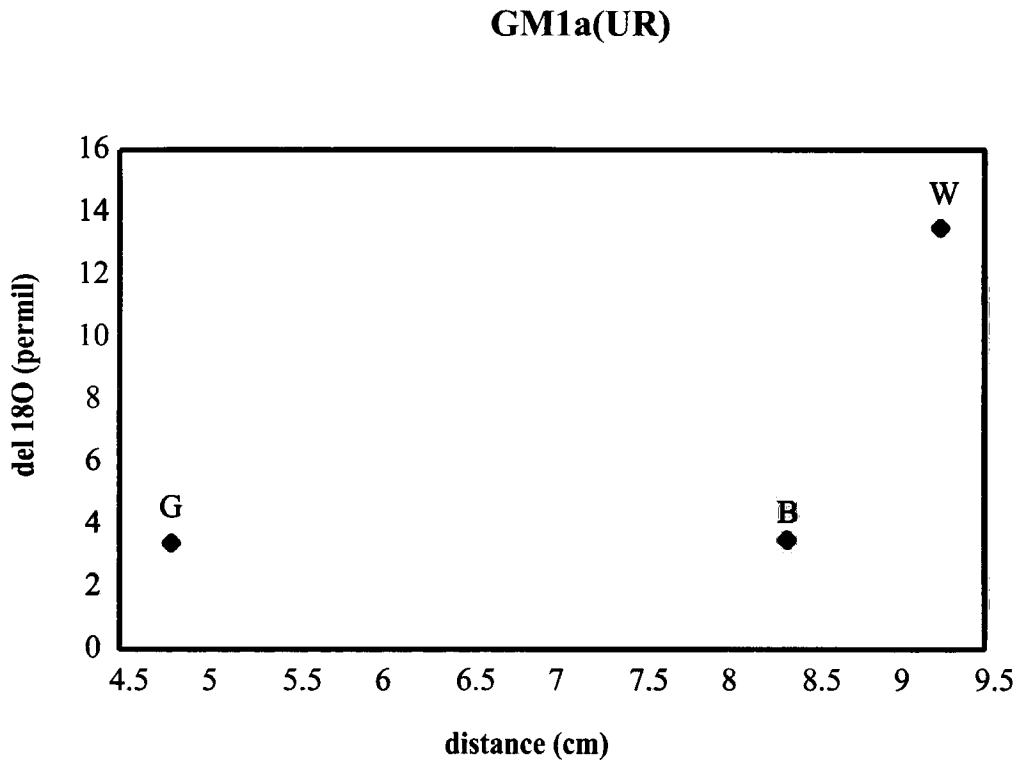


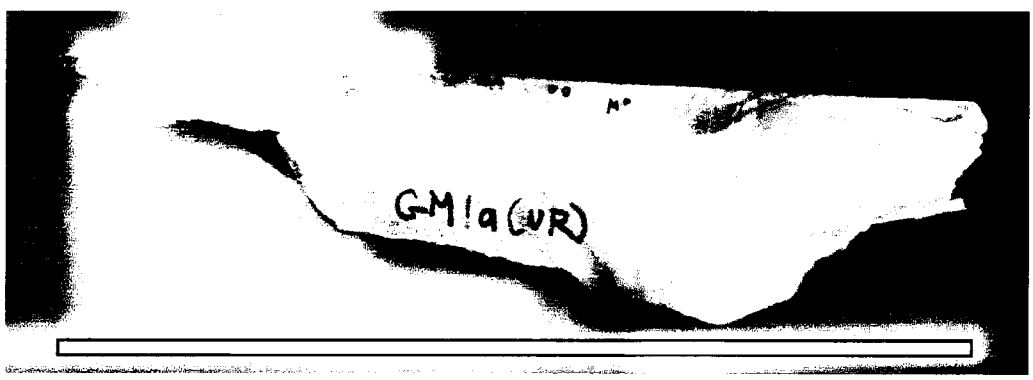


16 cm

Fig. 4.13. g) Centimeter-scale oxygen isotopic shifts in grid map sample GM1a(UR). All analyses derive from drilled powders from slabs (photo). G= grey marble, B= bleached marble, W= wollastonite skarn (see Table 4.1).

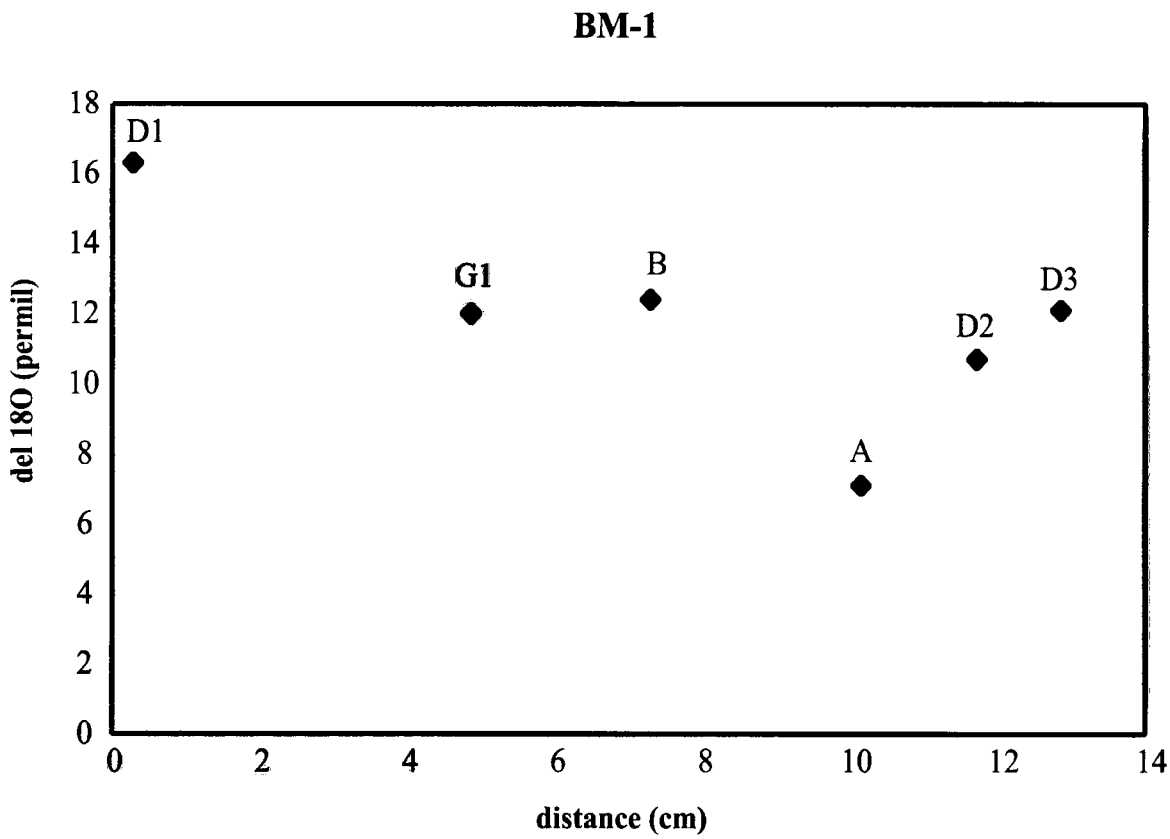


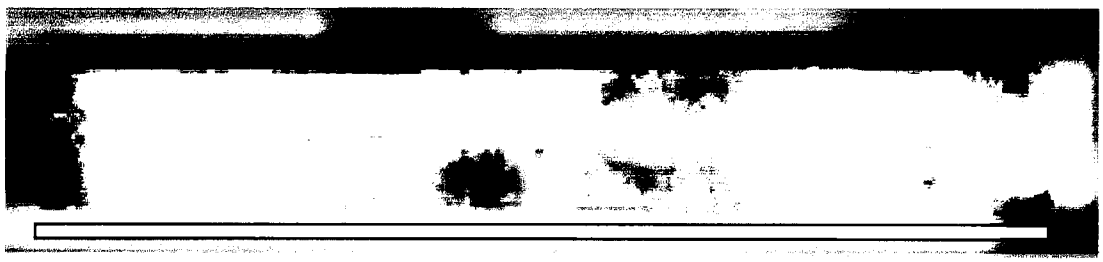

14.5 cm

Fig. 4.13. h) Centimeter-scale oxygen isotopic shifts in sample BM-1 from the Middle Bench. All analyses derive from drilled powders from slabs (photo). D= black marble, G= grey marble, B= bleached marble, A= clinozoisite augen; numbers indicate sample number (see Table 4.1).

equilibrated with magmatic volatiles. This is supported by the $\delta^{18}O$ value (7.1 permil) of a clinozoisite augen within sample BM-1. This composition is consistent with values of mafic igneous rocks, suggesting interaction with magmatic volatiles.

### 4.6 $\delta^{18}O$ variation of wollastonite skarn and marble

All analyzed samples have depleted $\delta^{18}O$ values relative to inferred protoliths (igneous and sedimentary), suggesting that all examined rocks in the study area exchanged $^{18}O$ with an isotopically light fluid. The shift toward lower carbon and oxygen isotopic values within the roof pendant at Mineral Hill can be the result of a number of different processes. Samples with isotopic compositions lower than the unmetamorphosed equivalents (i.e. marble to wollastonite skarn) are often considered to have been altered by fluid-rock interaction [*Valley*, 1986]. However, metamorphic reactions can occur that release volatiles ($H_2O$ and $CO_2$) as reaction products. These reactions (devolatilization) fractionate carbon and oxygen isotopes between the host rock and volatile phase, and, as a result, the $\delta^{13}C$ and $\delta^{18}O$ values of the host rock are lowered [*Rumble*, 1982; *Valley*, 1986]. Hence, fractionation due to devolatilization reactions could account for some of the observed isotopic depletion. Therefore, to evaluate the nature of the fluid infiltration, any samples whose isotopic shifts can solely be attributed to devolatilization reactions must be withdrawn [*Roselle et al.*, 1999].

The $\delta^{18}O$ values of wollastonite skarn decrease from 19.8 to as low as 3.3 permil, and the $\delta^{13}C$ values of the marbles fraction from 0.3 to –6.2 permil. Increases in temperature drive decarbonation reactions in calc-silicate rocks. The effects of devolatilization in relation to natural processes fall between two extremes; batch and Rayleigh devolatilization. *Valley* [1986] gives an excellent overview of the derivations for isotopic shifts for these end-members. Batch devolatilization implies a closed system in which fluid escapes in a single episode. However, in

reality, the large volume increase that accompanies volatilization requires a gradual escape of fluid. Therefore, batch processes set a minimum value for isotopic shifts due to devolatilization reactions. On the other hand, Rayleigh devolatilization implies an open system where a continuous release of fluid occurs in small increments.

Using the devolatilization reaction,

$$CaCO_3 + SiO_{2(qtz)} = CaSiO_3 + CO_2 \qquad \text{R3}$$

we can evaluate the largest possible devolatilization effects to produce wollastonite skarn. The mole fraction of oxygen remaining in the rock ($F_{(oxygen)}$) after all the fluid has left the system is dictated by the stoichiometry of this reaction. R3 has an $F_{(oxygen)}$-value of 0.6. For values of $F_{(oxygen)} \geq 0.6$ (known as the 'calc-silicate' limit) the amount of $^{18}O$ depletion by Rayleigh distillation is very similar to that of a batch process. Figure 1 in *Valley* [1986], illustrates the range of isotopic depletion due to decarbonation reactions. It shows that $\delta^{18}O$ depletion is restricted by the calc-silicate limit ($F_{(oxygen)} \geq 0.6$), and therefore, only small differences (at most 2 permil) are seen between Rayleigh and batch calculations.

Carbon isotopes are much more susceptible to change by devolatilization and $F_{(carbon)}$ can approach zero. Figure 7 in *Nabelek et al.* [1984] illustrates as $F \rightarrow 0$, isotopic shifts in $\delta^{13}C$-values for marble can be as large as 12 permil. Thus, large depletion in $^{13}C$ in carbonate rocks can occur as reaction reaches completion and nearly all carbon is converted to $CO_2$ [*Valley*, 1986].

As such, we contend that the change in $\delta^{13}C$ values in marble down to –6.2 permil can be attributed solely to decarbonation reactions. However, the amount of $CO_2$ released (in the extreme example given by R3) cannot produce $\delta^{18}O$ shifts of $> 3$ permil recorded in wollastonite skarn samples. Therefore, we reject total oxygen isotopic shifts as a function of devolatilization reactions.

Fractionation of $^{18}O$ between calcite and wollastonite dictates that they will have different $\delta^{18}O$ values at equilibrium. This equilibrium fractionation factor, $\Delta_{woll\text{-}cc}$, is temperature dependent and ranges from -5.0 permil at 400°C to -3.4 permil at 600°C [*Zheng,* 1993a], where $\Delta_{woll\text{-}cc} = \delta_{woll} - \delta_{cc}$.

Mineral Hill and Marble Hill wollastonite skarn tends to have greater $^{18}O$-content than spatially related marble resulting in values ranging from –2.6 to 14.8 permil for $\Delta_{woll\text{-}cc}$ (Fig. 4.8). Because $\Delta_{woll\text{-}cc}$ –values do not range between –5.0 and -3.4 permil [*Zheng*, 1993a], calcite and wollastonite could not have been in equilibrium at 400°C to 600°C at Mineral Hill.

To conclude, it is likely that $\delta^{18}O$ was lowered by infiltration and exchange of externally derived fluids out of equilibrium with the host rocks, however $\delta^{13}C$ isotopic shifts could have resulted from devolatilization reactions and/or the exchange with graphite or organic matter. Graphite is observed in grey marbles at Mineral Hill.

$\delta^{18}O$ values of marbles and silicates less than 5 permil indicate exchange with meteoric/and or seawater. Other $\delta^{18}O$ values of marbles and silicates between 19.8 and 8.0 permil suggest exchange with magmatic water.

## 4.7 Discussion

Although powders were taken from the freshest part of each sample, there were samples in which veining and alteration was so extensive within skarn that contamination is likely. All igneous samples show retrograde alteration. Moreover, depleted $^{18}O$ values (1.8 to 0.8 permil) in the latest diking event (D3) require interaction with a low $^{18}O$ fluid. Therefore, it is likely that igneous rocks were depleted after the first skarn formation event. Even though igneous rocks at Mineral Hill exchanged with a late isotopically light oxygen reservoir, these samples are not excluded from the suite as they hold evidence to the timing of this low $^{18}O$ fluid event. However,

their $\delta^{18}O$ values are not used to directly determine the nature of fluid flow during skarn formation.

Some highly veined skarn samples include TB13a (garnetite) and MB3b (clinopyroxene skarn). In other samples a moderate amount of veins were observed in thin section. Although most powders are relatively vein-free, some contamination is expected, especially for analyzed powders taken from whole rock. Moreover, petrographic examination of low $\delta^{18}O$ silicates (< 5 permil) indicates on average moderate alteration of peak mineral grains. In all of these samples, opaque minerals were observed, although not exclusive to samples with $\delta^{18}O < 5$ permil. Because retrograde alteration and veining is apparent in these low $\delta^{18}O$ units (garnetite, garnet-wollastonite skarn, and clinopyroxene skarn) they have been excluded in the interpretation of infiltration history involved in anhydrous skarn genesis at Mineral Hill.

Likewise, two wollastonite skarn samples yield $\delta^{18}O$ values less than 5 permil; GM1g-W and W1d(w), at 3.3 and 3.6 permil, respectively. These wollastonite skarns could have been altered to meteoric oxygen signatures by late meteoric infiltration, or could have formed from pre-existing low $\delta^{18}O$ marbles. Late alteration of GM1g-W is considered likely because of the alteration and proximity to large calcite veins. The low $\delta^{18}O$ content of W1d(w) may reflect the $^{18}O$ composition of skarn at high temperature, however, because it is only one of thirty-three skarn samples, this interpretation cannot be made with confidence. This thesis will focus on the majority of skarn samples which record $\delta^{18}O > 5$ permil.

## 4.8 Infiltration History

Because devolatilization reactions cannot account for the $\delta^{18}O$ isotopic shifts observed in wollastonite skarn and marble, the study area must have been infiltrated by externally derived fluids. As discussed above, all samples from Mineral Hill record exchange with an isotopically

light oxygen reservoir. The following section interprets the timing and source of fluid(s) responsible for the $\delta^{18}O$ alteration in context to skarn formation and igneous activity.

### 4.8.1 Magmatic fluid event

Spatially extensive high temperature wollastonite production is prevalent in Mineral Hill skarns. Wollastonite formed from a relatively pure marble requires a source for $SiO_2$-bearing, $H_2O$-rich fluids. Moreover, magmatic volatiles must have infiltrated the roof pendant as evidenced by some skarn in $^{18}O$ exchange equilibrium with the pluton. Because the roof pendant is essentially a xenolith or wedge of country rock preserved within the Crowston Lake Pluton, it is likely that the intrusion is the source of magmatic fluid. Therefore, the spatially extensive skarn formation event at Mineral Hill likely occurred in the Late Jurassic.

### 4.8.2 Meteoric fluid event(s)

Meteoric $^{18}O$ isotopic signatures ($\delta^{18}O < 5$permil) occur within every unit sampled at Mineral Hill (Fig. 4.14). Almost all $\delta^{18}O$ alteration to values < 5 permil can be attributed to moderate temperature alteration mineral assemblages. We have identified at least two temporally separate high to moderate temperature meteoric fluid events at Mineral Hill: a prograde and retrograde event(s), respectively. This section discusses each separately, including evidence for high temperature meteoric alteration and timing of these events.

***Prograde meteoric fluid event***

*Evidence from low $\delta^{18}O$ signatures in marble*

In order to deplete a marble or limestone with an initial $\delta^{18}O$ signature of ~20 permil to ~0 permil, exchange and equilibrium with a very low $^{18}O$ fluid (i.e. meteoric/seawater) at high

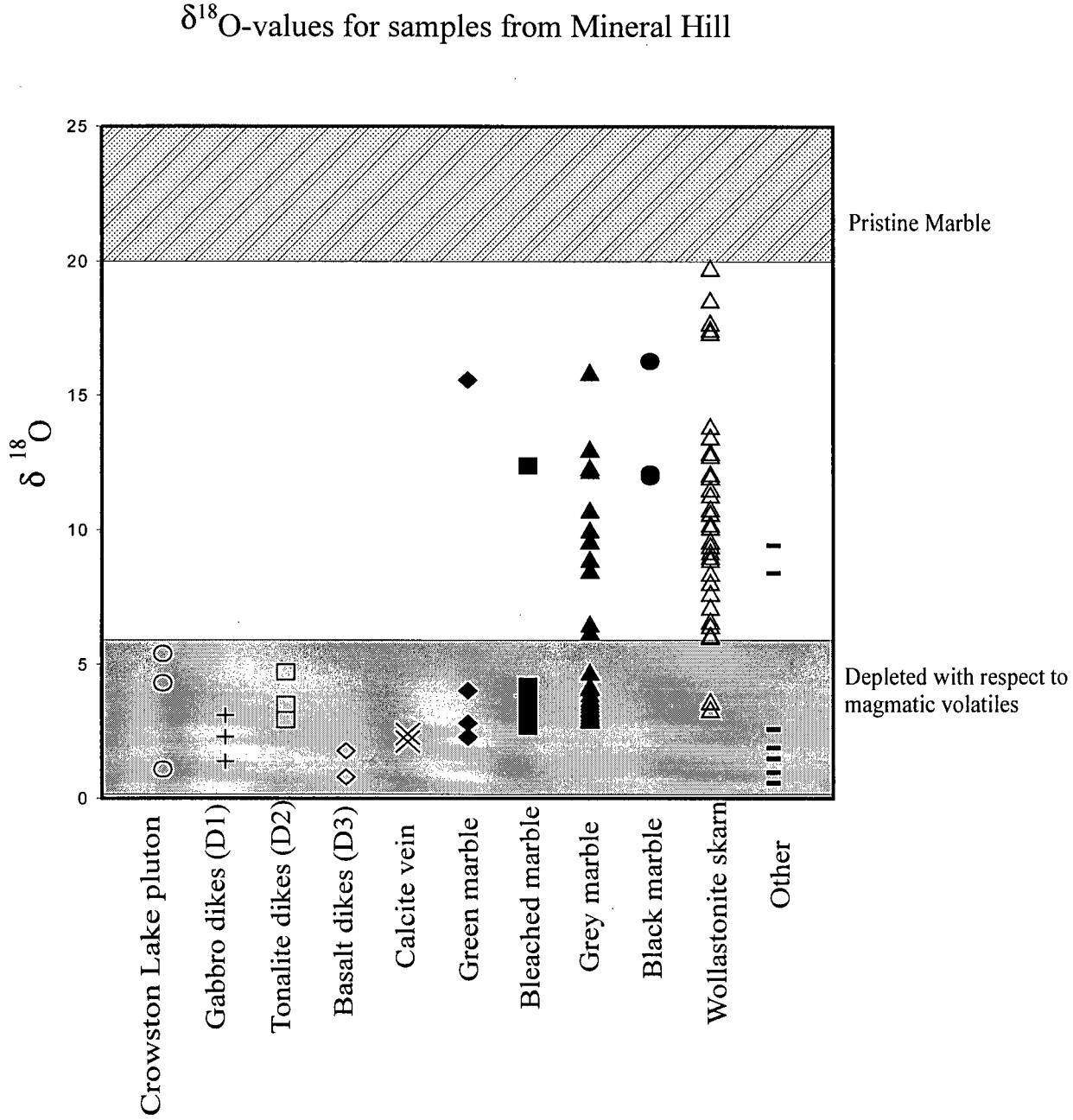


Fig. 4.14. $\delta^{18}O$ isotopic compositions for all samples collected at Mineral Hill. Grey hashed field represents $\delta^{18}O$ isotopic composition range for pristine marbles. Grey field represents samples depleted in oxygen isotopes with respect to magmatic fluids ($\delta^{18}O < \sim 6$ permil).

temperatures (~400°-500°C) must have occurred (Fig. 4.15). Marble is pervasively altered on a large scale (up to 10 meters; see section 4.9.3) to values as low as 2.3 to 5 permil. Alteration over this length scale reflects fluid advection. Therefore, the new composition (2.3 to 5 permil) emulates the composition of the fluid source, after correcting for equilibrium fractionation. Isotope fractionation is temperature dependent. Fig. 4.15 illustrates what combinations of fluid composition and temperature can produce a marble near 0 permil. A fluid source of < 0 permil is not included (even though meteoric water can be < than 0 permil) since there is no evidence in vein or alteration compositions that reflect negative $\delta^{18}O$ exchange equilibrium. As such, we conclude that high temperatures (> 400°C if fluid $\delta^{18}O$= 0 permil) must have accompanied the meteoric fluid that equilibrated with marble at Mineral Hill.

*Timing of hi-T meteoric fluid event*

It is interpreted that low $\delta^{18}O$ signatures in marble occurred due to reaction with meteoric fluid at high temperatures. However, the timing of this event must be evaluated. There are three possible scenarios for a high temperature event that would have allowed meteoric water to deplete marble to $\delta^{18}O$-values < 5 permil: (1) pre-pluton emplacement (Triassic to Mid-Jurassic), (2) syn-pluton emplacement (Late Jurassic), and (3) post-pluton emplacement (Cretaceous).

High temperature depletion of marbles could have occurred during the Triassic to Mid-Jurassic period. Although this possibly cannot be completely ruled out, it is unlikely since the depleted marbles have such a strong spatial association with the Crowston Lake Pluton. Moreover, there is no evidence regionally for Triassic- mid-Jurassic large scale intrusive events.

Therefore, marble depletion either occurred as a result of a syn-pluton, pre-skarn formation or post-pluton, post-skarn formation meteoric fluid event. A syn-pluton emplacement,

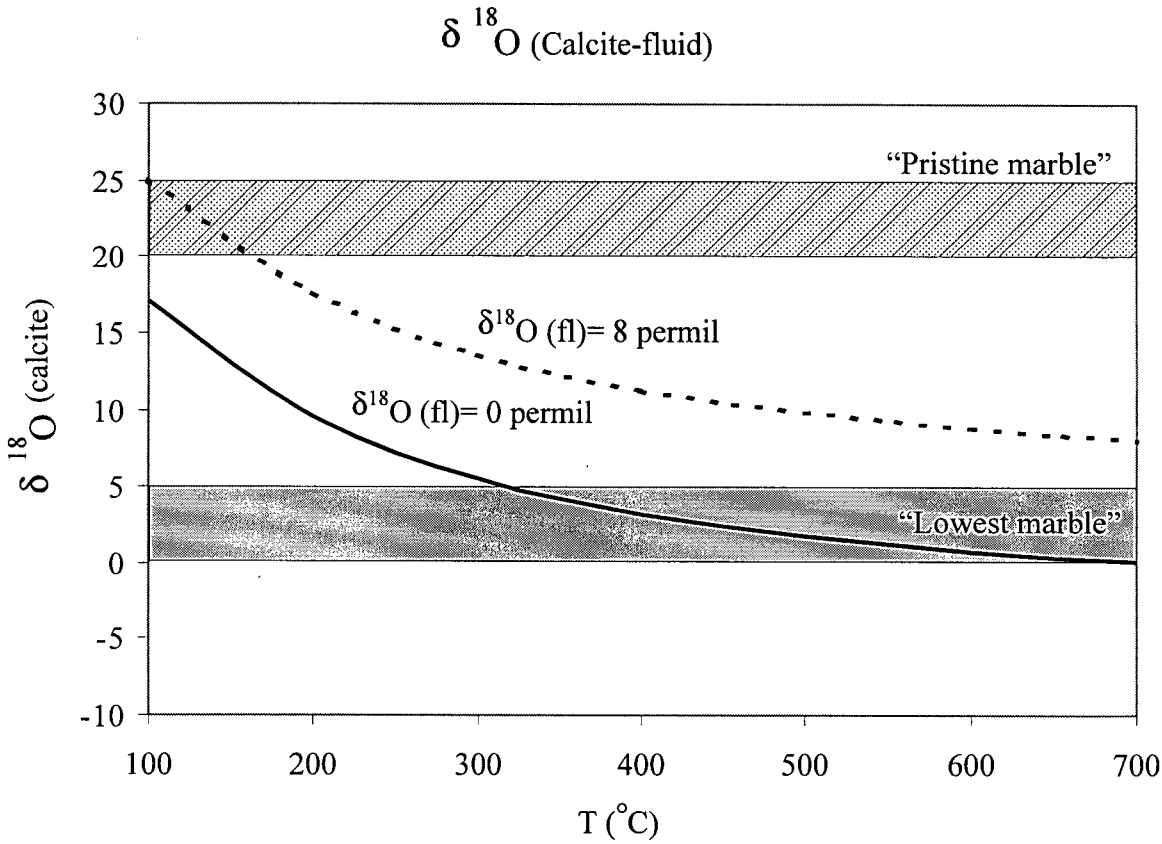


Fig. 4.15. $\delta^{18}O$ (cc-$H_2O$) versus temperature plot. Dashed line indicates path of marble $^{18}O$-depletion with increasing temperture that has been infiltrated by a fluid with a $\delta^{18}O$= 8 permil (magmatic). Solid line indicates path of marble $^{18}O$-depletion with increasing temperture that has been infiltrated by a fluid with a $\delta^{18}O$= 0 permil (conservative meteoric/seawater). Lines calculated by $\Delta^{18}O$ (cc-fl)= $A(10^6/T^2) + B$, A=2.78; B=-2.89 [*Friedman and O'Neill,* 1977]. Fields show values of "pristine marble" and the lowest marble values at Mineral Hill. Intersection of lowest marble values ($\delta^{18}O \sim 3$) and the meteoric fluid line at ~ 450 °C, indicates that lowest marble at Mineral Hill must have exchanged and equilibrated with meteoric fluids at high temperature.

pre-skarn formation depletion of marbles is supported by evidence and observations made within the study area at Mineral Hill. Spatially, low $\delta^{18}O$ values for marble are isolated near the Crowston Lake Pluton (i.e. Marble Hill); marble samples collected distal to the pluton have higher $\delta^{18}O$ values (i.e. Upper Marble Quarry and NE extension). It is possible that the contact between the pluton and the roof pendant could have been a conduit for meteoric water to depths typically unavailable to meteoric fluid. The proximity to the pluton would have provided the temperatures needed to deplete marble $\delta^{18}O$ isotope compositions. Moreover, the homogeneously low isotopic signatures of marble in areas of convex and concave interfingering of wollastonite skarn suggest that high temperature depletion was not post pluton and skarn formation. First, it is unlikely that late meteoric fluids would mimic the irregular, lobate wollastonite skarn/marble contact. Secondly, if the fluid was post-pluton, then concave areas along the wollastonite skarn/ marble boundary would have been sheltered from exchange with meteoric water (Fig. 4.16). However, at Mineral Hill, detailed cm-scale sampling along this highly irregular lobate boundary (see Figs. 4.13a-g) suggest that no areas of marble were sheltered from depletion, except those distal (i.e.Upper Marble Quarry and North-east Extension) to the Crowston Lake Pluton. Therefore, it is most likely that the high temperature $\delta^{18}O$ marble depletion was associated with Late Jurassic pluton emplacement and that skarn overprinted this low $^{18}O$ alteration event (Fig. 4.17). Furthermore, the porphyritic and fine-grained nature of dikes D2 and D3 indicate that the region was cool during subsequent igneous activity.

***Retrograde meteoric fluid event(s)***

*Evidence from low $\delta^{18}O$ signatures igneous and skarn units*

Petrographic observations from rock with low $^{18}O$-values (< 5.4 permil) suggest that the meteoric signatures in the Crowston Lake Pluton were attained during moderate temperature

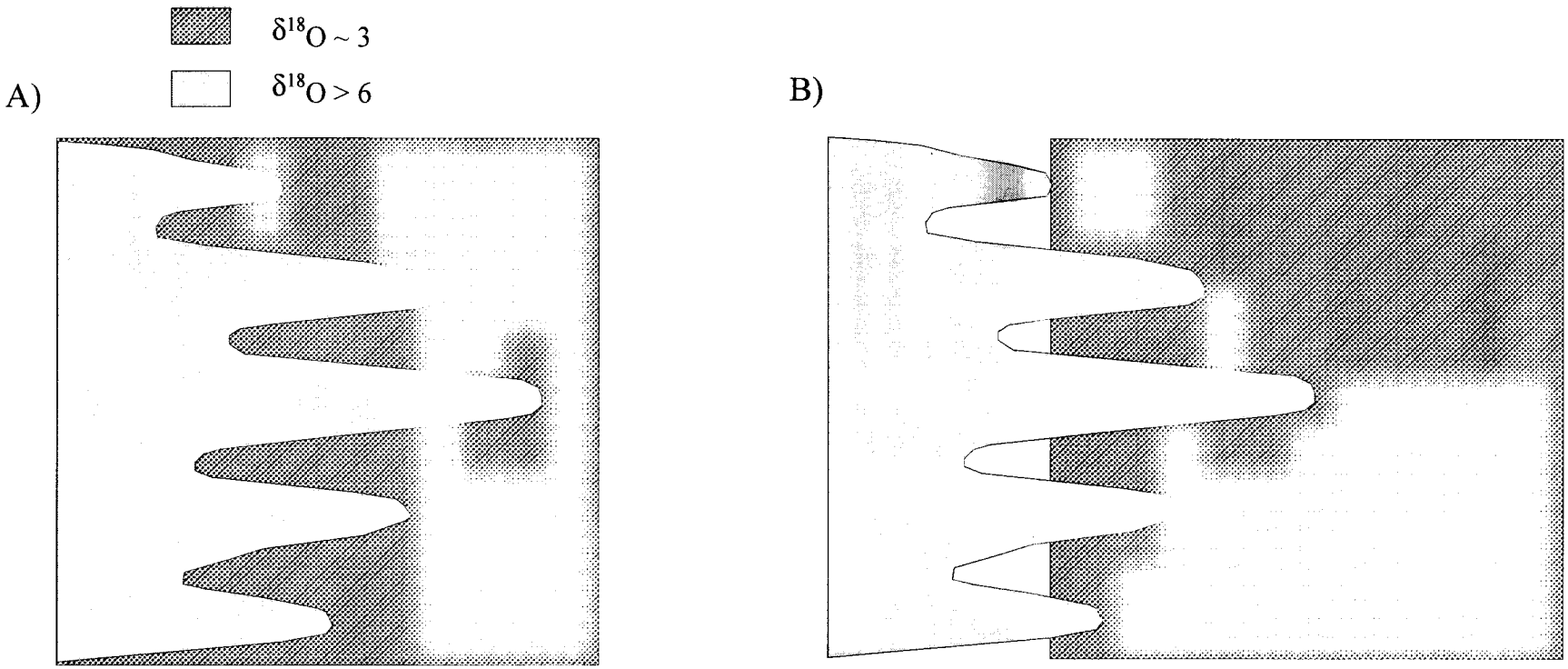


Fig. 4.16. Schematic showing spatial distribution of low $\delta^{18}O$ –values ($\delta^{18}O \sim 3$ permil) in marble in reference to a lobate front (wollastonite skarn with $\delta^{18}O > 6$ permil). $\delta^{18}O$ data and distance relationships are plotted in Fig. 4.15a-d. A) At Mineral Hill we see low $\delta^{18}O$ –values for marble samples in concave and convex areas outboard of the skarn front, indicating meteoric fluid infiltration prior to skarn formation. B) Illustration showing the distribution of low $\delta^{18}O$ –values for marble farther away from concave areas. This scenario indicates post-skarn formation infiltration of meteoric fluid, since concave areas along the skarn front would have sheltered marble from meteoric fluid exchange.

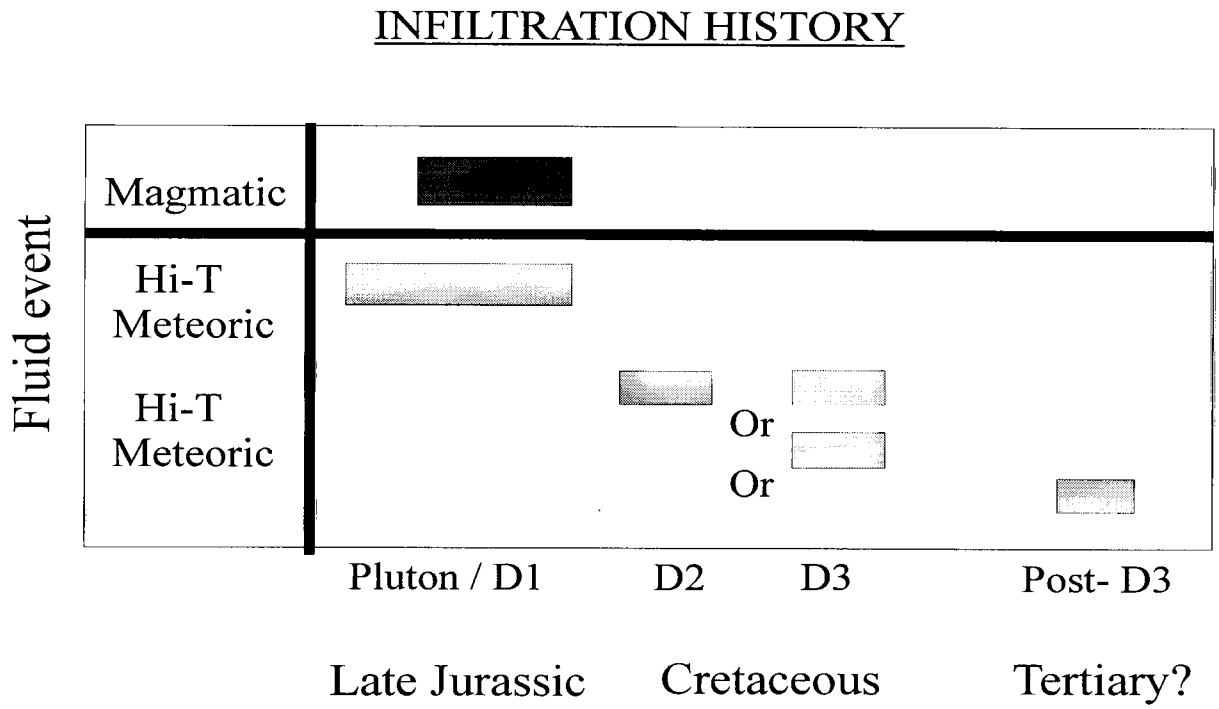


Fig. 4.17. Fluid History associated with igneous activity at Mineral Hill. 1). The emplacement of the Late Jurassic Crowston Lake Pluton resulted in contact metasomatism of a Triassic roof pendant producing garnet and wollastonite skarn zones by infiltration of magmatic fluid. 2) High temperature meteoric fluid associated with the pluton depletes marble $\delta^{18}O$-values to < 5 permil pre- to syn-skarn formation. A late high temperature meteoric event is supported by depleted isotopic signatures and retrograde alteration in all igneous units including Cretaceous-aged D2 and D3 dikes and sills. Three models for late infiltration of meteoric water: a) meteoric fluid response to each thermal event (D2 and D3) and/or b) meteoric fluid event during D3 emplacement which altered all previous igneous units and/or c)all meteoric fluid could be post-dike events (late) possibly during the Tertiary.

alteration (i.e. $^{18}O$ alteration associated with chlorite, hornblende alteration). Moreover, depleted values of $\delta^{18}O$ in the Cretaceous tonalitic (D2) and basaltic (D3) dikes of ~5.0 -0.8 permil indicate exchange with meteoric and/or seawater.

Most garnet-wollastonite skarn, garnetite, clinopyroxene skarn, and quartzite samples also have $^{18}O$-values < 3.1 permil. Petrographic observations suggest that these meteoric signatures were attained during moderate temperature alteration (i.e. chlorite and epidote alteration). It is concluded that this alteration event post-dated skarn formation (and pluton emplacement) because these retrograde minerals overprint skarn assemblages.

*Timing of retrograde meteoric fluid event(s)*

Several scenarios are possible for the timing of skarn and igneous $\delta^{18}O$ retrograde meteoric alteration at Mineral Hill (Fig. 4.17). Meteoric fluid infiltration and exchange during Late Jurassic, post skarn formation could have depleted skarn samples. However, because Cretaceous-aged D2 and D3 rocks are also depleted in $\delta^{18}O$, it could not have been an isolated retrograde meteoric fluid episode. Depletion of $\delta^{18}O$-values in D2 and D3 could have occurred as a meteoric fluid response to thermal perturbations in the Cretaceous. Reaction with this fluid event could have altered all igneous and skarn rocks. Furthermore, alteration could be due to a post-Cretaceous meteoric fluid event(s) (Tertiary?). Even though any or all of these scenarios are possible, it should be noted that because D3 is depleted in $\delta^{18}O$, and is the last intrusive event observed in the study area, a retrograde meteoric event had to occur either syn-D3 emplacement or by a post-D3 meteoric event. One retrograde meteoric fluid event could have depleted all igneous and skarn rocks, but is unlikely considering that meteoric fluid alteration seems prevalent in the history of the area (i.e. prograde and retrograde events).

## 4.9 Nature and evolution of syn-metamorphic permeability

### 4.9.1 Introduction

Igneous, meta-sedimentary and skarn units have $^{18}O$-values that indicate exchange and equilibrium not only with magmatic fluid (internal to the system), but also with a low $^{18}O$ fluid such as meteoric water (external to the system). Due to the proximity to the pluton, and preserved $\delta^{18}O$ signatures of wollastonite skarn, it is concluded that magmatic fluids were the main control for mineralogy, geochemistry and stable isotope geochemistry in skarn genesis at Mineral Hill.

This final section investigates the role of fluids during the most spatially extensive skarn-forming event by interpreting petrographic and isotopic constraints on the system. In particular, we focus our discussion on the flow geometry and distribution of multiple reaction fronts at the periphery of skarn formation (wollastonite/marble interface) at Mineral Hill.

### 4.9.2 Background

Mineral reaction may determine the pathways and rates of fluid flow by changing permeability and fluid pressure gradients during Darcian fluid flow. Permeability changes in the system result from volume change due to precipitation or dissolution of minerals. *Dipple and Gerdes* [1998] found that a decrease in permeability due to reaction closes the permeability networks in marble layers and focuses flow into regions of high permeability (Fig. 4.18a). Although the rate of skarn formation slows due to the lowered permeability of the entire system, these focused networks have the potential to serve as conduits for later ore-bearing fluids. On the other hand, an increase in permeability produces a small increase in the rate of formation since exhaust fluid must escape downstream through a permeable pathway [*Dipple and Gerdes*, 1998]. These fluid flow pathways can cause interfingering of wollastonite skarn and marble as seen at

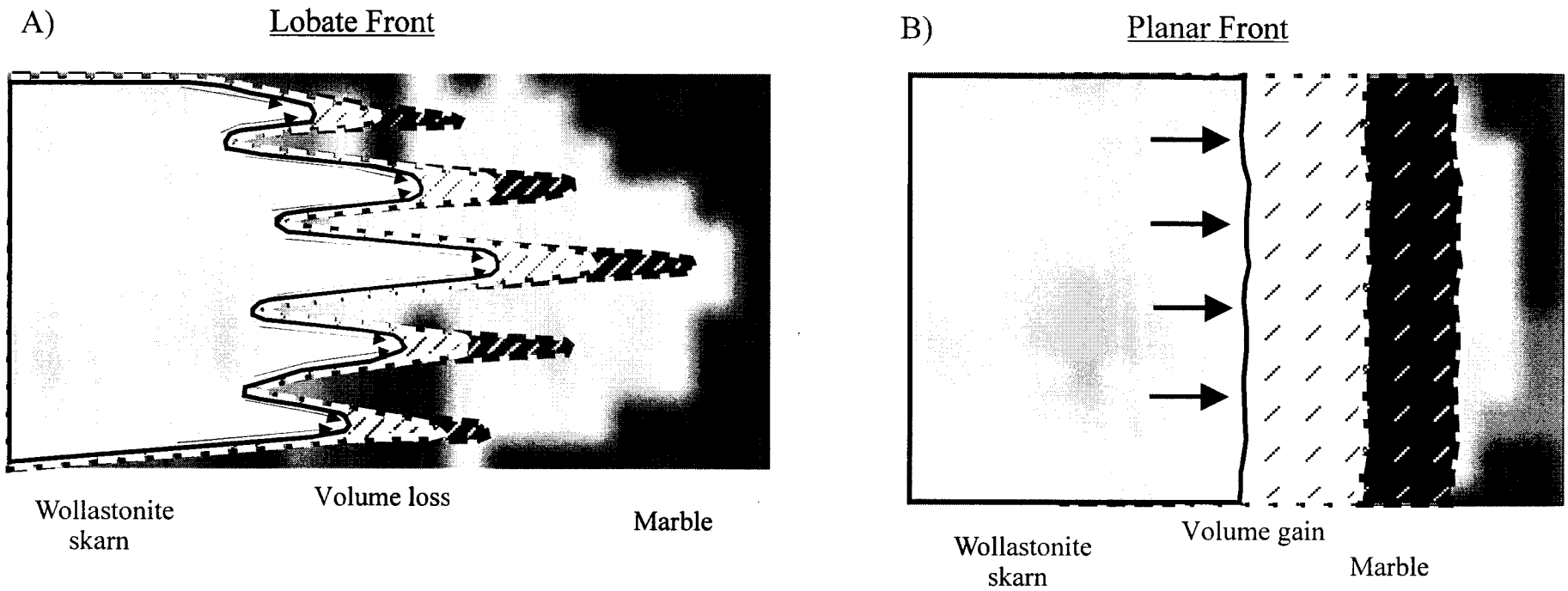


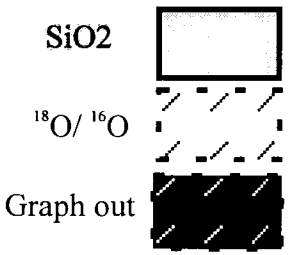


Fig 4.18. Schematic of lobate and planar reaction fronts. A) A volume loss creates porosity at the reaction front drives fluid (arrows) into focused areas of permeability. The wollastonite skarn/marble boundary acts as a transient aquifer. Skarn forms as fingerlike projections into marble. $SiO_2$ front extends only as far as wollastonite skarn forms; $^{18}O$- front graphite-out isograd are irregular and mimic $SiO_2$ front geometry. At sides, $^{18}O$- front and graphite-out isograd overlap $SiO_2$ front. At reaction front, $^{18}O$ signatures and graphite-out isograd extend into marble away from $SiO_2$ front due to faster propagation rate of reaction. At Mineral Hill, it is determined that the degraphitization front which defines the graphite-out isograd propagates at a faster rate than the $^{18}O$ –front. B) A volume gain will destroy porosity at the reaction front and will drive flow (arrows) into permeable areas and fluid will not be focused resulting in a planar front. $SiO_2$ front extends only as far as wollastonite skarn forms, however, $^{18}O$ signatures and the graphite-out isograd will uniformly extend into marble away from $SiO_2$ front.

Mineral Hill (discussed later). Thus, propagation rates of reaction, and permeability creation or destruction not only influence the size of the skarn, but can also be used to pattern the geometry of the fluid flow event.

### 4.9.3 Reaction Transport Theory: One-dimensional distribution of multiple reaction fronts

Because syn-metamorphic permeability is destroyed by compaction we use reaction-transport theory to deduce paleo-fluid flow. The propagation rate ($u$) of a reaction front (e.g. $SiO_2$, $^{18}O/^{16}O$) can be related to the time-integrated fluid flux (TIFF) and the distance the front has travelled:

$u = \Delta z / q_v$

where $q_v$ is the time-integrated Darcy flux and $\Delta z$ is the distance of reaction front propagation [*Korzhinskii*, 1970; *Dipple and Gerdes*, 1998]. As briefly discussed in Chapter 3, several studies have documented that different reactions will propagate at different rates [*Korzhinskii*, 1970; *Bickle and Baker*, 1990; *Dipple and Gerdes*, 1998]. This one-dimensional concept is illustrated in Fig. 3.22. Geochemical fronts such as Fe, Al, and $SiO_2$ start at the same interface (t=0), but through time spread apart. At Mineral Hill, partial control on skarn zonation is attributed to the distance the Fe, Al, Mg?, and $SiO_2$ reaction front has travelled and is reflected in map view with garnet skarn proximal to the pluton to distal wollastonite skarn in contact with marble (see Fig. 3.20). The contact between wollastonite skarn and marble marks the extent of aqueous silica infiltration.

This study uses multiple tracers (i.e. $SiO_2$, $^{18}O/^{16}O$ and degraphitization alteration) in order to image fluid flow geometry at the wollastonite skarn-marble interface. Fig. 4.18b illustrates a one-dimensional map view $SiO_2$, $^{18}O/^{16}O$ and degraphitization reaction fronts (t=n) at such an interface. Because the $SiO_2$ front propagates at a slower velocity, $^{18}O/^{16}O$ and degraphitization reaction fronts are distributed outboard of the wollastonite skarn-marble contact.

Moreover, each front occurs as a planar boundary since one-dimensional reaction-transport theory does not accommodate heterogeneous permeability distribution; fluid pervasively flows perpendicular across all alteration fronts (i.e. reaction front).

At Mineral Hill, the degraphitization front (denoted by the disappearance of graphite from bleached marble to grey marble) appears to travel at a faster rate than the $^{18}O/^{16}O$ front since the graphite-out isograd occurs a few centimeters outboard of the wollastonite skarn-marble contact (see Fig 4.18). This distance is attributed to diffusion mass transfer of fluids across the contact, however the small scale observation of the graphite-out isograd ahead of the $^{18}O/^{16}O$ front probably mimics the large scale scenario. The extent of the $SiO_2$ front and the graphite-out isograd is recorded by the spatial extent of wollastonite skarn and bleached marble, respectively. These alteration fronts are mappable in the field. Moreover, the $SiO_2$ front is noted as the distinct chemical change from ~4 wt percent $SiO_2$ in marble to ~50 wt % $SiO_2$ in wollastonite skarn.

In order to evaluate the extent of the $^{18}O/^{16}O$ front, the $\delta^{18}O$ values of wollastonite skarn and marble were plotted as a function of distance from the skarn/marble boundary on cm-scale (Fig. 4.13a-f) and m-scale (Fig. 4.19a-d). $\delta^{18}O$ values of marble and wollastonite skarn differ because magmatic volatiles (carrying aqueous silica) from a pluton react with marbles to create wollastonite skarn. Wollastonite forms at or near isotopic equilibrium with the fluid. In other skarn systems it has been noted that skarn adopts a magmatic $\delta^{18}O$ signature while marble retains it's primitive signature (20-30 permil) (Fig. 4.20b) [e.g. *Taylor and O'Neill*, 1977]. At Mineral Hill, some wollastonite skarn samples are at or near $^{18}O$ exchange equilibrium with magmatic volatiles. However, directly across the contact, marble $\delta^{18}O$ values are less than 5 permil, up to ~10 m outboard the wollastonite skarn/marble boundary, suggesting $^{18}O$ exchange equilibrium with meteoric/ seawater (Fig. 4.19b). Therefore, the $\delta^{18}O$ alteration front is spatially coincident

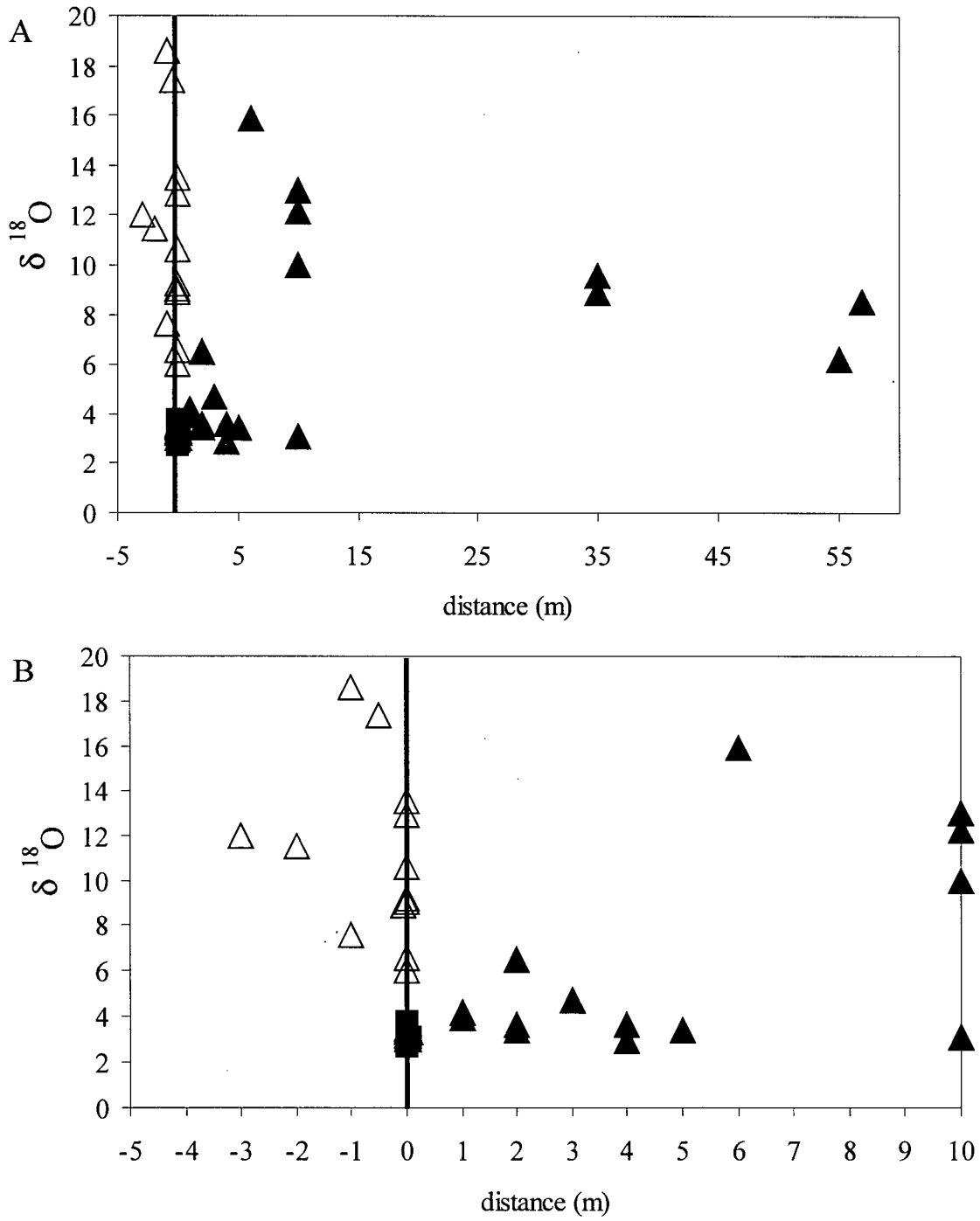


Fig. 4.19. A) $\delta^{18}O$ vs. distance plot. Distance= 0 at the wollastonite skarn/marble boundary. Range includes all samples in the study area (wollastonite skarn-open triangles, bleached marble-squares, grey marble-closed triangles). B) same plot as A) with range of 10 meters outboard wollastonite skarn/marble boundary.

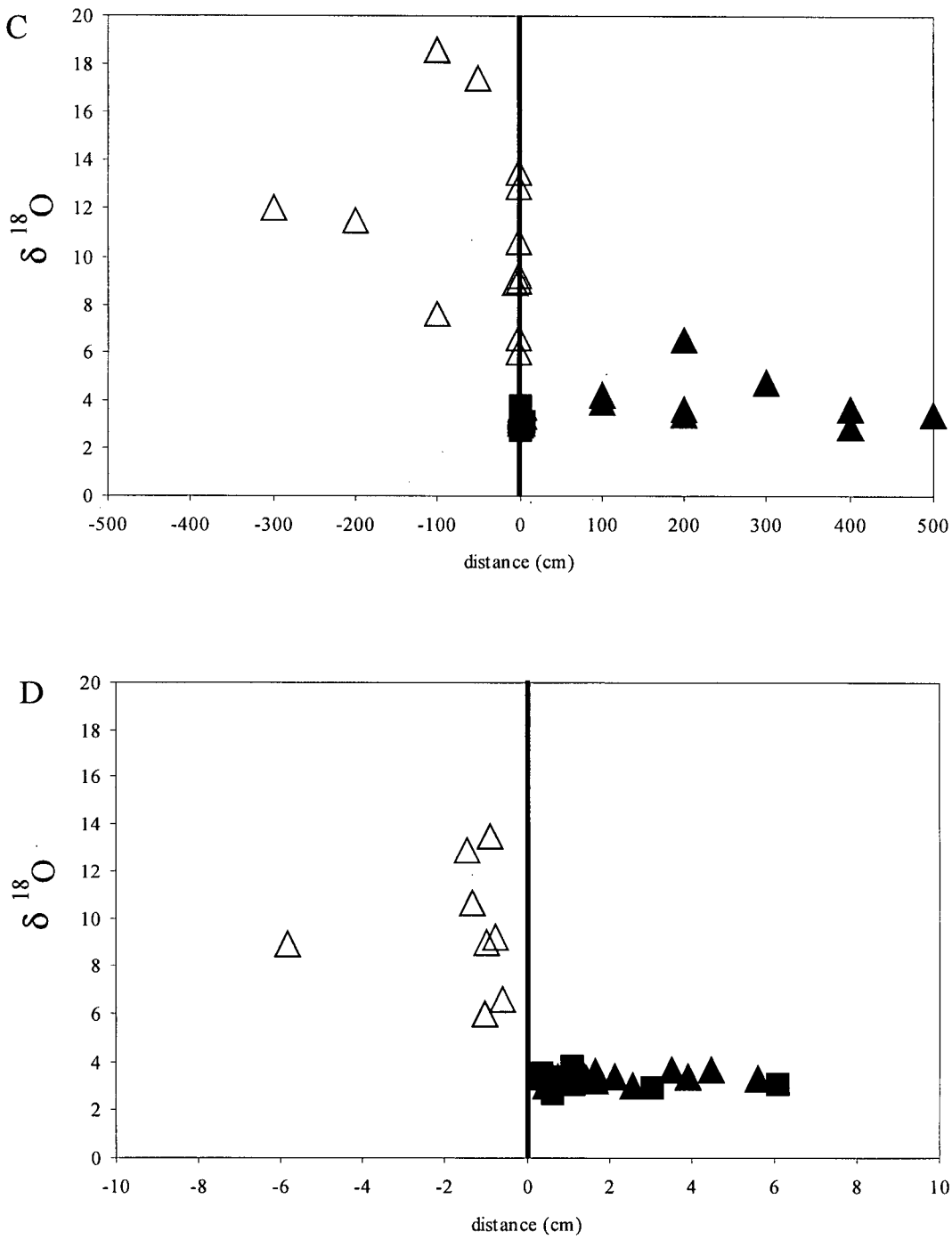


Fig. 4.19. C) $\delta^{18}O$ vs. distance plot. Distance= 0 at the wollastonite skarn/marble boundary. Range includes all samples 500 centimeters outboard of the wollastonite skarn/marble boundary (wollastonite skarn-open triangles, bleached marble-squares, grey marble-closed triangles). D) same plot as C) with range of 10 centimeters outboard wollastonite skarn/marble boundary. Note sharp isotopic variation of wollastonite skarn and marble.

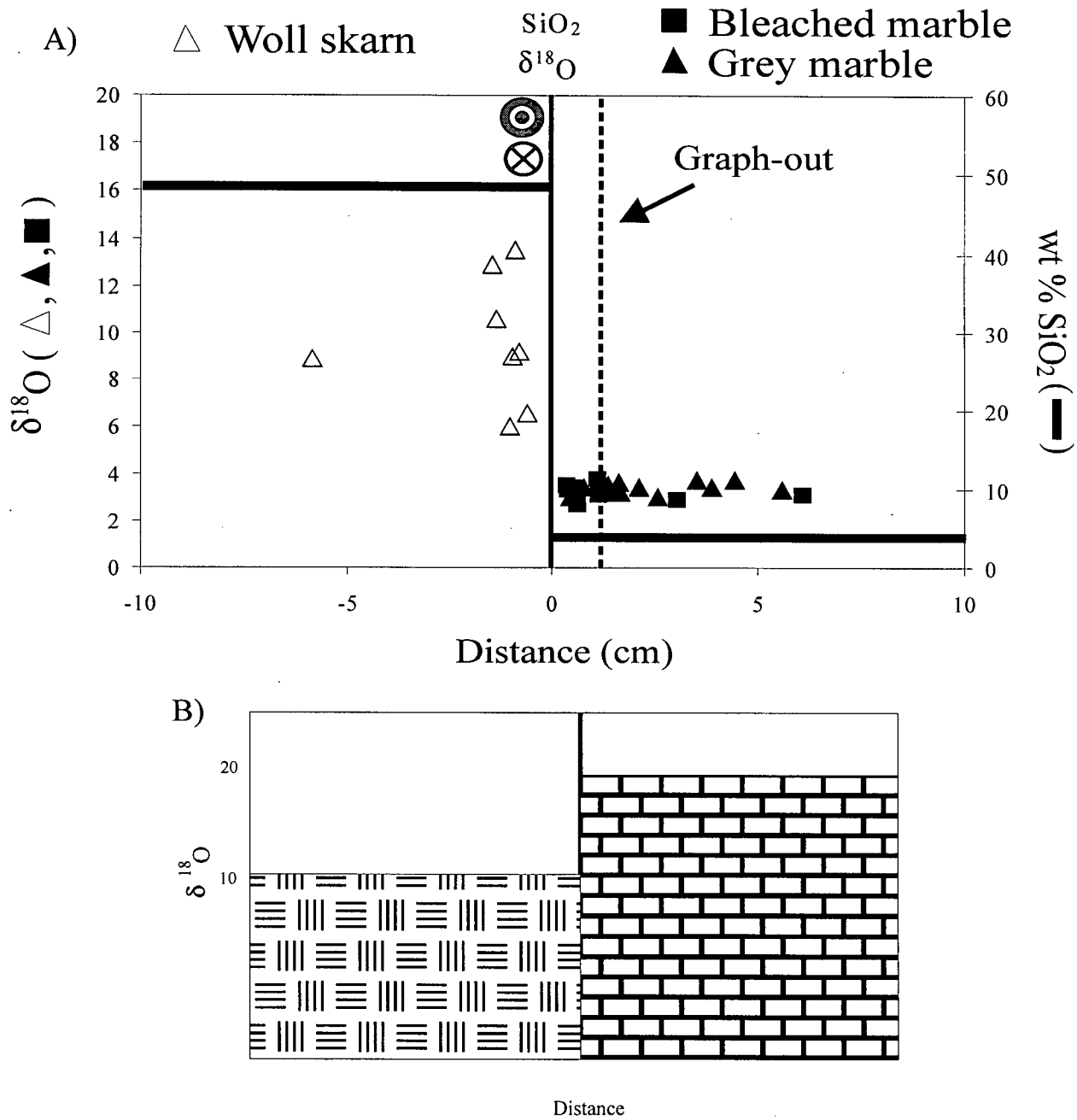


Fig. 4.20. A) $\delta^{18}O$ vs. distance plot with range of 10 centimeters outboard and inboard of the wollastonite skarn/marble boundary denoted by the increase in $SiO_2$ from ~4 wt % in marble to ~50 wt % in wollastonite skarn. A sharp isotopic shift from wollastonite skarn in 18O exchange equilibrium with magmatic volatiles to marbles depleted to $\delta^{18}O$ values < 5 permil, indicate the $^{18}O/^{16}O$ front overlaps the $SiO_2$ front. The graphite-out isograd, the extent of bleached marble outboard wollastonite skarn, generally does not exceed a few centimeters. This distance can be accommodated for by diffusional mass transfer across the skarn front. The spatial stacking of multiple tracers indicates that flow is parallel to the wollastonite skarn/marble boundary (reaction/infiltration side). B) Schematic of typical oxygen isotopic shifts between wollastonite skarn and marble due to infiltration of magmatic fluids. Wollastonite skarn adopts a magmatic oxygen isotopic signature (~10 permil) while marble more or less maintains it's primitive signature (20-25 permil), minus depletion due to devolatilization reactions.

with the $SiO_2$ front. Plots of $\delta^{13}C$ versus distance from the wollastonite skarn/ marble interface show no systematic variation in values (Fig. 4.21a,b).

The graphite-out isograd was determined by the distance bleached marble extends outboard wollastonite skarn. Generally, bleached marble does not occur more than a few centimeters past the interface; a distance easily accommodated by diffusion or bi-metasomatism across this boundary.

This spatial stacking of multiple tracers is not consistent with one-dimensional reaction transport theory in which tracers should be spread apart due to perpendicular flow across the reaction front. Instead, stacking of tracers suggests flow parallel to alteration fronts, known as reaction or infiltration sides [*Dipple and Gerdes*, 1998]. Moreover, based on a molar TIFF on the order of $10^5$ moles/cm$^2$ (see section 3.7.3), the $^{18}O/^{16}O$ front should have moved approximately 12 kilometers [cf. *Dipple and Ferry*, 1992]. Samples record $^{18}O/^{16}O$ alteration no farther than the $SiO_2$ front (~65m). This is consistent with the interpretation of reaction sides documented in samples along the wollastonite skarn-marble interface. However, it is important to note that this analysis is predicated on the assumption that marble ($\delta^{18}O$) was altered by meteoric fluids prior to skarn formation. This assumption is justified in section 4.8.2. An alternative explanation for the variations in $\delta^{18}O$ in the vicinity of the marble-skarn interface is that marble was depleted through interaction with meteoric fluids after wollastonite skarn formation. In this scenario, the isotopic alteration of marble during skarn formation was obliterated by subsequent infiltration of meteoric water. Even in this instance, the interpretation that the sampled marble-skarn contacts are infiltration sides is still supported by the limited development of bleached marble.

Furthermore, one-dimensional reaction transport theory cannot account for the observed wollastonite skarn-marble contact geometry. Detailed mapping at Mineral Hill reveals that the

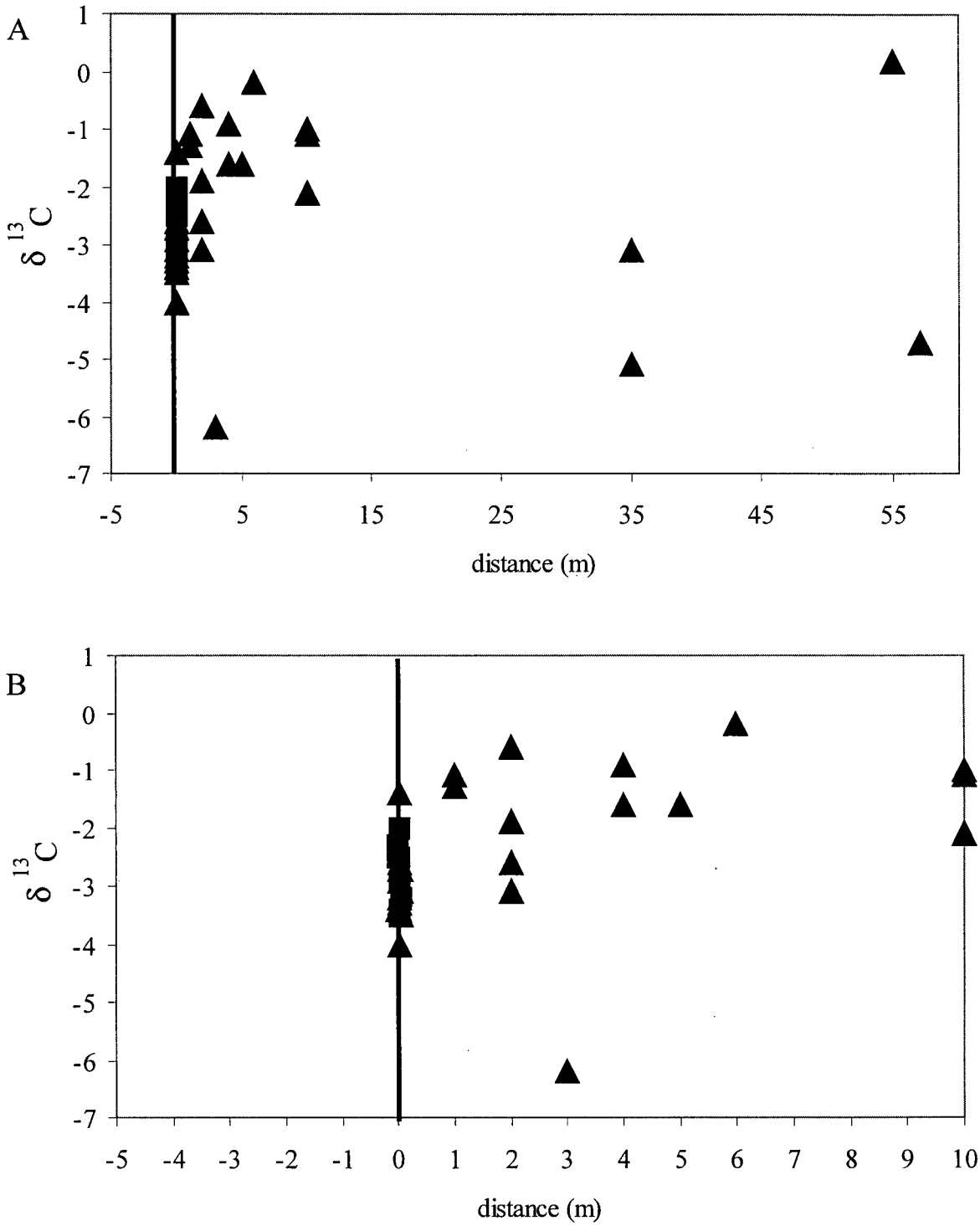


Fig. 4.21. A) $\delta^{13}C$ vs. distance plot. Distance = 0 at the wollastonite skarn/marble boundary. Range includes all marble samples in the study area (bleached marble- squares, grey marble-triangles). B) Same plot as A) with range of 10 meters outboard of wollastonite skarn/marble boundary.

lithologic contact between wollastonite skarn and marble (i.e. $SiO_2$ front) is not planar, but highly irregular and fingered (Fig. 1.9).

### 4.9.4 Reaction-infiltration instabilities at the skarn front: Implications on flow geometry

The morphology of the reaction front (e.g. planar versus lobate fronts) is controlled by the initial permeability structure of the country rocks, reaction infiltration feedbacks and mechanical processes such as compaction [*Balashov and Yardley*, 1998; *Dipple and Gerdes*, 1998]. In fact, it is essential that the host rocks be chemically reactive and permeable for skarn to be produced.

The extent of the $^{18}O$ front is observed to overlap the $SiO_2$ front (Fig. 4.20a). If the timing of the meteoric exchange and equilibrium with marble is pre-skarn formation (see section 4.8.2), most of the wollastonite skarn/marble boundary samples represent an infiltration or reaction side and not a front. Therefore, dominant flow (advection) is parallel to the wollastonite skarn/marble interface probably with diffusional exchange occurring across this boundary. The isotopic evidence of mostly reaction sides supports a lobate morphology since a planar front would result in mostly reaction fronts.

The bleached marble represents a graphite out isograd and occurs by a reaction such as:

$2C + 2H_2O = CH_4 + CO_2$ [from *Todd*, 1990]

Since this zone only occurs within centimeters between wollastonite skarn and grey marble, the degraphitization can be attributed to diffusive mass transfer of an $H_2O$- rich fluid along an infiltration side [*Todd*, 1990]. If the bleached zone was extensive (100's of meters to kilometers) then we would be located along an exhaust pipe of a infiltration front or in a geometrically planar front (Fig. 4.18). Some examples of extensive bleached marble zones outboard of skarn are Magistral, Peru [*Floyd,* 2001], Antamina, Peru [*O'Connor*, 2001] and Texada Island, B.C [W*ebster and Ray*, 1990.]

In addition, petrological evidence shows that the reaction creating wollastonite skarn from marble (R1) resulted in a volume loss of ~20 percent. It has been documented that volume losses at the reaction boundary focuses flow such that the geometry of the boundary becomes lobate [*Dipple and Gerdes*, 1998]. On the other hand, a volume gain (destruction of permeability networks) would divert flow from the reaction site and result in a geometrically planar front [*Dipple and Gerdes*, 1998].

## 4.10 Conclusions

The emplacement of the Late Jurassic Crowston Lake Pluton drove a convection cell of meteoric fluid into Triassic sediments (preserved as a roof pendant). This early high temperature meteoric fluid event is preserved in low $\delta^{18}O$ marbles that are spatially coincident with the pluton contact. Farther from the pluton contact, the marbles are depleted to magmatic signatures (~15 to 9 permil).

Magma in the pluton reached volatile saturation and exsolved magmatic fluids into the roof pendant resulting in contact metasomatism producing the first spatially extensive garnet and wollastonite skarns. The lobate or interfingering geometry of the reaction front at the wollastonite skarn/marble interface at Mineral Hill is deduced from 2m by 2m grid mapping, cm-scale bleached marble zone, calculation of volume loss, and stacking of geochemical and isotopic fronts. Planar fronts are limited by how permeable the host rock is prior to infiltration. However, at Mineral Hill, we conclude that reaction drove infiltration and resulted in volume loss and local increase in permeability (reaction-infiltration instabilities) focusing fluid along the wollastonite/marble boundary toward and out through exhaust pipes at the reaction front (unsampled). Reaction enhanced permeability has several implications for skarn formation. Positive reaction-infiltration feedback provides a two-dimensional picture of a transient aquifer. If skarn reaction creates porosity, a small increase in rate of formation occurs which, in turn, can

influence the size of the skarn deposit. Moreover, because flow focusing creates conduits for late fluid, it is possible that ore mineralization may be concentrated in these areas [*Dipple and Gerdes*, 1998].

**References**

Ague, J.J., 1994, Mass Transfer during Barrovian Metamorphism of Pelites, South-Central Connecticut. II: Channelized Fluid Flow and the Growth of Staurolite and Kyanite: *American Journal of Science*, vol. 294, pp. 1061-1134.

Balashov, V.N, and Yardley, B.W.D., 1998, Modeling metamorphic fluid flow with reaction-permeability feedbacks and at a range of effective stresses: *American Journal of Science*, vol. 298 pp. 441-470.

Barrell, J., 1902, Physical effects of contact metamorphism: *American Journal of Science*, 4th Series, vol. 13, pp. 279-296.

Barton, M.D., Ilchik, R.P., and Marikos, M.A., 1991, Metasomatism. In: Kerrick, D.M., ed., *Contact Metamorphism*, Reviews in Mineralogy, vol. 26, pp. 321-350.

Bau, M., 1991, Rare-earth element mobility during hydrothermal and metamorphic fluid-rock interaction and the significance of the oxidation state of europium: *Chemical Geology*, vol. 93, pp. 219-230.

Baumgartner, L.P. and Olsen, S.N., 1995, A Least-Squares Approach to Mass Transport Calculations Using the Isocon Method: *Economic Geology*, vol. 90, pp. 1261-1270.

Beaty, D.W., and Taylor, H.P., 1982, Some petrologic and oxygen isotopic relationships in the Amulet Mine, Noranda, Quebec, and their bearing on the origin of Archaean massive sulfide deposits: *Economic Geology*, vol. 77, pp. 95-108.

Bickle, M.J., and Baker, J., 1990, Migration of reaction and isotopic fronts in infiltration zone: assessments of fluid flux in metamorphic terrains: *Earth and Planetary Science Letters*, vol. 98, pp. 1-13.

Bickle, M.J., Chapman, H.J., Ferry, J.M, Rumble, D., and Fallick, A.E., 1997, Fluid Flow and Diffusion in the Waterville Limestone, South-Central Maine: Constraints from Strontium, Oxygen and Carbon Isotope Profiles: *Journal of Petrology*, vol. 38, no. 11, pp.1489-1512.

Boulvais, P., Fourcade, S., Moine, B., Gruau, G., and Cuney, M., 2000, Rare-earth elements distribution in granulite-facies marbles: a witness of fluid-rock interaction: *Lithos*, vol. 53, pp.117-126.

Bowman, J.R., O'Neil, J.R, and Essene, E.J., 1985, Contact skarn formation at Elkhorn, Montana. II. Origin and evolution of C-O-H fluids: *American Journal of Science*, vol. 285, pp. 621-660.

Brownlow, A.H., 1996, *Geochemistry*. 2nd Edition, Prentice Hall, 580 pages.

Bucher, K., and Frey, M., 1994, *Petrogenesis of Metamorphic Rocks*, Springer-Verlag, 318 pages.

Clayton, R.N., and Mayeda, T.K., 1963, The use of bromine pentafluoride in the extraction of oxygen from oxides and silicates for isotopic analysis: *Geochimica et Cosmochimica Acta*, vol. 27, pp. 43-52.

Criss, R.E., Champion, D.E., and McIntyre, D.H., 1985, Oxygen isotope, aeromagnetic and gravity anomalies associated with hydrothermally altered zones in the Yankee Fork Mining District, Custer County, Idaho: *Economic Geology*, vol. 80, pp.1277-1296.

Criss, R.E., Fleck, R.J, and Taylor, H.P., 1991, Tertiary meteoric hydrothermal systems and their relation to ore deposition, Northwestern United States and Southern British Columbia: *Journal of Geophysical Research*, vol. 96, pp.13335-13356.

Cui,Y., and Russell, J.K., 1995, Nd-Sr-Pb isotopic studies of the southern Coast Plutonic Complex, southwestern British Columbia: *GSA Bulletin*, vol. 107, no. 2, pp. 127-138.

Dallmeyer, R.D., and Van Breeman, O., 1981, Rb-Sr whole rock and $^{40}K/^{39}Ar$ mineral ages of the Togus and Hallowell quartz monzonite and Three Mile Pond granodiorite plutons, south-central Maine: their bearing on post-Acadian cooling history: *Contributions to Mineralogy and Petrology*, vol. 78, pp. 61-73.

Debon, F., and Le Fort, P., 1982, A chemical-mineralogical classification of common plutonic rocks and associations: *Transactions of the Royal Society of Edinburgh*: Earth Sciences, vol. 73, no. 3, pp.135-149.

Dipple, G.M. and Ferry, J.M., 1992, Fluid flow and stable isotopic alteration in rocks at elevated temperatures with applications to metamorphism. *Geochimica et Cosmochimica Acta*, vol. 56, pp. 3539-3550.

Dipple, G.M. and Ferry, J.M., 1992, Metasomatism and fluid flow in ductile fault zones, *Contributions to Mineralogy and Petrology*, vol.112, pp.149-164.

Dipple, G.M. and Gerdes, M.L., 1998, Reaction-Infiltration Feedback and Hydrodynamics at the Skarn Front. In: Lentz, D.R., ed., *Mineralized Intrusion-Related Skarn Systems*, mineralogical Association of Canada Short Course Series, vol. 26, pp. 71-97.

Ditson, C.I., 1987, Geologic and diamond drill report for Candol Developments Ltd., Sechelt Carbonate Group, Sechelt Peninsula, British Columbia: Vancouver Mining Division.

Eastwood, G.E.P., 1968, Geology of the Kennedy Lake area, Vancouver Island, British Columbia: *Bulletin- British Columbia Department of Mines and Petroleum Resources*, 63 pages.

Einaudi, M.T. and Burt, D.M., 1982, A Special Issue Devoted to Skarn Deposits, Introduction-Terminology, Classification, and Composition of Skarn Deposits: *Economic Geology*, vol. 77, no. 4, pp. 745-753.

Ferry, J.M., 1988, Contrasting mechanisms of fluid flow through adjacent stratigraphic units during regional metamorphism, south-central Maine, USA: *Contributions to Mineralogy and Petrology*, vol. 9, pp. 1-12.

Ferry, J.M., 1989, Contact metamorphism of roof pendants at Hope Valley, Alpine County, California, USA: *Contributions to Mineralogy and Petrology*, vol. 101, pp. 402-417.

Ferry, J.M., 1994, Overview of the petrologic record of fluid flow during regional metamorphism in northern New England: *American Journal of Science*, vol. 294, pp. 905-988.

Floyd, A., 2001, Magistral: *Eighteenth Annual Cordilleran Roundup Abstracts*, B.C. and Yukon Chamber of Mines, p. 59.

Freidman, R.M., and Armstrong, R.L., 1995, Jurassic and Cretaceous geochronology of the southern Coast Belt, British Columbia, 49° to 51° N, *in* Miller, D.M., and Busby, C., *Jurassic Magmatism and Tectonics of the North American Cordillera*: Boulder, Colorado, Geological Society of America Special Paper 299.

Freidman, R.M., Mahoney, J.B., and Cui, Y., 1995, Magmatic evolution of the southern Coast Belt: constraints from Nd-Sr isotopic systematics and geochronology of the southern Coast Plutonic Complex: *Canadian Journal of Earth Sciences*, vol. 32, pp. 1681-1698.

Friedman, I., and O'Neil, J.R., 1977, Compilation of stable isotope fractionation factors of geochemical interest: In: *Data of Geochemistry*, 6th Edition, M. Fleischer, ed., U.S. Government Printing Office, Washington, D.C.

Green, G.R., Ohmoto, D., Date, J., and Takahashi, T., 1983, Whole-rock oxygen isotope distribution in the Fukazawa-Kosaka Area, Hokuroko District, Japan and its potential application to mineral exploration: *Economic Geology Monogram*, vol. 5, pp. 395-411.

Goldsmith, L.B. and Kallock, P., 1988, Geological Mapping, Diamond Drilling and Reserve Estimates of Wollastonite Deposit Mineral Hill claim group, Sechelt area, B.C. Vancouver Mining Division NTS 92G/12 W: unpublished report for *Tri-Sil Minerals Inc.*, 25 pages.

Grant, J.A., 1986, The Isocon Diagram—A Simple Solution to Gresens' Equation for Metasomatic Alteration: *Economic Geology*, vol. 81, pp. 1976-1982.

Gresens, R.L., 1967, Composition-Volume Relationships of Metasomatism: *Chemical Geology*, vol. 2, pp. 47-65.

Hess, P.C., 1989, *Origins of Igneous Rocks*: Harvard University Press, Cambridge, MS, 336 pages.

Hoefs, J., 1997, *Stable Isotope Geochemistry, 4th Edition* : Springer-Verlag, Berlin, 201 pages.

Irvine, T.N., and Baragar, W.R.A., 1971, A guide to the chemical classification of the common volcanic rocks: *Canadian Journal of Earth Sciences*, vol. 8, no. 5, pp. 523-548.

James, L.P., 1976, Zoned alteration in limestone at porphyry copper deposits, Ely, Nevada: *Economic Geology*, vol. 71, pp. 488-512.

Jeletzky, J.A., 1976, Mesozoic and ?Tertiary rocks of Quatsino Sound, Vancouver Island, British Columbia: *Bulletin- Geological Survey of Canada*, vol. 242, 243 pages.

Journeay, J.M., and Friedman, R.M., 1993, The Coast Belt Thrust System: Evidence of Late Cretaceous shortening in southwest British Columbia: *Tectonics*, vol. 12, no. 3, pp. 756-775.

Journeay, J.M., Williams, S.P., and Wheeler, J.O., 2000, Tectonic assemblage map, Kootenay Lake, British Columbia-Alberta-U.S.A.: *Geological Survey of Canada-Open File* 2948b.

Korzhinskii, D.S., 1936, Mobility and inertness of components in metasomatism: Akd. Nauk SSSR Izv. Otdel. matem. i estestven, nauk, no.1, pp. 35-65 (translated and reprinted in Mather, K.F., ed., 1967, *Source book in geology, 1900-1950*: Cambridge, Harvard University Press, pp. 290-303, summary in Burt, 1982).

Korzhinskii, D.S., 1970, *Theory of metasomatic zoning* (translated by Jean Agrell), Oxford Clarendon, Oxford, 162 pages.

Kwak, T.A.P., 1978, Mass Balance Relationships and Skarn-Forming Processes at the King Island Scheelite Deposit, King Island, Tasmania, Australia: *American Journal of Science*, vol. 278, pp. 943-968.

Kwak, T.A.P., and Askins, P.W., 1981, Geology and genesis of the F-Sn-W (-Be-Zn) skarn (wrigglite) at Moina, Tasmania: *Economic Geology*, vol. 76, pp. 439-467.

Lawson, A.C., 1914, Ore deposition in and near intrusive rocks by meteoritic waters: *University of California Department Geology Bulletin*, vol. 8, pp. 219-242 (summary in Burt, 1982).

Le Maitre, R.W. (ed.), Bateman, P., Didek, A, Keller, J., Lemeyre, J, Le Bas, M.J., Sabine, P.A., Schmid, R., Sorensen, H., Streckeisen, A., Wooley, A.R., Zanettin, B., 1989, *A classification of igneous rocks and glossary of terms*. Blackwell Sci. Publ. Oxford, U.K., 193 pages.

Lentz, D.R., Walker, J.A., and Stirling, J.A.R., 1995, Millstream Cu-Fe skarn deposit: an example of a Cu-bearing magnetite-rich skarn system in northern New Brunswick.: *Exploration Mining Geology*, vol. 4, pp. 15-31.

Lentz, D.R., and Susuki, K., 2000, A low-F, pegmatitic-related Mo skarn from the southwestern Grenville Province, Ontario, Canada: phase equilibria and petrogenetic implications: *Economic Geology*, vol. 95, pp. 1319-1337.

Lindgren, W., 1902, The character and genesis of certain contact deposits: *American Institute of Mining Engineers Transactions*, vol. 31, pp. 226-244 (summary in Burt, 1982).

Lindgren, W., 1924, Contact Metamorphism at Bingham, Utah: *Geological Society of America*

*Bulletin*, vol. 36, pp. 247-261.

Maniar, P.D., and Piccoli, P.M., 1989, Tectonic discrimination of granitoids: *Geological Society of America Bulletin*, vol. 101, no. 5, pp. 635-643.

McCrea, J.M., 1950, The isotopic chemistry of carbonates and a paleotemperature scale: *J Chem Phys*, vol. 18, pp. 849-857.

McDonough, W.F., and Sun, S.S., 1995, The Composition of the Earth. In: McDonough, W.F. (ed.), Chemical evolution of the mantle, *Chemical Geology*, vol. 120, no. 3-4, pp. 223-253.

Meinert, L.D., 1992, Skarns and Skarn Deposits: *Geoscience Canada*, vol. 19, no. 4, pp. 145-162.

Muller, J.E., Northcote, K.E., and Carlisle, D., 1974, Geology and Mineral Deposits of the Alert Bay-Cape Scott map area, Vancouver Island, British Columbia: *Paper- Geological Survey of Canada*, vol. 74-8, 77 pages.

Murphy, K.G., 1999, A Preliminary Assessment of the Mineral and Aggregate Potential of the South Central Sechelt Peninsula Sechelt, B.C.: Vancouver Mining Division, NTS: 92G12W.

Nabelek, P.I., Labotka, T.C., O'Neil, J.R., and Papike, J.J., 1984, Contrasting fluid/rock interaction between the Notch Peak granitic intrusion and argillites and limestones in western Utah: evidence from stable isotopes and phase assemblages: *Contributions to Mineralogy and Petrology,* vol. 86, pp. 25-34.

Nabelek, P.I., 1991, Stable Isotope Monitors. In: Kerrick, D.M., ed., *Contact Metamorphism*, Reviews in Mineralogy, vol. 26, pp. 395-435.

O'Connor, K., 2001, Antamina: *Eighteenth Annual Cordilleran Roundup Abstracts*, B.C. and Yukon Chamber of Mines, p. 58.

Ortoleva, P., Chadam, J., Merino, E., Sen, A., 1987, Geochemical self organization II; the reactive-infiltration instability: *American Journal of Science*, vol. 287, no. 10, pp. 1008-1040.

Osberg, P.H., 1979, Buchan-type metamorphism of the Waterville pelite, south-central Maine. In: Osberg, P.H. (ed.) *Geology of east-central and north-central Maine*. University of Maine, Orono, pp. 210-222.

Rae, D.A., Coulson, I.M., and Chambers, A.D., 1996, Metasomatism in the North Qoroq centre, South Greenland; apatite chemistry and rare-earth element transport: *Mineralogical Magazine*, vol. 60, pp. 207-220.

Ray, G.E. and Kilby, C.E., 1996, Geology of Mineral Hill-Wormy Lake Skarns, B.C. (92G/12W): *B.C. Ministry of Energy, Mines and Petroleum Resources,* Open File 1996-6,

1:10 000 scale.

Ray, G.E. and Kilby, C.E.,1996, The Geology and Geochemistry of the Mineral Hill-Wormy Lake Wollastonite Skarns. Southern British Columbia (92G/12W): *in* Geological Fieldwork 1995, *B.C. Ministry of Energy, Mines and Petroleum Resources,* Paper 1996-1, pages 227-241.

Roddick, J.A. and Woodsworth, G.J., 1979, Geology of Vancouver, West Half, and Mainland Parts of Alberni: *Geological Survey of Canada,* Open File 611.

Roselle, G.T, Baumgartner, L.P., and Valley, J.W., 1999, Stable isotopic evidence of heterogeneous fluid infiltration at the Ubehebe Peak contact aureole, Death Valley National Park, California: *American Journal of Science*, vol. 299, pp. 93-138.

Rumble, D., 1982, Stable isotope fractionation during metamorphic devolatilization reactions. In: *Characterization of Metamorphism Through Mineral Equilibria*, J.M. Ferry (ed.), Reviews in Mineralogy, Mineralogical Society of America, vol. 10, pp. 327-353.

Russell, J.K. and Nicholls, J., 1988, Analysis of Petrologic hypotheses with Pearce element ratios: *Contributions to Mineralogy and Petrology*, vol. 99, pp. 25-35.

Russell, J.K. and Stanley, C.R. (eds.), 1990, *Theory and application of Pearce element ratios to geochemical data analysis*, Geological Association of Canada Short Course Volume no. 8, Vancouver, B.C.

Samson, S.D., Patchett, P.J., McClelland, W.C., and Gehrels, G.E., 1991, Nd and Sr isotopic constraints on the petrogenesis of the west side of the northern Coast Mountains batholith, Alaskan and Canadian Cordillera: *Canadian Journal of Earth Sciences*, vol. 28, pp. 939-946.

SPSS Inc., 1997, *Sigma Plot 4.0 for Windows*, http://www.spss.com.

Taylor, B.E. and O'Neil, J.R., 1977, Stable isotope studies of metasomatic skarns and associated metamorphic and igneous rocks, Osgood Mountains, Nevada: *Contributions to Mineralogy and Petrology*, vol. 63, pp. 1-49.

Todd, C.S., 1990, Bleaching of limestones in the Notch Peak contact-metamorphic aureole, Utah: *Geology*, vol. 18, pp. 83-86.

Valley, J.W., 1986, Stable isotope geochemistry of metamorphic rocks. In: Valley, J.W., Taylor, H.P., O'Neil, J.R. (eds.), *Stable isotopes in high temperature geological processes.* Reviews in Mineralogy, vol. 16, pp. 445-489.

Vander Auwera, J. and Andre, L., 1991, Trace elements (REE) and isotopes (oxygen, carbon, strontium) to characterize the metasomatic fluid sources from the skarn deposit (iron, tungsten, copper) of Traversella (Ivrea, Italy): *Contributions to Mineralogy and Petrology*, vol. 106, pp. 325-339.

Veizer, J., Ala, D. Azmy, K, Bruckschen, P., Buhl, D., Bruhn, F., Carden, G.A.F., Diener, A.,

Ebneth, S., Godderis, Y., Jasper, T., Korte, C., Pawellek, F., Podlaha, O.G., Strauss, H., 1999, $^{87}Sr/^{86}Sr$, d$^{13}C$ and d$^{18}O$ evolution of Phanerozoic seawater: *Chemical Geology*, vol. 161, pp. 9-88.

Webster, I.C.L. and Ray, G.E., 1990, Geology and Mineral Occurrences of Northern Texada Island: *B.C. Ministry of Energy, Mines and Petroleum Resources,* Open File 1990-3, 1:20 000 scale.

Westphal, M., Coulson, I.M., Dipple, G.M., and Russell, J.K., 1999, Mantle signature versus crustal contamination in arc-magmatism: an example from Zippa Mountain. In: Cook, F. and P. Erdmer (compilers), *Slave-Northern Cordillera Lithospheric Evolution (SNORCLE) Transect and Cordilleran Tectonics Workshop Meeting* (March 5-7), University of Calgary, Lithoprobe Report no. 69, pp.146-152.

Whitney, P.R., and Olmsted, J.F., 1998, Rare-earth element metasomatism in hydrothermal systems: The Willsboro-Lewis wollastonite ores, New York, USA: *Geochimica et Cosmochimica Acta*, vol. 62, pp. 2965-2977.

Winkler, H.G.F., 1976, *Petrogenesis of Metamorphic Rocks*, Springer-Verlag, 334 pages.

Zharikov, V.A., 1970, Skarns: *International Geology Review*, vol. 12, pp. 541-559, 619-647, 760-775.

Zheng, Y.F., 1993a, Calculation of oxygen isotope fractionation in $SiO_2$ and $Al_2SiO_5$ polymorphs: effect of crystal structure: *European Journal of Mineralogy*, vol. 5, pp. 651-658.

# APPENDIX 1:
# STRUCTURAL MEASUREMENTS

App. 1. Structural measurments for Mineral Hill. Magnetic declination is 20 degrees. Corresponding localities found in Fig 1.4 (UB, TB, UMQ) and Fig 1.5 (MB, LB).

| location | strike | dip |
|---|---|---|
| 1 | 235 | 77NW |
| | 220 | 84NW |
| | 240 | 84NW |
| 2 | 25 | 70SE |
| | 35 | 55SE |
| | 21 | 86SE |
| 3 | 250 | 75NW |
| | 230 | 55NW |
| | 255 | 85NW |
| 4 | 250 | 80NW |
| | 290 | 80NW |
| | 255 | 90 |
| 5 | 280 | 65NW |
| | 280 | 53NW |
| | 280 | 68NW |
| 6 | 250 | 72NW |
| | 230 | 80NW |
| | 115 | 75SW |
| 7 | 255 | 75NW |
| | 250 | 90 |
| 8 | 260 | 76N |
| | 280 | 75NW |
| | 258 | 80N |
| 9 | 240 | 71N |
| | 230 | 88NW |
| | 214 | 86N |
| | 218 | 71N |
| | 212 | 69N |
| | 205 | 69N |
| 10 | 255 | 25NE |
| | 168 | 62E |
| | 160 | 64E |
| | 355 | 80NE |
| 11 | 182 | 72E |
| | 197 | 86E |
| | 184 | 82E |
| 12 | 240 | 85NW |
| | 235 | 73NW |
| | 220 | 80NW |
| | 205 | 85W |
| | 211 | 70W |
| | 215 | 64W |
| | 209 | 73W |
| | 240 | 71W |
| | 222 | 71W |
| | 227 | 68W |
| | 225 | 65W |
| | 209 | 73W |
| | 315 | 65N |
| | 325 | 70N |
| | 324 | 64N |
| | 337 | 74N |
| | 304 | 70N |
| | 337 | 45N |
| | 330 | 58N |
| | 352 | 53E |
| 13 | 255 | 76NW |
| | 75 | 85SE |
| | 344 | 76E |
| | 115 | 85SE |
| | 126 | 69S |
| | 325 | 87NE |
| | 185 | E |
| | 30 | 80SE |
| | 330 | 70NE |
| 14 | 302 | 84N |
| | 110 | 85S |
| | 112 | 85S |
| | 265 | 75NW |
| 15a | 300 | 76NW |
| | 275 | 88NW |
| | 270 | 79NW |
| | 285 | 82N |
| | 104 | 86S |
| 16a | 240 | 70NW |
| | 215 | 75NW |
| | 34 | 87E |
| | 213 | 71W |
| | 205 | 75NW |
| | 215 | 80NW |
| 16b | 202 | 71W |
| | 205 | 80NW |
| 16b | 215 | 71W |
| | 204 | 83W |
| 15b | 350 | 90 |
| | 300 | 86N |
| 16c | 220 | 80NW |
| | 206 | 76W |
| | 205 | 80NW |
| | 30 | 60SE |
| 15c | 295 | 85NE |
| | 296 | 90 |
| 17 | 255 | 75NW |
| | 240 | 75NW |
| | 225 | 90 |
| | 242 | 66NW |
| | 213 | 82NW |
| | 252 | 81NW |
| | 285 | 80NW |
| 18a | 277 | 71NW |
| | 295 | 80NW |
| | 275 | 75NW |
| 19 | 305 | 20NW |
| | 25 | 75E |
| | 260 | 80NW |
| | 235 | 90 |
| 20 | 340 | 75NE |
| 18b | 267 | 70NE |
| 21 | 200 | 90 |
| | 30 | 84E |
| | 195 | 85E |
| | 45 | 88E |
| | 29 | 90 |
| 22 | 223 | 69NW |
| | 170 | 70SW |
| | 210 | 75W |
| | 290 | 71W |
| | 290 | 85NW |
| 23 | 235 | 70NW |
| | 260 | 62NW |
| | 276 | 52N |
| | 265 | 55NW |
| | 253 | 58NW |
| 24 | 265 | 76NW |
| | 275 | 80NW |
| 25 | 323 | 64NW |
| | 321 | 79NW |
| | 327 | 75NW |
| | 225 | 85W |

| location | strike | dip | location | strike | dip | location | strike | dip | |
|---|---|---|---|---|---|---|---|---|---|
| 26 | 225 | 86SE | 32a | 20 | 90 | 41 | 302 | 78N | |
| | 250 | 85NW | 34 | 277 | 70N | | 299 | 83N | |
| | 22 | 84SE | | 300 | 63N | 42 | 265 | 65NW | |
| 27 | 245 | 84NW | | 289 | 73N | | 185 | 57W | |
| | 245 | 80NW | | 285 | 55N | | 70 | 10NW | (APPROX) |
| | 230 | 90 | | 298 | 59N | 43 | 58 | 68SE | |
| 28 | 245 | 80NW | | 291 | 51N | | 102 | 86S | |
| | 245 | 62NW | | 326 | 50NE | | 94 | 76S | |
| | 260 | 64NW | | 298 | 69N | | 94 | 52S | |
| | 260 | 60NW | | 330 | 80NE | | 64 | 80SE | |
| | 265 | 90 | | 249 | 70NW | 44 | 250 | 80NW | |
| | 225 | 82NW | | 250 | 34NW | | 260 | 85NW | |
| | 230 | 88NW | 35 | 190 | 23W | | 250 | 88NW | |
| | 245 | 89NW | 33 | 210 | 10W | 45 | 230 | 75NW | |
| | 235 | 90 | | 285 | 90 | | 255 | 68NW | |
| | 50 | 81SE | 36 | 246 | 80NW | | 42 | 52SE | UPPER LIMB |
| | 85 | 80SE | | 50 | 83SW | | 70 | 67SE | UPPER LIMB |
| 29 | 285 | 45NW | | 228 | 74NW | | 62 | 75SE | UPPER LIMB |
| | 75 | 40NW | | 237 | 38NW | 46 | 265 | 70NW | |
| | 290 | 65NW | | 230 | 66NW | 47 | 290 | 85NW | |
| | 40 | 40SE | | 135 | 80NE | | 245 | 68NW | |
| | 40 | 80SE | | 242 | 84NW | | 260 | 85NW | |
| | 210 | 90 | | 235 | 65NW | 48 | 244 | 77NW | (APPROX) |
| | 200 | 77W | | 245 | 90 | | 68 | 82SE | (APPROX) |
| | 240 | 42NW | 37 | 56 | 89SE | 49 | 270 | 75NW | |
| | 275 | 60NW | | 242 | 89NW | | 255 | 70SW | |
| 30 | 235 | 60NW | | 230 | 75NW | | 90 | 80SE | |
| | 260 | 60NW | | 74 | 85SE | | 235 | 55NW | |
| | 285 | 85NW | | 270 | 76NW | | 235 | 88NW | |
| | 205 | 70NW | | 48 | 63SE | 50 | 234 | 81NW | |
| 31 | 270 | 64NW | 38 | 198 | E | | 254 | 86NW | |
| | 225 | 80NW | 39 | 35 | 80SE | | 250 | 82NW | |
| | 270 | 65NW | | 45 | 78SE | 51 | 62 | 53SE | |
| | 280 | 72NW | | 30 | 90 | | 54 | 60SE | |
| | 225 | 88NW | | 35 | 79SE | | 64 | 63SE | |
| | 245 | 75NW | | 40 | 85SE | 52 | 240 | 85NW | |
| | 225 | 70NW | | 30 | 78SE | | 65 | 75SE | |
| 32 | 235 | 82NW | | 140 | 85SW | | 70 | 76SE | |
| | 225 | 84NW | | 45 | 90 | 53 | 62 | 89SE | |
| | 219 | 20W | 40 | 212 | 83NW | | 76 | 85SE | |
| | 244 | 44NW | | 214 | 78NW | | 82 | 82SE | |
| 33 | 235 | 40W | | 214 | 88W | 54 | 255 | 72NW | |
| | 20 | 89SE | | 214 | 89W | | 225 | 75NW | |
| | 200 | 80NW | | 36 | 88E | 55 | 73 | 85SE | |
| | 264 | 25NW | | 222 | 64W | | 260 | 55NW | |
| | 225 | 64NW | 41 | 280 | 90 | | 82 | 80SE | |

| location | strike | dip |
|---|---|---|
| | 250 | 81NW |
| | 255 | 75NW |
| | 265 | 68NW |
| 56 | 160 | 70NW |
| | 268 | 60NW |
| | 280 | 69N |
| | 282 | 72N |
| | 275 | 87N |
| 57 | 250 | 76NW |
| | 250 | 83NW |
| | 265 | 80NW |
| | 240 | 43NW |
| | 295 | 65NW |
| | 272 | 70N |
| | 266 | 72N |
| 58 | 50 | 88SE |
| | 242 | 75NW |
| | 262 | 59NW |
| 59 | 60 | 85SE |
| | 230 | 90 |

| location | strike | dip |
|---|---|---|
| H | 155 | 75 |
| H | 180 | 85 |
| H | 175 | 65 |
| H | 195 | 86 |
| H | 344 | 85 |
| H | 150 | 76 |
| H | 175 | 75 |
| H | 225 | 51 |
| H | 245 | 77 |
| H | 160 | 77 |
| H | 158 | 70 |
| H | 275 | 68 |
| H | 255 | 80 |
| H | 170 | 77 |
| H | 155 | 90 |
| H | 140 | 70 |
| H | 175 | 45 |
| H | 200 | 57 |
| H | 165 | 80 |
| H | 150 | 90 |
| H | 125 | 86 |
| H | 155 | 70 |
| H | 330 | 75 |
| H | 145 | 90 |
| H | 315 | 70 |
| H | 325 | 75 |
| H | 325 | 80 |
| H | 325 | 73 |
| H | 325 | 85 |
| H | 310 | 75 |
| H | 325 | 65 |
| H | 315 | 75 |
| H | 330 | 75 |
| H | 295 | 68 |
| H | 290 | 72 |
| H | 315 | 83 |
| H | 300 | 65 |
| H | 120 | 75 |
| H | 345 | 65 |
| H | 0 | 75 |
| H | 120 | 80 |
| H | 315 | 60 |
| H | 110 | 75 |
| H | 110 | 75 |
| H | 335 | 88 |
| H | 100 | 90 |
| H | 320 | 75 |

| location | strike | dip |
|---|---|---|
| H | 110 | 85 |
| H | 305 | 80 |
| H | 160 | 73 |
| H | 310 | 60 |
| H | 155 | 75 |
| H | 300 | 75 |
| H | 305 | 83 |
| H | 305 | 80 |
| H | 280 | 90 |
| H | 280 | 75 |
| H | 5 | 85 |
| H | 225 | 65 |
| H | 140 | 70 |
| H | 235 | 35 |
| H | 180 | 75 |
| H | 180 | 70 |
| Sheer zo | 120 | 78 |